

The Synthesis and Applications of
Pillar[n]arene in Selective Guest
Binding and Surface Modification

By

Alexander Lewis

A thesis submitted to the University of Birmingham for
the degree of DOCTOR OF PHILOSOPHY

School of Chemistry

The University of Birmingham

2022

ABSTRACT

Macrocyclic chemistry has garnered interest in a plethora of scientific fields. Whether in the exploration of new antibiotics, or in the adsorption of greenhouse gases, the breadth of macrocyclic research is constantly extending. Underpinning most of this research, however, is a key theme; to bind and encapsulate a particular species. Natural processes provided the foundations of such research, from ion capture in hemoglobin, to the protein binding antimicrobial qualities of erythromycin and clarithromycin. Consequently, the subsequent biomimetic approach to the synthetic design of macrocycles was the dominant force in synthetic macrocyclic research. That was until the works from the likes of Pederson, Lehn and Cram, who introduced not only new chemical motifs, but a new approach to the design of macrocycles.

Pillar[*n*]arenes were introduced to the family of synthetic macrocycles by Tomoki Ogoshi in 2008. They were heralded for their simplicity, rigidity, and their promising host-guest properties. These para-bridged symmetrical macrocycles have since become a guiding force in macrocyclic research, aided by their ease of synthesis, and the almost endless possibilities for functionalization. Akin to other macrocycles, research into the host-guest properties of pillar[5]arene has been demonstrated as paramount to the macrocycle's success in pursuing real-world applications.

Although pillar[5]arenes selectivity towards cationic and electron poor molecules has been well established, this research has rarely expanded into specific applications. An example of such an application is presented herein, that is the selective binding of common pesticides and their metabolites. Pesticides perform a vital role in providing means to produce the ever-increasing supply of agrarian products needed for our expanding population. Parallel to their need, however, is the growing concern

surrounding the environmental and anthropomorphic damage that these agrochemicals provide. The safe management and control of these biocides are therefore paramount to ensuring a sustainable future. Herein, the host-guest properties of pillar[*n*]arenes are utilized to pursue a method of creating a selective 'kill-switch' to prevent the more harmful metabolites of nicotinoids and neonicotinoids. Through proton NMR titrations, the binding constants of the 5 and 6 membered pillar[*n*]arenes towards a series of insecticides and their respective metabolites are measured. Whereas the cationic nicotine metabolite, *N*-ethylnicotinium is successfully encapsulated, imidacloprid and its metabolite desnitroimidacloprid show contrary results. The results therefore demonstrate that our understanding of the host-guest chemistry of pillar[5]arene must propel solely beyond electrostatic interactions.

Surface chemistry plays a vital role in transferring the properties of molecules to the macromolecular scale. The adoption of macrocycles onto surfaces, therefore provides a unique opportunity to transplant the host-guest properties of a given molecule to a stable macromolecular platform. This work details a method of adsorbing pillar[5]arenes onto a gold surface using thiol chemistry. Through scanning tunneling microscopy, the topographic nature of the pillar[5]arene/ metal surface is examined.

An expansion to this surface modification is an attempt to affix the dynamic rotaxane to a porous material. Herein, a 'semi-modular' approach to rotaxane design where the asymmetric components of the rotaxane can be tailored to a specific surface is employed. Paired with these rotaxanes are novel metal organic frameworks containing moieties capable of covalent post-synthetic surface modification.

ACKNOWLEDGMENTS

Firstly, I would like to thank my supervisor Professor Neil Champness for his guidance and mentoring with my research. Without his help and willingness to let me explore the inherent creativity that arises from supramolecular chemistry, I would not have been able to pursue my work. Equally, I would like to thank my secondary supervisors Dr Alex Saywell and Dr Tim Barendt for their help. Pertinent is the funding for research, which was gratefully provided by initially the EPSRC and then the University of Birmingham.

For my research to progress it was imperative that I took advice from those who had a greater understanding than myself. For specific analytical and spectroscopic instruments that was none-so relevant. For that reason, I would like to acknowledge my post-docs: Dr Sarah Griffin for her help with crystallography, Dr Georgia Orton with help with cyclic-voltammetry, and Dr Nic Pearce for his synthetic guidance. Equally, the contribution from the wonderful technicians that I have encountered within both universities of Nottingham and Birmingham was more than necessary. Especially that of Ben Pointer-Gleadhill and Cecile Le Duff who I owe a lot to.

I must also thank those who I have shared my PhD experiences with, my group members within Nottingham and Birmingham and those in other groups who have assisted both academically and personally. Equally, I could not of achieved all of my results without the assistance of my two masters students; Martin and Tash.

Lastly, to all those in my life who have sacrificed their time and effort into helping me, that is my parents, my sisters, my friends, my doctors, and Vera the cat.

CONTENTS

Abstract	ii
Acknowledgments	iv
List of Symbols and Abbreviations.....	xi
1. Introduction	1
1.1. Macrocycles.....	1
1.1.1. Synthetic Routes for Macrocycles	2
1.1.2. Applications of Macrocycles	3
1.1.3. Crown Ethers	4
1.1.4. Cyclodextrins.....	5
1.1.5. Calix[<i>n</i>]arenes	6
1.1.6. Cucurbit[<i>n</i>]urils	7
1.1.7. Other Macrocycles	9
1.2. Pillar[<i>n</i>]arenes	10
1.2.1. Nomenclature of Pillar[<i>n</i>]arenes	11
1.2.2. Mechanism of Pillar[5]arene Formation.....	11
1.2.3. Synthesis of Pillar[5]arene.....	13
1.2.4. Synthesis of Pillar[>5]arenes.....	15
1.2.5. Pillar[<i>n</i>]arenes; structural properties.....	16
1.2.5.1. Pillar[<i>n</i>]arene Cavity Dimensions	16
1.2.5.2. Conformation and Planar Chirality	17
1.2.5.3. Pillar[<i>n</i>]arene, Intermolecular Assemblies.....	19
1.2.6. Functionalisation of Pillar[<i>n</i>]arenes	20
1.2.7. Deprotection of Pillar[<i>n</i>]arenes	21
1.2.8. Cocyclisation and Pre-macrocyclization Functionalisation	23
1.2.9. Other Methods of Functionalisation.....	24
1.3. Host-Guest Properties of Pillar[<i>n</i>]arenes	25
1.3.1. Host-Guest Chemistry, a Brief History	25
1.3.2. Intermolecular Forces in Host-Guest Chemistry.....	27
1.4. Host-Guest Chemistry of Pillar[5]arene	31
1.4.1 Assessing Pillar[<i>n</i>]arene Host-Guest Complexes.....	32
1.4.2. Pillar[<i>n</i>]arenes With Cationic Guests.....	34
1.4.2.1. Dialkoxypillar[5]arene With Cationic Guests	34
1.4.2.2. Dihydroxypillar[5]arene With Cationic Guests.....	35
1.4.2.3. Water-soluble Pillar[5]arenes with Cationic Guests	36
1.4.2.4. Larger Pillar[<i>n</i>]arenes with Cationic Guests.....	37

1.4.3. Pillar[<i>n</i>]arene With Neutral Guests	39
1.4.3.1. Dialkoxypillar[5]arene With Neutral Guests	39
1.4.3.2. Larger Alkoxypillar[<i>n</i>]arenes With Neutral Guests	42
1.5. Thesis Outline	44
1.6 References	47
Chapter 2 Pillar[<i>n</i>]arenes and their complexations with neonicotinoids and nicotine derivatives	54
2.1. Introduction	55
2.2. Nicotine.....	55
2.2.1. Metabolites of Nicotine	57
2.2.2. Detection and Encapsulation of Nicotine and Nicotine Like Compounds	59
2.2.3 Alkylation of Nicotine.....	61
2.3. Neonicotinoids	62
2.3.1. A Brief History of Pesticide Usage	62
2.3.2. History of Neonicotinoids.....	63
2.3.3. Neonicotinoid Mode of Action.....	66
2.3.4. Transformation of Neonicotinoids.....	70
2.3.5. Metabolites of Neonicotinoids	74
2.3.6. Toxicity of Metabolites.....	76
2.3.7. Encapsulation of Neonicotinoids	77
2.4. Results and Discussion	80
2.4.1. Synthesis of Pillar[<i>n</i>]arenes.....	80
2.4.2. Synthesis of Alkylated Nicotine's.....	83
2.4.3. Synthesis of Imidacloprid and Desnitroimidacloprid	86
2.4.4. Nicotine binding studies	88
2.4.5 Nicotinium NMR Titrations.....	95
2.4.5. Imidacloprid Binding Studies	97
2.4.6. Imidacloprid NMR Titrations	100
2.4.7. Imidacloprid and Pillar[6]arene Titration, and Concentration Variations	105
2.4.8. Desnitro-imidacloprid Binding Studies.....	107
2.4.9. Desnitro-Imidacloprid NMR Titrations	110
2.5. Conclusions and Further Work	111
2.6. Materials and Methods	115
2.6.1. Synthesis.....	115
2.6.1.1. Dimethoxypillar[5]arene	115
2.6.1.2. Diethoxypillar[5/6]arene	116
2.6.1.3. Imidacloprid	119

2.6.1.4. N1-((6-chloropyridin-3-yl)methyl)ethane-1,2-diamine	119
2.6.1.5. Desnitro-imidacloprid	120
2.7. References	121
Chapter 3. Pillar[5]arene for the Synthesis of Rotaxane Decorated Metal Organic Frameworks	130
3.1. Introduction	130
3.2. Rotaxanes	130
3.2.1. Synthesis of Rotaxanes.....	131
3.2.2. Dynamics of Rotaxanes	133
3.2.3. Molecular Shuttles.....	133
3.2.4. Rotaxanes on Surfaces	135
3.3. Metal Organic Frameworks.....	137
3.3.1. Synthesis of MOFs.....	138
3.3.2. Surface Modification of MOFs	140
3.3.3. Rotaxanes and MOFs	142
3.4. Results and Discussion	144
3.5. Surface Modification of MOFs With Rotaxanes <i>Via CuAAC Click Chemistry</i>	144
3.5.1. Synthesis of an Azide Functionalised MOF	144
3.5.1.1. Synthesis of Dimethyl 2',5'-dimethyl-[1,1':4',1''-terphenyl]-4,4''-dicarboxylate	145
3.5.1.2. Synthesis of Dimethyl 2',5'-bis(bromomethyl)-[1,1':4',1''-terphenyl]-4,4''-dicarboxylate.....	146
3.5.1.3. Synthesis of Dimethyl 2',5'-bis(azidomethyl)-[1,1':4',1''-terphenyl]-4,4''-dicarboxylate	147
3.5.1.4. Synthesis of 2',5'-Bis(azidomethyl)-[1,1':4',1''-terphenyl]-4,4''-dicarboxylic acid	148
3.5.1.5. Synthesis of UIO-68 N ₃ MOF.....	148
3.5.2. Design and Synthesis of Rotaxane for Surface Modification of an Azide Functionalised MOF	148
3.5.2.1. Design of Rod Component	149
3.5.2.2. Synthesis of Rod Component	150
3.5.2.3. Design of Stopper Groups	152
3.5.2.4. Synthesis of Alkyne Functionalised Stopper	153
3.5.2.5. Coupling of Alkyne Functionalised Stopper to Rod Component	155
3.5.2.6. Design of Fluorescent Stopper	157
3.5.2.7. Testing of Fluorophore for Confocal Microscopy	157
3.5.2.8. Synthesis of Alkyne BODIPY	158
3.5.2.9. Confocal Microscopy of BODIPY functionalised MOF	160

3.5.2.10. Synthesis of Fluorescent Stopper Group	162
3.5.2.11. Design and Synthesis of Pillar[5]arene Macrocycle	164
3.5.2.12. Attempted Rotaxane Synthesis	165
3.5.3. Conclusions of Surface Modification of MOFs With Rotaxanes Via CuAAC Click Chemistry	167
3.6. Design and Synthesis of a MOF Capable of Methylhalide Functionalisation	168
3.6.1. Design of Pyridine Containing MOF	169
3.6.2. Synthesis of Shielded Pyridine MOF	170
3.6.2.1. Synthesis of Dimethyl 4,4'-(2-hydroxyacetyl)dibenzoate	170
3.6.3. Synthesis of Dimethyl 4,4'-oxalyldibenzoate	172
3.6.4. Synthesis of 4,4'-oxalyldibenzoic acid	173
3.6.5. Synthesis of Pyridine-2,6-bis(carboximidhydrazide).....	174
3.6.6. Synthesis of MOF-N7 linker	175
3.6.7. Synthesis of Shielded Pyridine MOF	177
3.6.8. Conclusion of the Synthesis of a MOF Capable of Methylhalide Functionalisation	179
3.7. Design and Synthesis of a MOF for Thiol-ene Surface Modification.....	180
3.7.1. Design and Synthesis of bis(alkene) Linker	181
3.7.1.1. Synthesis of 1,4-Dibromo-2,5-bis(bromomethyl)benzene.....	181
3.7.1.2. Synthesis of 1,4-Dibromo-2,5-divinylbenzene	182
3.7.1.3. Synthesis of bis(alkene) Linker.....	184
3.7.2. Synthesis of UiO-68 bis(alkene) MOF	184
3.7.3. Conclusions of the Synthesis of a MOF for Thiol-ene Surface Modification	185
3.8. Conclusions and Further Work	186
3.9 Materials and Methods	189
3.9.1 Synthesis of UiO6-8-N ₃ MOF	189
3.9.1.1. 2',5'-dimethyl-[1,1':4',1''-terphenyl]-4,4''-dicarboxylate	189
3.9.1.2. Dimethyl 2',5'-bis(bromomethyl)-[1,1':4',1''-terphenyl]-4,4''-dicarboxylate	190
3.9.1.3. Dimethyl 2',5'-bis(azidomethyl)-[1,1':4',1''-terphenyl]-4,4''-dicarboxylate	190
3.9.1.4. 2',5'-Bis(azidomethyl)-[1,1':4',1''-terphenyl]-4,4''-dicarboxylic acid..	191
3.9.1.5. UIO-68 N ₃ MOF	192
3.9.2. Synthesis of Alkene Rotaxane	192
3.9.2.1. 2-(6-bromohexyl)isoindole-1,3-dione	192
3.9.2.2. 2-(6-(1H-imidazol-1-yl)hexyl)isoindoline-1,3-dione	193
3.9.2.3. 6-(1H-imidazol-1-yl)hexan-1-amine	194

3.9.2.4. 4-Hydroxy-3,5-diisopropylbenzoic acid	194
3.9.2.5. Methyl 4-hydroxy-3,5-diisopropylbenzoate	195
3.9.2.6. Methyl 3,5-diisopropyl-4-(prop-2-yn-1-yloxy)benzoate.....	196
3.9.2.7. 3,5-Diisopropyl-4-(prop-2-yn-1-yloxy)benzoic acid	196
3.9.2.8. N-(6-(1H-imidazol-1-yl)hexyl)-3,5-diisopropyl-4-(prop-2-yn-1-yloxy)benzamide.....	197
3.9.2.9. 4-(Prop-2-yn-1-yloxy)benzaldehyde	198
3.9.2.10 4-(hydroxymethyl)benzaldehyde.....	199
3.9.2.11. 4-(Bromomethyl)benzaldehyde.....	200
3.9.2.12. Bromomethyl BODIPY	200
3.9.2.13. Attempted Rotaxane Synthesis	202
3.9.3. Synthesis of MOF-N7	203
3.9.3.1. Dimethyl 4,4'-(1-hydroxy-2-oxoethane-1,2-diyl)dibenzoate	203
3.9.3.2. Dimethyl 4,4'-oxalyldibenzoate	203
3.9.3.3. 4,4'-Oxalyldibenzoic acid	204
3.9.3.4. Pyridine-2,6-bis(carboximidhydrazide).....	204
3.9.3.5. MOF-N7 linker	205
3.9.3.6. MOF-N7 Synthesis	206
3.9.3.7. MOF-N4 Linker Synthesis.....	206
3.9.4. Synthesis of UiO-68 Alkene	207
3.9.4.1. 1,4-Dibromo-2,5-bis(bromomethyl)benzene	207
3.9.4.2. 1,4-Dibromo-2,5-divinylbenzene.....	207
3.9.4.3. Dimethyl 2',5'-divinyl-[1,1':4',1''-terphenyl]-4,4''-dicarboxylate.....	208
3.9.4.4. 2',5'-divinyl-[1,1':4',1''-terphenyl]-4,4''-dicarboxylic acid (bis(alkene) linker).....	209
3.9.4.5. UiO-68 bis(alkene) MOF	209
3.10 References	211
Chapter 4. Thiolated Pillar[5]arenes On Gold Surfaces.....	215
4.1. Introduction	216
4.2. Self-Assembled Monolayers	216
4.2.1. Common Self-Assembled Monolayer Motifs	218
4.2.2. Self-Assembled Monolayers of Thiolates on Gold.....	220
4.2.3. Mechanism of Thiolate-Gold SAM Formation.....	222
4.2.4. Structure and Bonding of Thiolate-Gold SAM	224
4.2.5. Macrocycles as Adsorbents for Thiolate-Gold SAMs	226
4.3. Thiolated Pillar[5]arenes on Gold Surfaces	227
4.3.1. Pillar[5]arene on Surfaces	228

4.3.2. Thiolated Pillar[5]arenes	230
4.3.3. Pillar[5]arenes on Gold Surfaces.....	232
4.3.4. Scanning Tunnelling Microscopy.....	232
4.4. Results and Discussion	234
4.4.1. Synthesis of Thiolated Pillar[5]arenes	235
4.4.1.1 Synthesis of 1,4-Bis(2-bromoethoxy)benzene	235
4.4.1.2 Synthesis of bis(bromoethoxy)-dimethoxycopillar[4+1]arene	237
4.4.1.3 Synthesis of Bis(bromoethoxy)pillar[5+6]arene	238
4.4.1.4 Structure of Bis(bromoethoxy)pillar[6]arene	239
4.4.1.5 Synthesis of bis(ethoxythiol)-dimethoxycopillar[4+1]arene and bis(ethoxythiol)pillar[5]arene.....	241
4.4.2. Thermal Decomposition and Adsorption Analysis	243
4.4.3. Scanning Tunnelling Microscopy of Bis(ethoxythiol)- dimethoxycopillar[4+1]arene on a Au(111) surface	244
4.5. Conclusions and Further Work	246
4.6. Materials and Methods	248
4.6.1. Synthesis of Thiolated Pillar[5]arenes	248
4.6.1.1. 1,4-Bis(2-bromoethoxy)benzene	248
4.6.1.2. Bis(bromoethoxy)-dimethoxybenzenecopillar[4+1]arene.....	248
4.6.1.3. Bis(ethoxythiol)-dimethoxybenzenecopillar[4+1]arene – method 1.	249
4.6.1.4. Bis(ethoxythiol)-dimethoxybenzenecopillar[4+1]arene – method 2.	250
4.6.1.5. Bis(bromoethoxy)pillar[5]arene.....	251
4.6.1.6. Bis(ethoxythiol)pillar[5]arene	252
4.7. References	254
Chapter 5. Conclusions	257
Chapter 6. Materials and Methods	262
6.1. Reagents and Purification.....	262
6.2. General Equipment.....	262
6.2.1. Nuclear Magnetic Resonance Spectroscopy (NMR)	262
6.2.2. Mass Spectrometry	262
6.2.3. Infrared Spectroscopy (IR)	262
6.2.4. Single crystal X-ray diffractometry (SCXRD).....	263
6.2.5. Procedure for Titrations by Nuclear Magnetic Resonance Spectroscopy	263
6.2.6 Scanning Tunnelling Microscopy.....	263
6.3. Computational Chemistry	264

List of Symbols and Abbreviations

Å	Angstrom
AcOH	Acetic acid
AIBN	Azobisisobutyronitrile
B24C8	Dibenzo-24-crown-8
BArF	Tetrakis(3,5-bis(trimethyl)phenyl)borate
BCE	Before Common Era
BODIPY	4,4-difluoro-4-bora-3a,4a-diaza-s-indacene
BPO	Dibenzoyl peroxide
BTB	4,4',4''-benzene-1,3,5-triyl-tris(benzoic acid)
CB	Cucurbituril
CD	Cyclodextrin
CDCl ₃	Deuterated Chloroform
COSY	Correlated Spectroscopy
CPM	6-chloropyrid-3-ylmethyl
CuAAC	Copper (I)-catalysed alkyne-azide cycloaddition
CYP	Cytochrome P450
DCC	Dicyclohexylcarbodiimide
DCE	Dichloroethane
DCM	Dichloromethane
DCTHIA	Descyanothiacloprid
DDT	Dichlorodiphenyltrichloroethane
DEP[5]A	Diethoxypillar[5]arene
DEP[6]A	Diethoxypillar[6]arene
DFT	Density functional theory
DIC	<i>N,N</i> -Diisopropylcarbodiimide
DIPEA	<i>N,N</i> -Diisopropylethylamine
DMF	<i>N,N</i> -Dimethylformamide
DMP[5]A	Dimethoxypillar[5]arene
DMSO	Dimethyl sulfoxide
DNA	Deoxyribonucleic acid
DNIMI	Desnitroimidacloprid
DPP[5]A	Dipropoxypillar[5]arene
e ⁻	Electron
EDC	1-Ethyl-3-(3-dimethylaminopropyl)carbodiimide
Et	Ethyl
EtOH	Ethanol
FAO	Food and Agriculture Organization of the United Nations
FeCl ₃	Iron (II) Chloride
FeSO ₄	Iron (II) Sulfate
FL	Fluorescence spectroscopy
FMO	Flavin-containing monooxygenase
H ₂ O ₂	Hydrogen Peroxide
H ₂ SO ₄	Sulfuric Acid

HCl	Hydrochloric Acid
HKUST	Hong Kong University of Science and Technology
HOBt	Hydroxybenzotriazole
hr	Hour
HSQC	Heteronuclear single quantum coherence spectroscopy
IC ₅₀	Half maximal inhibitory concentration
IMI	Imidacloprid
IPA	Isopropyl alcohol
ITC	Isothermal titration calorimetry
JMOD	J-modulated spin-echo
K _a	Binding Constant
LD ₅₀	Median Lethal dose
MALDI	Matrix-assisted laser desorption/ionisation
MeCN	Acetonitrile
MeOD	Deuterated Methanol
MIL	Matériaux de l'Institut Lavoisier
MiM	Mechanically interlocked molecules
MOF	Metal Organic Framework
MORF	Metal Organic Rotaxane Frameowrks
nAChR	Nicotinic acetylcholine receptor
NBS	N-bromosuccinimide
NMR	Nuclear magnetic resonance
NN	Neonicotinoid
OP	Organophosphate
OTMA	Octyltrimethyl ammonium hexafluorophosphate
Ox	Oxidation
PBS	Phosphate-buffered saline
PDMS	Polydimethylsiloxane
PF ₆	Hexafluorophosphate
Ph	Phenyl
pKa	Acid dissociation constant
PPE	Personal Protective Equipment
PPh ₃	Triphenylphosphine
R.T	Room Temperature
Ref	Reference
Rf	Retardation factor
SAM Mtase	S-adenosyl-L-methionine-dependent methyltransferases
tBuOK	<i>Tert</i> -potassium butoxide
TC	Thiocarbamate
TCE	1,1,2,2-tetrachloroethane
TEA	Triethylamine
THF	Tetrahydrofuran
THIA	Thiacloprid
TOF	Time of flight
Ts	Tosyl
UGT	Uridine 5'-diphospho-glucuronosyltransferase
UiO	University of Oslo
UV/VIS	Ultraviolet-visible
α4β2*	Alpha-4 beta-2 nicotinic receptor

1. INTRODUCTION

1.1. Macrocycles

Macrocycles are ring-shaped molecules comprised of several repeating monomers often referred to as subunits. The subunits are oligomerised in such a way that they form a closed ring, with a cavity or pore in the centre. The macrocycle complete, and its associated properties such as cavity size, solubility, polarity, and guest affinity, are largely dependent on the choice of subunit, but also on the bridging connections between the subunits. Macrocycles can be broadly split into two distinct categories: natural and synthetic. There are a multitude of naturally occurring macrocycles, including the antibiotic macrolides, erythromycin, clarithromycin, and azithromycin.¹ Antifungals such as amphotericin, ivermectin and nystatin, and immunosuppressants, with rapamycin and cyclosporine being two notable examples (*figure 1*).^{2,3} The bioactive nature of these molecules, sparked keen interest in biochemists and chemists alike to study further these molecules. Combined with these attractive qualities, however, is a difficulty in laboratory synthesis. Erythromycin for example, was discovered in 1952, but it would not be until 1981 when a ten step total-synthetic route was published.^{4,5} Amphotericin B equally, also took over 30 years to synthetically produce.^{6,7} The difficulty in synthesis due to their multiple stereogenic carbons and multiple asymmetric substitutions, led chemists to synthesise and isolate novel macrocycles which can be produced in a simple and consistent way.

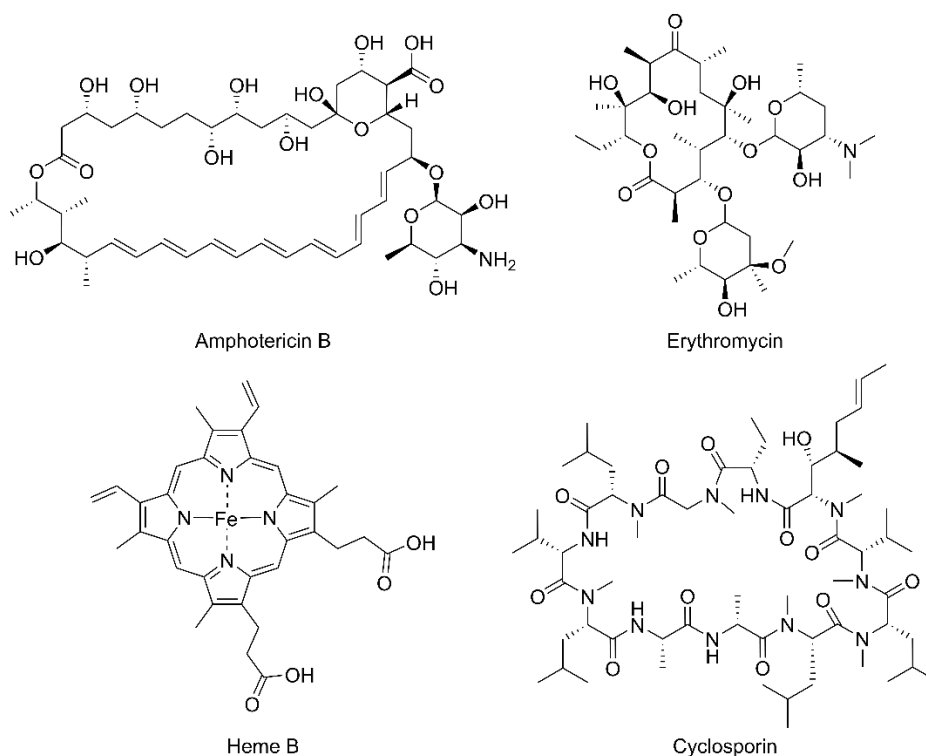


Figure 1. Examples of naturally occurring macrocycles.

1.1.1. Synthetic Routes for Macrocycles

The synthesis of macrocycles is simple in essence; smaller molecular building blocks are to be attached together in such a manner that they form a ring. The routes to macrocyclization thereby closely follow the same principles as polymerisation, and an equally large variety of chemical reactions can be employed to form these rings. This similarity, however, also causes the greatest difficulty in macrocycle synthesis, preventing the formation of linear polymers, and focussing the reaction towards macrocyclization. There are two remedies for this problem: high dilution and templating. The high dilution principle simply states that the more dilute a reaction is, the less likely collisions are between two adjacent small chains, and therefore increasing the probability of intramolecular ring closure. This principle was first

proposed by *Ruggli* and *Ziegler*, and although this was in reference to small 5 or 6 membered rings, the same principle is still used today with larger ring systems.^{8,9}

Alternatively, a template can be added to aid in macrocycle formation. Most commonly a metal ion, the template aids in the orientation of monomer units to allow for the optimum conformation for ring closure. The first demonstration of the increase in macrocycle formation efficiency *via* a template, was shown by *Busch* in 1968. Wherein, he described a 'kinetic coordination template effect' by a nickel (II) ion to hold a bis(thioether) containing molecule in a *cis configuration*, and thereby allowing for a macrocyclization reaction with an adjacent dibromobenzene (*figure 2*).¹⁰

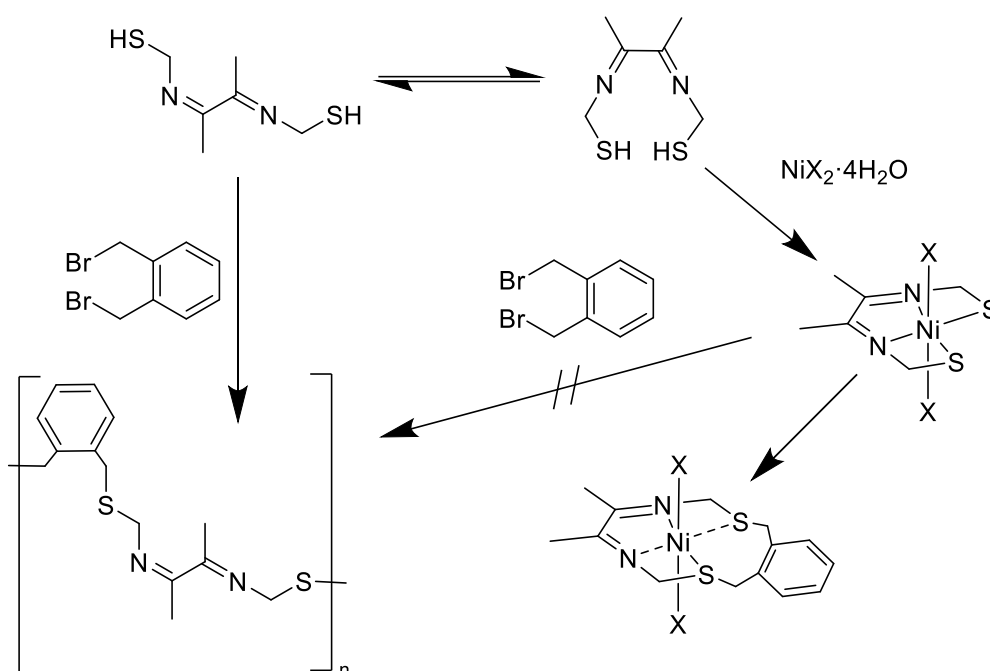


Figure 2. Reaction scheme, showing the products of the reaction between a bis(thioether) containing azapentadiene and 1,2-bis(bromomethyl)benzene with and without a nickel template.¹⁰

1.1.2. Applications of Macrocycles

The uses of macrocycle's ultimately, are the harnessing of their abilities to bind specific guests. This molecular encapsulation is not unique to macrocycles, porous materials

such as nanotubes, zeolites and metal organic frameworks have these same properties. Equally, in biochemical research, specific proteins and enzymes can be used to capture a particular substrate. However, how macrocycles differ is their relatively low molecular weight, mono-dispersity, and high symmetry when compared to previously mentioned examples. This allows for solvation in a wide range of solvents, a wider range of applicable spectroscopic and spectrometric analysis, and the ability to be further utilised in larger supramolecular assemblies.

As previously discussed, macrocycles can be utilised in medicinal chemistry. Research has shown the effective employment of macrocycles in various biochemical applications, including biosensing, drug delivery, and protein inhibitors.¹¹⁻¹³ In ecological studies multiple macrocycles have been proposed as prospects for gas capture and storage, as well as components in next generation renewable energy technologies.¹⁴⁻¹⁶ Molecular machines, those of which include; molecular shuttles, propellers, and switches, nearly always have macrocycles as the dynamic components within a larger supramolecular structure.¹⁷ Macrocycles, therefore, fulfil a role in a myriad of scientific branches, and as new macrocycles are developed, and as we obtain a greater understanding of existing, new opportunities are being presented.

1.1.3. Crown Ethers

One of the earliest synthetic macrocycles were crown ethers, first reported by *Pederson* in 1967.¹⁸ Crown ethers became not only the first lab-made macrocycle, but the first neutral synthetic compound that could form stable complexes with alkali metal cations (*figure 3*). The importance of macrocycles therefore propelled research further than just producing alternatives to natural products, but towards new and uncharted applications. Chemically, crown ethers are cyclic oligomers containing multiple

oxygens bound by organic linkers, most commonly ethylene's. Since their inception, the number of crown ethers has multiplied exponentially, with a vast array of different properties arising from each variant. The synthesis of crown ethers was, and largely still is templated by metal ions, with the size of the cation largely defining the number of subunits, and therefore size of the macrocycle. With crown ethers solubility in a range of solvents, ease of synthesis, large array in variations and their attractive host guest properties, they have cemented themselves as popular macrocycles in a wide range of applications to this day.

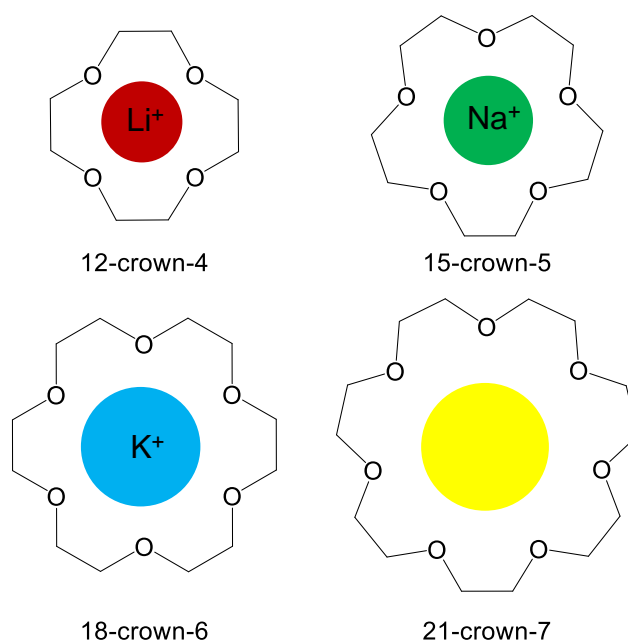


Figure 3. Chemical structures of common crown ethers with favoured cation in selective binding studies shown in cavity.¹⁹

1.1.4. Cyclodextrins

Cyclodextrins are naturally occurring macrocycles, consisting of several glucopyranose units bound *via* α -1,4-linkages (*figure 4*). These sugar based cyclic oligosaccharides, were first discovered in 1891 by *Villiers*, and were extensively studied since.²⁰ The most common commercially available cyclodextrins are; α -, β -

and γ -cyclodextrin, and consist of 6, 7 and 8 glucopyranose subunits respectively. The most widely used synthesis of cyclodextrins is *via* the enzymatic treatment of starch, and by altering the enzyme used, or alternatively by adding a solvent-based template, the size ratio of cyclodextrins formed is controlled.²¹ Due to the rims of cyclodextrin being decorated with hydroxyl groups, the outside of the cyclodextrin is hydrophilic, resulting in good solubility in aqueous media and polar solvents. Conversely, the inside of the cavity is hydrophobic, and can therefore accommodate a wide range of organic alkyl and aromatic guests.²² This water solubility, and ability to bind non-polar guests in aqueous conditions, combined with the ease and scalability of synthesis, have established cyclodextrins as important focal points in biological macrocyclic research.

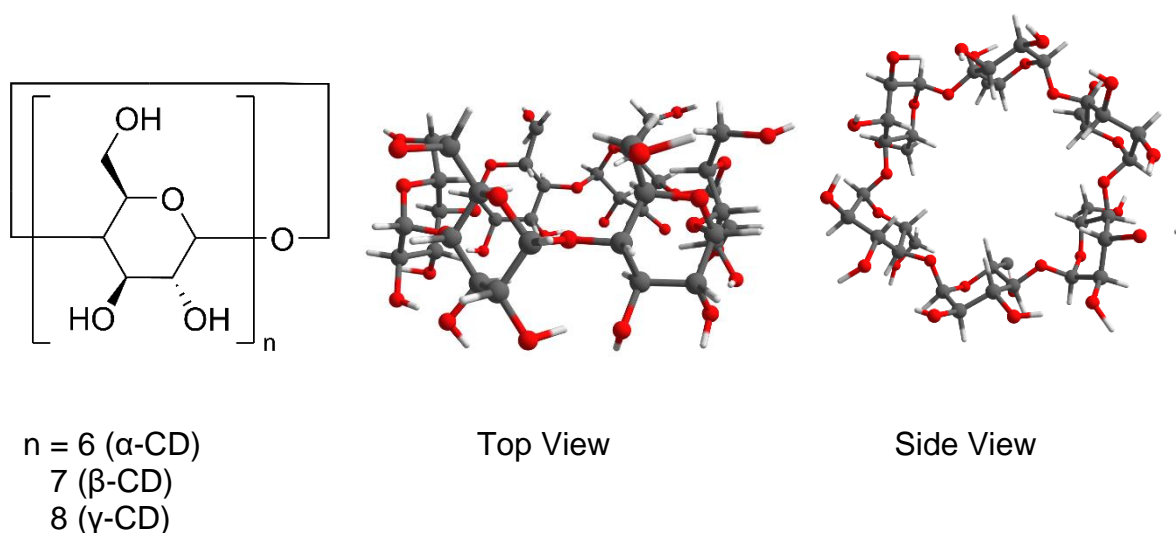


Figure 4. Chemical and X-ray crystal structure of cyclodextrin (β -CD for crystal structure).²³

1.1.5. Calix[n]arenes

Calix[n]arenes are macrocycles comprised of phenol subunits linked by methylene bridges in the *ortho* positions, synthesised *via* a phenol-formaldehyde condensation (*figure 5*). Calix[n]arenes were first synthesised in 1872 by *Baeyer*, but at that time characterisation methods were not equipped to fully understand the macrocycle. Interestingly, the same procedure involving phenols, strong acids and formaldehyde

would also become the precursor to forming the first synthetic plastic; Bakelite.²⁴ But it would not be until 1978 that Calix[*n*]arenes would be named as such by *Gutsche*, with the prefix 'calix' arising from the Greek word to mean cone or bowl. As the name suggests, the calix[*n*]arenes' asymmetric phenolic units, combined with their *ortho*-bridges, leads to an asymmetric macrocycle. Both rims can be functionalised before or after macrocycle formation, which allows for the synthesis of calix[*n*]arenes with varying structural and chemical properties. The phenolic subunits allow for an electron-donating cavity, and therefore cationic and electron poor molecules are suitable guests for the macrocycle.²⁵ The tunability, selectivity and low toxicity of the calix[*n*]arene, has elicited a vast amount of research into their potential drug delivery capabilities, and for the manufacturing of biomaterials.²⁶

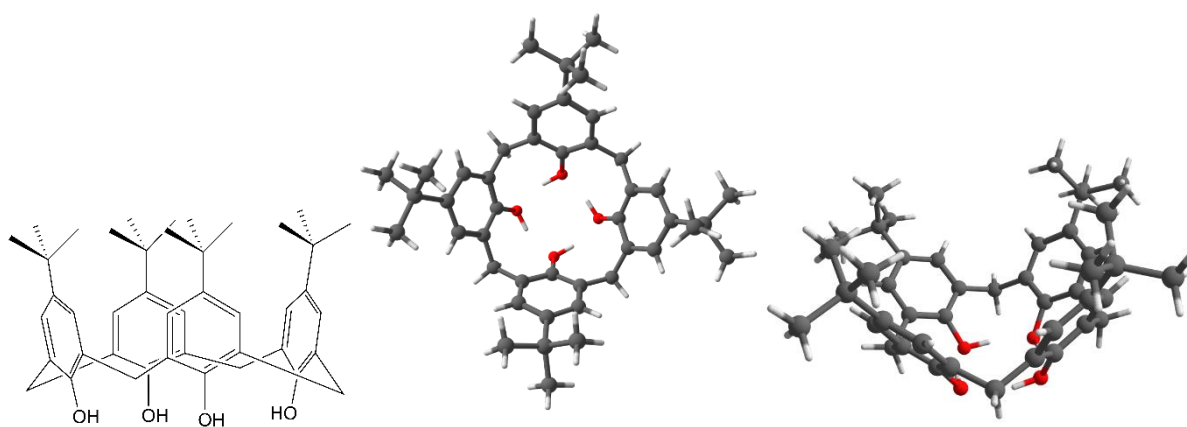


Figure 5. Chemical structure of calix[4]arene, and the top and side view of the X-ray crystal structure of calix[4]arene.²⁷

1.1.6. Cucurbit[*n*]urils

Cucurbit[*n*]urils are synthesised *via* an acid-catalysed condensation of formaldehyde and glycoluril (*figure 6*). The symmetric, barrel shaped macrocycle was first synthesised in 1905, and was noted as an insoluble product of condensation.²⁸ Due

to this insolubility, the macrocyclic structure would not be identified until 1981, with *Mock* reporting a crystal structure of cucurbit[n]uril.²⁹ Noting its pumpkin like shape, cucurbit[n]urils were named thus, after *Cucurbitaceae* the plant family containing the pumpkin. Research into the complexation behaviour of cucurbit[n]urils was stifled by cucurbit[6]uril's poor solubility. However, *Kim et al*, reported that by altering the reaction temperature, more soluble 5 and 7 member homologues could be synthesised and isolated.³⁰ The cavity of the macrocycle is highly symmetric and hydrophobic, whereas the carbonyl rims are electron rich. Therefore, water soluble cationic guests, such as alkyldiamines can form strong host-guest interactions with cucurbit[n]urils.

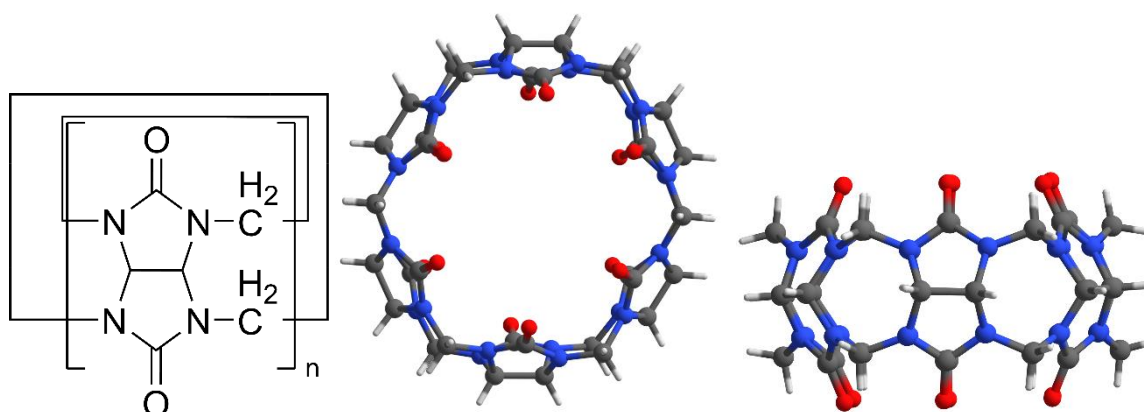


Figure 6. Chemical structure of Cucurbit[n]uril ($n > 4$), and top and side view from the x-ray crystal structure of cucurbit[6]uril.³¹

The size and volume of the cavity can be altered by expanding the number of glycoluril units to selectively tailor towards a specific guest. So, for cucurbit[5]uril, the cavity is too small to accommodate even the smallest alkyl or aromatic organic molecules, however this limited pore volume allows for effective gas adsorption for a wide range of gaseous molecules.³² Cucurbit[6]uril however, shows the strongest and most efficient host-guest complexes with aliphatic amines, allowing for the macrocycle to be used effectively in rotaxanes and molecular machines.³³ Cucurbit[7]uril, has a much

wider range of possible guests due to its larger size, so is able to bind aryl molecules and simple organometallics such as ferrocene and cobaltocene.³⁴ The larger cucurbit[*n*]urils with > 8 glycouril units can form complexes with even larger guests, this also includes multiple fully encapsulated guests, and other macrocycles forming so called ‘macrocycle within macrocycle’ complexes (*table 1*).^{35,36} The large variation in possible guests, and their high binding associations with cationic guests have made cucurbit[*n*]urils attractive options for the synthesis of molecular machines.

Properties	CB[5]	CB[6]	CB[7]	CB[8]	CB[10]	α-CD	β-CD	γ-CD
Cavity Diameter	4.4	5.8	7.3	8.8	11.3 - 12.4	4.7 - 5.3	6.0 - 6.5	7.5 - 8.3
Cavity Volume	82	164	279	479	870	174	262	427
Outer Diameter	13.1	14.4	16.0	17.5	20.0	14.6	15.4	17.5

Table 1. Table comparing the structural properties of cucurbit[*n*]urils (CB[*n*]) and cyclodextrins (x-CD). All data in Å and retrieved from *Barrow et al*, and *Valle et al*.^{35,37}

1.1.7. Other Macrocycles

As well as the main families of macrocycles previously mentioned, there are other examples of macrocycles with a smaller depth in structural variation (*figure 7*). Paraquat containing macrocycles were developed by *Stoddart et al*, and the cationic nature of the macrocycle allows for the trapping of electron-rich guests.³⁸ This affinity towards electron-rich guests, is contrary to that of most other macrocycles, which has propelled pyridinium based macrocycles in catenane synthesis, where two macrocycles are interlocked together.³⁹

There are several other macrocycles that also favour electron rich guests, for example the imidazolium based tetracationic ‘texas-sized box’, and the ‘cyano star’, with its hydrogen bonding cavity amplified by electron-withdrawing nitrile groups around the

rim.^{40,41} Cyclic phenylenes, are a rare example of an exclusively hydrocarbon based macrocycle, and aside from possible host-guest applications, have posed as potential precursors in alternative lower temperature carbon nanotube syntheses.⁴²

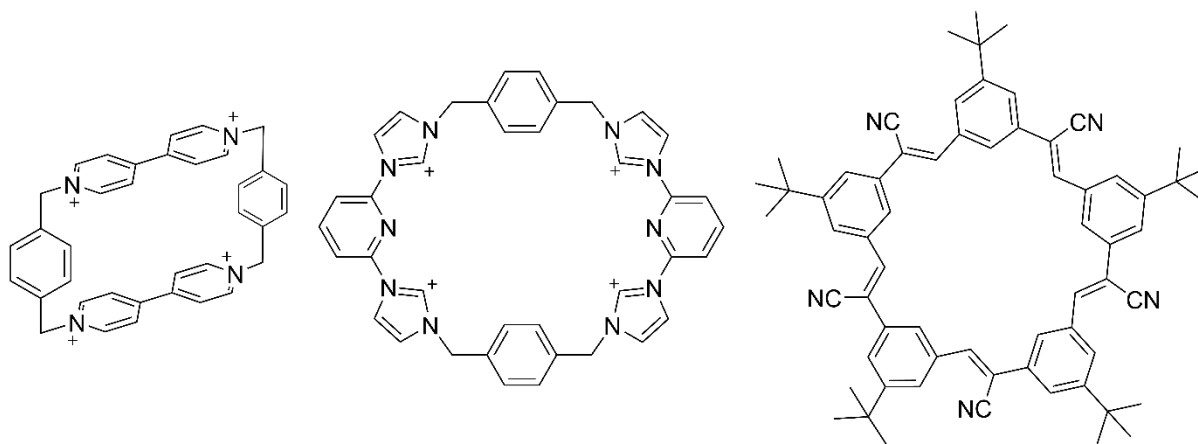


Figure 7. Chemical structures of cyclobis(paraquat-p-phenylene) 'blue-box', cyclo[2](2,6-di(1H-imidazol-1-yl)pyridine)[2](1,4-dimethylenebenzene) 'Texas-sized box', and penta-t-butylpentacyanopentabenzene[25]annulene 'cyanostar'.^{38,40,41}

1.2. Pillar[*n*]arenes

Pillar[*n*]arenes were first reported by *Ogoshi* in 2008, and since then a plethora of papers on the synthesis and applications of pillar[*n*]arene have been published, including a number of reviews on the macrocycle.^{43–50} The extensive use of pillar[*n*]arene, can be largely attributed to its ease of synthesis, high yield, and high degree of functionalisation. Pillar[*n*]arenes are stable macrocycles, consisting of hydroquinone subunit moieties, linked in the *para* position by methylene bridges. The composition and syntheses of pillar[*n*]arenes is like the aforementioned calixarene, however, the shape of the pillar[*n*]arene is a symmetrical, columnar structure, compared to the calixarene's basket architecture. This shape deviation, is due to the *para* linking of the subunits, compared to the *ortho* linking in the calixarene.⁵¹

1.2.1. Nomenclature of Pillar[*n*]arenes

To better understand pillar[*n*]arenes, the naming rules when discussing the macrocycle are important, not just to analyse the molecule as a whole, but also to help identify individual derivatives. *Pillar* refers to the shape of the macrocycle, which as previously stated is a highly symmetric columnar structure, with a well-defined cavity. The *arene* refers to the subunits of which pillar[*n*]arene is synthesised from, which are all based on aromatic hydrocarbons. The [*n*] refers to the number of subunits within the pillar[*n*]arene, this can also be expanded to [*n+m*] if there is more than one subunit within the pillar[*n*]arene. These copillar[*n+m*]arenes, where there are multiple subunits, have a generalised naming rule where the simplest subunit is labelled as [*n*], and therefore the further functionalised subunit is [*m*]. Functionalisation of the pillar[*n*]arene subunits is most often stated as a prefix, for example dipropoxypillar[*n*]arene, refers to pillar[*n*]arene with two propoxy groups attached in the 1- and 4- positions of the aryl subunits.

1.2.2. Mechanism of Pillar[5]arene Formation

The synthesis of pillar[*n*]arenes occurs *via* a controlled condensation polymerisation, akin to the synthesis of cucurbit[*n*]urils and calix[*n*]arenes. When compared to calix[*n*]arenes however, there is a major discrepancy in how macrocyclization is controlled. For calix[*n*]arenes the alcohol on the phenol directs electron density to the 2- and 6- positions of the aryl ring, thus ensuring that each subunit is linked in the same positions. However, with pillar[*n*]arenes which are mainly synthesised from 1,4-alkoxybenzenes, these electronic effects do not occur due to the unsubstituted positions on the ring being equivalent. The formation of pillar[*n*]arenes is instead controlled by sterics (*figure 8*). When a monomer unit and paraformaldehyde initially react, there are three carbons which could logically be the subsequent reaction target:

the adjacent carbon, or the *meta*- and *para*- carbons on the opposite side of the ring. The *ortho*- carbon is sterically hindered due to the newly substituted methanol group and adjacent alkoxy group. The *meta*- position is also sterically hindered; the addition of the methanol group forces the alkyl chain on the adjacent alkoxy group to face towards the *meta*- carbon. Therefore, directing further formaldehyde reaction to exclusively the *para*- position.

Efficient macrocycle synthesis *via* condensation relies on consistent reaction sites, but also there needs to be a kinetic or thermodynamic driving force to avoid polymerisation of the monomer units. Kinetic control of macrocycle synthesis involves careful tailoring of reaction conditions to ensure single product formation, and often require an additional substrate or reagent to stabilise the transition state of the desired product. This is due to kinetically controlled reactions involving the formation of irreversible covalent bonds. However, when the mechanism of pillar[5]arene was studied, it was found to proceed *via* a series of Friedel-Crafts alkylation reactions, and the reversible nature of the formed bonds allowed for thermodynamic control of the products.⁵² Solvent also assists in acting as a template for the macrocycle formation. It was noted that for small linear chlorinated solvents; dichloromethane (DCM) and 1,2-dichloroethane (DCE), yields of 81 % could be reached, however when bulkier 'branched' solvents such as chloroform and 1,1,2,2-tetrachloroethane (TCE) were used yields decreased to 15 % and 7 % respectively.⁵³ Additionally, when crystal structures of pillar[5]arene with chlorinated guests were examined, DCM formed a series of non-covalent interactions with the macrocycle cavity; CH/ π hydrogen bonds and Cl/ π halogen bonds.

1.2.3. Synthesis of Pillar[5]arene

There are several possible routes for the synthesis of pillar[5]arene and pillar[5]arene derivatives, but there are four essential components for macrocyclization to be achieved efficiently (*figure 8*). The essential reagents of this synthesis are, a 1,4-dialkoxybenzene derivative, a halogenated solvent, a Lewis acid and a formaldehyde forming species; most commonly paraformaldehyde, but 1,3,5-trioxane has been used in substitute.⁵⁴ The choice in Lewis acid is varied; initially boron trifluoride diethyl dietherate was used as the catalyst, but metal based Lewis acids, for instance; iron (III) chloride, zinc (II) chloride and aluminium (III) chloride have been implemented, and have seen success, especially in co-pillar[n+m]arene synthesis.^{43,52,55} A multitude of organic and mineral acids have also been trialled, with varying success; organic acids such as trifluoroacetic acid and sulfonic acid produced high yielding pillar[n]arene in ambient conditions, conversely acetic acid and mineral acids; hydrochloric acid and sulfuric acid, have been shown to be unsuccessful.^{53,56,57}

Pre-organisation is also possible in the synthesis of pillar[5]arenes; where an addition of substituent 'arms' in the 2 and 5 positions of the subunit dictate orientation of pillar[5]arene formation. This has also been displayed as a viable route to both unfunctionalized pillar[n]arene, and more complicated specifically ordered pillar[n]arene derivatives.

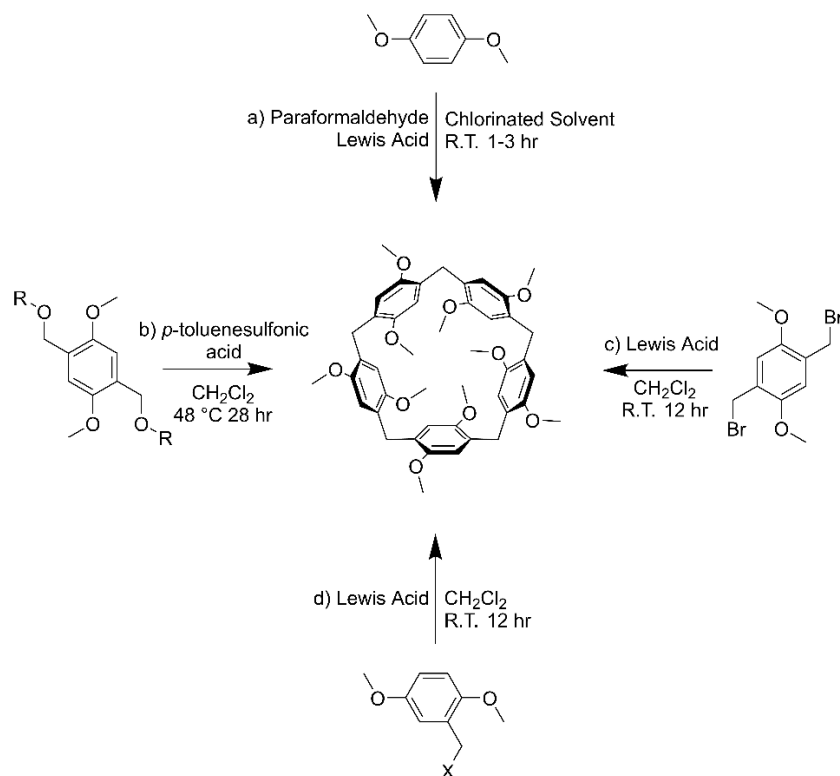


Figure 8. Schematic of various synthetic routes for dimethoxypillar[5]arene

Synthetic Route	Acid	Solvent	Time (hours)	Yield (%)	Ref
A	FeCl ₃	CH ₂ Cl ₂	3	59	55
A	BF ₃ .OEt ₂	CICH ₂ CH ₂ Cl	0.5	71	43
A	TFA	CICH ₂ CH ₂ Cl	2.5	81	53
A	<i>p</i> -TsOH	CH ₂ Cl ₂	50	66	57
B, R=Bn	<i>p</i> -TsOH	CH ₂ Cl ₂	2	75	58
B, R=nBu	<i>p</i> -TsOH	CH ₂ Cl ₂	24	75	58
B, R=Et	<i>p</i> -TsOH	CH ₂ Cl ₂	3-4	89	58
B, R'=Me	<i>p</i> -TsOH	CH ₂ Cl ₂	3-4	92	58
B, R'=H	<i>p</i> -TsOH	CH ₂ Cl ₂	4-5	84	58
C	AlCl ₃	CH ₂ Cl ₂	12	61	52
C	ZnCl ₂	CH ₂ Cl ₂	12	55	52
C	FeCl ₃	CH ₂ Cl ₂	12	63	52
D	AlCl ₃	CH ₂ Cl ₂	12	71	52
D	ZnCl ₂	CH ₂ Cl ₂	12	49	52
D	FeCl ₃	CH ₂ Cl ₂	12	39	52

Table 2. Relative yields of pillar[5]arene synthesis for the methods described in *figure 9* using a variety of acids.

1.2.4. Synthesis of Pillar[>5]arenes

Pillar[5]arene was shown to be the most favourable thermodynamic product of the macrocyclization of 1,4-alkoxybenzene, due to in part its bond angles which are the closest to that of the ideal sp³ hybridized carbon – carbon bond.⁵² Nonetheless, larger pillar[*n*]arenes are possible, with the largest isolated pillar[*n*]arene having 13 subunits.⁵⁹ To access these larger macrocycles modifications to the synthetic procedure, have to be made. For pillar[6]arene, either a kinetic or thermodynamic approach can be used, with solvent being the key factor in selecting larger pillar[*n*]arenes. When chloroform is used as the solvent, the cyclization is carried out under partial-kinetic control, this is due to chloroform not acting as a template for either pillar[5]arene or pillar[6]arene. This is in contrast to DCM and DCE which thermodynamically stabilise the pentamer. The deviation from the ‘linear’ chlorinated solvents, results in an almost equal percentage of both macrocycles being synthesised in chloroform (*table 3*).^{60,61} Conversely, when chlorocyclohexane (Cl-CyC6) is used as the solvent, the reaction proceeds *via* thermodynamic control, with the larger cyclohexyl solvent templating the formation of the hexamer, increasing the yield of pillar[6]arene to 87 % (pillar[5]arene 3 % yield).⁶⁰ Equally, choline chloride was shown to be a capable additive to increase the selectivity towards pillar[6]arene, when used in conjunction with iron (III) chloride and DCM as the solvent.⁶² Pillar[*n*]arene’s with more than 6 subunits can be synthesised and isolated, however as of yet, no templating solvent which enables thermodynamic control has been reported, so chloroform is used, and larger pillar[*n*]arenes are only isolated as minor products. Furthermore, to increase the relatively low yields of pillar[>6]arenes, the reaction time is reduced to only 20 minutes, further showing the kinetic control in this reaction.⁶³

Solvent	Lewis Acid	n = 5	n = 6	ref
CHCl ₃	FeCl ₃	30 %	34 %	61
CHCl ₃	BF ₃ OEt ₂	20 %	15 %	63
CH ₂ Cl ₂	FeCl ₃ /Choline Chloride	35 %	53 %	62
Cl-CyC6	BF ₃ OEt ₂	3 %	87 %	60

Table 3. Relative yields of diethoxypillar[5]arene and diethoxypillar[6]arene in several solvents and Lewis acids.

1.2.5. Pillar[*n*]arenes; structural properties.

1.2.5.1. Pillar[*n*]arene Cavity Dimensions

Pillar[5]arene is the smallest synthetically available pillar[*n*]arene, and as previously discussed is the major product when DCM is used as the solvent. *Ogoshi et al* reported the cavity size of pillar[5]arene to be 5 Å, which is similar to that of other macrocycles such as α-cyclodextrin (*ca* 4.7 Å) and cucurbit[6]uril (*ca* 5.8 Å).⁶⁴ The cavity size of the next largest pillar[*n*]arene; pillar[6]arene, was reported to be 7.5 Å, similar to cucurbit[7]uril (*ca* 7.3 Å) and β-cyclodextrin (*ca* 6.0 Å).⁶⁴ Pillar[7]arene is the last strictly symmetrical pillar[*n*]arene, after which deformations occur. The cavity size of the 7 membered pillar[*n*]arene is approximately 7.3 Å, and again is similar to the next largest cucurbituril and cyclodextrin (8.8 Å and 7.5 Å respectively).⁶⁵ Pillar[*n*]arenes with more subunits than 7 form structures with multiple cavities, due to an inward bend in the centre of the macrocycle, formed to alleviate ring strain. 8, 9 and 10 pillar[*n*]arenes all have two cavities, comprised of two pentagons, one hexagon and one pentagon, and two pentagons respectively (*figure 9*). The two cavities in the larger pillar[*n*]arenes, are approximately equal to the geometrically related smaller pillar[*n*]arenes.⁶³ Larger pillar[*n*]arenes (11-15) have been reported, and their synthesis is performed *via* a ring expansion of pillar[5]arene.⁵⁹ The pillar[8-10]arenes obtained with this method do not display the same inward contortion as the previously mentioned example, with cavities

of 8.2, 9.3 and 10.5 Å respectively. Pillar[*n*]arenes 11-14 synthesised with this method have cavity sizes of 11.6, 12.7, 13.8 and 14.9 Å respectively.⁵⁹

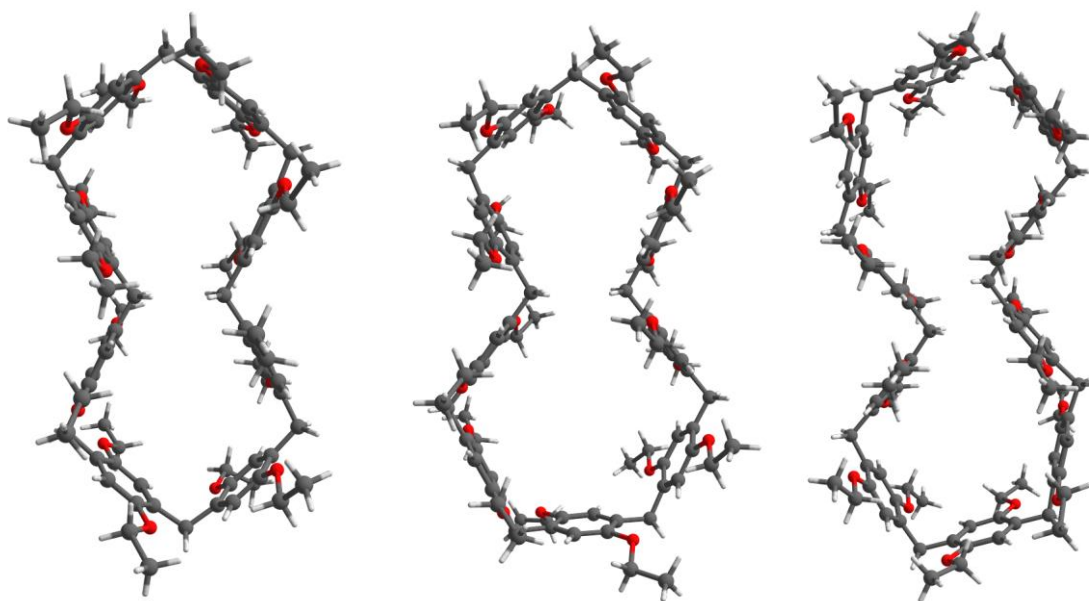


Figure 9. Left to right : crystal structures of diethoxypillar[8], [9], and [10]arene.⁶³

1.2.5.2. Conformation and Planar Chirality

To assess the conformational mobility of pillar[5]arene it is first important to place it within context to other macrocycles. Rigid macrocycles, for example cucurbiturils, which possess double methylene bridges are conformationally fixed. In contrast, calix[4]arenes are defined as conformationally flexible with the ability to form four distinct conformers: cone, partial cone, 1,2-alternate and 1,3-alternate.⁶⁶ Pillar[5]arene aligns with the former, due to the ability of the subunits to rotate 180° through *annulus*, having four diastereoisomers as well as four corresponding enantiomers. Stereoisomer **a/a'** has all monomer units facing the same direction so has C_5 symmetry, whereas **b/b'**, **c/c'** and **d/d'** have C_2 symmetry (Figure 11). For dialkoxypillar[5]arenes, the **a/a'** conformer is the most stable structure, due to the avoidance of steric hindrance between alkyl chains. However, with per-

hydroxypillar[5]arene **d/d'** was shown to be the most stable, due to the hydroquinone's ability to form intramolecular hydrogen bonds with neighbouring subunits.⁶⁷ Efforts to limit the rotation of the subunits within pillar[5]arene, and therefore inhibit the interconversion between isomers have been made. Firstly, it was noted that as alkyl chain lengths of the alkoxy benzenes was increased, the energy barrier of rotation was proportionately increased.⁶⁸ However, it was not until the incorporation of bulkier cyclohexylmethyl groups where rotation was halted.⁶⁹ This control of planar chirality was also demonstrated with the incorporation of chiral guests.⁷⁰

Pillar[6]arene has five diastereoisomers with five analogous enantiomers, and also has three *meso* forms, equalling thirteen distinct conformers. Diastereoisomers **a/a'**, **b/b'**, **c/c'**, **d/d'** and **e/e'** have C_6 , C_1 , C_2 , C_2 , and D_2 assigned symmetries respectively. Equally, the *meso* forms (**e**, **f** and **g**) are assigned with the symmetry labels; C_s , C_{3v} and C_{2h} respectively (*figure 10*). Contrary to perhydroxypillar[5]arene, perhydroxypillar[6]arene can form a continuous, alternating, 'up-down' hydrogen bonded network due to its even number of subunits, thereby making **g** the most stable conformer (*figure 10*). The same methods of rotation inhibition documented for pillar[5]arene, have been unsuccessful when transferred directly to pillar[6]arene. With the larger cavity of pillar[6]arene being cited as the rationale for the cyclohexyl groups inability to halt rotation.⁷¹

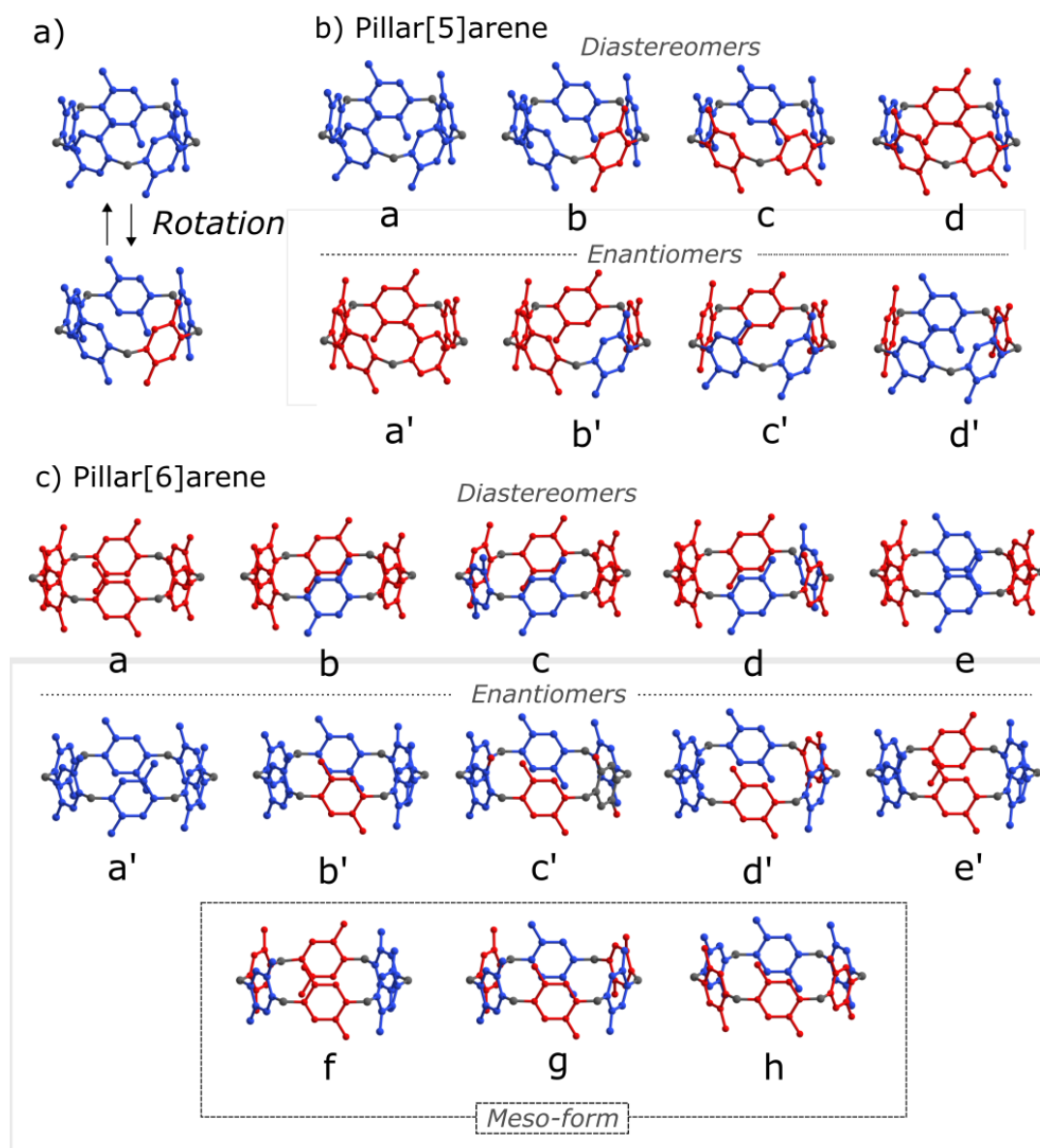


Figure 10. (a) the rotational mode of the subunits in pillar[*n*]arenes. (b) conformers of pillar[5]arene. (c) conformers of pillar[6]arene. Adapted from *Ogoshi et al.*⁷²

1.2.5.3. Pillar[*n*]arene, Intermolecular Assemblies

Due to the structure of pillar[*n*]arene being highly symmetrical, the assembled structures of pillar[*n*]arene found crystallographically, should show a high degree of order. Indeed, when X-ray structures of pillar[*n*]arenes are examined, they can form one of three discrete assemblies. As to which of the assemblies' forms is dependent on a myriad of factors; substituents on the pillar[*n*]arene, number of subunits and

conditions in which the crystal was grown. The three assemblies can be categorised as herringbone, 1D channels, and slipped stacking, and are similar to assemblies formed by other macrocycles. A herringbone structure is when the pillar[*n*]arenes are arranged perpendicular to each other, with the cavity of one pillar[5]arene facing the edge of its neighbour. 1D channels are, as the name suggests, layers of 1D arrays of pillar[*n*]arenes with the cavities all facing the same direction. Finally, slipped stacking is similar to 1D channels, except the cavities of each layer do not overlap, and it's the rims which overlap, normally due to intermolecular interactions between rim substituents.

An example of how solvent conditions affect assembly is, in the case of diethoxypillar[5]arene, where recrystallisation from acetone yields 1D channels but slow evaporation of hexane into chloroform yields a herringbone structure.⁷³ Equally, in regards to substituents; when the alkyl groups are removed, the perhydroxypillar[5]arene yields a slipped stacking structure due to intermolecular hydrogen bonding between phenolic groups.⁵¹

1.2.6. Functionalisation of Pillar[*n*]arenes

The sheer variation in functionalised pillar[*n*]arenes that have been reported, is a testament to one of the largest advantages of the macrocycle, the ease of modification. Functionalisation of pillar[*n*]arenes most commonly involves adding substituents on the rims of the macrocycle, and such substituents can affect the physical properties. Solubility, conformation, host-guest properties, and reactivity can all be affected, and tailored by adding or removing components of the pillar[*n*]arene, and therefore have become a recurring feature in pillar[*n*]arene based research. It's important to note that due to the relative ease of synthesis and high yields, pillar[5]arene has garnered the most attention in the pursuit of new functionalisation possibilities. But equally, as

pillar[6]arene research has progressed there has been more examples of the hexamer being modified. To better understand the parameters of functionalisation, it is important to split functionalised pillar[*n*]arenes into two distinct categories, based on the approaches to synthesising these homologues. Firstly, an exchange or deprotection approach; where the alkyl chains are removed from the rim, and etherification can be subsequently performed to implement a new functional group. Secondly, a 'pre-macrocyclization' approach; where modified subunits are synthesised and then reacted together in an analogous manner to unsubstituted pillar[*n*]arene to form the fully rim-substituted pillar[5]arene. Alternatively, the modified subunit can be reacted alongside a 1,4-dialkoxybenzene subunit, to form a 'copillar[*n*]arene'.

1.2.7. Deprotection of Pillar[*n*]arenes

Deprotection or exchange formation, was one of the first routes to pillar[*n*]arene functionalisation, deprotection specifically refers to the removal of the alkyl groups from the rims of the macrocycle to form a reactive phenolic intermediate. The deprotection step is usually performed with boron tribromide and pillar[*n*]arenes containing alkoxy subunits, but hydrogenation of a benzyloxy containing pillar[*n*]arenes can also form the reactive phenolic derivatives (*figure 11*).^{43,74} Optimisation of the deprotection reaction, has increased yields and lowered reaction times, but the issue of inseparable isomers, when > *mono-deprotection* is performed, limits the potential of *deprotection* as a route to selective functionalisation. To try and circumvent this issue, *Han et al* firstly established that deprotection occurs in a stepwise manner at lower temperatures under kinetic control, and therefore by manipulating the reaction temperature the relative isomers can be controlled.⁷⁵ Equally, the isomers of the hydroxypillar[5]arenes could be separated *via* the

replacement of the deprotected hydroxyls with triflate groups. Equally, an oxidation/reduction method can be used to target specific subunits within the pillar[5]arene structure. A benzoquinone unit, can be produced within the pillar[5]arene structure, with an oxidant (most commonly cerium ammonium nitrate), then reduction with, for example, sodium borohydride, obtains a phenolic monomer unit.^{76,77} Alternatively, in the pursuit of creating rim-differentiated pillar[5]arenes *Drouhard et al*, implemented an asymmetric subunit, with a methoxy benzene, and a benzyloxy group in the *para*-position.^{78,79} This subunit pre-oriented the pillar[5]arene formation so that two distinct rims will be formed, one with a methoxy group, and one with the benzyloxy group. The benzyloxy group could be removed *via* hydrogenation, and then a series of further reactions could be performed to successfully assemble a series of rim-differentiated or *tiara*-pillar[5]arenes.

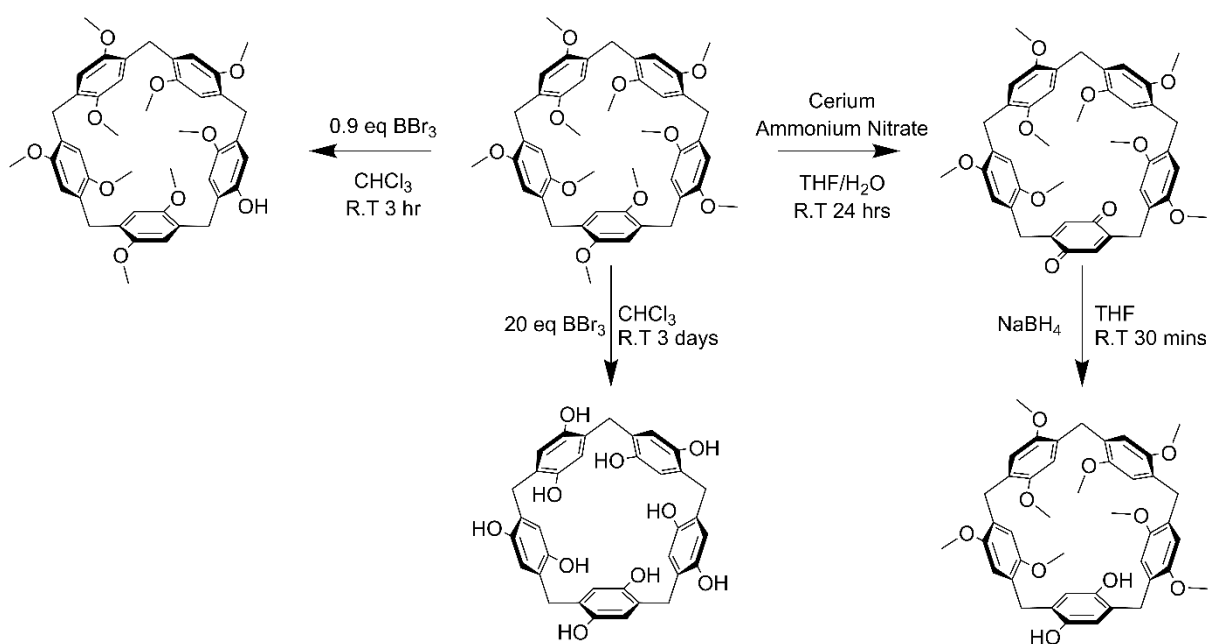


Figure 11. Routes to forming deprotected phenolic pillar[5]arenes using either boron tribromide or oxidation/reduction.^{51,80,81}

1.2.8. Cocyclisation and Pre-macrocyclization Functionalisation

Functionalised pillar[*n*]arenes can also be synthesised prior to the macrocyclization step. Following similar principles to conventional pillar[5]arene synthesis, synthesising modified pillar[5]arenes requires a subunit, a Lewis acid and paraformaldehyde in a chlorinated solvent. There are however prerequisites for the monomer subunit to ensure successful macrocyclization and pillar[5]arene formation. The intrinsic properties necessary are not fully understood, but there are several suggestions to predict whether a subunit is appropriate. Firstly, the reactive 2,5- positions on the benzene ring cannot be significantly sterically hindered, and equally, strongly deactivating groups, for example nitro or cyano groups will inhibit macrocyclization. Additionally, groups which disturb solubility in halogenated solvents, or react with the Lewis acid are inappropriate choices.⁷² Consequently, the most common examples of 'non-alkoxy' subunits, are in fact still alkoxy based. Alkoxy groups with differing terminal functional groups have been demonstrated to form pillar[5]arenes, that of which includes, bromides, alkynes and esters.^{82–84} Manipulations of this nature, could be expanded by having two or more different subunits, which leads to mono-, di- and tetra- functionalised pillar[*n*]arenes.^{55,85}

The pre-cyclisation method of functionalisation is therefore useful, but also limited as to what groups can be incorporated *via* this method. However, due to pillar[5]arenes structural and chemical stability, a high degree of further reactions can be performed on the previously mentioned modified pillar[5]arenes. For the alkyl bromide pillar[5]arenes this includes catenation with pyridines, amines, imidazoles, and phosphines, leading to water soluble pillar[5]arenes.^{86–90} Williamson ether syntheses are also possible with alkyl bromide pillar[5]arenes, leading to a large variety of functionalised macrocycles. Equally, azide-alkyne click reactions are possible, either

with the alkyne pillar[5]arene, or by reacting the bromide pillar[5]arene with sodium azide to synthesis an azide adorned pillar[5]arene.^{82,91,92}

1.2.9. Other Methods of Functionalisation

Aside from the rim functionalisation methods previously discussed, there are two other possible positions in the pillar[*n*]arene capable of functionalisation. Lateral functionalisation, or methylene-bridge-substitution, refers to the addition of a functional group onto the methylene bridges between subunits. As of yet, this has only been achieved by bromination with N-bromosuccinimide, but it does provide a platform for further routes of functionalisation.⁹³ Equally, lateral functionalisation allows new secondary structures to be accessed, for example with the bromine laterally-functionalised pillar[5]arene being able to form covalently bonded 2D polymers when reacted with a diamine linker.⁹⁴

Ortho-functionalisation is the other possible route for pillar[*n*]arene functionalisation (*figure 12*). Due to the steric hindrance of the alkoxy groups, direct addition of functional groups has not yet been achieved, however by utilising rearrangement reactions *ortho*-substitution has been realised. Initially, *Bojtár et al* reacted a *mono*-deprotected pillar[5]arene with 3-bromo-1-propene *via* a Williamson ether synthesis, a subsequent Claisen rearrangement yielded a *ortho*-functionalised propenyl pillar[5]arene.⁹⁵ The depth of possible functionalisation was expanded by *Wang et al*, who also utilised a rearrangement reaction. The initial pillar[5]arene was converted to a pillar[4+1]quinone with cerium ammonium nitrate, a series of Grignard reagents were then reacted with the macrocycle affording pillar[5]arenes with *para*-substituted quinols. A dienone-phenol rearrangement reaction could then be achieved using HCl, providing the aforementioned *ortho*-functionalised pillar[5]arenes.⁹⁶

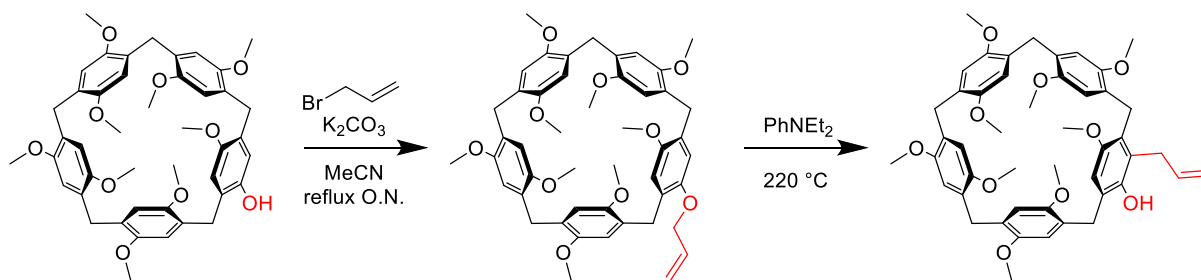


Figure 12. *Bojtár et al*, method for the synthesis of *ortho*-functionalised pillar[5]arenes.

1.3. Host-Guest Properties of Pillar[*n*]arenes

Arguably, the most important property of a macrocycle is its ability to form strong intermolecular interactions with other molecules. From ribosomal binding in antibiotic macrocycles such as erythromycin and clarithromycin, to switchable binding in molecular machines, studying and utilising macrocycle complexations is essential in a myriad of disciplines.

1.3.1. Host-Guest Chemistry, a Brief History

'*Host-guest*' interactions would not be popularised as a named concept to supramolecular chemistry until the late 60s with works by Dietrich, Sauvage, Pederson, Cram and Lehn.^{18,97–99} However, it could be argued the concept itself dates further back, composed of a conglomeration of theories from several scientific fields. The notion of intermolecular forces; that is attractive or repulsive interactions between molecules that are not covalently linked, could be dated as far back as Empedocles in 450 B.C. Empedocles explored such attractive and repulsive forces and defined what we would later call magnetism and electrostatic interactions. Such rudimentary and reductive notions of intermolecular interactions would form the basis of our scientific understanding for the next 2000 years. It would not be until the 1500s where the move from metaphysics into experimental science, which would see the likes of Bacon, Galileo, Boyle and Newton expand physical chemistry, introducing terms like *energy*

and *force*.¹⁰⁰ Arguably the greatest contribution to the notion of intermolecular forces arose from the works of van der Waals, who attributed the deviation of the ideal gas law in real gases to intermolecular interactions. From that initial notion, was developed the notions of hydrogen bonding by Latimer and Rodebush in 1920, dipole-dipole interactions in 1921 by Keesom, and dispersion forces by *London* in 1930.^{101–103} These key forces, would later become the framework in how host-guest chemistry is defined and explained.

Parallel to the previously described physical forces, was a biological description of how enzymes and substrates interact. In 1894 *Fischer* published 'Effect of Configuration on the Activity of Enzymes'¹⁰⁴ which contained the comparison of the enzyme substrate interaction to a 'lock and key,' and stated that the 'phenomenon itself is transferred from the biological to the chemical realm'. This not only introduced chemical theory into the molecular scale of biology, but also propelled the notion of molecular interactions away from merely forces, but also due to how complementary the geometries of each molecule are. This concept would be later expanded to include non-biological systems with *Cramer's* 'inclusion compounds' in 1954, and was to be later refined with *Henrich* in 1965 (*figure 13*).¹⁰⁵ With these principles of an ideal, complementary fit, supplemented with the theories and quantitative approaches of intermolecular forces, arose the unified field of supramolecular chemistry, and with it the understandings of the mechanics, importance and application potential of host-guest chemistry.

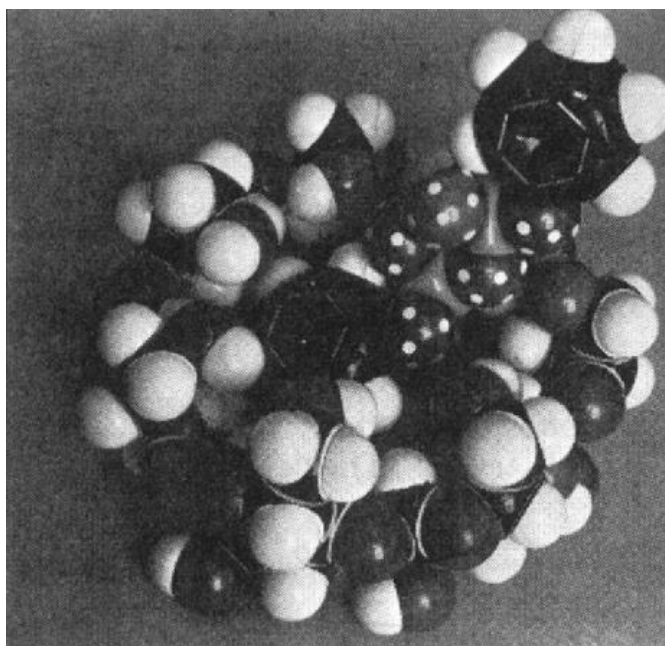


Figure 13. *Hennrich and Cramer's* model of their β -cyclodextrin/ diphenyl pyrophosphate 'inclusion compound'. Extracted from their 1965 paper: 'the catalysis of the fission of pyrophosphates by cyclodextrin. A model reaction for the mechanism of enzymes.'¹⁰⁵

1.3.2. Intermolecular Forces in Host-Guest Chemistry

As mentioned previously, a plethora of intermolecular forces can be contributory factors in host-guest chemistry and successful complexation. The possible non-covalent interactions can be broadly split into three categories; charged electrostatic interactions, van der Waals forces, and π -interactions. With large variations in bond strength, the type and extent of intermolecular interactions can cause large variations in binding association.

Charged electrostatic interactions are forces that arise when both components associate electrostatically through, at-least, partial charges. Coulombic forces between two oppositely charged species produce some of the strongest non-covalent bonds seen within host-guest systems. An example of such a system, utilised a macrocycle which was dicationic due to its two ammonium cations. Such a macrocycle was shown to not only form strong interactions with anionic guests, but could also

selectively bind to specific alkyl dianionic guests, depending on the alkyl chain length and their relative substituents (*figure 14*).¹⁰⁶

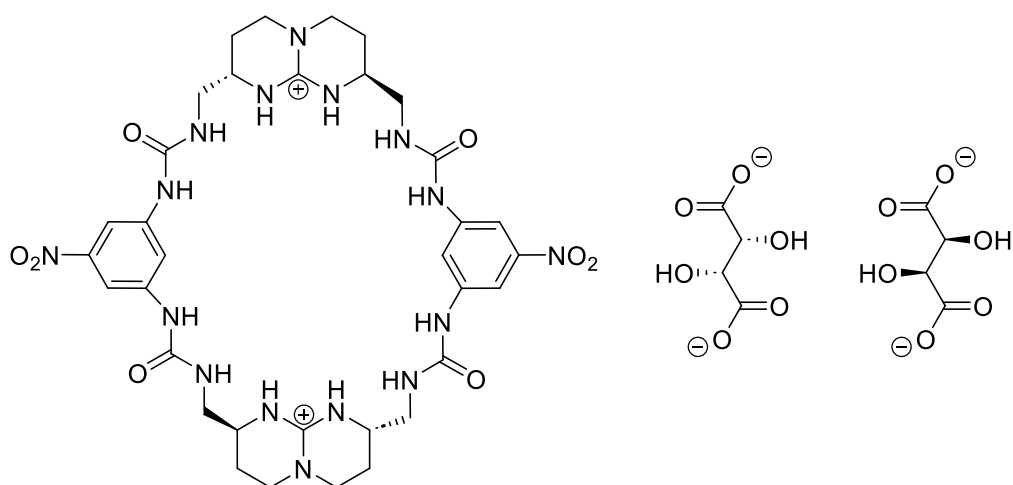


Figure 14. Example of a host-guest system with a dicationic macrocycle host, and two dianionic chiral guests.¹⁰⁶

Neutral macrocycles can also interact with cationic guests due to their electron dense cavities, for example cucurbiturils with viologens, or with crown ethers and alkaline earth metal cations.^{18,107} The former of which, is an example of a complex containing explicit charge transfer between guest and host as was made evident with UV/Vis spectroscopy. Equally, charged macrocycles such as cyclobis(paraquat-*p*-phenylene) can form complexes with neutral electron rich guests such as catechol and tetrathiafulvalene.^{108,109}

Van der Waals forces are interactions between two or more molecules that involve permanent or induced dipole-dipole interactions. Although considered a subset of electrostatic interactions, they are normally weaker than the aforementioned charged electrostatic interactions. The interaction between two molecules with permanent dipoles is often described as a dipole-dipole interaction or Keesom force. These forces are strongly associated with molecules containing electronegative atoms: oxygen,

nitrogen, fluorine etc. A common occurrence in macrocyclic host-guest systems, dipole-dipole interactions are a popular motif, especially with macrocycles which bare multiple hydroxyl or amino groups, for example cyclodextrins or azacrown ethers.^{110,111} London dispersion forces are weaker dipole-dipole forces where both dipoles are induced, this induction is caused by the temporary repulsion of electrons away from an adjacent molecule's electrons, forming two partial dipoles; one positive and one negative in charge. Such forces can be seen between molecules without electronegative heteroatoms, in for example alkanes and alkenes. Dispersion forces are generally too weak to form efficient host-guest complexes by themselves, but as the number of contact points increase, dispersion forces' contribution to binding becomes more important.

Lastly π -interactions, these non-covalent bonds are akin to other electrostatic interactions, but for π -interactions the electron-donor is the electron-rich π -system of most commonly, a benzene unit (*figure 14*). There are multiple moieties capable of forming intermolecular non-covalent bonds, those of which include electron accepting or cationic groups, and other π -systems. Cation- π interactions are generally regarded as one of the stronger intermolecular bonds, having similar binding strengths as hydrogen bonds.¹¹² Due to these strong bonds, and most macrocycles consisting of multiple connected arenes, the binding strengths of cations and aryl macrocycles are among the highest of all host-guest systems. Additionally, unlike other ion-quadrupole interactions, the cation- π bond is less sensitive to directionality of the bond, therefore lowering the geometric constraints for host-guest bonding.¹¹³ In a similar manner, classic examples of hydrogen bond donors such as NH, OH and to a lesser extent CH are also capable of forming intermolecular bonds with π -systems (*table 4*). Comparing the interactions of different hydrogen bond donors and a model π -system (in this case

benzene) shows a large difference between heteroatoms, with OH/ π having double the bond energy of CH/ π (-3.02 and -1.45 kcal mol⁻¹ respectively).¹¹⁴ However, one of the most important features of the CH/ π bond is that is cooperative in nature, indicating, that multiple CH's can interact with a single π -electron system. Ergo, the larger the CH system is, the stronger the intermolecular bond energy will be, as is evidenced when cyclooctane was shown to have triple the bond energy of methane when interacting with benzene.¹¹⁵

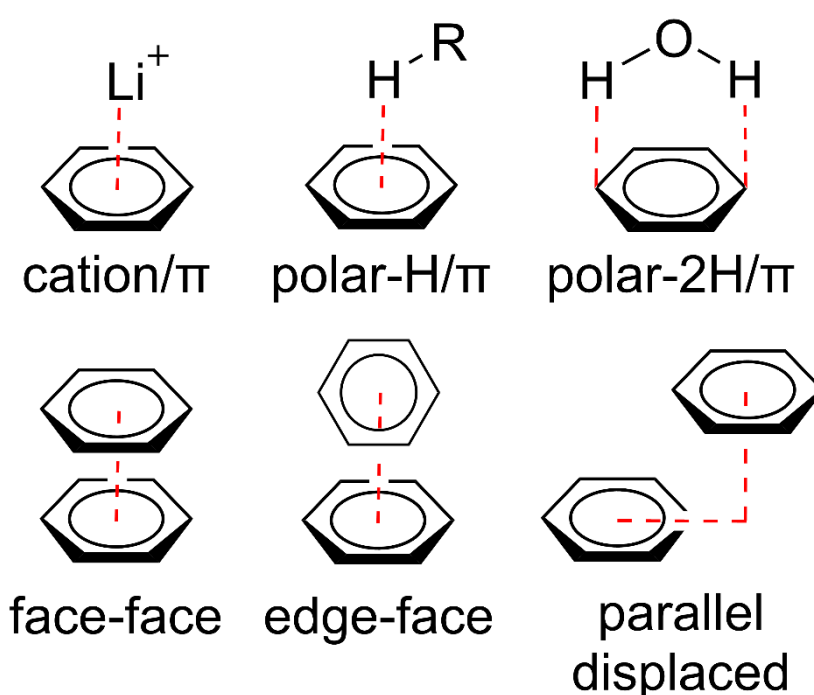


Figure 14. Several π -interactions

Aromatic systems will also interact with other neighbouring aromatic systems, to form π - π bonds. The criterion for such bonds is that the distance between π -systems must be between 4.5 - 7 Å, and the dihedral angle must be between 30° and 90°.¹¹⁶ The interactions between two aromatic rings has been observed in three orientations; face-face stacking, edge to face stacking and parallel displaced. The binding energies of a model benzene-benzene system were calculated using computational chemistry.¹¹⁷

The research detailed that the binding energies of the edge to face and parallel displaced are almost isoenergetic with respective binding energies of 2.7 and 2.8 kcal mol⁻¹. However, for the face-face interaction there is a lowering of binding energy to 1.8 kcal mol⁻¹, indicating the stability of aromatic-aromatic interactions are increased when the π -systems are not directly parallel from each other.

Electron Acceptor/Donor	Example	Interaction Energy (kcal mol ⁻¹)	ref
Cation/ π	Li+	-32.91	118
Cation/ π	NH ₄ ⁺	-14.12	118
Cation/ π	N(CH ₃) ₄	-6.34	118
CH/ π	CH ₄	-1.05	115
CH/ π	C ₂ H ₆	-1.76	115
CH/ π	C ₃ H ₈	-2.29	115
CH/ π	Cy-C ₅ H ₁₀	-3.02	115
CH/ π	Cy-C ₈ H ₁₆	-3.38	115
CH/ π	CH ₂ Cl ₂	-4.5	119
CH/ π	CHCl ₃	-5.6	119
OH/ π	H ₂ O	-3.02	120
NH/ π	NH ₃	-2.22	120

Table 4. Calculated interactions energies of a series of electron acceptors and benzene.

1.4. Host-Guest Chemistry of Pillar[5]arene

The myriad of complexes that have been documented for pillar[5]arene is vast and varying. With pillar[5]arene's π -electron rich aryl backbone, and its rims usually consisting of electron-donating hydroxyl/alkoxy groups, the cavity of pillar[5]arene is perfectly suited towards cations and other electrophilic guests.¹²¹ The possibilities, in reference to the intermolecular bonds detailed above are vast, allowing for a large variety of guest molecules. Additionally, by further modifying the pillar[5]arene macrocycle with functional groups, directionality and specificity can be introduced.

1.4.1 Assessing Pillar[n]arene Host-Guest Complexes

Before a discussion on the host-guest chemistry of pillar[n]arenes, it is important to note how the stability of potential formed complexes are assessed. By far the most widely used measurement for the binding association between host and guest is *via* titration experiments. Titrations are used to calculate and assess the binding constants for most host-guest systems, not only pillar[n]arenes. The instrumentation used to carry these titrations out depends on the molecules in question, however for pillar[n]arene the methods used are most commonly: nuclear magnetic resonance (NMR), ultraviolet-visible spectroscopy (UV/Vis), fluorescence spectroscopy (FL), and isothermal titration calorimetry (ITC). It is also important to note that UV/VIS and FL can only be used when complexation results in a significant colour or fluorescence change, which is mostly only seen in examples with charge transfer between host and guest.

The largest issue with such measurements, and more specifically making quantitative comparisons of pillar[5]arene complexes, is the effect solvent has on complexation. *Schönbeck* suggested that reducing complexation to only the attraction between host and guest oversimplifies the role solvent has in complex formation.¹²² Instead, three associations need to be accounted for: host-guest, host-solvent and guest-solvent. The accompanying study used computational model to detail how changes in the solvent, can cause deviations in the calculated binding constants. The findings report that non-polar solvents such as xylene and toluene promote host-guest binding, whereas polar solvents like acetone and acetonitrile hinder binding. There are multiple explanations for the origins of this solvent effect, but they can all be grouped into two contributions: guest/host-solvent interactions and complex-solvent interactions. So, if a solvent interacts favourable with the guest or host in their free state then the

equilibrium is pushed towards the un-complexed state, and *vice versa*. This can also be seen experimentally when a bis(imidazolium) guest was used with dihydroxypillar[5]arene. *Li et al*, reported that the binding constant between these two molecules could be increased when the polarity of the solvent was lowered, from $5.5 \times 10^4 \text{ M}^{-1}$ in DMSO, to $3.1 \times 10^3 \text{ M}^{-1}$ in 1:1 acetone:chloroform.¹²³ Equally, with a dinitrilealkane the binding constant decreased 10 fold with the introduction of DMSO.¹²⁴

Another widely used indicator of host-guest formation is upfield shifting in proton NMR. Not exclusive to only pillar[*n*]arenes, as a guest enters into the cavity of an aryl macrocycle the proton environments of the encapsulated guest will be shielded by the surrounding arenes.¹²⁵ This is observable *via* upfield shifting of the relative proton environments from the free guest to the complex (*figure 15*). The extent of which peaks are shifted can give a good estimate of enclosure geometry, however there are multiple factors affecting shielding. For example, proximity of the guest towards the arenes, proton environment being shielded, and again solvent. This will be explored in more detail with implications for pillar[*n*]arene complexes in chapter 2.

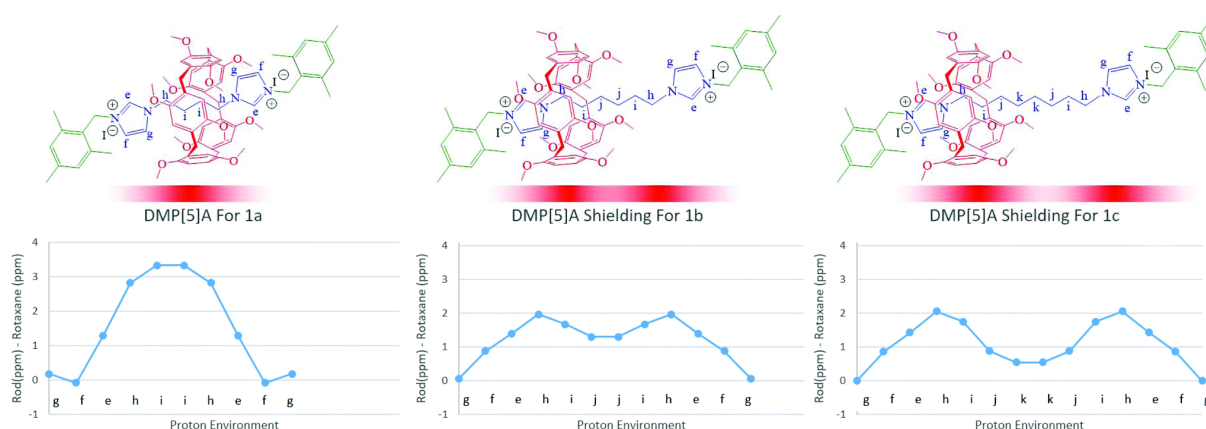


Figure 15. Example of upfield shifts being used to determine residency of a macrocycle upon a guest molecule. Reproduced with permission from *Langer et al.*¹²⁶

1.4.2. Pillar[*n*]arenes With Cationic Guests

Cation/ π intermolecular bonds are dominant within pillar[*n*]arene host-guest chemistry. As previously shown, in isolation, the intermolecular bonds formed between a cation and an electron rich system are among the strongest of the non-covalent bonds due to dominant electrostatic interactions. This effect is further amplified with the introduction of a macrocycle akin to the pillar[*n*]arene. Where its cavity of π -electron rich arenes introduces a space with multiple points of interaction with a cation.

1.4.2.1. Dialkoxypillar[5]arene With Cationic Guests

For alkoxy pillar[5]arenes the complexations formed with cationic guests are among the largest in binding energy. An issue, however, is the limited solubility of alkoxypillar[5]arenes; being only readily soluble in halogenated solvents and aryl solvents, paired with the general preference for more polar solvents for cationic species. Therefore, there are only a few select examples of cationic/alkoxypillar[5]arene complexes, with most having an alkyl ammonium guest. Alkyl ammonium guests are popular choices for alkoxypillar[5]arenes, this is in part due to their solubility in chloroform, the ease of synthesis, and the tunability of the alkyl substituents. However, minor changes to the guest can alter the binding, so for example, anion exchange from the weakly coordinating PF_6^- to the smaller, more strongly binding Cl^- inhibited host-guest complexation.¹²⁷ This was further extended by exchanging PF_6^- with the weaker coordinating BArF^- anion, wherein an increase from $(6.1 \pm 0.8) \times 10^4 \text{ M}^{-1}$ to $(3.4 \pm 0.4) \times 10^4 \text{ M}^{-1}$ in the binding constants is reported with BArF^- .¹²⁸ Not just the guest, but also the composition of the pillar[5]arene can enhance or decrease the binding association. An example of this was seen when the alkyl groups on the rims of the pillar[5]arene were altered to more or less sterically hindering groups. For pillar[5]arene with linear butyl substituents the binding constant with

octyltrimethyl ammonium hexafluorophosphate (OTMA) was $(4.1 \pm 0.4) \times 10^3 \text{ M}^{-1}$, whereas with a branched (S)-methylbutyl substituted pillar[5]arene there was a slight decrease to $1.3 \times 10^3 \text{ M}^{-1}$.^{70,85} The justification for this decrease, was that the steric hindrance around the rim of the pillar[5]arene would decrease the stability of the host-guest complex by 'attenuating the cationic/ π interactions'.⁷² This was further exacerbated by increasing the steric hindrance with the introduction of cyclohexylmethyl substituents, lowering the binding constant to $8.3 \times 10^2 \text{ M}^{-1}$.

1.4.2.2. Dihydroxypillar[5]arene With Cationic Guests

Dihydroxypillar[5]arene, where the alkoxy groups on pillar[5]arene's rim are deprotected and substituted with hydroxy groups, has altered solubility. Due to the hydroxyl groups on the rim, dihydroxypillar[5]arene favours more polar solvents, for example methanol, acetone, and dimethyl sulfoxide. This allows for a wider range of cationic guests to be introduced for the study of host-guest complexes. Pyridinium salts are capable of forming complexes with dihydroxypillar[5]arene, and some bipyridinium guests can form charge-transfer complexes with the hydroxyl containing macrocycle. In fact, the first reported pillar[5]arene paper, published by *Ogoshi et al* in 2008, showed this exact phenomenon, when dihydroxypillar[5]arene was mixed with bis(octyl)viologen, with a significant colour change being witnessed, cited as evidence for the formation of a charge transfer complex.⁴³ However, not all pyridinium guests will form these charge transfer complexes, as was shown evident by substituting viologens with bis(pyridiniums) where the two pyridinium units are connected with alkylene linkers.¹²⁹ The dihydroxypillar[5]arene/ viologen complex's in this research all showed the distinctive charge-transfer band at 460 nm when measured *via* UV/VIS spectroscopy, however the bis(pyridinium) complex's did not. This was theorised to be due to the pyridinium being a weaker electron-acceptor, when compared to viologen.

This study also varied the length of the alkyl linker in the bis(pyridinium) guests, from ethyl to hexyl. It was reported that the butyl derivative showed the most stable host-guest complex with dihydroxypillar[5]arene, indicating the four membered chain allows for the best fit for the size of the pillar[5]arene cavity.

1.4.2.3. Water-soluble Pillar[5]arenes with Cationic Guests

Water-soluble pillar[5]arenes are a relatively new class of pillar[5]arene derivatives, and although the range of substituents on the pillar[5]arene that allow for water solubility is vast, they all have commonalities. Nearly all the so far published water-soluble pillar[5]arenes contain one or more cationic or anionic substituents, with most utilising cationic ammonium moieties.^{130–135} Anionic pillar[5]arenes have also been demonstrated, using carboxylate or phosphonate groups.^{136–138} There are also sparing amounts of neutral water-soluble pillar[5]arenes, with all utilising ethylene oxide substituents to produce an amphiphilic pillar[5]arene.^{139,140} The possible guests available for water-soluble pillar[5]arenes is further expanded to now include, exclusively water soluble guests, that of which includes metal salts and multiply charged organic cations. Due to coulombic repulsions, cationic water-soluble pillar[5]arenes are inefficient at encapsulating cationic guest molecules, and instead have been utilised with anionic or electron-rich guests.^{89,131,141} However, for anionic pillar[5]arenes such as the carboxylate decorated pillar[5]arene, there is a sharp increase in binding energies. For example, with viologens a deca-substituted carboxylate pillar[5]arene was reported to have an association constant with paraquat of $8.2 \times 10^4 \text{ M}^{-1}$, 70 times more than that of perhydroxypillar[5]arene and bis(octyl)viologen.^{43,136} Equally, with a butyl linked bis(pyridinium) guest, the association constant rose from $4.5 \times 10^2 \text{ M}^{-1}$ in perhydroxypillar[5]arene to $1.1 \times 10^6 \text{ M}^{-1}$ with dicarboxylatopillar[5]arene (*figure 16*).^{129,142} This increase was attributed to the

multiple electrostatic interactions between the anionic carboxylate moieties on the rim of the pillar[5]arene and the cationic guest. Equally, for guests containing hydrophobic groups like the pyridinium guests detailed above, the hydrophobic cavity of pillar[5]arene will additionally push the equilibria towards encapsulation, as it provides an 'escape' for the guest away from the aqueous solvent medium.

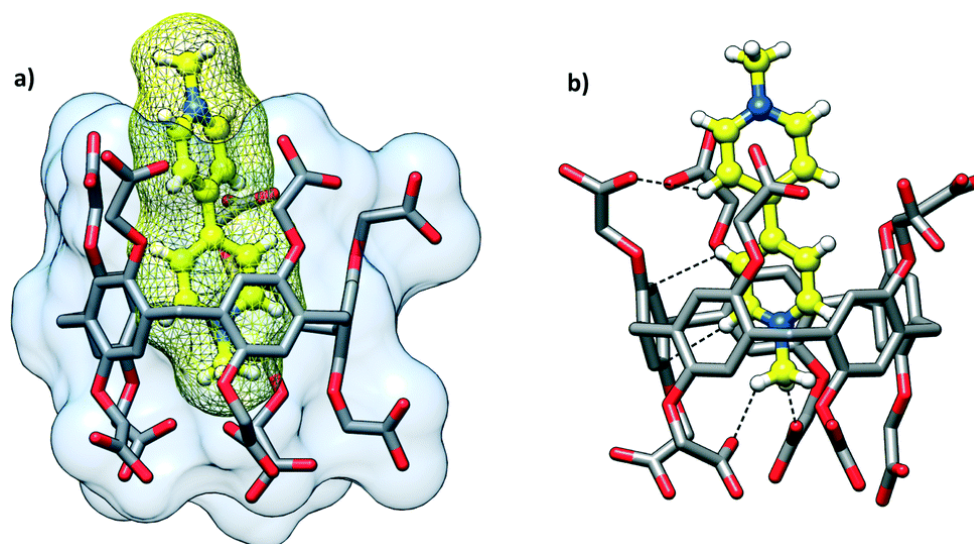


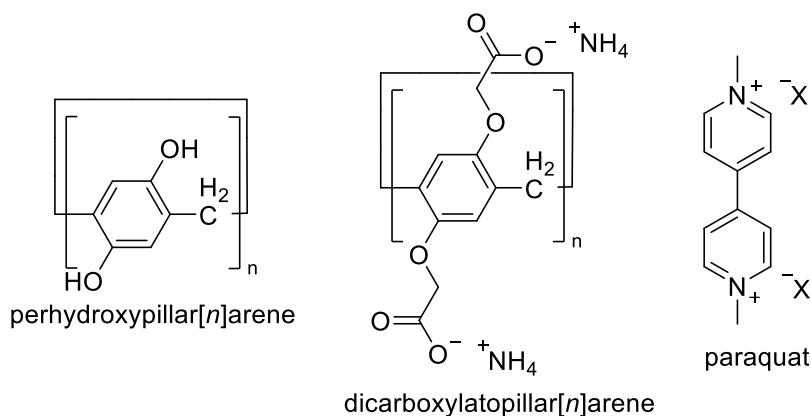
Figure 16. The inclusion complex between a paraquat guest and a dicarboxylatopillar[5]arene host. (a) inclusion mode. (b) CH/ π and CH/O interactions between guest and cavity. Reproduced with permission from Butkiewicz et al.¹⁴³

1.4.2.4. Larger Pillar[n]arenes with Cationic Guests

For pillar[n]arenes with more than 5 subunits, the cavities are also π -electron rich, with similar guest-binding preferences. However, the larger cavities do lend themselves to accommodate larger guests. For example, with a triethylammonium guest, diisobutoxypillar[5]arene was unable to form adequate host-guest interactions due to the bulky ethyl groups, diisobutoxypillar[6]arene however, was able to form a complex with said guest.¹⁴⁴ This selectivity towards the larger pillar[6]arene is also observed with other bulky groups, with adamantyl and 1,4-diazabicyclo[2.2.2]octane groups also shown to only be appropriate for larger pillar[n]arenes.^{128,145} However, the larger cavity of pillar[6]arene can also inhibit some intermolecular bonding when smaller guests are

introduced. An example of which uses OTMA as the guest, this linear ammonium guest had a binding constant with dimethoxypillar[6]arene half of that of the equivalent pentamer.⁶³ Conversely, whereas the previously mentioned isobutyloxy functionalised pillar[5]arene was too sterically hindered to form a complex with OTMA, the hexamer could form a 1:1 complex with said guest.¹⁴⁴ This specificity for cationic guests towards specific pillar[*n*]arenes is further established *via* use of a cationic tropylium guest. The 7-membered cationic ring was shown to be too large for the pillar[5]arene, but equally with pillar[7]arene insufficient intermolecular bonding resulted in no complexation being observed. However, when pillar[6]arene was used, a complex with a moderate $2.3 \times 10^2 \text{ M}^{-1}$ association constant was observed. Further highlighting how important geometric considerations are in the host-guest chemistry of pillar[*n*]arenes.

For anionic water-soluble pillar[*n*]arenes however, this size specificity is as stringent. For example when the carboxylate decorated pillar[6]arene is compared to its smaller derivative in paraquat complexation, there is a more than 100 times increase in association constant (*figure 17*).¹⁴⁶ Furthermore, as we increase the number of subunits to 7 there is a further increase in association constant to $2.96 \times 10^9 \text{ M}^{-1}$, and in fact, it is only with dicarboxylatopillar[9]arene where the binding constant decreases in value.^{147,148} Indicating, that for anion containing pillar[*n*]arenes the number of negatively charged atoms will dominate the strength of binding, up until the macrocycle becomes so large that cation/anion intermolecular bonds can not be efficiently formed.



Pillar[n]arene	Binding Constant (M^{-1})	Ref
Perhydroxypillar[5]arene	<i>a</i>	129
Perhydroxypillar[6]arene	2.2×10^2	149
Dicarboxylatopillar[5]arene	8.2×10^4	131
Dicarboxylatopillar[6]arene	1.02×10^8	146
Dicarboxylato[7]arene	2.96×10^9	147
Dicarboxylato[9]arene	2.27×10^6	148
Dicarboxylato[10]arene	1.25×10^7	150

Figure 17 and Table 5. Comparison of binding constants between paraquat and a series of pillar[n]arenes.

a. Value too small to be calculated

1.4.3. Pillar[n]arene With Neutral Guests

Nullifying the strong electrostatic interactions between a cation and the electron rich cavity of pillar[n]arene weakens the bonding behaviour between macrocycle and guest. However, neutral guests can still form complexes with pillar[n]arene, with multiple hydrogen bonding, π/π or van der Waals interactions being possible for a single system.

1.4.3.1. Dialkoxypillar[5]arene With Neutral Guests

For the encapsulation of neutral guests dialkoxypillar[5]arene's are the most prevalent pillar[n]arene to be used. The ease of synthesis of the dialkoxypillar[5]arene allows for facile trialling of a large range of chloroform soluble guests in a short period (*table 6*). This compares to the dihydroxypillar[5]arene which relies on a further

deprotection step and is in itself a macrocycle that will decompose in a short period of time. This is no further exemplified by what is arguably one of the largest compilations of works in the field of neutral guest encapsulation by dialkoxypillar[5]arene's by *Wang et al.*¹²¹ By comparing almost 50 neutral guests, a broader understanding on the nature of pillar[5]arenes host/guest chemistry without cationic contributions was understood.

Haloalkanes are among the smallest of guests which have shown complexation behaviour with pillar[5]arenes.¹⁵¹ For butylhalides the binding constant increases with the atomic radii of the halide; with bis(iodo)butane having the greatest complexation ability, and the fluorine derivative having the worst. These results highlight, that even though the fluoro derivative has the possibility of forming the strongest dipole-dipole and CH/ π interactions with pillar[5]arene. The greater dispersion forces granted by the larger halides are the dominant factor in complexation. For other disubstituted alkanes the binding constant is much lower. For aliphatic hydrocarbons there is a slight preference for alkynes over alkanes, but the binding constant is still 2 orders of magnitude lower than the iodoalkane.¹⁵² Equally aliphatic esters, aldehydes and ketones were either characterised as non-binding or only weakly binding.¹⁵³ However, when nitriles were introduced significant complexation could be observed, with the dipole-dipole, CH/ π , CH/O and CH/N interactions being highlighted as contributory factors to the strong bonding.¹²⁴ This study also highlighted the stringent requirement of 'good-fit' in host-guest complexation. By decreasing or increasing the alkyl chain length away from the preferential dinitrilebutane, significant drops in binding constant can be seen. Thus, showing that with neutral guests, careful consideration needs to be taken when choosing a suitable chain length to ensure the most efficient intermolecular bonding.

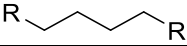
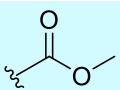
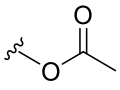
Host (Solvent)	Guest (R=)	Binding Constant K_a (M^{-1})	ref
DEP[5]A (DMSO- d_6 :CDCl ₃ 1:9)	CN 	$(1.5 \pm 0.3) \times 10^4$	124
DEP[5]A (CDCl ₃)	F	86 ± 5	151
DEP[5]A (CDCl ₃)	Cl	$(1.9 \pm 0.2) \times 10^3$	151
DEP[5]A (CDCl ₃)	Br	$(4.9 \pm 0.3) \times 10^3$	151
DEP[5]A (CDCl ₃)	I	$(1.0 \pm 0.1) \times 10^4$	151
DEP[5]A (CDCl ₃)	OH	$(5.4 \pm 0.3) \times 10^2$	151
DEP[5]A (CDCl ₃)	N ₃	$(3.5 \pm 0.4) \times 10^2$	151
DEP[5]A (CDCl ₃)	-C≡CH	82 ± 5	152
DEP[5]A (CDCl ₃)	-CH=CH ₂	12 ± 2	152
DEP[5]A (CDCl ₃)	-CH ₂ -CH ₃	<u>a</u>	152
DEP[5]A (CDCl ₃)		<u>a</u>	153
DEP[5]A (CDCl ₃)		27 ± 3	153

Table 6. Binding constants between neutral disubstituted butanes and diethoxypillar[5]arene
a. Binding constant too small to be measured

When comparing neutral nitrogen heterocycles, interesting results were found with seemingly similar heterocycles (table 7). Han et al, measured the binding constants between a series of alkoypillar[5]arenes and 4 nitrogen heterocycles.¹⁵⁴ The heterocycles that were chosen were all 5-membered rings, with the two-nitrogen containing; pyrazole and imidazole, as well as 1,2,3- and 1,2,4-triazole's being measured. For the two-nitrogen rings, imidazole had a binding constant 300 times that of pyrazole. Additionally, for the triazole substituents both 1,2,3 and 1,2,4 had similar binding constants. However, when the alkyl chain connected in the 2- position on the 1,2,3 triazole instead of the 1- position, there was an almost 1500 times decrease in binding constant. Their hypothesis for this finding, was that the dominant force for neutral nitrogen heterocycle and pillar[5]arene binding were the multiple CH/N bonds forming between the alkyl chains of pillar[5]arene and the outermost nitrogen of the heterocycle. Therefore, due to the 2-substituted triazole not having an outer nitrogen capable of binding, the binding constant is low. This was also demonstrated by altering

the chain length of the alkoxypillar[5]arene's rims, with the larger butoxypillar[5]arene having a slightly higher binding constant than the ethoxypillar[5]arene, and also significantly higher binding than the methoxypillar[5]arene.

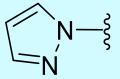
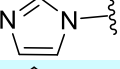
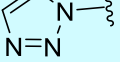
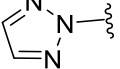
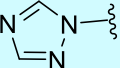
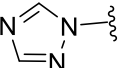
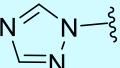
Host (Solvent)	Guest (R=)	Binding Constant K_a (M^{-1})	ref
DEP[5]A ($CDCl_3$)		66 ± 2	146
DEP[5]A ($CDCl_3$)		20000 ± 3000	146
DEP[5]A ($CDCl_3$)		16000 ± 3000	146
DEP[5]A ($CDCl_3$)		11 ± 1	146
DEP[5]A ($CDCl_3$)		6600 ± 400	146
DBuP[5]A ($CDCl_3$)		7300 ± 500	146
DMP[5]A ($CDCl_3$)		1200 ± 300	146

Table 7. Binding constants of disubstituted butyl chains containing neutral nitrogen heterocycles with alkoxypillar[5]arenes.

1.4.3.2. Larger Alkoxypillar[*n*]arenes With Neutral Guests

As was previously discussed, the complexation between hydroxypillar[5]arene and neutral guests is seldom reported. This could be due to as early stated; relative difficulties in synthesising, or alternatively, due to the alkane chains (that of which hydroxypillar[5]arene lacks) providing significant driving forces for complexation. There are, however, a few available examples of neutral guests with larger alkoxypillar[*n*]arenes, mostly with diethoxypillar[6]arene. *Yuan et al*, used a series of cyanide substituted guests which including alkyl, benzyl, adamantyl and naphthyl nitriles.¹⁵⁵ The results showed a stark difference between the pentamer and hexamer in binding with these guests. For the alkyl guest, butane-1,4-dicarbonitrile, the binding constant was 1500 times less with diethoxypillar[6]arene. However, for the larger

benzyl guests, such as 1,4-phenylenediacetonitrile, compared to diethoxypillar[5]arene which could not form a complex with said guest, the larger diethoxypillar[6]arene was successful in encapsulation of the guest. Crystal data from the diethoxypillar[6]arene/phenylenediacetonitrile complex suggested ten CH/N hydrogen bonds between the ethyl chains of the pillar[6]arene and the nitrile. Additionally, there was a further eight intramolecular bonds arising from the protons in the guest and the oxygens in the alkoxy pillar[6]arene.

For haloalkanes, the larger macrocyclic hexamer is too large to accommodate the linear guests. However, *Han et al*, was able to show some complexation behaviour between diethoxypillar[6]arene and pentaerythrityl halides.¹⁵⁶ The larger tetra-substituted haloalkanes were able to form intramolecular bonds with the cavity of diethoxypillar[6]arene, however the binding constants for both the chloride and bromide derivatives were incredibly low ($<10 \text{ M}^{-1}$) so it's difficult to draw any conclusions from this data.

1.5. Thesis Outline

This thesis examines potential applications of a series of both previously reported and novel pillar[*n*]arenes. With focus mainly affixed to the host-guest properties of these macrocycles, different sized pillar[*n*]arenes are compared and contrasted in a variety of functions.

A biochemical application for dialkoxypillar[*n*]arenes is examined in chapter 2. Where the pentamer and hexamer macrocycle are utilised in the selective encapsulation of cationic nicotine metabolites. Equally, in the pursuit of a method to better control the lifecycle of neonicotinoids. The complexation of imidacloprid and its metabolite desnitro-imidacloprid with pillar[*n*]arenes are to be assessed, and potential environmental impacts will be discussed. The aim would be to use the macrocycles potential selective affinity to capture the neonicotinoid metabolites most harmful to mammals.

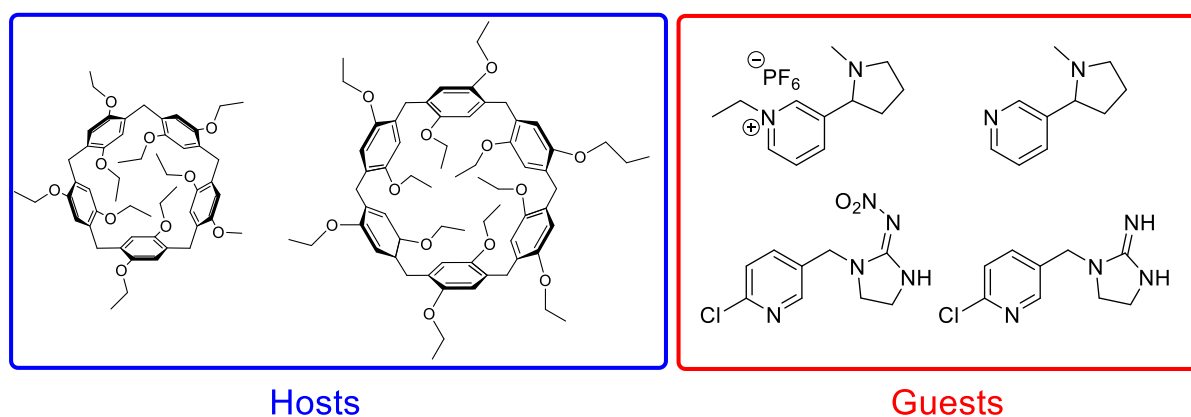


Figure 18. Chemical structures of the hosts and guests used herein.

In chapter 3, dipropoxypillar[5]arene will be utilised within a supramolecular structure. With the objective of synthesising a rotaxane decorated MOF, the synthesis of a suitable rotaxane, that of which is containing pillar[5]arene will be discussed and evaluated. With special attention paid to the synthesis of a rotaxane possessing

groups with the potential for fluorescence signalling, MOF attachment, and environment sensitive 'stations'. This will lead to the start of a collection of covalently functionalisable MOFs with corresponding rotaxanes capable of attaching to the MOF (figure 19).

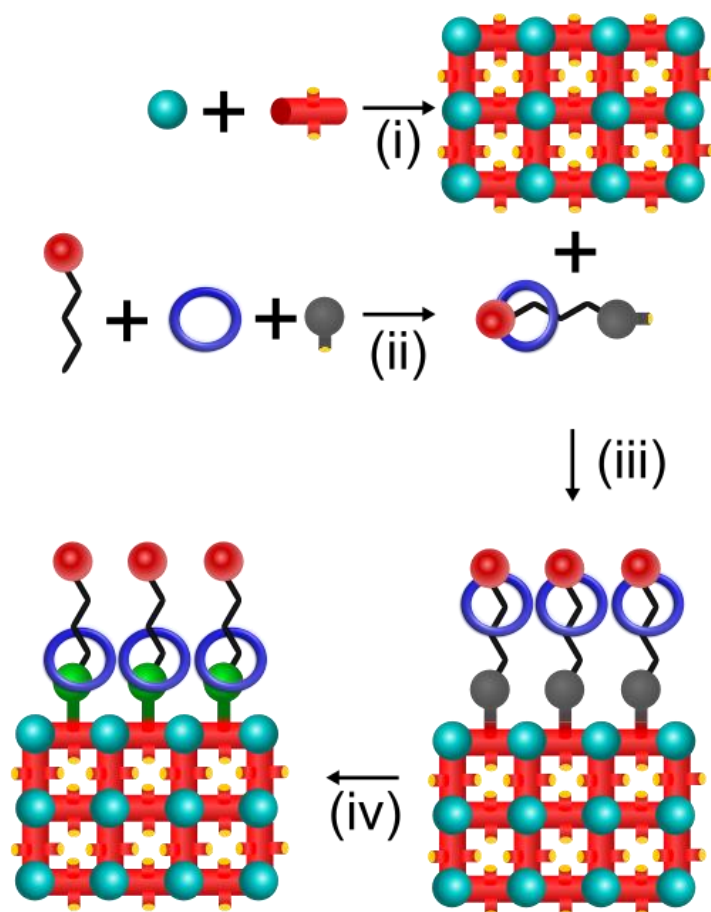


Figure 19. Graphic to show how a functionalised MOF can be post-synthetically modified with an environment sensitive rotaxane. i) Synthesis of a functionalised MOF with a metal node (teal) and linker (red). ii) Synthesis of an asymmetric rotaxane with a mono-stoppered rod (red and black), macrocycle (blue), and stopper with pendant functional group (grey) iii) Coupling reaction to attach the rotaxane to the MOF's surface e.g. CuAAC (azide and alkyne), thiolene (thiol and alkene), Suzuki (halide and boronic acid). iv) Environmental change that promotes the macrocycle to favour the encapsulation of one of the stoppers on the asymmetric rotaxane. Which in this example will lead to the blocking of the MOFs pores.

Chapter 4 will contain a thiol functionalised pillar[5]arene and will explore its function within self-assembled monolayers when attached to gold surfaces or electrodes. This chapter will also explore multiple synthetic procedures for producing thiolated pillar[5]arenes and assess the relative advantages and shortcomings of both. The intention of the macrocycle adsorbed surface would be to firstly evaluate the topography and molecular properties of the self-assembled monolayer, but also to then introduce an electron poor guest to the pillar[5]arene's cavity. This guest could for example, be an alkali metal cation for ion capture, but equally, the introduction of an alkane with electron poor groups attached could lead to *in-situ* rotaxane formation (figure 20).

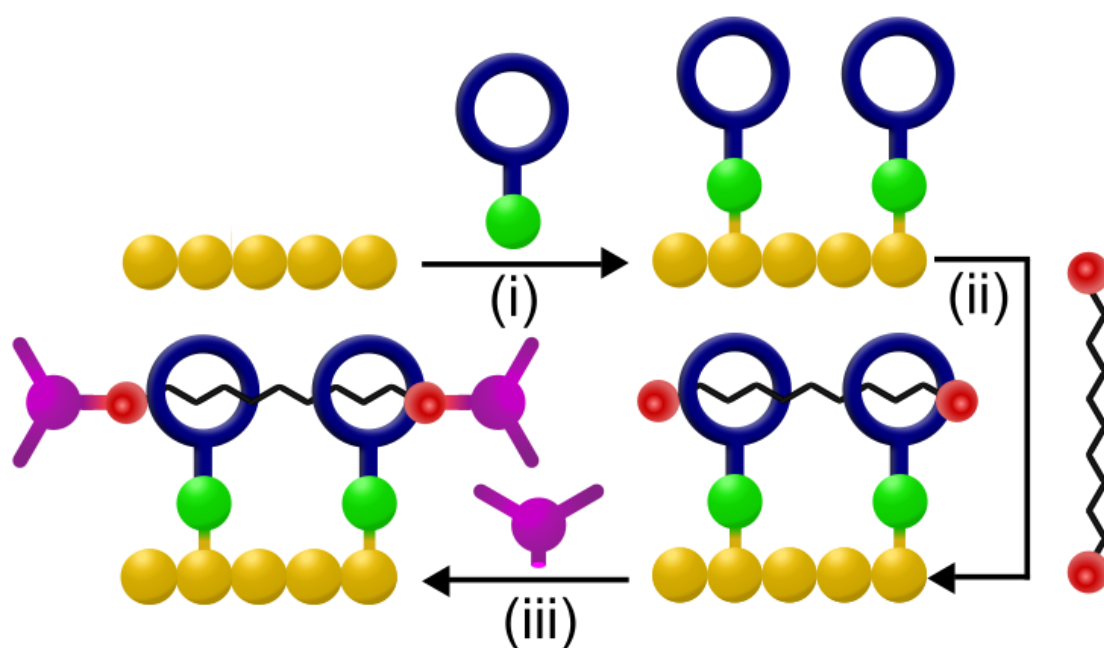


Figure 20. Proposed route for synthesising rotaxanes in situ on a gold surface. i) Adsorption of a thiol (green) functionalised pillar[5]arene (blue) to a bare gold Au(111) surface. ii) Addition of a rotaxane rod with electron deficient groups (red) on both ends of the alkane chain (black), forming the pseudo-rotaxane. iii) Bulky stopper groups (purple) attach to prevent dethreading of the macrocycle forming the rotaxane complete.

Finally, chapter 5 will summarise and discuss the key findings within the thesis, and detail how these results could be utilised in future research.

1.6. References

- 1 S. Kanoh and B. K. Rubin, *Clin. Microbiol. Rev.*, 2010, **23**, 590–615.
- 2 A. Crump, *J. Antibiot. (Tokyo)*, 2017, **70**, 495–505.
- 3 T. H. Keller, R. Hersperger and G. Della Cioppa, *Prog. Respir. Res.*, 2001, vol. 31, pp. 237–240.
- 4 J. M. McGuire, R. L. Bunch, R. C. Anderson, H. E. Boaz, E. H. Flynn, H. M. Powell and J. W. Smith, *Antibiot. Chemother. (Northfield)*, 1952, **2**, 281–283.
- 5 R. Woodward, E. Logusch, K. Nambiar, K. Sakan, D. Ward, B. Au-Yeung, P. Balaram, L. Browne, P. Card, C. Chen, R. Chênevert, A. Fliri, K. Froel, H. Gais, D. Garratt, K. Hayakawa, W. Heggie, D. Hessen, I. Hoppe and H. Wong, *J. Am. Chem. Soc.*, 1981, **103**, 3210–3213.
- 6 J. D. Dutcher, *Dis. Chest.*, 1968, **54**, 296–298.
- 7 K. C. Nicolaou, R. A. Daines, T. K. Chakraborty and Y. Ogawa, *J. Am. Chem. Soc.*, 1987, **109**, 2821–2822.
- 8 P. Ruggli, *Justus Liebigs Ann. Chem.*, 1912, **392**, 92–100.
- 9 K. Ziegler, H. Eberle and H. Ohlinger, *Justus. Liebigs. Ann. Chem.*, 1933, **504**, 94–130.
- 10 E. L. Blinn and D. H. Busch, *Inorg. Chem.*, 1968, **7**, 820–824.
- 11 P. G. Dougherty, Z. Qian and D. Pei, *Biochemical. J.*, 2017, **474**, 1109–1125.
- 12 J. Chen, Y. Zhang, L. Zhao, Y. Zhang, L. Chen, M. Ma, X. Du, Z. Meng, C. Li and Q. Meng, *ACS. Appl. Mater. Interfaces*, 2021, **13**, 53564–53573.
- 13 S. Lim, Y. Kuang and H. A. M. Ardoña, *Front. Chem.*, 2021, **9**.
- 14 C.-Y. Yao and A. P. de Silva, *Carbon Capture Sci. Technol.*, 2022, 100058.
- 15 A. Vlasceanu, S. L. Broman, A. S. Hansen, A. B. Skov, M. Cacciarini, A. Kadziola, H. G. Kjaergaard, K. V. Mikkelsen and M. B. Nielsen, *Chem. Eur. J.*, 2016, **22**, 10796–10800.
- 16 Y. Wang, Y. Zhang, T. Shan, Q. Wei, Z. Xu, Y. Zhao, J. Yang, Q. Bao, H. Jin, Z. Ma, H. Wei and H. Zhong, *J. Mater. Chem. A. Mater.*, 2021, **9**, 25629–25640.
- 17 S. Erbas-Cakmak, D. A. Leigh, C. T. McTernan and A. L. Nussbaumer, *Chem. Rev.*, 2015, **115**, 10081–10206.
- 18 C. J. Pedersen, *J. Am. Chem Soc.*, 1967, **89**, 2495–2496.
- 19 H. K. Frensdorff, *J. Am. Chem. Soc.*, 1971, **93**, 600–606.
- 20 G. Crini, *Chem. Rev.*, 2014, **114**, 10940–10975.
- 21 J. Szejtli, *Chem. Rev.*, 1998, **98**, 1743–1754.
- 22 M. V Rekharsky and Y. Inoue, *Chem. Rev.*, 1998, **98**, 1875–1918.
- 23 K. Harata, *Bull. Chem. Soc. Jpn.*, 1977, **50**, 1416–1424.

- 24 C. Wieser, C. B. Dieleman and D. Matt, *Coord. Chem. Rev.*, 1997, **165**, 93–161.
- 25 D. S. Guo and Y. Liu, *Acc. Chem. Res.*, 2014, **47**, 1925–1934.
- 26 E. S. Español and M. M. Villamil, *Biomolecules*, 2019, **9**.
- 27 E. B. Brouwer, K. A. Udachin, G. D. Enright, J. A. Ripmeester, K. J. Ooms and P. A. Halchuk, *Chem. Commun.*, 2001, 565–566.
- 28 R. Behrend, E. Meyer and F. Rusche, *Justus Liebigs Ann. Chem.*, 1905, **339**, 1–37.
- 29 W. A. Freeman, W. L. Mock and N. Y. Shih, *J. Am. Chem. Soc.*, 1981, **103**, 7367–7368.
- 30 J. Kim, I. S. Jung, S. Y. Kim, E. Lee, J. K. Kang, S. Sakamoto, K. Yamaguchi and K. Kim, *J. Am. Chem. Soc.*, 2000, **122**, 540–541.
- 31 W. A. Freeman, *Acta Crystallogr. B: Struct. Sci. Cryst. Eng. Mater.*, 1984, **40**, 382–387.
- 32 Y. Miyahara, K. Abe and T. Inazu, *Angew. Chem., Int. Ed. Engl.*, 2002, **41**, 3020–3023.
- 33 O. A. Efremova, Y. V. Mironov, N. V. Kuratieva and V. E. Fedorov, *Inorganica Chim. Acta.*, 2010, **363**, 4411–4415.
- 34 L. Cui, S. Gadde, W. Li and A. E. Kaifer, *Langmuir*, 2009, **25**, 13763–13769.
- 35 S. J. Barrow, S. Kaseira, M. J. Rowland, J. Del Barrio and O. A. Scherman, *Chem. Rev.*, 2015, **115**, 12320–12406.
- 36 E. A. Kovalenko, T. V. Mitkina, O. A. Geras'Ko, D. G. Samsonenko, D. Y. Naumov and V. P. Fedin, *Russ. J. Coord. Chem./Koord.*, 2011, **37**, 161–167.
- 37 E. M. M. Del Valle, *Process Biochem.*, 2004, **39**, 1033–1046.
- 38 W. R. Dichtel, O. Š. Miljanić, W. Zhang, J. M. Spruell, K. Patel, I. Aprahamian, J. R. Heath and J. F. Stoddart, *Acc. Chem. Res.*, 2008, **41**, 1750–1761.
- 39 P. R. Ashton, C. L. Brown, E. J. T. Chrystal, T. T. Goodnow, A. E. Kaifer, K. P. Parry, D. Philp, A. M. Z. Slawin, N. Spencer, J. F. Stoddart and D. J. Williams, *J. Chem. Soc.*, 1991, 634–639.
- 40 B. M. Rambo, H. Y. Gong, M. Oh and J. L. Sessler, *Acc. Chem. Res.*, 2012, **45**, 1390–1401.
- 41 S. Lee, C. H. Chen and A. H. Flood, *Nat. Chem.*, 2013, **5**, 704–710.
- 42 R. Jasti, J. Bhattacharjee, J. B. Neaton and C. R. Bertozzi, *J. Am. Chem. Soc.*, 2008, **130**, 17646–17647.
- 43 T. Ogoshi, S. Kanai, S. Fujinami, T. A. Yamagishi and Y. Nakamoto, *J. Am. Chem. Soc.*, 2008, **130**, 5022–5023.
- 44 K. Yang, Y. Pei, J. Wen and Z. Pei, *Chem. Commun.*, 2016, **52**, 9316–9326.
- 45 M. Cao, Y. Hao, Z. Xu, S. Hua Liu and J. Yin, *Curr. Org. Chem.*, 2015, **20**, 1299–1313.

- 46 F. Guo, Y. Sun, B. Xi and G. Diao, *Supramol. Chem.*, 2018, 30, 81–92.
- 47 T. Ogoshi, *J. Incl. Phenom. Macrocycl. Chem.*, 2012, 72, 247–262.
- 48 P. J. Cragg and K. Sharma, *Chem. Soc. Rev.*, 2012, 41, 597–607.
- 49 N. Song, T. Kakuta, T. aki Yamagishi, Y. W. Yang and T. Ogoshi, *Chem.*, 2018, 4, 2029–2053.
- 50 C. W. Sathiyajith, R. R. Shaikh, Q. Han, Y. Zhang, K. Meguellati and Y. W. Yang, *Chem. Commun.*, 2017, **53**, 677–696.
- 51 T. Ogoshi, T. Aoki, K. Kitajima, S. Fujinami, T. A. Yamagishi and Y. Nakamoto, *J. Org. Chem.*, 2011, **76**, 328–331.
- 52 M. Holler, N. Allenbach, J. Sonet and J. F. Nierengarten, *Chem. Commun.*, 2012, **48**, 2576–2578.
- 53 T. Boinski and A. Szumna, *Tetrahedron*, 2012, **68**, 9419–9422.
- 54 Y. Yao, J. Li, J. Dai, X. Chi and M. Xue, *RSC Adv.*, 2014, **4**, 9039–9043.
- 55 L. Liu, D. Cao, Y. Jin, H. Tao, Y. Kou and H. Meier, *Org. Biomol. Chem.*, 2011, **9**, 7007–7010.
- 56 S. Santra, D. S. Kopchuk, I. S. Kovalev, G. V. Zyryanov, A. Majee, V. N. Charushin and O. N. Chupakhin, *Green Chem.*, 2016, **18**, 423–426.
- 57 K. Wang, L. L. Tan, D. X. Chen, N. Song, G. Xi, S. X. A. Zhang, C. Li and Y. W. Yang, *Org. Biomol. Chem.*, 2012, **10**, 9405–9409.
- 58 D. Cao, Y. Kou, J. Liang, Z. Chen, L. Wang and H. Meier, *Angew. Chem., Int. Ed. Engl.*, 2009, **48**, 9721–9723.
- 59 T. Ogoshi, N. Ueshima, F. Sakakibara, T. A. Yamagishi and T. Haino, *Org. Lett.*, 2014, **16**, 2896–2899.
- 60 T. Ogoshi, N. Ueshima, T. Akutsu, D. Yamafuji, T. Furuta, F. Sakakibara and T. A. Yamagishi, *Chem. Commun.*, 2014, **50**, 5774–5777.
- 61 H. Tao, D. Cao, L. Liu, Y. Kou, L. Wang and H. Meier, *Sci. China. Chem.*, 2012, **55**, 223–228.
- 62 J. Cao, Y. Shang, B. Qi, X. Sun, L. Zhang, H. Liu, H. Zhang and X. Zhou, *RSC Adv.*, 2015, **5**, 9993–9996.
- 63 X. B. Hu, Z. Chen, L. Chen, L. Zhang, J. L. Hou and Z. T. Li, *Chem. Commun.*, 2012, **48**, 10999–11001.
- 64 T. Ogoshi and T. Yamagishi, *Chem. Commun.*, 2014, **50**, 4776–4787.
- 65 C. Han, Z. Zhang, X. Chi, M. Zhang, G. Yu and F. Huang, *Acta. Chimi. Sin.*, 2012, **70**, 1775–1778.
- 66 S. Karakurt, T. F. Kellici, T. Mavromoustakos, A. G. Tzakos and M. Yilmaz, *Curr. Org. Chem.*, 2015, **20**, 1043–1057.
- 67 T. Ogoshi, K. Kitajima, T. Aoki, T. A. Yamagishi and Y. Nakamoto, *J. Phys. Chem. Lett.*, 2010, **1**, 817–821.

- 68 T. Ogoshi, K. Kitajima, T. Aoki, S. Fujinami, T. A. Yamagishi and Y. Nakamoto, *J. Org. Chem.*, 2010, **75**, 3268–3273.
- 69 T. Ogoshi, K. Masaki, R. Shiga, K. Kitajima and T. A. Yamagishi, *Org. Lett.*, 2011, **13**, 1264–1266.
- 70 T. Ogoshi, R. Shiga, T. A. Yamagishi and Y. Nakamoto, *J. Org. Chem.*, 2011, **76**, 618–622.
- 71 T. Ogoshi, K. Demachi, K. Masaki and T. A. Yamagishi, *Chem. Commun.*, 2013, **49**, 3952–3954.
- 72 T. Ogoshi, T. A. Yamagishi and Y. Nakamoto, *Chem. Rev.*, 2016, **116**, 7937–8002.
- 73 T. Ogoshi, R. Sueto, K. Yoshikoshi, Y. Sakata, S. Akine and T. A. Yamagishi, *Angew. Chem., Int. Ed. Engl.*, 2015, **54**, 9849–9852.
- 74 T. F. Al-Azemi, M. Vinodh, F. H. Alipour and A. A. Mohamod, *J. Org. Chem.*, 2017, **82**, 10945–10952.
- 75 J. Han, X. Hou, C. Ke, H. Zhang, N. L. Strutt, C. L. Stern and J. F. Stoddart, *Org. Lett.*, 2015, **17**, 3260–3263.
- 76 T. Ogoshi, D. Yamafuji, D. Kotera, T. Aoki, S. Fujinami and T. A. Yamagishi, *J. Org. Chem.*, 2012, **77**, 11146–11152.
- 77 C. Han, Z. Zhang, G. Yu and F. Huang, *Chem. Commun.*, 2012, **48**, 9876–9878.
- 78 P. Demay-Drouhard, K. Du, K. Samanta, X. Wan, W. Yang, R. Srinivasan, A. C. H. Sue and H. Zuilhof, *Org. Lett.*, 2019, **21**, 3976–3980.
- 79 M. Guo, X. Wang, C. Zhan, P. Demay-Drouhard, W. Li, K. Du, M. A. Olson, H. Zuilhof and A. C. H. Sue, *J. Am. Chem. Soc.*, 2018, **140**, 74–77.
- 80 T. Ogoshi, K. Demachi, K. Kitajima and T. Yamagishi, *Chem. Commun.*, 2011, **47**, 7164–7166.
- 81 G. Wang, H. Qiang, Y. Z. Guo, J. Yang, K. Wen and W. B. Hu, *Org. Biomol. Chem.*, 2019, **17**, 4600–4604.
- 82 I. Nierengarten, S. Guerra, M. Holler, L. Karmazin-Brelot, J. Barberá, R. Deschenaux and J. F. Nierengarten, *Eur. J. Org. Chem.*, 2013, **18**, 3675–3684.
- 83 H. Deng, X. Shu, X. Hu, J. Li, X. Jia and C. Li, *Tetrahedron Lett.*, 2012, **53**, 4609–4612.
- 84 Y. Han, G. F. Huo, J. Sun, J. Xie, C. G. Yan, Y. Zhao, X. Wu, C. Lin and L. Wang, *Sci. Rep.*, 2016, **6**, 28748
- 85 Z. Zhang, B. Xia, C. Han, Y. Yu and F. Huang, *Org. Lett.*, 2010, **12**, 3285–3287.
- 86 W. Chen, Y. Zhang, J. Li, X. Lou, Y. Yu, X. Jia and C. Li, *Chem. Commun.*, 2013, **49**, 7956–7958.
- 87 T. Ogoshi, N. Ueshima, T. A. Yamagishi, Y. Toyota and N. Matsumi, *Chem. Commun.*, 2012, **48**, 3536–3538.
- 88 Y. Yao, M. Xue, X. Chi, Y. Ma, J. He, Z. Abliz and F. Huang, *Chem. Commun.*,

- 2012, **48**, 6505–6507.
- 89 Y. Ma, X. Ji, F. Xiang, X. Chi, C. Han, J. He, Z. Abliz, W. Chen and F. Huang, *Chem. Commun.*, 2011, **47**, 12340–12342.
- 90 T. Ogoshi, N. Ueshima and T. A. Yamagishi, *Org. Lett.*, 2013, **15**, 3742–3745.
- 91 I. Nierengarten, S. Guerra, M. Holler, J. F. Nierengarten and R. Deschenaux, *Chem. Commun.*, 2012, **48**, 8072–8074.
- 92 Y. Chang, K. Yang, P. Wei, S. Huang, Y. Pei, W. Zhao and Z. Pei, *Angew. Chem., Int. Ed. Engl.*, 2014, **53**, 13126–13130.
- 93 S. Fu, G. An, H. Sun, Q. Luo, C. Hou, J. Xu, Z. Dong and J. Liu, *Chem. Commun.*, 2017, **53**, 9024–9027.
- 94 F. Li, M. Zang, J. Hou, Q. Luo, S. Yu, H. Sun, J. Xu and J. Liu, *J. Mater. Chem. B.*, 2021, **9**, 5069–5075.
- 95 M. Bojtár, A. Simon, P. Bombicz and I. Bitter, *Org. Lett.*, 2017, **19**, 4528–4531.
- 96 Z. Wang, Y. A. Liu, H. Yang, W. B. Hu and K. Wen, *Org. Lett.*, 2022, **24**, 1822–1826.
- 97 D. J. Cram and J. M. Cram, *Science*, 1974, **183**, 803–809.
- 98 B. Dietrich, J. M. Lehn and J. P. Sauvage, *Tetrahedron Lett.*, 1969, **10**, 2889–2892.
- 99 J. M. Lehn, J. P. Sauvage and B. Dietrich, *J. Am. Chem. Soc.*, 1970, **92**, 2916–2918.
- 100 J. Israelachvili and M. Ruths, *Langmuir*, 2013, **29**, 9605–9619.
- 101 W. M. Latimer and W. H. Rodebush, *J. Am. Chem. Soc.*, 1920, **42**, 1419–1433.
- 102 W. M. Keesom, *Phys. Z.*, 1921, **22**, 129–141.
- 103 R. Eisenschitz and F. London, *Z. Phys.*, 1930, **60**, 491–527.
- 104 E. Fischer, *Ber. Dtsch. Chem.*, 1894, **27**, 2985–2993.
- 105 N. Henrich and F. Cramer, *J. Am. Chem. Soc.*, 1965, **87**, 1121–1126.
- 106 V. D. Jadhav and F. P. Schmidtchen, *Org. Lett.*, 2006, **8**, 2329–2332.
- 107 F. Biedermann and O. A. Scherman, *J. Phys. Chem. B.*, 2012, **116**, 2842–2849.
- 108 A. Owais, A. M. Djerdjev, J. M. Hook, A. Yuen, W. Rowlands, N. G. White and C. Neto, *J. Mater. Chem. A Mater.*, 2019, **7**, 12713–12722.
- 109 M. M. Cetin, Y. Beldjoudi, I. Roy, O. Anamimoghadam, Y. J. Bae, R. M. Young, M. D. Krzyaniak, C. L. Stern, D. Philp, F. M. Alsubaie, M. R. Wasielewski and J. F. Stoddart, *J. Am. Chem. Soc.*, 2019, **141**, 18727–18739.
- 110 D. Niether, T. Kawaguchi, J. Hovancová, K. Eguchi, J. K. G. Dhont, R. Kita and S. Wiegand, *Langmuir*, 2017, **33**, 8483–8492.
- 111 N. H. Evans, *Eur. J. Org. Chem.*, 2019, **21**, 3320–3343.

- 112 D. A. Dougherty, *Acc. Chem. Res.*, 2013, **46**, 885–893.
- 113 D. A. Dougherty, *Science*, 1996, **271**, 163–168.
- 114 M. Nishio, *CrystEngComm*, 2004, **6**, 130–158.
- 115 J. Ran and M. W. Wong, *J. Phys. Chem. A*, 2006, **110**, 9702–9709.
- 116 R. Anjana, M. K. Vaishnavi, D. Sherlin, S. P. Kumar, K. Naveen, P. S. Kanth and K. Sekar, *Bioinformation*, 2012, **8**, 1220–1224.
- 117 M. O. Sinnokrot, E. F. Valeev and C. D. Sherrill, *J. Am. Chem. Soc.*, 2002, **124**, 10887–10893.
- 118 D. Kim, S. Hu, P. Tarakeshwar, K. S. Kim and J. M. Lisy, *J. Phys. Chem. A*, 2003, **107**, 1228–1238.
- 119 S. Tsuzuki, K. Honda, T. Uchimaru, M. Mikami and K. Tanabe, *J. Phys. Chem. A*, 2002, **106**, 4423–4428.
- 120 S. Tsuzuki, K. Honda, T. Uchimaru, M. Mikami and K. Tanabe, *J. Am. Chem. Soc.*, 2000, **122**, 11450–11458.
- 121 Y. Wang, G. Ping and C. Li, *Chem. Commun.*, 2016, **52**, 9858–9872.
- 122 C. Schönbeck, H. Li, B. H. Han and B. W. Laursen, *J. Phys. Chem. B*, 2015, **119**, 6711–6720.
- 123 C. Li, L. Zhao, J. Li, X. Ding, S. Chen, Q. Zhang, Y. Yu and X. Jia, *Chem. Comm.*, 2010, **46**, 9016–9018.
- 124 X. Shu, S. Chen, J. Li, Z. Chen, L. Weng, X. Jia and C. Li, *Chem. Comm.*, 2012, **48**, 2967–2969.
- 125 F. Diederich and D. Griebel, *J. Am. Chem. Soc.*, 1984, **106**, 8037–8046.
- 126 P. Langer, L. Yang, C. R. Pfeiffer, W. Lewis and N. R. Champness, *Dalton Transactions*, 2019, **48**, 58–64.
- 127 C. Han, G. Yu, B. Zheng and F. Huang, *Org. Lett.*, 2012, **14**, 1712–1715.
- 128 C. Li, X. Shu, J. Li, J. Fan, Z. Chen, L. Weng and X. Jia, *Org. Lett.*, 2012, **14**, 4126–4129.
- 129 C. Li, Q. Xu, J. Li, Feina Yao and X. Jia, *Org. Biomol. Chem.*, 2010, **8**, 1568–1576.
- 130 Y. M. Zhang, X. P. Chen, G. Y. Liang, K. P. Zhong, Q. Lin, H. Yao and T. B. Wei, *New J. Chem.*, 2018, **42**, 10148–10152.
- 131 Q. Lin, F. Zheng, L. Liu, P. P. Mao, Y. M. Zhang, H. Yao and T. B. Wei, *RSC Adv.*, 2016, **6**, 111928–111933.
- 132 Q. Lin, P. P. Mao, F. Zheng, L. Liu, J. Liu, Y. M. Zhang, H. Yao and T. B. Wei, *New J. Chem.*, 2017, **41**, 12172–12177.
- 133 Q. Lin, L. Liu, F. Zheng, P. P. Mao, J. Liu, Y. M. Zhang, H. Yao and T. B. Wei, *RSC Adv.*, 2017, **7**, 34411–34414.
- 134 G. Zhao, X. Zhou, X. Ran, X. Tan, T. Li, M. Cao, L. Yang and G. Du, *Electrochim.*

- Acta.*, 2018, **277**, 1–8.
- 135 J. Sun, L. Shao, J. Zhou, B. Hua, Z. Zhang, Q. Li and J. Yang, *Tetrahedron Lett.*, 2018, **59**, 147–150.
- 136 T. Ogoshi, M. Hashizume, T. A. Yamagishi and Y. Nakamoto, *Chem. Commun.*, 2010, **46**, 3708–3710.
- 137 D. X. Chen, Y. L. Sun, Y. Zhang, J. Y. Cui, F. Z. Shen and Y. W. Yang, *RSC Adv.*, 2013, **3**, 5765–5768.
- 138 X. Tan, Y. Wu, S. Yu, T. Zhang, H. Tian, S. He, A. Zhao, Y. Chen and Q. Gou, *Talanta.*, 2019, **195**, 472–479.
- 139 T. Ogoshi, R. Shiga and T. A. Yamagishi, *J. Am. Chem. Soc.*, 2012, **134**, 4577–4580.
- 140 H. Zhang, X. Ma, K. T. Nguyen, Y. Zeng, S. Tai and Y. Zhao, *Chempluschem*, 2014, **79**, 462–469.
- 141 B. Gómez, V. Francisco, F. Fernández-Nieto, L. Garcia-Rio, M. Martín-Pastor, M. R. Paleo and F. J. Sardina, *Chem. Eur. J.*, 2014, **20**, 12123–12132.
- 142 C. Li, X. Shu, J. Li, S. Chen, K. Han, M. Xu, B. Hu, Y. Yu and X. Jia, *J. Org. Chem.*, 2011, **76**, 8458–8465.
- 143 H. Butkiewicz, S. Kosiorek, V. Sashuk and O. Danylyuk, *CrystEngComm*, 2021, **5**, 1075-1082.
- 144 C. Han, F. Ma, Z. Zhang, B. Xia, Y. Yu and F. Huang, *Org. Lett.*, 2010, **12**, 4360–4363.
- 145 T. Ogoshi, H. Kayama, D. Yamafuji, T. Aoki and T. A. Yamagishi, *Chem. Sci.*, 2012, **3**, 3221–3226.
- 146 G. Yu, X. Zhou, Z. Zhang, C. Han, Z. Mao, C. Gao and F. Huang, *J. Am. Chem. Soc.*, 2012, **134**, 19489–19497.
- 147 Z. Li, J. Yang, G. Yu, J. He, Z. Abliz and F. Huang, *Org. Lett.*, 2014, **16**, 2066–2069.
- 148 Z. Li, J. Yang, G. Yu, J. He, Z. Abliz and F. Huang, *Chem. Commun.*, 2014, **50**, 2841–2843.
- 149 Y. Ma, X. Chi, X. Yan, J. Liu, Y. Yao, W. Chen, F. Huang and J. L. Hou, *Org. Lett.*, 2012, **14**, 1532–1535.
- 150 J. Yang, X. Chi, Z. Li, G. Yu, J. He, Z. Abliz, N. Li and F. Huang, *Org. Chem. Front.*, 2014, **1**, 630–633.
- 151 X. Shu, J. Fan, J. Li, X. Wang, W. Chen, X. Jia and C. Li, *Org. Biomol. Chem.*, 2012, **10**, 3393–3397.
- 152 X. S. Hu, H. M. Deng, J. Li, X. S. Jia and C. J. Li, *Chin. Chem. Lett.*, 2013, **24**, 707–709.
- 153 X. Lou, H. Chen, X. Jia and C. Li, *Chin. J. Chem.*, 2015, **33**, 335–338.

- 154 K. Han, Y. Zhang, J. Li, Y. Yu, X. Jia and C. Li, *Eur. J. Org. Chem*, 2013, **2013**, 2057–2060.
- 155 M. Sen Yuan, H. Chen, X. Du, J. Li, J. Wang, X. Jia and C. Li, *Chem. Commun.*, 2015, **51**, 16361–16364.
- 156 C. Han, D. Zhao and S. Dong, *Chem. Asian. J*, 2020, **15**, 2642–2645.

CHAPTER 2 PILLAR[N]ARENES AND THEIR COMPLEXATIONS WITH NEONICOTINOIDS AND NICOTINE DERIVATIVES

2.1. Introduction

The usage and controlling of neonicotinoids present a challenge, not just chemically but geopolitically. From 1990 to 2018, the Food and Agriculture Organization of the United Nations (FAO) reported an 80 % increase in the usage of pesticides.¹ With neonicotinoids representing 25 % of the global pesticide market in 2014, and an estimated value of \$3 billion, neonicotinoids fulfil an important role in global agriculture and food production.^{2,3} However, as the damaging effect of neonicotinoids on ecosystems became better studied, countries and international organisations slowly started adding restrictions to the sale and usage of the pesticides.⁴⁻⁷

In this chapter, a novel selective encapsulation method has been proposed and studied using pillar[n]arene derivatives. The effectiveness of the complexation between the macrocycles and the elected guests, were explored using NMR titrations and compared to other commonly used macrocycles.

2.2. Nicotine

A naturally occurring psychoactive alkaloid, nicotine is found in members of the nightshade family including but not exclusive to; tomatoes, aubergines, potatoes and tobacco.⁸ Nicotine for these plants, act as a deterrent to ward off potential predators, and as early as 1690, treatments of crop yielding plants with tobacco was utilised to control invasive species of insects.^{9,10} Nicotine, or more specifically tobacco also plays a pivotal role in human history. From as early as 12,300 years ago humans have been

cultivating tobacco, and throughout history, the sociocultural impact the nicotine containing plant has had; from a religious devotion to a lucrative trade commodity cannot be underestimated.¹¹⁻¹³

Nicotine is an optically active molecule, having two enantiomeric forms: (*S*)-nicotine and (*R*)-nicotine. (*S*)-nicotine is the predominant naturally occurring isoform, with most plant derived nicotine products containing only 0.1-1.2 % (*R*)-nicotine (*Figure 1*).¹⁴ When the relative energies of each isomer are compared, the DFT measurements indicate a small, but significant Gibbs free energy difference of 18 kJ mol⁻¹. The physiological activities of the enantiomers also differs, with (*S*)-nicotine having be found to be more physiologically active and up to 18 times more toxic to mammals.^{15,16}

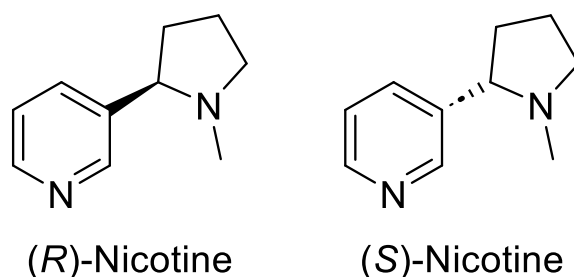


Figure 1. Optical isomers of nicotine.

The pharmacodynamics and pharmacokinetics of nicotine is complex, and the effects it may produce in mammals are differing and multifactorial, even within the same species.¹⁷⁻²⁰ The primary mechanism of nicotine however, is the binding to nicotinic acetylcholine receptors (nAChRs) within the central nervous system and skeletal muscle. For most nAChRs, the nicotine will act as a receptor agonist, but for nAChR α 9 and nAChR α 10, receptor antagonism occurs.²¹ The binding of nicotine to these gated ion channels will cause a rapid opening of the cation channel, allowing for an increased intake of potassium, sodium and calcium cations.²² Resultingly, the combination of this disruption of the nAChRs, and other minor biological pathways, causes the release of

numerous neurotransmitters including dopamine, adrenaline, gamma aminobutyric acid, and serotonin.²³ The swift activation of these 'reward pathways' coupled with the nAChRs propensity to desensitise leads to nicotine's addictiveness.²⁴

2.2.1. Metabolites of Nicotine

The metabolisation of nicotine for mammals occurs in the liver, with the major metabolite found in urine being cotinine and cotinine derivatives (ca 75 %).²⁵ Alternate metabolism pathways lead to minor pharmacologically active metabolites, with the most relevant for this work being the nicotine isomethonium ion (*N*-methylnicotinium) (*figure 2*). The *N*-methylation pathway of nicotine was shown to be *via* S-adenosyl-L-methionine as the methyl source, and amine *N*-methyltransferase as a catalyst.^{26,27} Interestingly, the methylation pathway *in vivo* is stereospecific; with only the minor (*R*)-enantiomer undergoing this biochemical transformation.²⁸ This differs from synthetic methylation of nicotine, which appears to react indiscriminate to the enantiomer, which further indicates the complexity of the isomer specific biochemical reactions of nicotine.²⁹ Alkylated nicotine species also partake in differing, and often converse binding to nAChR receptors. For example for the $\alpha 4\beta 2^*$ subtype, which has been known as a high affinity nicotine receptor since the 1980s, (*S*)-nicotine will act as a receptor agonist.^{30,31} However, an alkylated nicotine dimer was shown to act as a functional antagonist towards the $\alpha 4\beta 2^*$ receptor, inhibiting the dopamine response evolved from nicotine binding, with the length of the bridging alkane also altering the efficiency of binding.^{32,33} Therefore, by tailoring the presence and availability of alkylated nicotine species, the stimulating effect of nicotine can be controlled. Additionally, alkylated nicotine's were shown to excel (*S*)-nicotine as antimicrobials, further highlighting the need to further study the cations.³⁴

The excretion route for nicotine and its metabolites in animals is through urine, and through this water sources can get contaminated *via* domestic wastewater streams.³⁵ The negatives effects of this contamination are little understood, but some studies have shown the potential ecotoxicity of nicotine and cotinine.^{36–38} The damage caused by other naturally formed nicotine derivatives, however, are poorly understood and long term effects may yet to be seen.³⁹ One study conducted in 1948 concluded that *N*-methylated nicotine, like that of which is metabolised in mammals, has a lower toxicity towards arthropods.⁴⁰ However, it has also been established for other methylated pyridines that toxicity is increased post methylation.⁴¹ This severe ecotoxicity of methyl pyridiniums is no better studied than for *N,N'*-dimethyl-4,4'-bipyridinium dichloride (paraquat). Paraquat is a methyl viologen, first synthesised in 1882 and is still widely used in agriculture as a herbicide, with an annual consumption of 4,500 tons in the USA.^{42,43} Due to the large quantities of paraquat, and its extended use for the last 70 years, research into the ecotoxicology of paraquat is extensive. In mammals paraquat is acutely toxic by ingestion even in doses as low as 22 mg/kg.⁴⁴ Chronic effects of paraquat are also seen in frequent users, with increased risk of Parkinson's disease, impaired lung function, depression, renal failure and sterility for both the users, but also ambient exposures from water contamination and consumption.^{45–49}

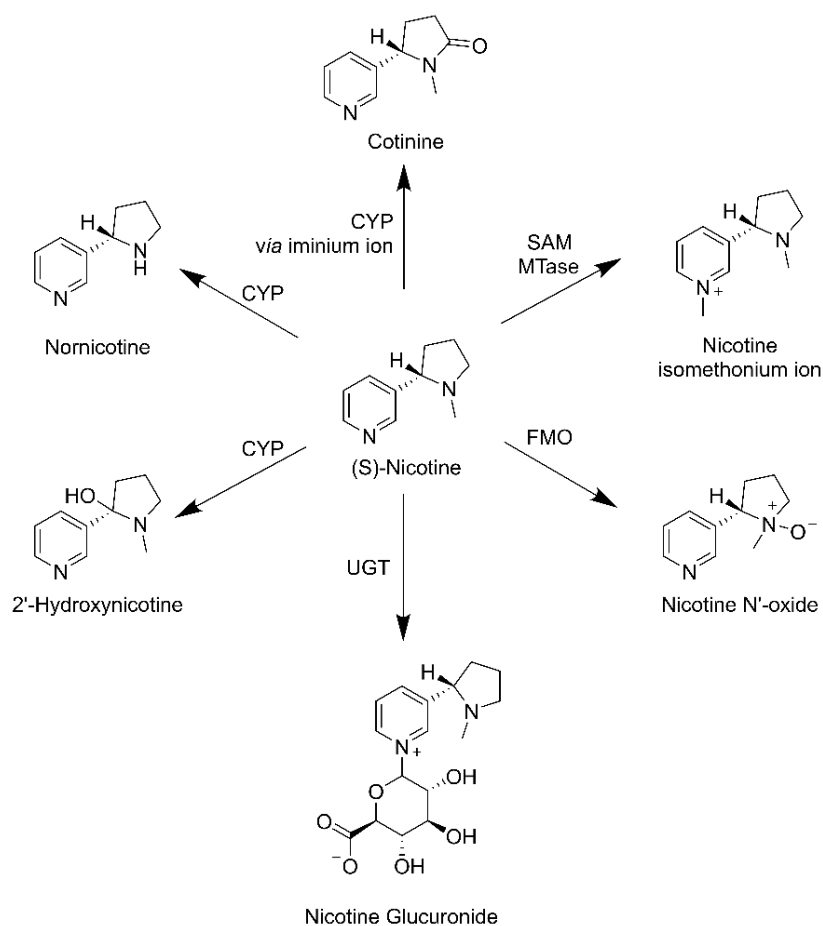


Figure 2. Primary metabolic pathway for (S)-nicotine. *Adapted from Hukkanen et al.*²⁵

2.2.2. Detection and Encapsulation of Nicotine and Nicotine Like Compounds

A consequence of paraquat's toxicity, and its ability to sequester in water sources, has led to a recent influx of research to detect and/or capture paraquat. Solid state materials such as metal organic frameworks (MOFs), zeolites and polymers, have all been shown to be effective paraquat detection methods.^{50–56} Macrocycles have also been implemented to form complexes with paraquat. Calixarenes functionalised with sulfonates were demonstrated to form 1:1 complexes with paraquat in water, with an increase in binding constant as the number of monomer units in the calixarene increase ($8.0 \times 10^2 \text{ M}^{-1}$, $1.7 \times 10^3 \text{ M}^{-1}$, $2.0 \times 10^3 \text{ M}^{-1}$ for C4, C6, and C8 respectively).⁵⁷

A pyridine containing cryptand was also reported, which has a 1600 fold increase in association constant with paraquat, when compared to that of a diphenyl crown ether.⁵⁸ Pillar[n]arenes have also shown efficient binding with paraquat and other viologens. *Ogoshi et al* showed that pillar[5]arene could form 1:1 complexes with hexyl substituted viologen, and *Huang et al* synthesised a water-soluble pillar[6]arene with pendant carboxylate groups that forms a stable 1:1 complex with paraquat in water with a high association constant of $(1.02 \pm 0.10) \times 10^8 \text{ M}^{-1}$.^{59,60}

For neutral nicotine metabolites, some advancements have been made to selectively detect and capture particular metabolites. A zinc porphyrin functionalised with phenoxyacetamides was able to selectively recognise nicotine (when compared to cotinine and myosmine). This was achieved *via* the pendant acetamides acting as 'pincers' to preferentially bind to nicotine's pyrrolidine.⁶¹ Equally a copper MOF was shown to be able to trap up to 40 wt % of nicotine within its mesoporous cavities.⁶²

For alkylated nicotine species little research in comparison has been undertaken, possibly due to the low natural occurrence as a natural nicotine metabolite. However some attempts to bind the molecules have been made, a molecular cage assembled using a linker comprised of a naphthalene core with pendant catechols, and gallium was one such example.⁶³ In this example however, the molecular cage wasn't employed to detect or capture the *N*-methylnicotinium ion, instead the cation's inherent chirality was employed to isolate the enantiomers of the cage. The single-molecule kinetics of this was further studied by affixing the cage to an α -hemolysin protein nanopore.⁶⁴ The results of both studies showed a strong binding between the nicotine cation and the cage, and the nicotinoid's ability to outperform other ammonium cations, for example tetramethylammonium as a competing guest. A macrocycle shown capable of *N*-methylnicotinium complexation, was a chiral upper-rim-bridged

calix[4]arene (*figure 3*).⁶⁵ The calix[4]arene was capable of binding the nicotinium, with NMR studies showing preferential binding towards the methylated pyridinium, indicated by the relative shifts of the guest protons. Although the nicotinium guest and the macrocycle were both inherently chiral, no significant difference was observed between the binding association of the two calix[4]arene enantiomers. The lack of difference was attributed to the chiral centre of the nicotine showing little involvement with the complexation, and therefore not providing chiral selectivity.

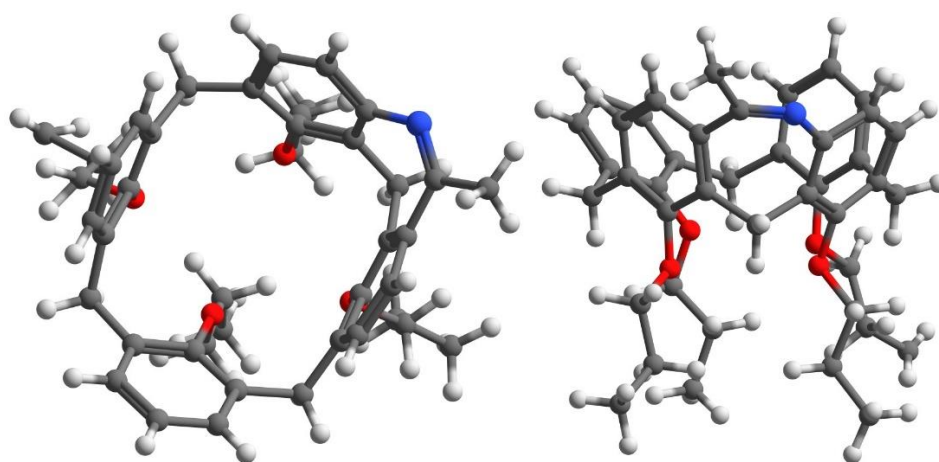


Figure 3. Top and side view respectively of calix[4]arene capable of *N*-methylnicotinium encapsulation.⁶⁵

2.2.3 Alkylation of Nicotine

The synthesis of any *N*-alkylated nicotine can be performed easily using alkyl halides, most commonly iodoalkanes, but bromoalkanes can also be used (*figure 4*).^{66–68} The reaction is clearly very similar to other pyridine alkylations, which have been produced synthetically from the late 1800s, with work pioneered by Hantzsch.^{69,70} Equally, previously discussed paraquat, is most commonly synthesised by addition of methyl iodide to 4,4'-bipyridine.^{42,71} Distinctively though for nicotine, the reaction itself is a rare case of competitive nitrogen alkylation. When performed in a polar solvent, the reaction yields a 2.5:1 mixture of both the *N'*-methylnicotinium and *N*-methylnicotinium

respectively (*figure 4*). To circumvent this, modification of the reagents can be used to increase the product specificity. Switching to acetic acid as the solvent led to analytically pure *N*-methylnicotinium, and equally adding sodium carbonate to the reaction in acetonitrile could give *N*-methylnicotinium after workup.⁷² Anion metathesis can also be easily performed on the nicotinium salts *via* reaction with a metal salt containing the desired anion, this exchange proves vital in tailoring solubility.⁷³

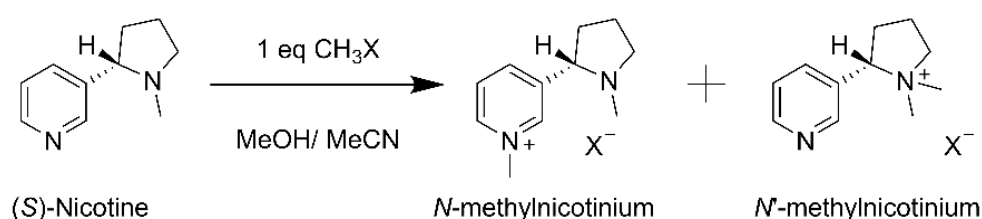


Figure 4. Methylation of Nicotine using alkyl halides.

2.3. Neonicotinoids

2.3.1. A Brief History of Pesticide Usage

Pesticides have been deemed essential to the development of mass agriculture and has supported the growth of civilisations. Since as early as 3700 BCE in the Rig veda, references to the protection of plants *via* the use of an external pest deterrent have been recorded.⁷⁴ For almost six thousand years, pesticides were either mineable elemental resources, for example sulfur, arsenic and mercury, or plant based pest deterrents like nicotine and pyrethrins.^{75–77} That was until 1939 when Paul Hermann Müller studied the insecticidal properties of dichlorodiphenyltrichloroethane (DDT), a discovery that would later see him awarded the Nobel prize in physiology and medicine.⁷⁸ Although first synthesised in 1874, 25 years before Müller's birth, it's insecticidal properties were not evaluated until Müller's research.⁷⁹ DDT's

controversial history begins in the trenches of World War Two, it was used extensively as an insecticide, but also was implemented as a 'cure all' to control the spread of typhus, typhoid, dysentery and malaria.⁸⁰ In 1944 DDT became available commercially, but as quickly as general use started, criticisms and concerns began getting raised.⁸¹ Questions about the possible harms it could cause on the ecosystem were presented as early as 1946, but it was not till the release of *Silent Spring* by Rachel Carson in 1962 where public opinion started to sway, and by 1972 it was banned in the USA.^{82,83}

Organophosphates saw a similar rise and fall in popularity, although synthesised since the early 19th century, organophosphates would not see their use as a pesticide until after the Second World War.⁷⁵ The surge in organophosphate research arose from a two pronged research campaign by Germany in 1938; to synthesise insecticides that were safe for mammals, but also to develop highly toxic organophosphates for use as poison gases.^{84,85} From this research arose that of Sarin, Tabun and Soman, but also vital developments in organophosphates as insecticides. After the war British and American companies utilised this research to market the first organophosphate pesticides, and their usage peaked after the banning of DDT and similar organochlorine insecticides in the 1970s. And up until recently, organophosphates such as glyphosate were the dominant pesticide for agricultural use, but from 2000 to 2012 their market share decreased from 71 % to 33 %.⁸⁶

2.3.2. History of Neonicotinoids

Chemically related to nicotine, neonicotinoids are still widely used today, and were welcomed as a perceived safer alternative to organophosphates and carbamates.⁸⁷ Research pioneered in the 1970s by Shell's biological research centre, identified possible candidates to be used as insecticides. Starting from an alkyl nitrate

substituted pyridine, Shell tested a series of nitrogen containing heterocycles for use as insecticides. This eventually led to nithiazine, which displayed high activity towards a plethora of insects, but importantly; low toxicity towards plants and mammals.^{88,89} The largest issue with nithiazine, and some other later discovered molecules such as 1-(6-chloropyrid-3-ylmethyl)-2-(nitromethylene)imidazoline, was their photoinstability.⁹⁰ Eventually, in 1985, imidacloprid was patented by Bayer, with an additional 2-(*N*-nitro-imino) chromophore photodegradation was limited, and the addition of the 6-chloropyrid-3-ylmethyl (CPM) group increased the biological efficacy 125 fold.⁹¹⁻⁹³ Imidacloprid was introduced to market in 1991, and since then has become the most successful insecticide, still being the leading neonicotinoid in production and sales as of 2011 (*table 1*).⁸⁷

Other neonicotinoids, namely acetamiprid (1995) and nitenpyram (1995) and thiacloprid (2000) were further developed, and still utilised the CPM group (year of patent).⁹⁴⁻⁹⁶ The CPM group was neglected in some more recently developed neonicotinoids; substitution to a furan group led to the development of dinotefuran (2002).⁹⁷ Equally, Thiamethoxam (1998) and clothianidin (2001) employed a 2-chlorothiazole site in place of the CPM group. The former of which; thiamethoxam, was one of the first in a new line of '2nd generation' neonicotinoids, and since 2012 has surpassed imidacloprid in market share (37.6 % compared to imidacloprid's 33.5 %).²

Insecticide and Year of introduction 2,98,99	Chemical Structure	Global Annual Turnover 2009 (US \$ Million) 100–102	Acute contact toxicity to Bees (LD ₅₀ µg/Bee) 103–106	Acute oral toxicity to rats (LD ₅₀ mg/kg) 93,98,107,108	Selectivity factor 93,109	ref
Imidacloprid 1991		1091	0.0179	450	565	2, 99, 102, 92
Thiamethoxam 1998		627	0.0299	1563	>20	2, 99, 102, 92
Clothianidin 2001		439	0.0218	>5000	1591	2, 99, 102, 92
Acetamiprid 1995		276	7.07	182	84	2, 99, 102, 92
Thiacloprid 2000		112	14.6	640	319	2,99, 102, 92
Dinotefuran 2002		79	0.0750	2400	>111	2,99, 102, 92
Nitenpyram 1995		8	0.0138	1628	3500	2,99, 102, 92
(S)-Nicotine		N/A	LC ₅₀ 2000 ppm	50	0.002	103, 97
Sodium Metam 1989		131.32 ^a	36.26	1294-1428	16 ^b	97, 100, 104, 106, 108
Glyphosate 1974		9,300 ^a	309	4320-5000	33 ^b	98, 101, 105, 107, 108

Table 1. Table showing the most commonly used neonicotinoids as of 2009, and two other widely used pesticides of different chemical class.

^a As of 2020

^b Selectivity for the carbamates and organophosphates pesticide class respectively

2.3.3. Neonicotinoid Mode of Action

The pharmacodynamics of neonicotinoids mimic that of (S)-nicotine; binding to the nAChRs of animals, but unlike (S)-nicotine, show highly selective toxicity towards insects and other invertebrates.^{93,110} Fortunately, there have been large swathes of research studying this selectivity towards invertebrates, partially due to the large global demands for insecticides. Just like (S)-nicotine, the mechanism of interaction between the neonicotinoids and the nAChRs is complex and multifaceted. The condensed mode of action is the neonicotinoid, once ingested, will irreversibly bind with nAChRs. This binding triggers the signalling of the nerve, opening the ion channels. Finally, unlike for the endogenous agonist acetylcholine, neonicotinoids can not be broken down by acetylcholinesterase, which in chronic doses concludes in hyperexcitation, paralyzes, then death.¹¹¹ *Zwart et al*, studied an early neonicotinoid which is structurally similar to imidacloprid, and their actions upon several receptors. The receptors were nAChRs obtained from mouse cell cultures (muscle and neuroblastoma) and those of which taken from locust neurones.¹¹² The results obtained showed a significant difference between the actions of the nitromethylene moiety, for the locust neurones there was both a potent agonist and antagonist action. Whereas for the mouse neurone, there was only a weak antagonist effect, and there was no effect at all on the muscle cells. Equally, imidacloprid was shown to have little, if any binding affinity for mammalian nAChRs, whilst still displaying high binding affinity for that of insects.¹¹³ This high affinity for insect nAChRs, and relatively low affinities for mammal receptors were deemed a large contributor to their selective toxicities. Thereafter, evidence was further provided when a significant correlation was seen for binding affinity and toxicity in flies.¹¹⁴

As to why this high affinity towards the nAChRs of insects occurs, is more complicated. Isolating a molecular fragment of the neonicotinoid responsible for its insecticidal nature is difficult, as is clear with the various chemical structure differences between the 1st and 2nd generation neonicotinoids. Imidacloprid was compared to (+)-epibatidine in its ability to preferentially bind to insect nAChRs. As both of these toxins contain the 2-chloropyridine moiety, previously thought responsible for neonicotinoid action, similar responses were assumed. Conversely, when the two pyridyl containing molecules were introduced to both a chicken nAChR, and a hybrid nAChR containing the melanogaster neuronal alpha subunit from a *Drosophila*, significant differences were found. Epibatidine was a full agonist towards both the chicken and hybrid receptor, whereas for imidacloprid the binding affinity was significantly increased with addition of the *Drosophila* subunit.¹¹⁵ Therefore, the pyridyl moiety cannot be seen as the sole driving force towards selectivity, and that the adjacent chromophore and bridging atom must also play an important role.

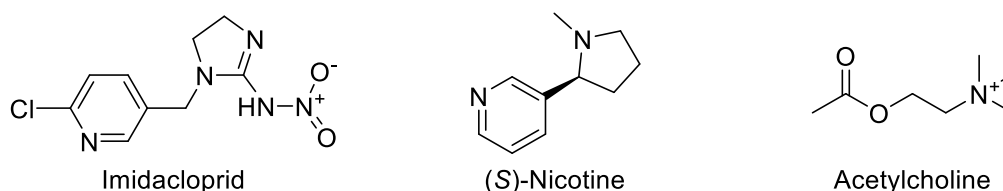


Figure 5. Chemical structures of nAChR active molecules

The current and most convincing theory as to why selectivity occurs is two-part; the structural differences of insect and mammal's nAChRs, and the relative basicity and electrochemical properties of neonicotinoids when compared to that of nicotinoids.¹¹⁶ As neonicotinoids, nicotinoids like nicotine, and acetylcholine all bind to nAChRs but show converse selectiveness, it is important to compare the structures of these molecules (*figure 5*). X-ray structures show important similarities, for imidacloprid the

distance between the van der Waals surface of the pyridyl nitrogen and the tertiary amine in the imidazolidine is 5.45 - 6.06 Å. This is mimicked between the two nitrogen's in nicotine, and between the ammonium nitrogen and carboxyl oxygen of acetylcholine.¹¹⁷ Differences though, start appearing once electronic contributions are scrutinised. For nicotine and other nicotinoids, the nitrogen on the pyrrole is mostly protonated once it reaches physiological conditions (89 % of nicotine protonated).¹¹⁸ Although this protonation assists in mimicking acetylcholine's quaternary ammonium ion, and therefore inhibits binding. It has a secondary effect of reducing nicotine's ability to cross the ion sensitive barrier which surrounds the central nervous system of insects.¹¹⁶ Imidacloprid however, like most other neonicotinoids, are less prone to protonation due to the conjugation of the imidazolidine ring through resonance of the nitroimino group. What the nitro substitute also confers, is a positive polarization due to its electron withdrawing nature. When combined, this produces a molecule capable of crossing the 'ion-impermeable' membrane, whilst still being able to hydrogen bond with the subunits in the nAChR.¹¹⁹

The nature of the nAChR in insects and mammals also furthers the explanation of neonicotinoid's affinity towards insect receptors, and *vice versa* for nicotine and mammals. The architecture of insect nAChRs are poorly understood when compared to mammalian nAChRs, so a full picture can not be easily ascertained. Although, by labelling a neonicotinoid with a radioisotope of iodine it was possible to define the subunit where binding occurred.¹²⁰ The radioisotope studies, when viewed in conjunction with gene co-factor studies, and later crystallographic studies, show important distinctions in the binding of nicotinoids and neonicotinoids.^{121,122} *Casida et al* illustrated the importance of the nitro group in imidacloprid's selectivity, by using both radiolabelled neonicotinoids and X-ray crystallography (*figure 6*). Through the

use of a binding protein surrogate of the nicotinic receptor, different bindings were seen for nicotinoids and neonicotinoids. For both neonicotinoids and nicotinoids, the pyridyl unit was positioned the same within the receptors, whereas only for the neonicotinoids does the imidazolidine interact with loop C tyrosine-188. Additionally, the oxygen of the nitro group shows affinity for the alcohol and thiol groups of cysteine-190/serine-189 respectively. Importantly, the previously stated serine-189 in the binding protein equates to a glutamate in a vertebrate's neuronal $\alpha 4$ and $\alpha 7$ nAChRs. The substitution of the hydrogen bond donating alcohol of serine to the electron rich carboxylate of glutamate, can therefore lead to repulsion of the nitro group and disrupt binding.¹²¹ This also explains nicotinoids inverse effect, and equally why substituting the nitroimine or cyanoamide to an amine reproduces the 'nicotinoid' bias towards mammal receptors.¹²³

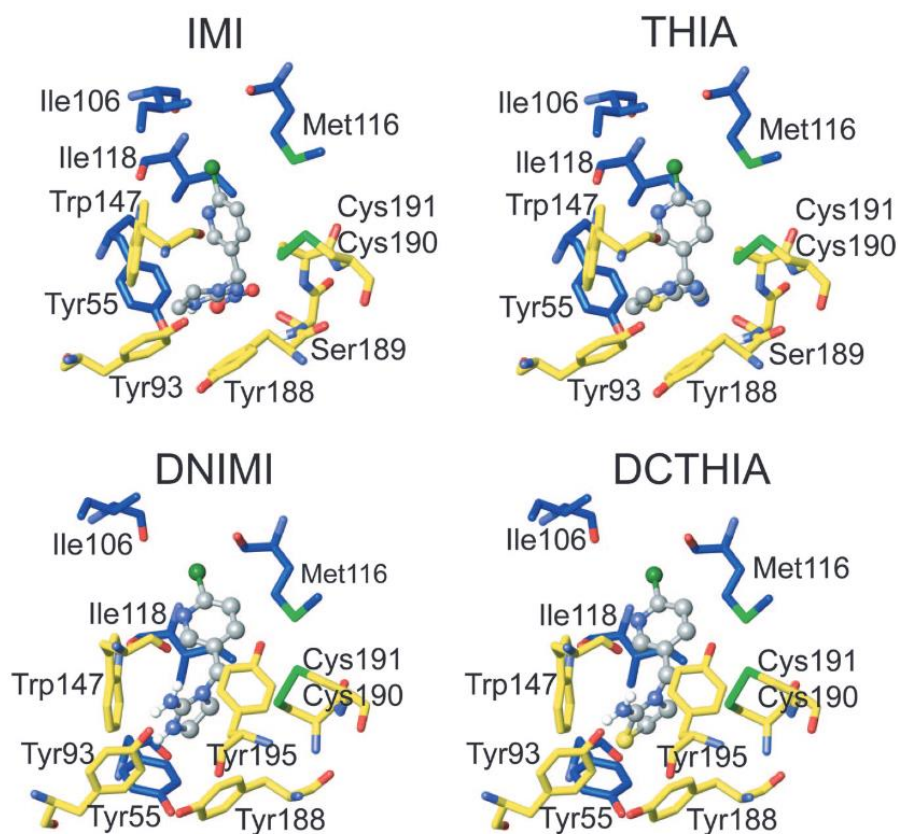


Figure 6. Models showing the pharmacophore of neonicotinoids: imidacloprid (IMI) and thiacloprid (THIA) and nicotinoids: desnitro imidacloprid (DNIMI) and descyanothiacloprid (DCTHIA) with the binding site of the acetylcholine binding protein. *Figure reproduced with permission from Casida et al.*¹²¹

2.3.4. Transformation of Neonicotinoids

The degradation of neonicotinoids differs depending both on the neonicotinoid, and where and how the transformation is taking place. The routes of transformation can be broadly split into three categories for ease of description and classification: physical, biological, and chemical.

Physical transformation of neonicotinoids is dominated by photolysis. Laboratory studies show that photodegradation of neonicotinoids can occur as quickly as a few minutes, but also raise awareness to the difficulties of generalising these results to real-world examples.¹²⁴ For imidacloprid, the photoproducts were found to consist

mainly of the desnitro-imidacloprid and the urea-imidacloprid, with exact ratios differing based on the medium in which photolysis was trialled. For most solution studies however, desnitro-imidacloprid formed the major photolysis product.^{125–127} The mechanism for the transformation of imidacloprid with light is not fully understood. One computational model suggests it proceeds *via* photodissociation of NO₂ which can recombine with the radical desnitro-imidacloprid; forming urea-imidacloprid and N₂O. Alternatively, protonation of the radical desnitro-imidacloprid will yield desnitroimidacloprid, releasing NO₂.¹²⁸ However when in protic organic solvents, other mechanisms have been proposed; an OH radical is released with the oxygen from imidacloprids' nitro group and a proton from the surrounding organic solvent. Where it can either release further NO forming the desnitro-imidacloprid, or release N₂ and perform an intramolecular rearrangement forming the urea-imidacloprid.¹²⁶ In an aqueous media however, this mechanism is altered after the initial release of the OH radical. Water is proposed to react with the imidacloprid's remaining NO group forming desnitro-imidacloprid and HNO₂, and after subsequent photodissociation of the recently formed NH₂, and further reaction with water, urea-imidacloprid and NH₃ are formed (*figure 7*).¹²⁷

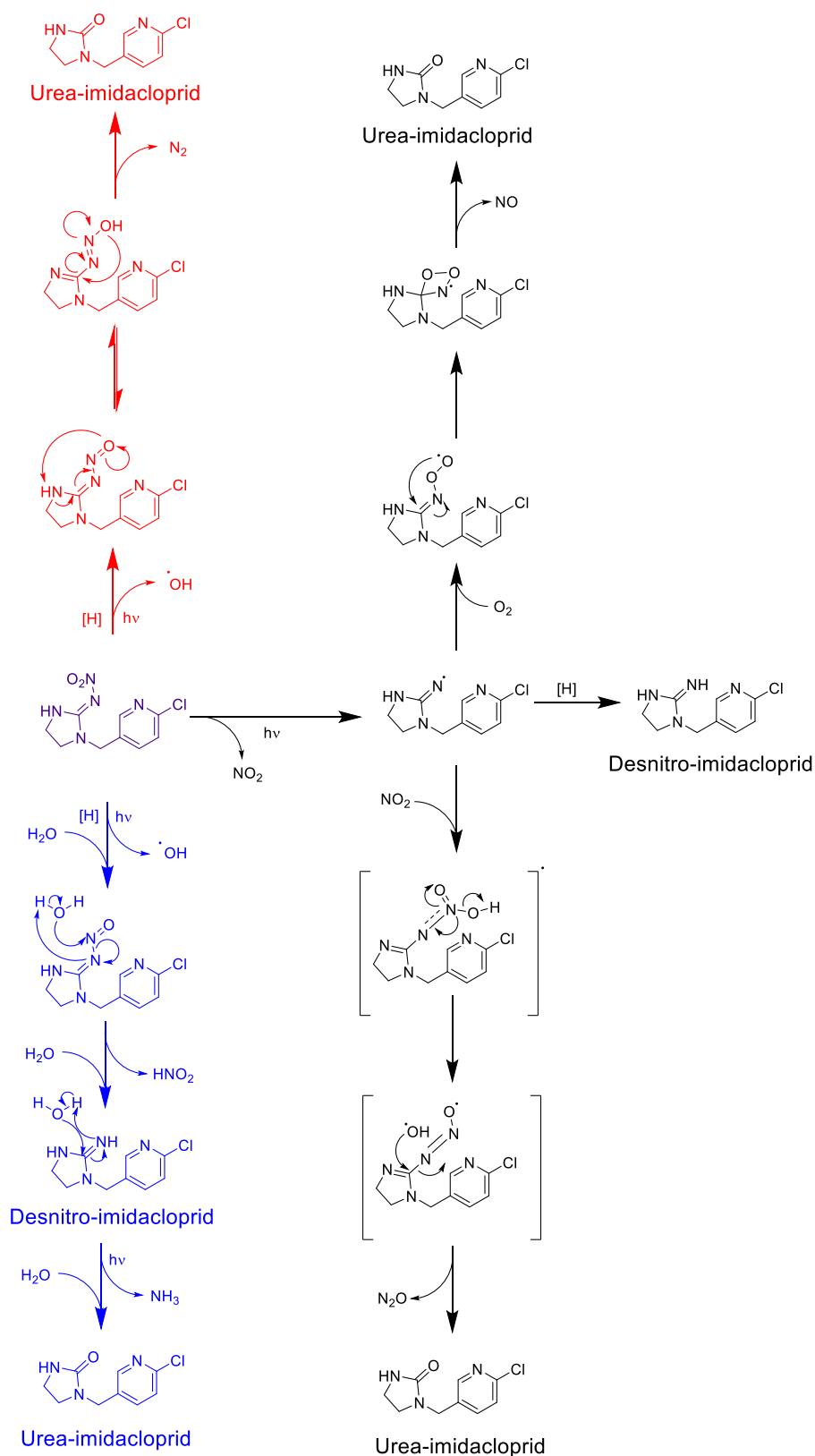


Figure 7. Proposed mechanisms for the photoinduced transformation of imidacloprid to urea-imidacloprid and desnitro-imidacloprid. Mechanism in blue represents in aqueous conditions, red in protic solvents, and black for solid phase.^{126–128}

Hydrolysis of neonicotinoids is seen as the most environmentally significant chemical reaction, due to their sustained presence in natural water systems. However, aside from hydrolysis, neonicotinoids will also react similarly to their parent compounds, for example; alkylation and halogenation of the pyridyl and/or imidazolidine nitrogen.^{129,130} Hydrolysis at pH ~ 7 is rare, in fact it is reported only thiamethoxam will undergo hydrolysis at neutral pH, and only after 29 days.¹³¹ Base-catalysed hydrolysis however, is seen with other neonicotinoids (nitenpyram, imidacloprid, clothianidin and acetamiprid) (*figure 8*). For all neonicotinoids the products formed after hydrolysis are primarily urea derivatives, and hydrolysis only occurred at meaningful rates with a pH above 10.¹³² The high pH needed may give the illusion that hydrolysis is not an environmental risk, however the base catalysed hydrolysis products of thiamethoxam have been found in naturally alkaline soil samples.¹³³ Equally, water conditioning treatments that use lime softening have been observed to produce the urea-neonicotinoid products.¹³⁴

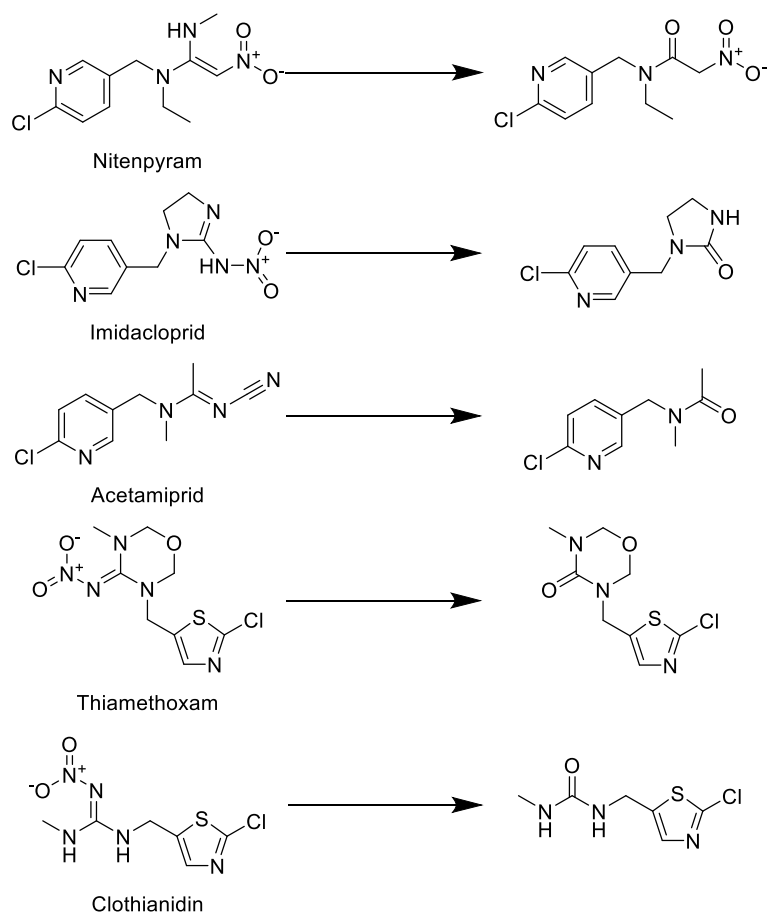


Figure 8. Base catalysed hydrolysis products of five neonicotinoids, identified by *Arnold et al.*¹³²

2.3.5. Metabolites of Neonicotinoids

The biotransformation of neonicotinoids has been observed and studied in numerous living organisms. The number of possible metabolites increases exponentially within biological transformations, but reoccurring themes are seen within initial products; with the urea and desnitro products again being major products.

The understanding of the transformation of neonicotinoids *via* plants is surprisingly little understood. Even though the primary use of neonicotinoids is in agriculture and plant maintenance, only a few studies have investigated the neonicotinoid by-products of plant metabolises. One example compared the metabolites of seven neonicotinoids in spinach seedlings and mice. Remarkably, similar results were seen within the plant

and mammal candidates for phase I metabolises, but as expected; unique phase II metabolites were formed.¹³⁵ Just as for photodissociation; desnitro-imidacloprid and urea-imidacloprid were formed *via* the reduction of the nitro group, but olefination, hydroxylation, demethylation, sulfoxidation and dichlorination were also noted. In total over 22 metabolites were observed unique to plant metabolises, including amino acid conjugates and glucosides.

Microbes have a crucial role in the breakdown of neonicotinoids in soil. The transformation products of imidacloprid and thiamethoxam, were detected after exposure to soil containing the bacterium *Pseudomonas* sp. 1G.¹³⁶ Interestingly, the degradation only occurs when the neonicotinoid is not the sole carbon source. These results are further seen, when seven other bacterium were shown to transform imidacloprid when a secondary carbon source was added.¹³⁷ After microbial metabolises, desnitro-imidacloprid and urea-imidacloprid are again detected, but additionally 5-hydroxyl imidacloprid and olefin-imidacloprid were produced, that latter of which showed high insecticidal activity.¹³⁷ For the cyano containing neonicotinoids (acetamiprid and thiacloprid), the major products are the amine derivatives, which proceed *via* a carbamoylimine or amide intermediate.^{138–140}

In mammals, the liver is where most of the metabolises of neonicotinoids occurs, with the most important enzymes being; cytochrome P450 enzymes, and aldehyde oxidase.^{141–143} Several metabolism pathways are possible for neonicotinoids, *via* several previously mentioned core reactions. Reduction of the nitro-group such as in imidacloprid, yields the urea and desnitro products. The cyano group, as for thiacloprid, can be hydrolysed or cleaved forming the *N*-carbamoylimine and guanidine respectively. Also, dealkylated, olefinated and hydroxylated metabolites have been found in mammals.¹³⁵ The last stage of biotransformation in mammals is unique to

each neonicotinoid subtype. For chloropyridinyl containing products (imidacloprid, nitenpyram, thiacloprid and acetamiprid) 6-chloronicotinic acid is the last major metabolite formed. The chlorothiazole derivatives (thiamethoxam and clothianidin) ultimate biotransformation is to 2-chloro-1,3-thiazole-5-carboxylic acid. Finally, dinotefuran will form furoic acid, and each of these metabolites will be excreted mainly through the urine after conjugation to either glucuronic acid or glycine. Complete biotransformation however, does not regularly occur in mammals, and multiple metabolites, and equally their parent compounds can be found in the blood, liver and urine.^{144,145} The amount of the parent compound unchanged in the urine depends largely on the neonicotinoid, but also on the species, with for example, clothianidin being metabolized significantly faster in rats compared to cats and dogs.^{143,146}

2.3.6. Toxicity of Metabolites

Arguably, the biggest risk to human health for neonicotinoids arises not from the parent compounds, which as previously discussed have excellent selectivity towards insects. The risk, however, is mainly determined by the metabolites that are formed either *in vivo* or by other transformation pathways. Perhaps the greatest example of this is the relative toxicity of imidacloprid and one of its main metabolites; desnitro-imidacloprid. Desnitro-imidacloprid as previously discussed, is the metabolite of imidacloprid formed after cleavage of the nitro group. The removal of the electronegative nitro 'tip' and revealing of the electron poor amine largely transforms the binding properties of the molecule.¹²³ Ultimately, the conversion to desnitro-imidacloprid grants the neonicotinoid with nicotinoid properties, and as such has a similar pharmacokinetic profile to (S)-Nicotine.¹⁴² This change in toxicity can also be seen in the descyano transformations, in thiacloprid for example; where the removal of the cyano group increases the mammalian selectivity *via* the subsequently formed primary amine.¹²³

The vast toxicological differences between the parent compounds and some of their metabolites, combined with the socioeconomic requirement for pesticides in agriculture, gives strong incentives to develop systems to better control neonicotinoids.

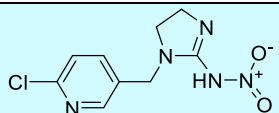
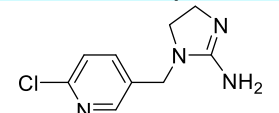
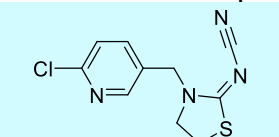
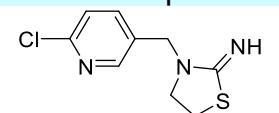
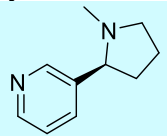
Compound	IC ₅₀ Insect nM	IC ₅₀ Mammal nM	LD ₅₀ Insect µg/g	LD ₅₀ Mammal mg/kg	ref
 Imidacloprid	4.6	2600	0.02- 0.07	40-50	114,122,147
 Desnitro-imidacloprid	1530	8.2	>5	6-9	114,122,147
 Thiachloprid	2.7	860	0.03	25-30	114,122,147
 Descyano-thiachloprid	200	4.4	>5	0.7-1.5	114,122,147
 (S)-Nicotine	4000	7.0	>50	6-8	146,122,147

Table 2. Table showing the half maximal inhibitory concentration (IC₅₀) and the median lethal dose (LD₅₀) of neonicotinoids; imidacloprid and thiachloprid and their metabolites.

2.3.7. Encapsulation of Neonicotinoids

An alternative to degradation or destruction of neonicotinoids is selective removal *via* encapsulation. For a molecule to be able to selectively encapsulate the neonicotinoid there are several inherent properties that are imperative. Favourable intramolecular bonds or interactions between the neonicotinoid and its host will of course be necessary for efficient binding, but factors such as cavity size and shape are also

fundamental. Therefore, due to these demands, only a few molecules have been shown to grant efficient encapsulation of the pesticide. One method of encapsulation uses macrocycles, these molecular rings contain a cavity, which depending on the macrocycle can range anywhere from 0.6-15 Å.^{147,148} One of the first examples of a neonicotinoid being encapsulated by a macrocycle, uses a calix[4]arene with sulfonate groups decorated around one of the rims.¹⁴⁹ Importantly though, this study focuses on the detection of acetamiprid, and not the encapsulation of the neonicotinoid, and as such no binding information is given. Nonetheless, when the calix[4]arene was adsorbed upon a cadmium tellurium quantum dot, the detection limit was extremely low 3.4×10^{-8} M suggesting strong binding.

Additional macrocycle and neonicotinoid binding studies used cyclodextrins, more specifically the β -cyclodextrin (β -CD) derivative containing 7 glucose subunits. The initial study into this partnership, explored the solid and solution state relationships between the host/guest complex (*figure 9*).¹⁵⁰ It was observed that in both solid state and within solution, acetamiprid and β -CD formed stable 1:1 complexes, and that the 6-chloro-3-pyridyl moiety is responsible for the binding in β -CD. This results suggests that other chloro-pyridinyl based neonicotinoids will have equally efficient binding.¹⁵⁰ Subsequent research using β -CD, reasserted the relationship between the macrocycle and chloro-pyridinyl neonicotinoids. Imidacloprid was shown to equally favour the cavity of β -CD, and by embedding the cyclodextrin-imidacloprid complex within a polymer network, controlled capture and release of the neonicotinoid could be achieved.^{151,152}

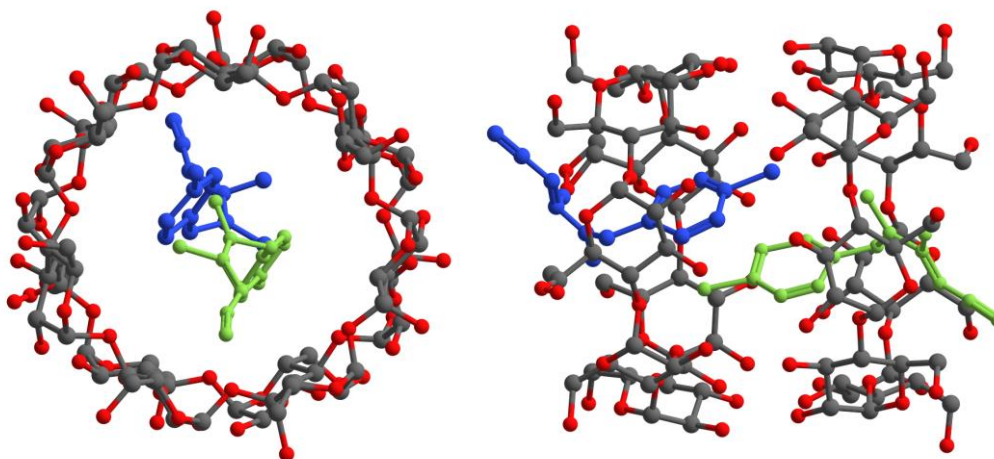


Figure 9. Top and side views of the β -cyclodextrin/ acetamidrid association, showing a (2:2) dimeric complex, with acetamidrid shown as blue and green, and hydrogens hidden for clarity.¹⁵⁰

Cyclodextrins were further employed, within a magnetic metal organic framework (MOF) containing system.¹⁵³ A copper MOF with a simple tridentate organic linker, was interlaced between layers of Fe_4O_3 and β -CD doped graphene oxide. The adsorption capacities of the material towards neonicotinoids, was then measured using high-performance liquid chromatography with tandem mass spectrometry. The adsorption capacities at 100 mg/L for acetamidrid, clothianidin, dinotefuran, imidacloprid, nitenpyram, thiacloprid and thiamethoxam, were 2.96, 2.88, 1.77, 3.11, 2.56, 3.30 and 2.88 respectively. Indicating moderate selectivity not just for, but also between the neonicotinoids. Additionally, another MOF designed for neonicotinoid capture was prepared from amino acids, and contained thioether based residues.¹⁵⁴ Three thioether derived calcium(II)/strontium(II)-copper(II) based MOFs were synthesised, where different amino acids were able to be incorporated within the structure; altering the hexagonal channels. The most successful, comprised of the

methionine and methyl cysteine amino acids, was reported to be able to fully capture acetamiprid and thiacloprid within 30 seconds.

2.4. Results and Discussion

This research focussed on measuring the relative binding and selectivity of pillar[*n*]arenes towards several nicotinoids and neonicotinoids. Pillar[*n*]arenes were selected as the macrocycle host due to their ease of synthesis and functionalisation, stability against photolysis and thermolysis, and their known propensity towards encapsulating electron poor guests. A series of pillar[*n*]arenes were synthesised using previously reported methods. Equally, the nicotinoid and neonicotinoid guests were synthesised using modified procedures based on known synthetic routes.

2.4.1. Synthesis of Pillar[*n*]arenes

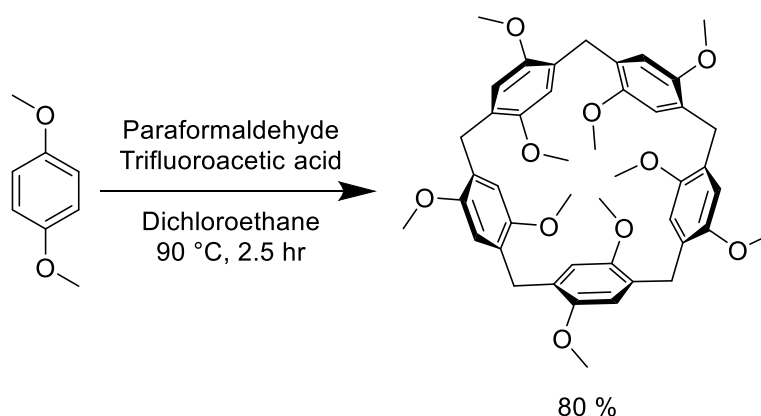


Figure 10. Synthetic route for dimethoxypillar[5]arene.

The first pillar[*n*]arene; dimethoxypillar[5]arene (DMP[5]A), was synthesised using a modified route developed by *Boinski and Szumna* (figure 10).¹⁵⁵ This direct synthesis method uses the dimethoxybenzene subunit, paraformaldehyde, and trifluoroacetic acid as the acid catalyst. The solvent used was dichloroethane, the choice of solvent was extremely important as the complexation between the solvent and the resulting

macrocycle, provides the thermodynamic stability required for efficient pillar[5]arene synthesis. This method was chosen primarily due to its consistent high yields, but equally, due to the change from Lewis acid to trifluoroacetic acid, the reaction no longer requires moisture free conditions. The DMP[5]A could be subsequently purified, by dissolving the post-reaction solid in 1:1 ratios of chloroform and acetone and collecting the solid formed thereafter.

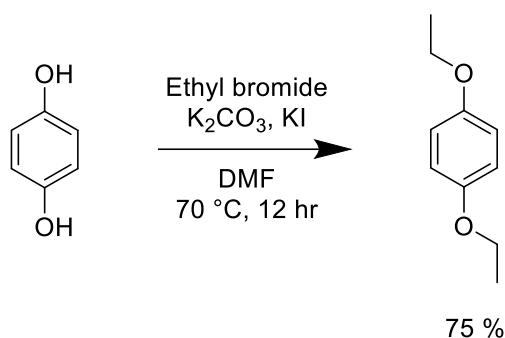


Figure 11. Synthetic route for the pillar[5]arene subunits, in this example diethoxybenzene. With potassium carbonate (K₂CO₃) as the base, potassium iodide (KI) to increase reactivity, and N,N'-dimethylformamide (DMF) as the solvent.

For the pillar[5]arenes with larger alkyl chains; ethyl and propyl, the subunit had to first be synthesised *via* hydroquinone and an alkyl halide (*figure 11*). The synthesis of the alkoxybenzenes is performed *via* a Williamson ether synthesis.¹⁵⁶ Wherein, the hydroquinone's alcohol groups are deprotonated with an inorganic base, in this case potassium carbonate. A subsequent concerted S_N² nucleophilic substitution occurs between the nucleophilic alkoxide, and the alkyl chain, with the halide acting as a leaving group. Ultimately forming the dialkoxybenzene and a sodium halide salt. The reaction rate was increased by use of potassium iodide. Potassium iodide and the alkyl bromides perform halogen exchange *via* the Finkelstein reaction, and due to the iodides increased ability as a leaving group, the etherification proceeds using lower temperatures and at a faster rate.

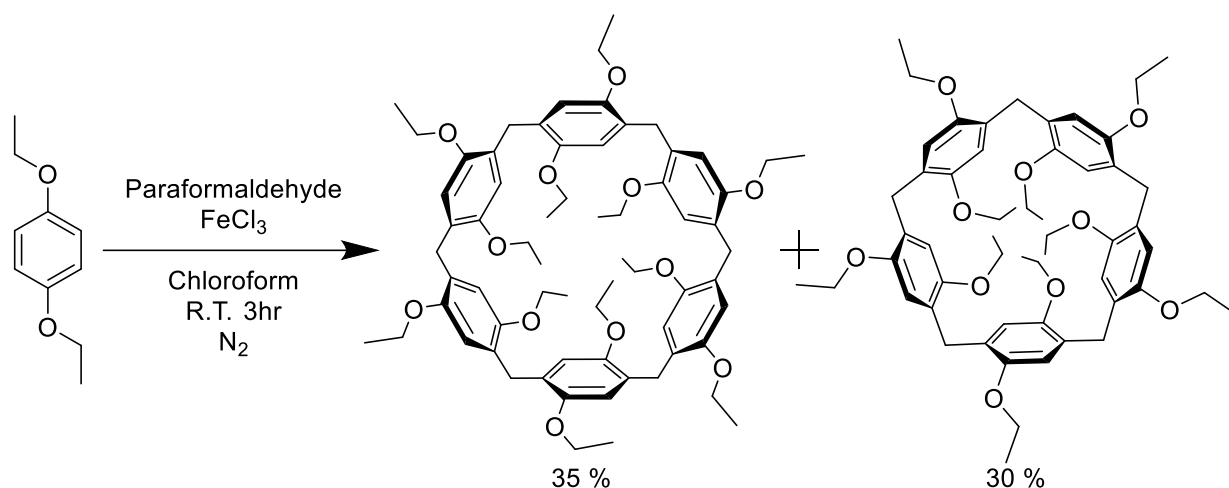


Figure 12. Synthetic route for pillar[6]arenes, showing yields for both the 6 and 5 subunit derivatives.

Diethoxypillar[5]arene (DEP[5]A) and dipropoxypillar[5]arene (DPP[5]A) were synthesised using a method adapted from *Liu et al.*¹⁵⁷ The alkoxy benzenes were mixed with a 3 times excess of paraformaldehyde or trioxane in dichloromethane. Iron chloride was consistently used as the Lewis acid, but several other acids were trialled, including trifluoroacetic acid. This acid was ultimately chosen due to higher yields being found, when compared to the previously stated trifluoroacetic acid for the longer alkyl subunits.

The larger diethoxypillar[6]arene (DEtP[6]A) was synthesised in a similar method to its 5 membered counterpart. However, the solvent was altered from dichloromethane to chloroform (*figure 12*). Chloroform, as previously mentioned, increases the selectivity towards larger pillar[*n*]arenes compared to dichloromethane, due largely to dichloromethane's strong templating effects towards the synthesis of the 5 membered pillar[*n*]arene. The chloroform solvated synthesis produced pillar[*n*]arenes of sizes up to 12 subunits, as seen by MALDI-TOF. However, when purification with column chromatography of the pillar[*n*]arene was performed, only pillar[5]arene and

pillar[6]arene were isolated, due to the difficulties in purifying ≥ 7 membered pillar[*n*]arenes.

2.4.2. Synthesis of Alkylated Nicotine's

For binding and selectivity measurements for pillar[5]arene and nicotinoid guests, careful consideration needed to be taken to find an alkylated guest which is cationic, but still highly chloroform soluble. Therefore, a series of mono- and di-alkylated cationic nicotine's were synthesised, using methods adapted from *Heckel et al* and *Whidby et al.*^{72,73}

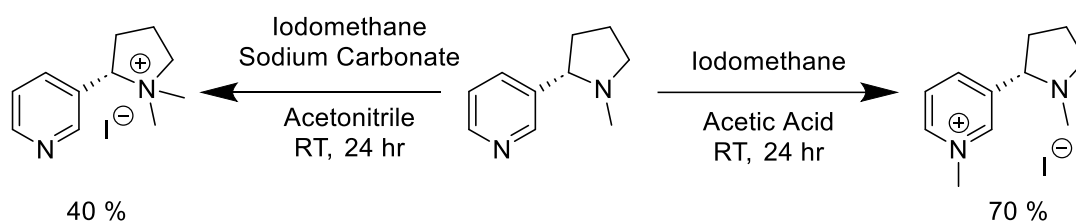


Figure 13. Synthetic route for both N'-methylnicotinium and N-methylnicotinium from nicotine.

There were several candidates for the cationic nicotine, but due to several factors *N*-ethylnicotinium was chosen. Logically, the initial cationic nicotine's were the methylnicotiniums. Both the pyridyl methylated and pyrrolidyl methylated nicotine's were synthesised with methods adapted from *Whidby et al.*⁷² Both nicotine derivatives were successfully synthesised with iodomethane, however solubility in chloroform was low at the high concentrations needed for the NMR titrations. This problem was further exacerbated when both nitrogen's were methylated, the solubility in chloroform was greatly reduced, even with anion exchange to hexafluorophosphate.

To aid in solubility, a dodecylated nicotine was synthesised from (*S*)-nicotine and dodecylbromide, and although solubilities in chloroform were adequate, the NMR of the product was inappropriate for host-guest studying. This was due to the protons in

the large dodecyl chains covering the nicotine peaks, therefore hindering the ability to measure peak shifts before and after adding the host. Additionally, the dodecyl nicotine was a viscous oil which proved difficult to handle. Nevertheless, the dodecyl nicotine derivative did show interesting properties when used in co-crystallisation experiments with pillar[5]arene in chloroform. The assembled structure after the crystallisation of DMP[5]A with the dodecyl nicotine, was the herringbone structure. Although not unique, this structure is usually only found when polar aprotic solvents such as acetone or acetonitrile are used as co-solvents (with chloroform as the solvent). Whereas, when alkyl solvents such as hexane are used, this will normally confer a 1D channel conformation. Furthermore, the rate in which crystallisation occurs with the dodecyl nicotine is approximately 1 hour, whereas for acetone for example, it was found it would take at least a day for crystals to start appearing. Ultimately though, as previously stated, the dodecyl nicotine was not applicable for the host-guest titrations and binding studies, so other variants were trialled.

After several iterations, including those stated above, the alkyl nicotine most appropriate for this study was an ethylated nicotine, where the ethyl chain is attached *via* the pyridyl nitrogen (*figure 14*). The *N*-ethylnicotinium was synthesised by reacting iodoethane with a slight excess of (*S*)-Nicotine (1:1.5) in acetic acid, and the reaction mixture was stirred overnight at 50 °C. After removal of the acetic acid *in vacuo*, diethyl ether was used to wash away and remove excess (*S*)-nicotine, giving *N*-ethylnicotinium as a yellow solid. Although solubility in chloroform at this stage was satisfactory, anion exchange to a non-coordinating anion, namely hexafluorophosphate, was performed (*figure 15*). The crystal structure obtained from *N*-ethylnicotinium hexafluorophosphate shows retention of chirality of its (*S*)-Nicotine

parent, with the CH₃ in the ethyl chain facing parallel to the pyrrolidine's methyl group (figure 15). This is highlighted by the Flack parameter, which is reported as -0.01.

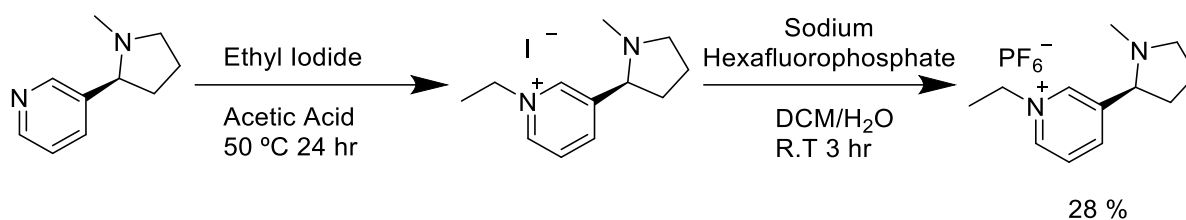


Figure 14. Synthesis route for *N*-ethylnicotinium hexafluorophosphate

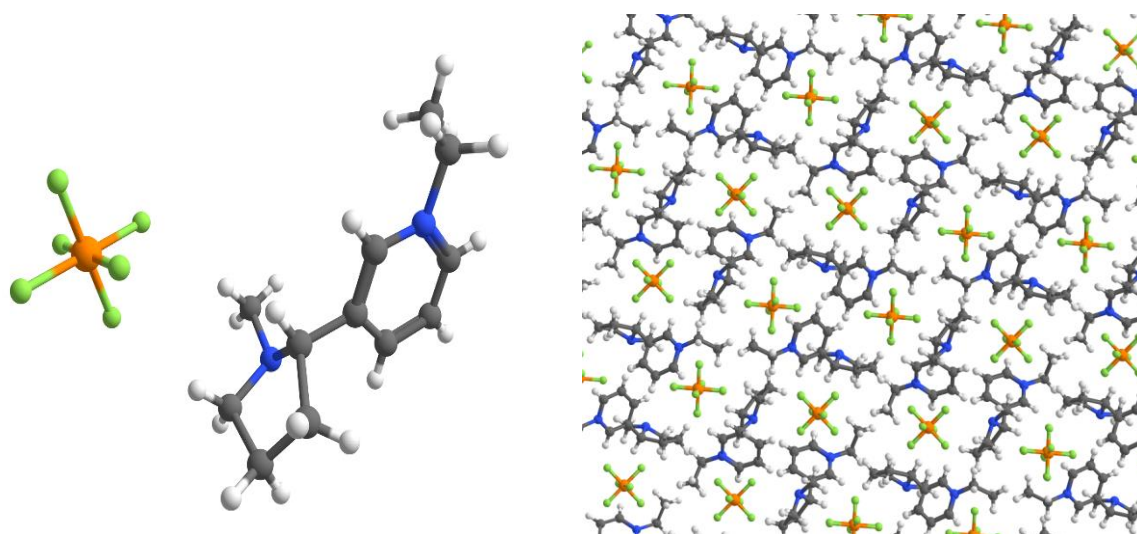


Figure 15. Crystal structure of *N*-ethylnicotinium hexafluorophosphate (left) packing conformation of *N*-ethylnicotinium.

The proton ¹H NMR of *N*-ethylnicotinium also confirms chiral specificity is maintained. This can be seen most clearly when assessing the pyrrolidines proton environments. For example, the two protons attached to the ortho-carbon (10 and 11), where proton 10 appears as a doublet of doublet of doublets at 3.29 ppm, with splitting arising from protons 11, 9 and 8. However, proton 11 appears initially as a quartet, but upon closer examination is determined as a triplet of doublets *via* equal splitting from protons 8 and 9, and splitting from proton 10, as confirmed by previous literature, COSY and proton-carbon HSQC NMR.⁷³ These large shift discrepancies of protons on the same

carbon due to chirality, are equally seen in the parent (*S*)-Nicotine, indicating retention of (*S*) chirality (figure 16).

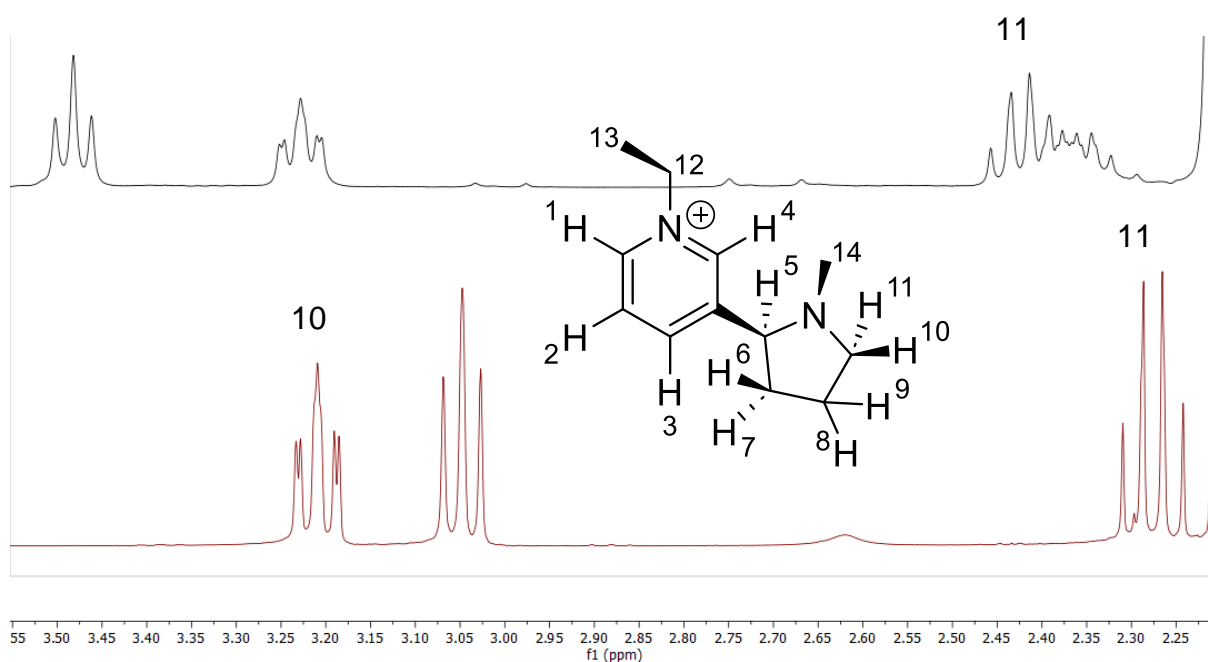


Figure 16. Partial Proton NMR spectra of *N*-ethylnicotinium (black) and (*S*)-Nicotine (purchased from TCI) (red). 400 MHz in CDCl₃.

2.4.3. Synthesis of Imidacloprid and Desnitroimidacloprid

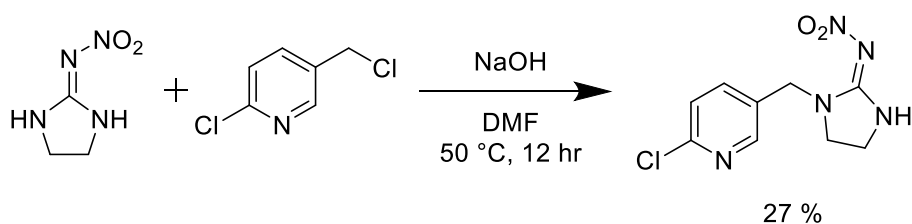


Figure 17. Synthetic route for Imidacloprid

The synthesis of imidacloprid proceeded *via* a previously described method (figure 17).¹⁵⁸ Where, 2-(nitroimino)imidazolidine is initially deprotonated with sodium hydroxide in *N,N*-dimethylformamide. 2-chloro-5-(chloromethyl)pyridine is subsequently added, and after acidification of the unreacted amine with hydrochloric

acid, imidacloprid was collected as a pale-yellow solid in high yields. Other methods are possible for the synthesis of imidacloprid; N-[(6-Chloro-3-pyridinyl)methyl]-1,2-ethanediamine and N-nitrodithiocarbamate can be reacted together without the use of base. However, due to availability or lack thereof, the aforementioned method was used.

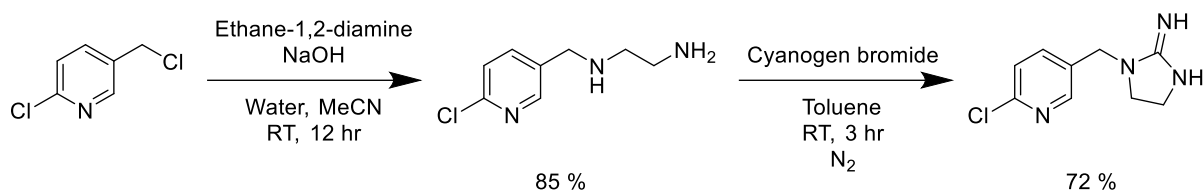


Figure 18. Synthetic route for desnitroimidacloprid.

Synthesis of desnitroimidacloprid did however use N-[(6-Chloro-3-pyridinyl)methyl]-1,2-ethanediamine, this precursor was synthesised *via* a method adapted from *Söftje et al (figure 18)*.¹⁵⁹ Wherein, an excess of ethane-1,2-diamine is deprotonated with sodium hydroxide, 2-chloro-5-(chloromethyl)pyridine is then added which after purification gives N-[(6-Chloro-3-pyridinyl)methyl]-1,2-ethanediamine as a yellow oil. Desnitro-imidacloprid was then synthesised *via* a method adapted from *Latli et al*.¹⁶⁰ Cyanogen bromide was reacted with the previously mentioned diamine precursor in degassed toluene, with desnitroimidacloprid hydrobromide precipitating as a white solid.

Due to cyanogen bromide's high toxicity and its reaction with water to form HBr and HCN, caution was taken when using the chemical. All manipulations were performed in a fumehood, with the reaction's nitrogen exit pipe inserted into a sodium hydroxide/bleach solution to decompose any potential cyanogen bromide waste.

2.4.4. Nicotine binding studies

To assess and measure the binding of the nicotine derived guests towards pillar[*n*]arenes, proton NMR was used. The preferential position of the guest within the macrocycle, and the strength of binding can be estimated using the relative shifts between the free guest and host-guest complex. Upfield shifting occurs when a guest is encapsulated within the macrocycle, this is due to an anisotropic shielding effect from the pillar[*n*]arenes aromatic rings. Equally, the outside alkyl rims of the pillar[*n*]arene will deshield nearby protons causing downfield shifts. Therefore, by measuring the relative shifts of the protons in the guest, an estimated complex structure can be formed. The host-guest interactions between the nicotinoids and a range of pillar[*n*]arenes (differing in alkyl chain length and number of subunits), were also compared to other macrocycles, namely benzo-24-crown ether and cyclodextrins.

(*S*)-Nicotine as previously discussed contains two nitrogen containing heterocycles, a pyridine and a methyl pyrrolidine. There are several literature examples of pillar[*n*]arene's association with neutral nitrogen heterocycles, suggesting the possibility of a complex forming between nicotine and the macrocycles in this study.^{161,162} The initial binding studies were performed by taking a ¹H NMR of a 1:1 20mM solution of the guest and the macrocycles. Before these shift differences were measured however, a fully assigned NMR of the free guest had to be established. There are literature examples of NMR assignments for (*S*)-nicotine.¹⁶³ However, due to the relative difficulty in assigning chiral molecules, and the age of the literature examples, both ¹H NMR and ¹³C JMOD NMR, in conjunction with 2D techniques; ¹³C-¹H HSQC, and COSY techniques were used to confirm these assignments (*figures 19 and 20*).

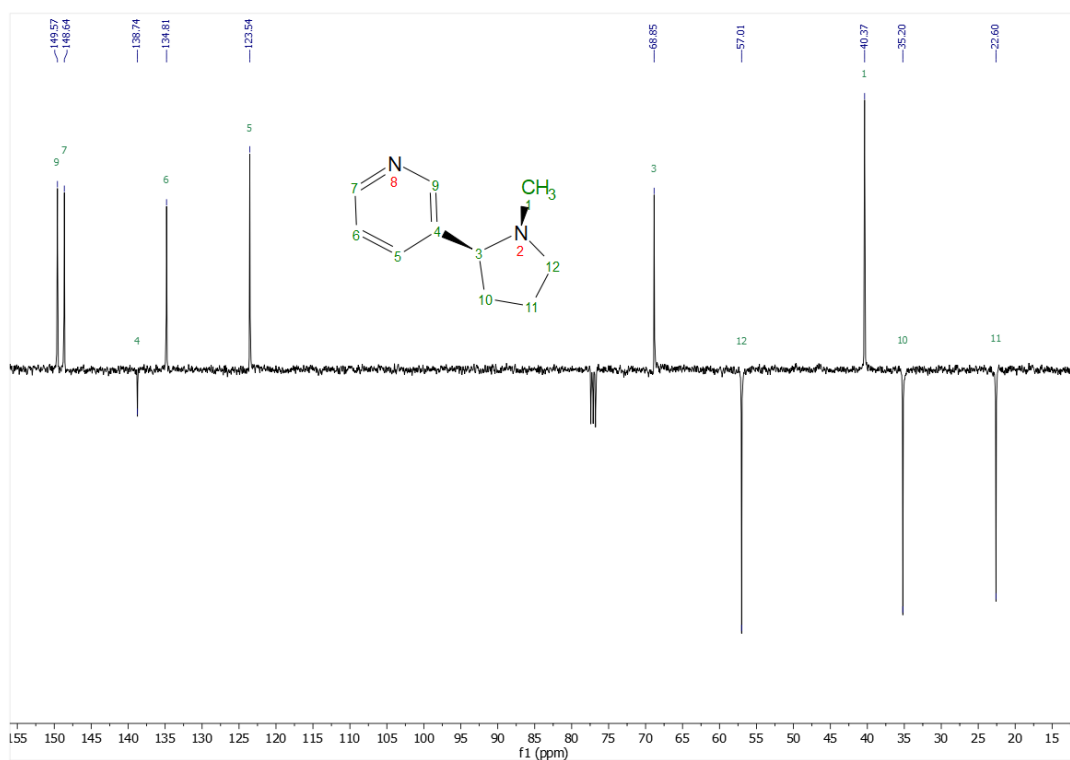
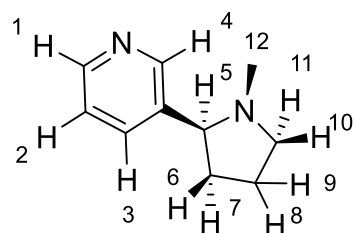


Figure 19. Assigned ^{13}C JMOD NMR of (*S*)-nicotine, 20 Mm in CDCl_3 (quaternary and CH_2 down, CH and CH_3 up)



E – 10 I – 12

F – 5 J – 8

G – 11 K – 9

H – 7 L – 6

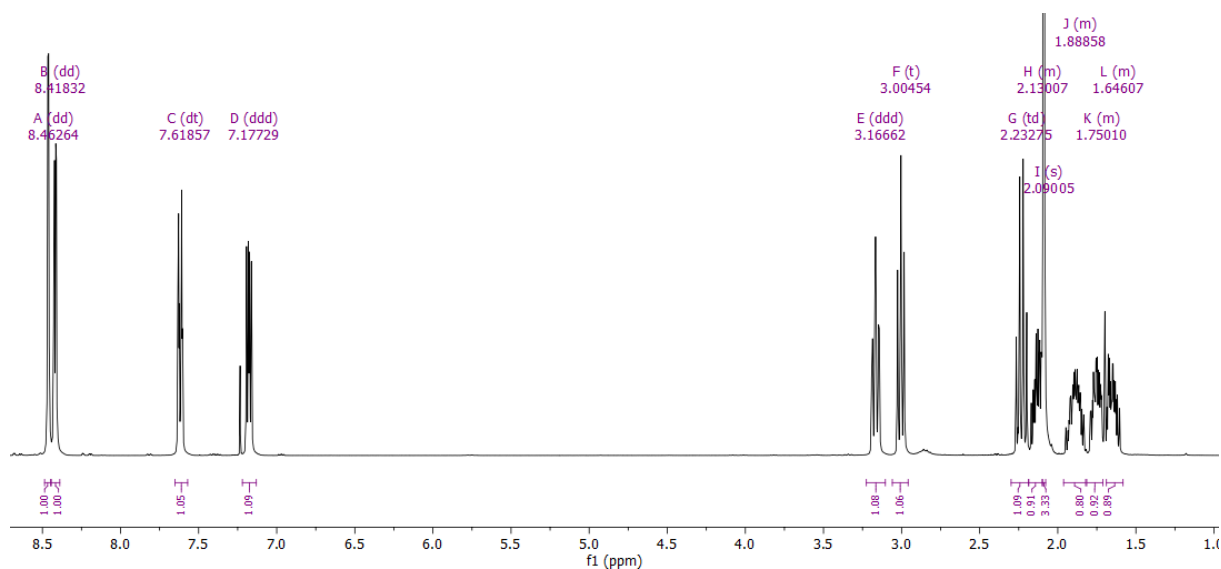


Figure 20. Assigned ^1H NMR for (*S*)-nicotine, 20 mM in CDCl_3 referenced to polydimethylsiloxane. (400 MHz CDCl_3 , – 7.23 ppm and water – 2.87, not labelled).

With all the previously stated NMR techniques, accurate assignments were made. When macrocycles hosts were added however, no significant upfield shifts were observed. The largest peak shift obtained was with DEP[5]A's interaction with pyridyl peaks 2 and 3 (-0.0016 and -0.002 respectively) (*figure 21*). Although this suggests a minor level of interaction, the shift values are too low to ascertain a definitive complex formation. Therefore, with the data obtained, it could be stated, that there is little, if any binding between (S)-nicotine and the pillar[*n*]arenes. Furthermore, when the relative shifts of each macrocycle are compared to each other, no logical trends are observed. Equally, there is no clear or obvious nicotine proton environment which are shifted more or less than others. These factors combined give strong evidence for no complexation occurring.

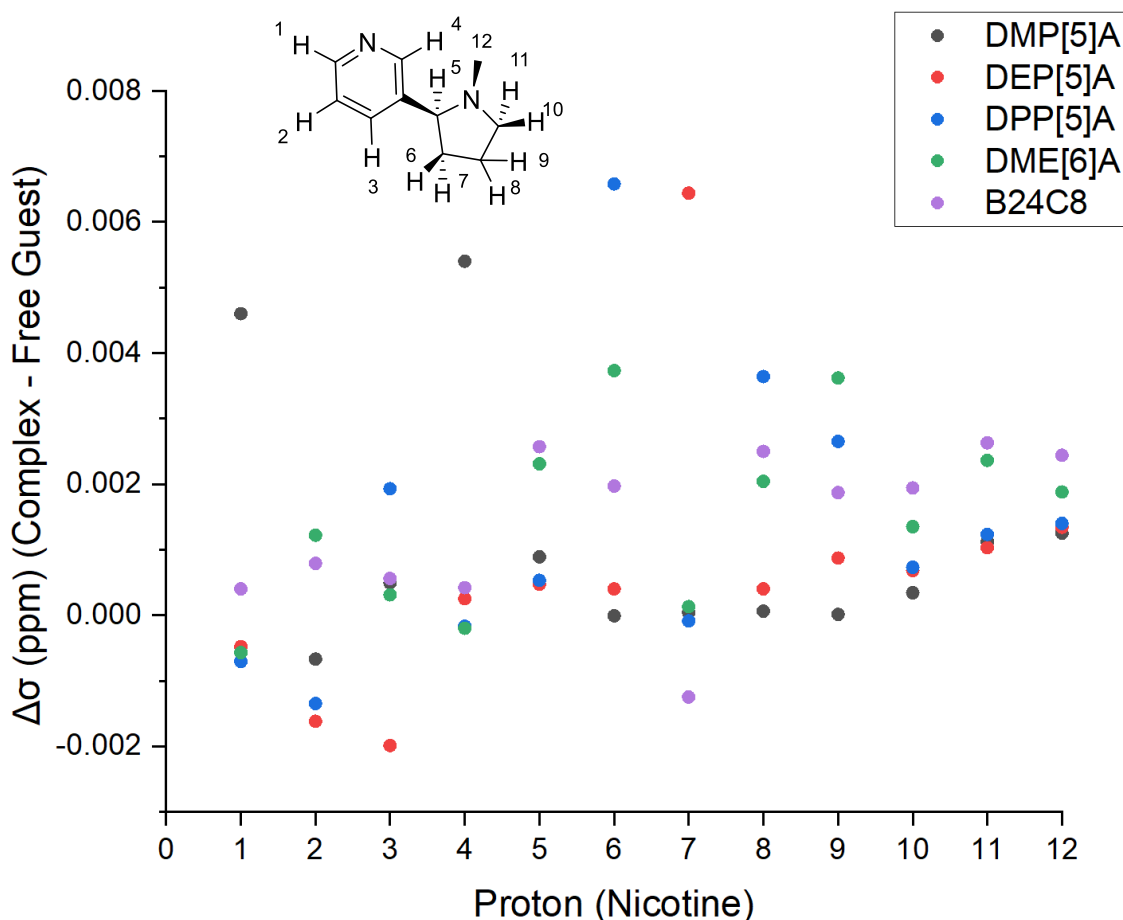


Figure 21. Graph showing the relative shifts of (*S*)-nicotine when in solution with a series of macrocycles. (400 MHz CDCl₃, 1:1 20mM (*S*)-nicotine : macrocycle). N.B. benzo-24-crown-8 (B24C8) used as a comparison for a different class of macrocycle.

However, when this experiment was repeated with the ethylated cationic nicotine, different results were observed (*figure 22*). Before proton shifts could be assessed though, a problem was encountered. Proton 8 was upfield shifted in the cation, becoming entrenched within the peak of the ethyl CH₃. Therefore unfortunately, an accurate value for proton 8 could not be established in *N*-ethylnicotinium, so was discarded from the measurements. Ultimately though, with the other proton on that carbon being measurable, the host/guest complex could still be assessed. Initial assessments of the complexes showed there was only one set of signals related to each proton environment in the guest. This is a good indication that the complexation

is fast and within the NMR time scale, which was a positive result when practical considerations for NMR titrations were assessed. Nonetheless, there is broadening of peaks, especially those which are heavily upfield shifted, obscuring some clarity of the doublets and triplets. This phenomena, as per literature, indicates either exchange of free and bound guests, or alternatively and more appropriately for this study; tumbling or rotating of the guest within the macrocycle.¹⁶⁴

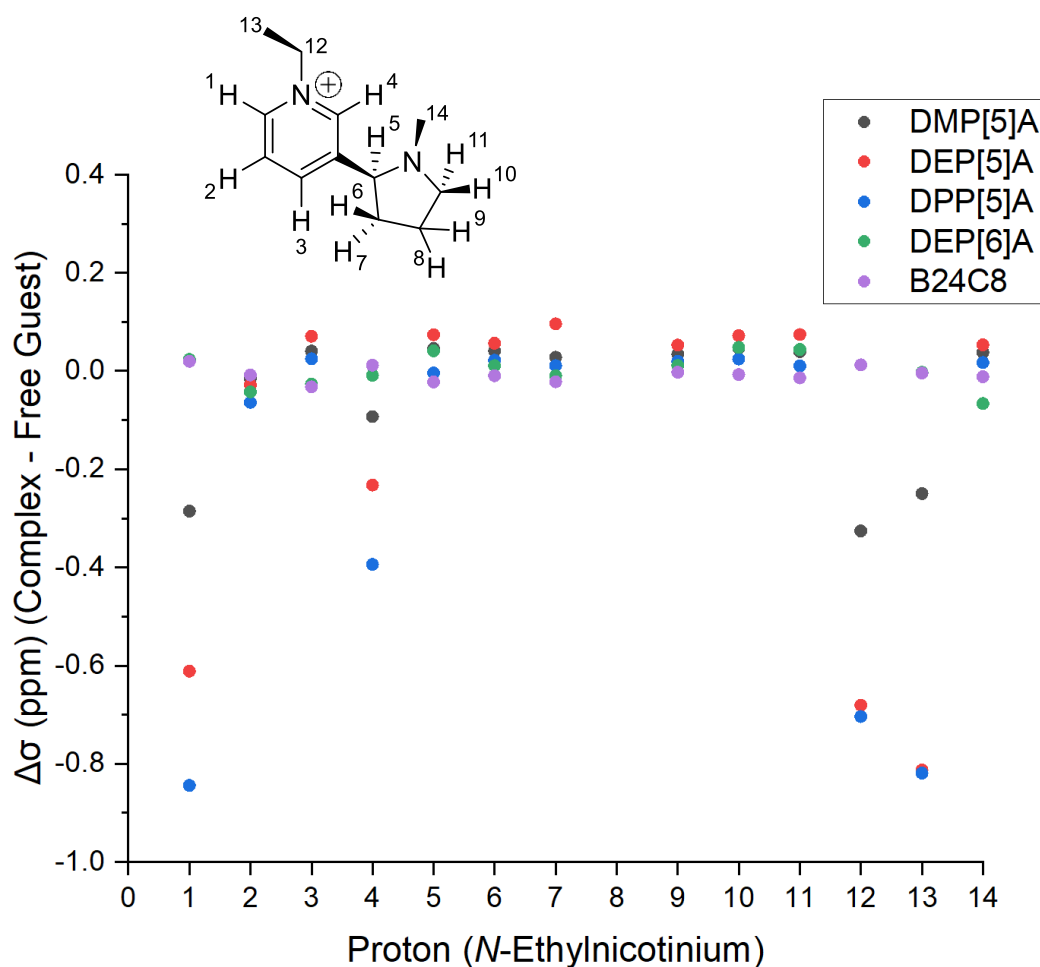


Figure 22. Graph showing the relative shifts of *N*-Ethylnicotinium hexafluorophosphate when in solution with a series of macrocycles. (400 MHz CDCl₃, 1:1 20mM *N*-Ethylnicotinium hexafluorophosphate: macrocycle).

There are two interesting trends that are observable within the data gathered. Firstly, there is a clear affinity for the macrocycle towards the pyridyls' cationic nitrogen. This

strong association has been previously noted, *Ogoshi et al* documented the inclusion complex formed between dihydroxypillar[5]arene and viologen, with an association constant of $1.20 \times 10^3 \text{ M}^{-1}$.⁵⁹ Therefore, these results are as expected, with pillar[5]arenes electron rich cavity and the nicotinium's positive charge. The second, and arguably more unexpected trend was observed with the effect of changing the alkoxy chain length for the pillar[5]arenes. The extent of guest upfield shifting proceeds *via* propyl > ethyl > methyl, which suggests a further interaction beyond the electronic contributions (*figure 22*). There could be several explanations for this trend, firstly van der Waals dispersion forces between the alkyl chains and nicotinium's ethyl or methyl group. Equally, CH/ π interactions between pillar[5]arene's alkyl chains and pyridiniums aromatic core will increase with the longer chain length. *Wang et al*, when studying the relative binding energies of different pillar[5]arenes and guests, highlighted the importance of the CH/N interaction for 'stabilizing host-guest complexes', which could also be a reasonable explanation.¹⁶⁵ Alternatively, it may not be a separate intramolecular force, but the longer alkyl chains acting as steric barriers to slow the rate of guest release. This effect should be identifiable *via* the relative broadening of the guest peaks, which, as stated previously is the direct result of free movement of the guest within the host. However, when comparing the broadness of the most upfield shifted peak, proton 1, the opposite effect is found (*figure 23*). This indicates it is most likely from a secondary intramolecular force, although establishing the actual force would involve further experiments with modified guests, those of which will be discussed in the conclusions.

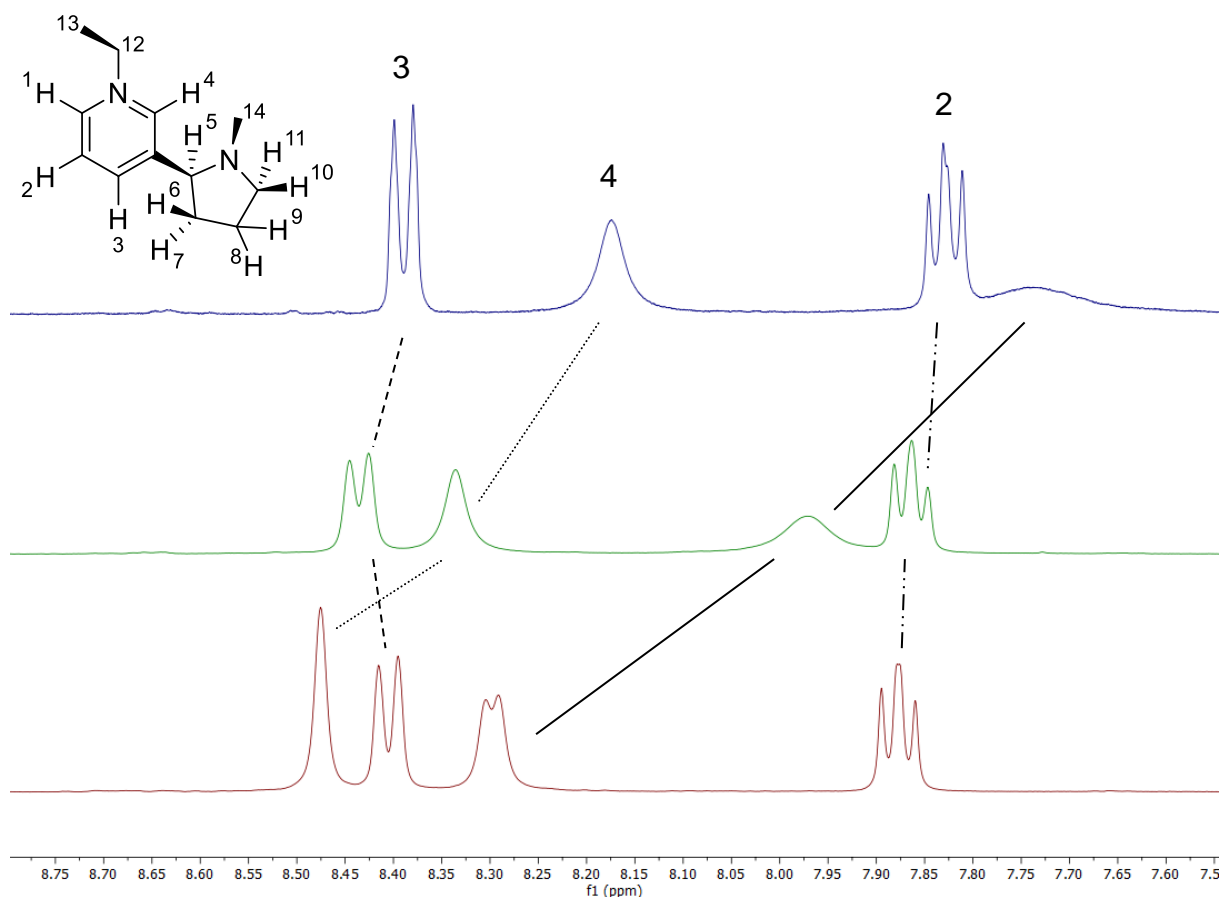


Figure 23. Comparison of the ^1H NMR spectra of *N*-ethylnicotinium with DPP[5]A (blue), DEP5A (green) and DMP[5]A red. (400 MHz CDCl_3 , 1:1 20mM *N*-Ethylnicotinium hexafluorophosphate: macrocycle)

There is also a large difference between the behaviours of the 5 and 6 membered pillar[*n*]arene. With a cavity difference of almost 2 Å, it would be reasonable to assume that the cavity of pillar[6]arene is too large for the pyridinium to form adequate coulombic interactions. *Ma et al* found similar results *and* reported an association constant of $(2.2 \pm 0.3) \times 10^2 \text{ M}^{-1}$ for perhydroxypillar[6]arene, 50 times less than perhydroxypillar[5]arene $(1.2 \pm 0.2) \times 10^4 \text{ M}^{-1}$ for their relative associations with paraquat. The explanation for this was that the cavity in the P[6]A was too large to form the stable host-guest complex. Equally, their crystal structure data showed no π -stacking between the larger macrocycle and the guest, π -stacking being seen as a large driving force for complexation.^{166,167}

2.4.5 Nicotinium NMR Titrations

To determine the association constant and stoichiometry for the pillar[*n*]arenes and *N*-ethylnicotinium complex, ¹H NMR titration experiments were performed. For the titrations the concentration of the host pillar[*n*]arenes were constant (1 mM in CDCl₃) and aliquots of guest (50 mM) were added so that equivalents of 0.2, 0.4, 0.6, 0.8, 1, 1.2, 1.4, 1.6, 2, 2.5, 4, 5 and 7, could be achieved. The lowering concentration of host due to dilution when adding the guest, were taken into consideration when calculating the binding constants. Each titration was repeated in triplicate to authenticate results (aside from DEP[5]A and *N*-ethylnicotinium where one dataset was unfortunately lost). Initially, higher concentrations were trialled, with the constant concentration of pillar[*n*]arenes at 20 mM, however precipitation of guest was observed above 4 equivalents, therefore the lower concentration of 1 mM was implemented. Polydimethylsiloxane (PDMS) was used as the NMR reference, the reason for this was firstly, chloroform could not be used as it is readily encapsulated within pillar[*n*]arene as is evident with the broad chloroform peaks in pillar[*n*]arene NMR spectra. Secondly, other more widely used references, for example, trimethylsilane, have the prerequisites for encapsulation with alkyls being a recorded guest motif. Therefore, with PDMS' long polymer chains, there is a greater chance of uncomplexed reference peaks, thereby making it more suitable.

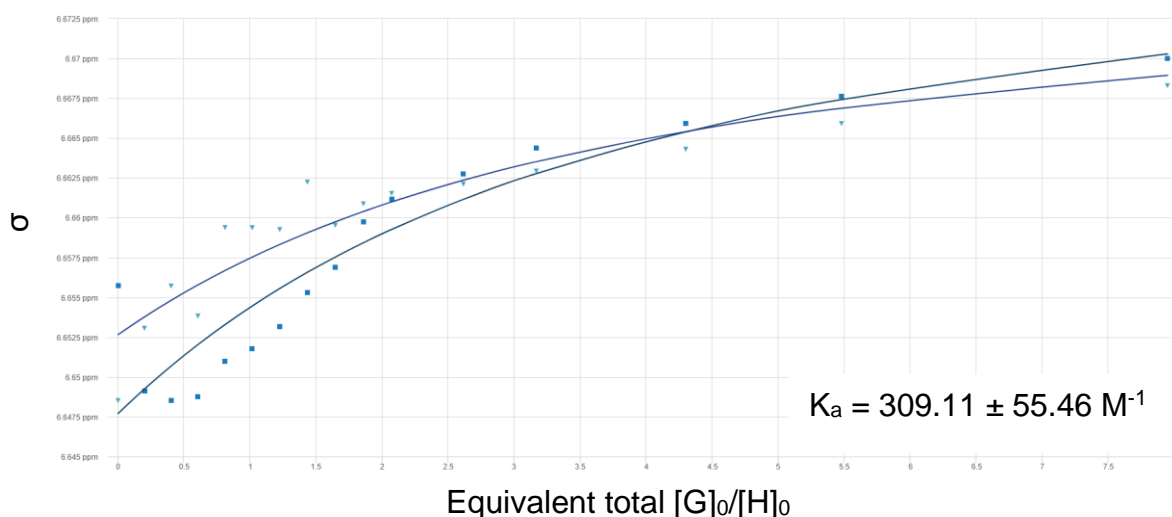


Figure 24. Graph showing the results of the titration between DEP[5]A and *N*-ethylnicotinium, with each of the two repeats fitted using the BindFit software to give the calculated binding constant and error.

To calculate the association constants (K_a) and stoichiometry the Bindfit application was used.^{168–170} Using the Nelder-Mead simplex algorithm the K_a value for DEP[5]A and ethylnicotinium was determined as $(3.09 \pm 0.55) \times 10^2 \text{ M}^{-1}$, with a 1:1 stoichiometric ratio (*figure 24*). The crystal structure of the guest suggests the angle between the cationic pyridyl, and the pyrrolidine's methyl group is 48° , which is a large disruption of the planarity that is key to successful complexation. For the larger DEP[6]A the results mirrored the previous upfield shift study, with the binding constant calculated as $(8.21 \pm 0.28) \times 10 \text{ M}^{-1}$. The large difference between the binding associations is assumably due to the larger cavity in pillar[6]arene, which as previously discussed can hinder efficient complexation, through the disrupting of key intramolecular forces.

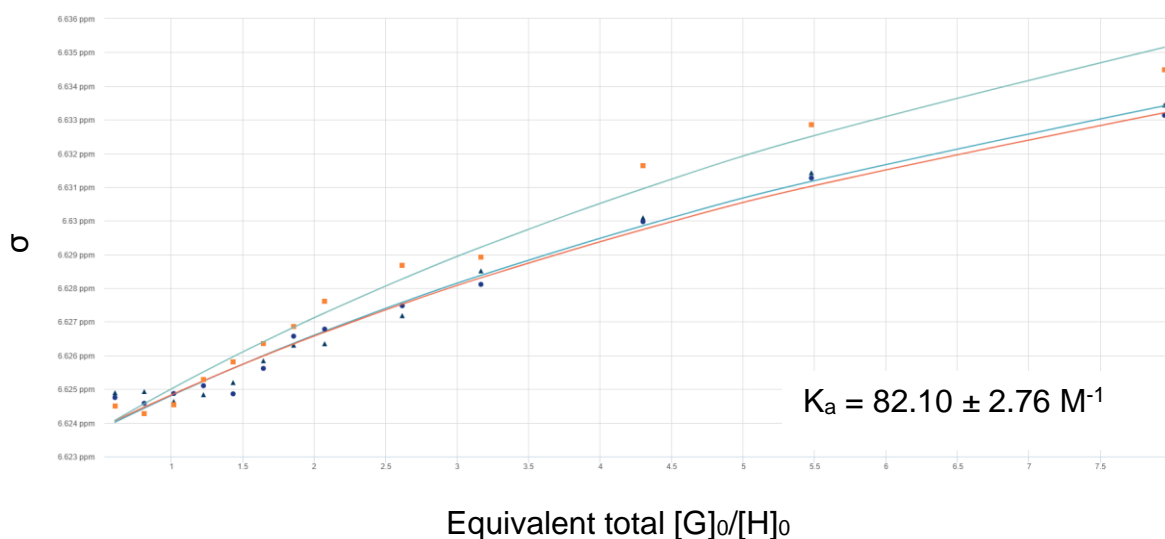


Figure 25. Graph showing the results of the titration between DEP[6]A and *N*-ethylnicotinium, with each of the three repeats fitted using the BindFit software to give the calculated binding constant and error.

2.4.5. Imidacloprid Binding Studies

Our second investigation compared the relative binding of imidacloprid, and its metabolite desnitro imidacloprid with pillar[*n*]arenes. The same macrocycles were used as in the nicotine studies, to ensure direct comparisons can be made between the two pyridyl species. For the initial NMR studies, 20 mM solutions of 1:1 imidacloprid : macrocycle in CDCl₃ were measured by ¹H NMR. The peaks of the imidacloprid were then compared to that of the free imidacloprid. As before a fully characterised NMR spectrum of imidacloprid was necessary, which due to imidacloprid not being chiral, was inherently simpler. It is however important to note that the spectra of imidacloprid in different solvents can differ largely. It was found that when comparing the pyrrolidinyl region in MeOD, DMSO and CDCl₃, large differences, especially in the NH peak occur. Methanol especially, as the NH peak does not appear, most likely due to deuterium exchange with the solvent. This unfortunately concluded with a discarding of cyclodextrin as a possible macrocycle comparison, as it was not chloroform soluble.

However, as all of the other macrocycles were soluble in chloroform this was not an issue, and dibenzo-24-crown-8 (B24C8) was used in place of cyclodextrin, due to its similar cavity size to pillar[5]arenes, and similar preferred cationic guests.¹⁷¹

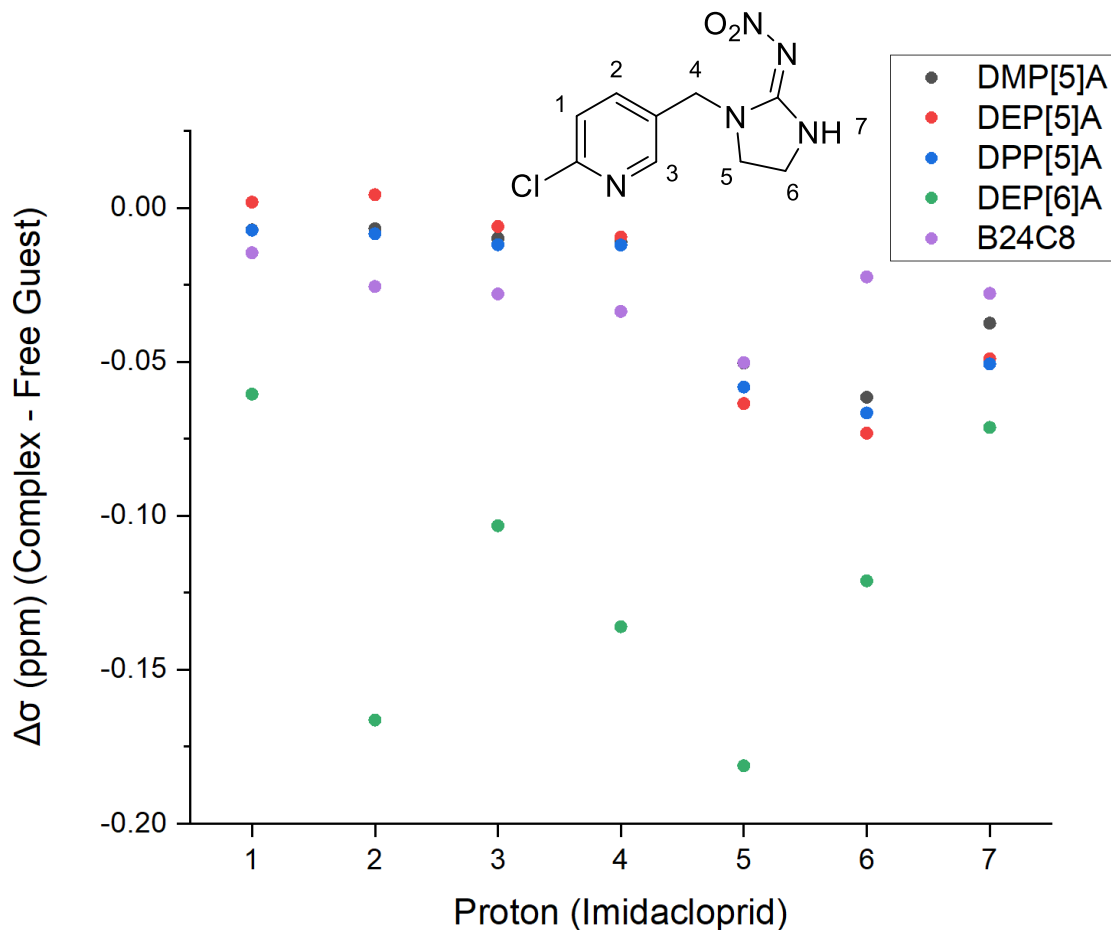


Figure 25. Graph showing the relative shifts of imidacloprid when in solution with a series of macrocycles. (400 MHz CDCl₃, 1:1 20mM imidacloprid : macrocycle).

For the pillar[5]arene's, unlike with *N*-ethylnicotinium there is no clear trend between the upfield shift and the length of alkoxy chain on the pillar[5]arene (*figure 25*). This suggests that some of the secondary alkyl intramolecular driving forces in the nicotinium are not present in the imidacloprid. Aside from the coulombic interactions arising from the positive charge on the pyridine, determination of the missing driving forces are difficult, especially as there are still opportunities in imidacloprid for alkyl van der Waals dispersion forces and CH/ π and CH/N interactions with the pyridine.

There is, however, a clear preference towards encapsulation of the imidazolidine of imidacloprid, compared to the pyridine. This can be explained by the relative electron density for imidacloprid, a computation study by *Moreira et al*, calculated the lowest electron density was found 'scattered on the guanidine group' (*figure 26*).¹⁷² Which, as previously stated would be the most probable point of encapsulation due to pillar[5]arenes electron rich cavity. This could also go towards an explanation of no trends being seen for the alkoxy chain length in the macrocycle. If the pillar[5]arene is only situated along the periphery of the imidazolidine, the longer alkyl chains may not be close enough to the guest to form intramolecular interactions, this being aided by the imidacloprids' methyl connection adding additional distance.

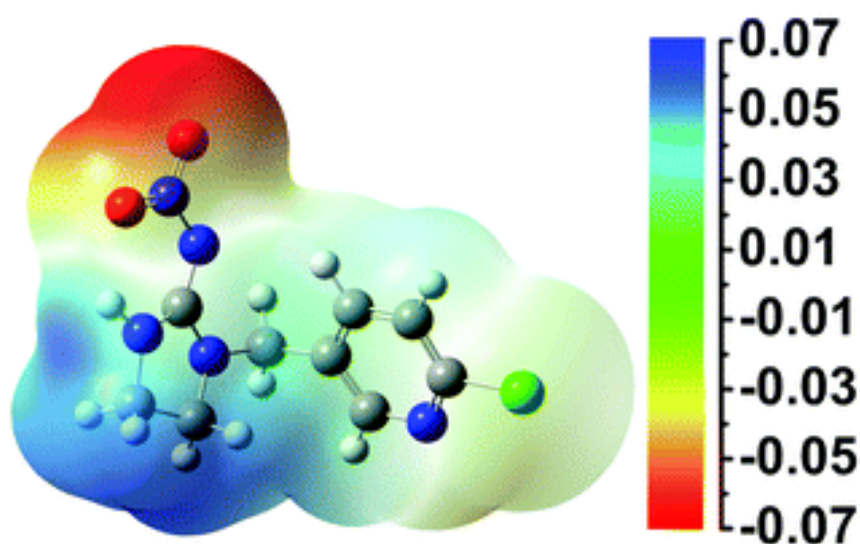


Figure 26. Total charge density for imidacloprid at pH 7.4, calculated using density functional theory employing the 6-311++G(d,p) basis set and M06-2X exchange correlation potential. *Figure reproduced with permission from Moreira et al.*¹⁷²

The upfield shift study indicates, pillar[6]arene shows a different biases towards imidacloprid, sitting over the middle of the molecule (*figure 25*). The increase in size for the 6 membered macrocycle cavity, does allow for larger molecules to become fully encapsulated. However, why this is somewhat surprising is by sitting over the middle

of the molecule, the pillar[6]arene has lower contact with the preferred electron poor pyrrolidine amine, and instead will put it within closer proximity to the electron rich nitro group.

2.4.6. Imidacloprid NMR Titrations

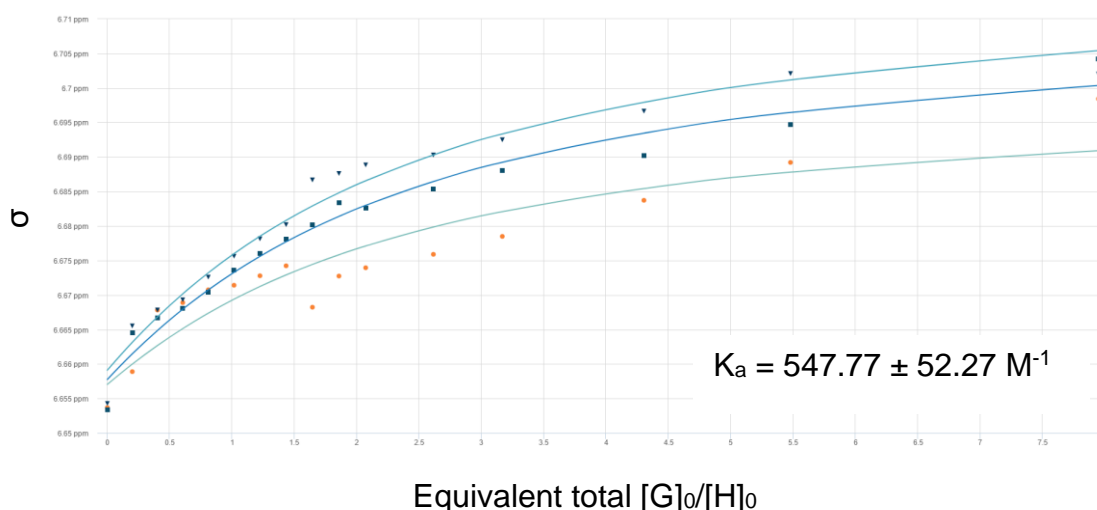


Figure 27. Graph showing the results of the titration between DEP[5]A and imidacloprid, with each of the three repeats fitted using the BindFit software to give the calculated binding constant and error.

The method for NMR titrations was the same as for *N*-ethylnicotinium; with 1mM solutions of diethoxypillar[*n*]arene in CDCl₃ and 50 mM solutions of imidacloprid being added so that equivalents of 0.2, 0.4, 0.6, 0.8 1, 1.2, 1.4, 1.6, 2, 2.5, 4, 5 and 7, could be achieved. Pillar[5]arene remarkably showed a binding association constant (K_a) of $(5.48 \pm 0.52) \times 10^2 \text{ M}^{-1}$, almost double that of the nicotinium (*figure 27*). This result contradicts the upfield shift study previously mentioned, where the imidacloprid peaks were shifted a maximum of -0.073 ppm, almost 10 times less than that of the nicotinium species. This firstly, highlights the importance in conducting and comparing titrations in conjunction with upfield shift studies. Equally, it proposes an issue with

defining the probability of the pillar[*n*]arene to guest association, as proportional only to electron density.

To supplement this, computational chemistry was employed to calculate the atomic charge distribution in (*S*)-nicotine, *N*-ethylnicotinium, and imidacloprid (*table 4*). Mulliken population analysis and Löwdin atomic charge calculations, were performed using density functional theory, employing 6-311++G(d,p) as the basis set and the M06-2X exchange correlation potential. The results are as expected, the alkylated cationic pyridyl nitrogen has the least negative atomic charge, and the secondary amines in the guanidine are less negatively charged than the pyrrolidine nitrogen. These results, along with the measured pKa's of (*S*)-nicotine and imidacloprid (3.09 and 1.56 respectively), can provide a foundation to explain why imidacloprid can form complexes with pillar[*n*]arene, whereas nicotine showed little complexation behaviour.¹⁷³ However, these results also further point to a secondary factor beyond electrostatic interactions as to why pillar[5]arene has a stronger affinity to the neutral imidacloprid, compared to the cationic nicotinium.

Molecule	Pyridyl Nitrogen	Pyrrolidine/ imidazolidine ^a nitrogen
(<i>S</i>)-Nicotine	-0.132 (L), -0.131 (M)	-0.192 (L), -0.051 (M)
<i>N</i> -ethylnicotinium	0.081 (L), 0.324 (M)	-0.081 (L), -0.018 (M)
Imidacloprid	-0.11 (L), 0.102 (M)	0.1557, -0.167, 0.011, 0.174 (L), -0.236, 0.100, 0.111, -0.357 (M)
Desnitroimidacloprid	-0.110 (L), 0.104 (M)	0.104, -0.362, -0.048 (L), -0.251, -0.629, 0.075

Table 4. Mulliken atomic charge (M) and Löwdin atomic charges, of the nitrogens in the 4 guests. Calculated with density functional theory employing 6-311++G(d,p) as the basis set and the M06-2X exchange correlation potential.

- a. Nitrogen's in imidazolidine are secondary amine, amine adjacent to nitro group, tertiary amine, nitrogen from nitro, respectively for imidacloprid. For desnitroimidacloprid, secondary amine, primary amine, tertiary amine respectively.

Although there are no conclusive explanations for these findings, there are several reasonable suggestions based on the properties of each guest molecule. The first consideration is the flexibility of the two molecules. The two rings of imidacloprid are separated by a methylene bridge, this added flexibility should allow the rings to better find favourable interactions with the pillar[5]arene. Compared with the nicotinium which has a rigid structure, where the pyrrolidine can only rotate on one axis to supplement binding. However, if this was the sole contributing factor, it would be expected that alkylamines display binding affinities beyond that of imidacloprid. Conversely, 1,8-diaminooctane was found to have a binding constant of only $(7.0 \pm 1.0) \times 10^4 \text{ M}^{-1}$.¹⁷⁴

Therefore, other driving forces must be present that favour imidacloprid binding. The three additional or altered secondary binding sites in imidacloprid, when compared to nicotinium are; the chlorine, the pyridyl and the nitro group. Halogen bonding from the chlorine to the oxygen in pillar[5]arenes is a possibility, halogen bonds can have a bond energy ranging from 10-200 kJ mol⁻¹ so would be strong enough to elevate imidacloprid's affinity.¹⁷⁵ However, if the position of the chlorine on the pyridyl, and the relative position of the alkoxy oxygen to the pillar[5]arene cavity is assessed, it becomes less likely. Equally halogen bonds with chlorine donors are usually weak, so there is unlikely to be a strong enough halogen bond to form this favourability towards imidacloprid. The angle between the imidazolidine secondary amine and the chlorine is 40° (from crystal structure), therefore for the chlorine to achieve an effective halogen bond distance of 2.6 - 3.3 Å, the bond angle would have to increase to *ca* 80° (if the encapsulation of the imidazolidine is as in the upfield shift study is assumed).¹⁷⁶ Equally, if a halogen bond was formed between the chlorine and the alkoxy oxygen, an upfield shifting or downfield shifting of the pyridyl protons would be expected (depending on whether the pyridyl was tilted into or out of the cavity respectively).

The chloropyridynl group is not limited to only halogen bonds though, the conjugated π -system can also provide intramolecular interactions. Although weaker than halogen and hydrogen bonds, with energies of *ca* 6-10 kJ mol⁻¹, the CH/ π bond can be crucial in the formation of supramolecular structures.¹⁷⁷ The strength and stability of the CH/ π can be affected by; the proton donating ability of the CH, the electron density of the π -system, and importantly the number of CH groups capable of bonding, as CH/ π is notably a cooperative process. When comparing and estimating the relative CH/ π between the nicotinium and imidacloprid, the relative electron density of the pyridyls π system, and the position of the guest within the pillar[5]arene cavity would need to be assessed, as to assess the possible number of CH/ π interactions. Electron density is easier to qualitatively assess, the nicotinium has a positive charge within the pyridyl, and for imidacloprid there is an electron donating chlorine and the pyridine is neutral, so one would logically expect the π -electron density to be greater in imidacloprid. Harder to predict however, is the position of the guest in relation to the macrocycle, and therefore how many possible CH/ π bonds can be made.

Finally, the nitro group may be important in stabilising the complex. Nitro groups have been shown to perform as hydrogen bond acceptors with alkoxy groups, and form π/π interactions with aromatic rings.^{178,179} Without an accurate structure showing binding conformation however, assessing how important these 'secondary' intermolecular interactions are, is not facile. Using the upfield shift studies it is possible to give an approximate guest directionality, but position of the guest within 3D-space is more difficult. To assist in gathering the nature of the host-guest complex, the Autodock Vina software was used (*figure 28*).¹⁸⁰ The software generated an inclusion complex for pillar[5]arene and both *N*-ethylnicotinium and imidacloprid, starting from the host and guest as two separated molecules. For the nicotinium, the estimated binding looks

sensible, with the ethyl chain fully encapsulated and the rest of the molecule tilting inwards, showing bias towards carbon 1, which supports the 1H NMR data. However, for imidacloprid the calculated binding is contrary to the evidence that was gathered, with the chloropyridyl within the cavity. Thus, further highlighting the difficulty in assessing binding characteristics, and therefore establishing causes for the differences in binding association.

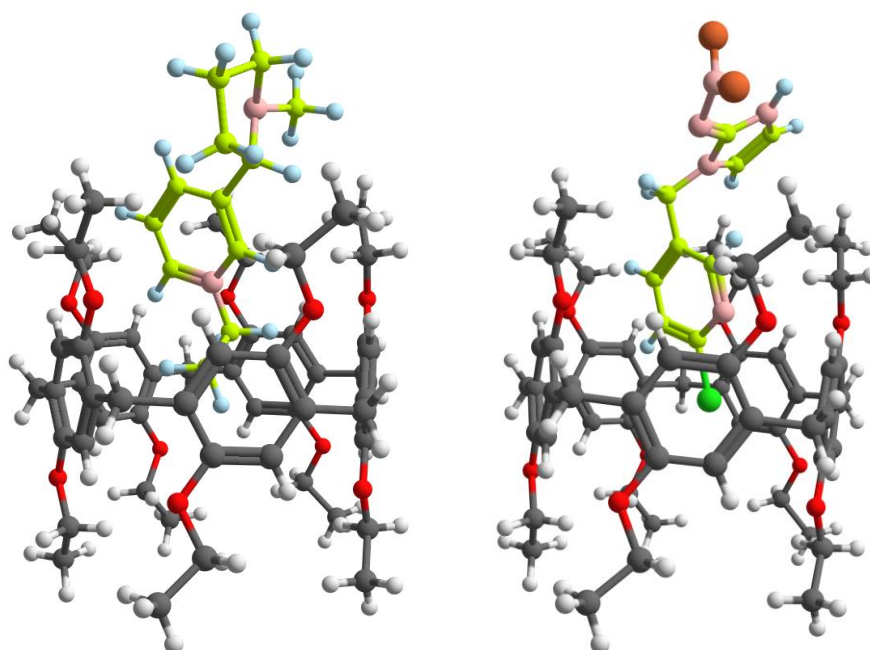


Figure 28. Computational models of the *N*-ethylnicotinium and imidacloprid complexes with pillar[5]arene, calculated using the AutoDock Vina software package. (for guest molecules Carbon – Green, Nitrogen – Pink, Hydrogen – Teal, Oxygen - Orange).

2.4.7. Imidacloprid and Pillar[6]arene Titration, and Concentration Variations

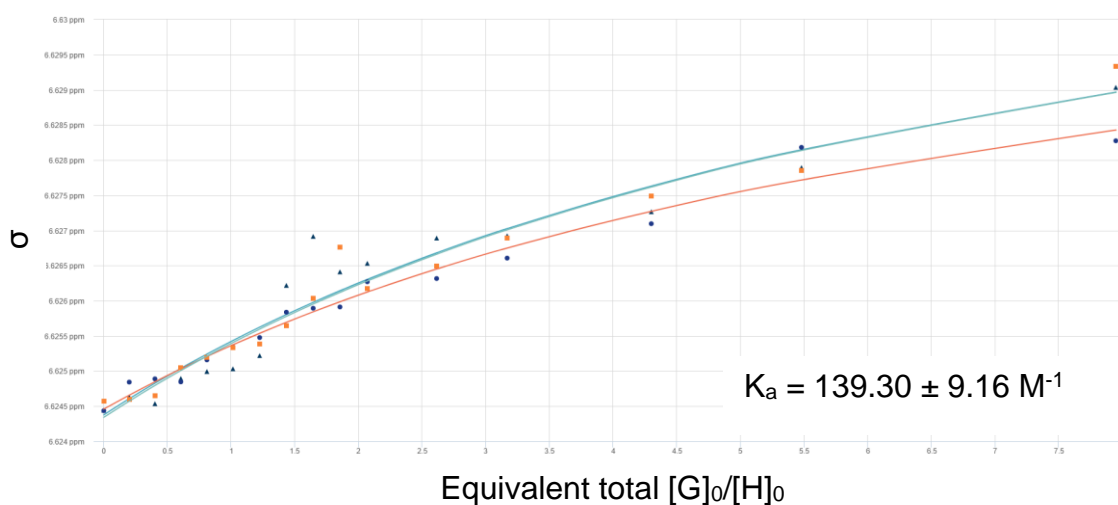


Figure 29. Graph showing the results of the titration between DEP[6]A and imidacloprid, with each of the three repeats fitted using the BindFit software to give the calculated binding constant and error.

For the titrations with pillar[6]arene, a greater binding constant with imidacloprid was expected when compared with pillar[5]arene. This prediction was due to the results gained from the upfield shift study, with DEP[6]A causing significantly greater upfield shifting across all the guests' protons. However, the results of the titrations with a macrocycle concentration of 1mM countered these original claims. The binding constant calculated for pillar[6]arene was $(1.39 \pm 0.09) \times 10^2 \text{ M}^{-1}$, almost 5 times less than pillar[5]arene (*figure 29*). Initially, the reasoning for this relatively low binding constant was a concentration effect. Due to chloroform having a known affinity for the cavity of pillar[*n*]arenes, it can be assumed that the binding of a guest molecule is not only controlled by the guest's association, but also the dissociation of solvent from the pillar[*n*]arenes cavity. The cavity of pillar[6]arene being larger, and therefore encapsulating more solvent, will thus require greater concentrations of guest to dissociate the solvent molecules. Two methods of assessing the contributions from the solvent were attempted. Firstly, titrations were performed at different host and

guest concentrations, and secondly the shift in peaks were measured relative to the chloroform peak to quantitatively measure the dissociation.

Two additional titrations were performed, one where the concentration of pillar[6]arene was 4 mM, and one where the concentration of pillar[6]arene was 20 mM. It is important to note however that for the 20 mM titration, the equivalents of guests did not exceed 4, due to issues in solubility. The results surprisingly showed the opposite effect. At 4 mM the binding constant was $(7.93 \pm 0.66) \times 10^2 \text{ M}^{-1}$ and at 20 mM the binding constant was $(6.71 \pm 0.62) \times 10^2 \text{ M}^{-1}$. Equally, when the peaks were referenced to chloroform *via* the equation $(\sigma_{\text{P6Apeak}} - \sigma_{\text{Chloroform}}) / \sigma_{\text{Chloroform}}$, a decrease in binding associations was found. For 1 mM the binding association decreased to $(1.08 \pm 0.08) \times 10^2 \text{ M}^{-1}$ and for 5 mM there was a slight decrease to $(6.96 \pm 0.59) \times 10^2 \text{ M}^{-1}$. The implication of these results is that instead of chloroform acting only as a solvent to dissociate, it may be capable of cooperatively binding with the pillar[6]arene and imidacloprid, aiding formation of the complex through NO₂/Cl halogen bonding.

The discrepancies between the titrations and the upfield shift study are not solved by this explanation. When other literature is examined for pillar[6]arene and guests, similar effects are seen. *Zhang et al* used (ferrocenylmethyl)trimethylammonium as the guest, and for pillar[6]arene the binding association was similar to the results observed herein for imidacloprid $(8.8 \pm 1.4) \times 10^2 \text{ M}^{-1}$. Importantly, the upfield shifts for the guest protons were also in the same range (-0.074 to 0.252 ppm).¹⁸¹ These supporting results indicate that although the relative upfield shifts can be considered proportional to the binding association, direct comparisons cannot be made when considering other sized macrocycles. In fact, when examining the difference in complex structure for P[6]A and P[5]A, and explanation for these results becomes apparent. Using the AutoDock Vini software, the calculated structures of pillar[6]arene

and pillar[5]arene with *N*-ethylnicotinium were compared (figure 30). The guest is clearly better enveloped within the pillar[6]arene when complexed, whereas in pillar[5]arene the full pyridyl ring cannot enter the cavity due to their relative sizes. This deeper position within the cavity results in greater shielding from the surrounding aryls, but equally the larger cavity allows the guest to enter and exit the macrocycle freely giving the low binding associations.

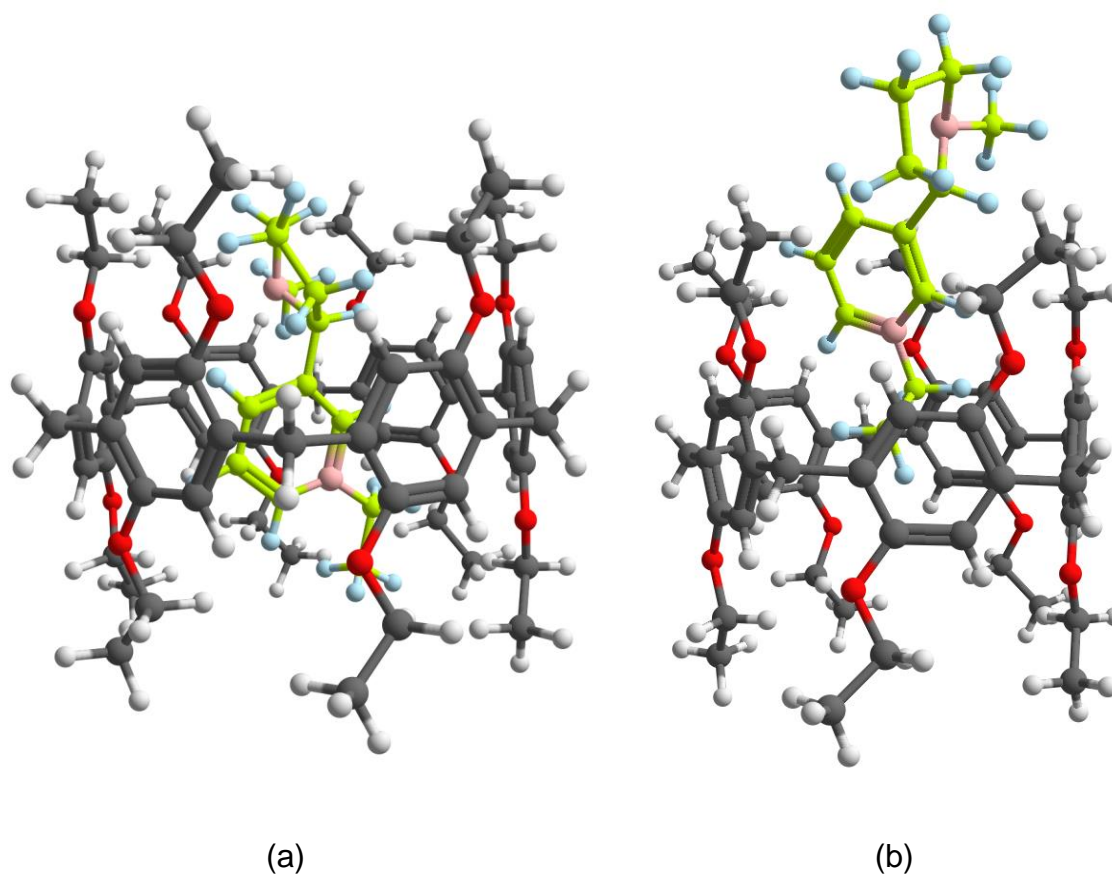


Figure 30. Computational models of the *N*-ethylnicotinium complexes with pillar[6]arene (a) and pillar[5]arene (b), calculated using the AutoDock Vina software package. (for nicotinium molecules Carbon – Green, Nitrogen – Pink, Hydrogen – Teal).

2.4.8. Desnitro-imidacloprid Binding Studies

As previously mentioned, for the synthesis of desnitro-imidacloprid the product yielded is in the form of the hydrobromide salt. Attempts were made to remove the HBr

component; sodium hydroxide was added, and chloroform was used to extract the free desnitro-imidacloprid. Unfortunately, this formed product was very unstable and within a few minutes decomposed into an unidentified yellow liquid. Therefore, to ensure that the studies could continue, and that no decomposition effects would be seen in the later titrations, the HBr salt was used for the binding studies.

The HBr salt of the desnitro-imidacloprid was however, not soluble in pure chloroform, so for the NMR upfield shift studies, a different approach was used. A 60 mM solution of desnitro-imidacloprid in DMSO- d_6 was made, then 0.1 mL of said solution was added to 0.5 mL of 10 mM solutions of the macrocycles in $CDCl_3$ (figure 31). A lower concentration of pillar[n]arene was required as the pillar[n]arenes would begin precipitating when the low amount of DMSO was added at 20 mM.

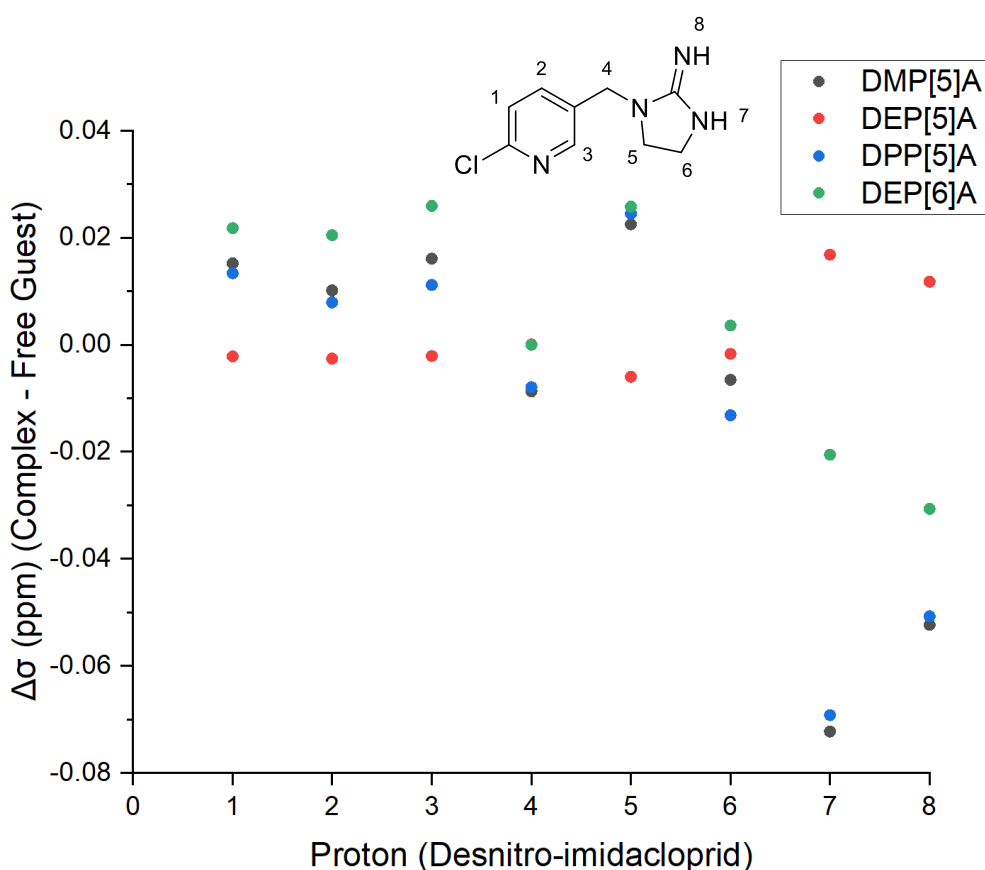


Figure 31. Graph showing the relative shifts of desnitro-imidacloprid when in solution with a series of macrocycles. (400 MHz $CDCl_3$ -DMSO- d_6 (5:1), 1:1 10mM desnitro-imidacloprid : macrocycle).

The results of the upfield shift study show interesting findings. As expected for the most electron deficient group, the guanidinium NH signals are upfield shifted the most. However, for methyl and propyl pillar[5]arene the secondary amine is shifted more, whereas for the larger pillar[6]arene the amine (proton 7) which has the propensity to be primary shows the largest shift. The larger pillar[6]arene also downfield shifts the pyridyl protons more than the smaller derivatives. There could be several reasons for this, but it is important to reiterate that as previously expressed, upfield shift data cannot be directly compared between different sized macrocycles. With that being said, there could be several reasons for these findings, most likely, the larger cavity is allowing for a conformation that cannot be accessed with the smaller pillar[5]arene. Additionally, when the NMR spectra of the pillar[6]arene with the desnitro-imidacloprid is examined, the peaks have broadened significantly. As previously discussed, peak broadening is caused by movement of the guest, which can be either rotational within the cavity, or translational in and out of the ring.

Secondly, and perhaps more importantly, when compared to imidacloprid the protons are significantly less upfield shifted. This may not be indicative to the binding being weaker than for imidacloprid however, as upfield shifts and binding associations are not always directly proportional. There is nonetheless an indication that desnitro-derivative may not be forming efficient complexes, with the 6 membered pillararene showing significant decreases in upfield shifts compared to the pillar[5]arene (*figure 32*).

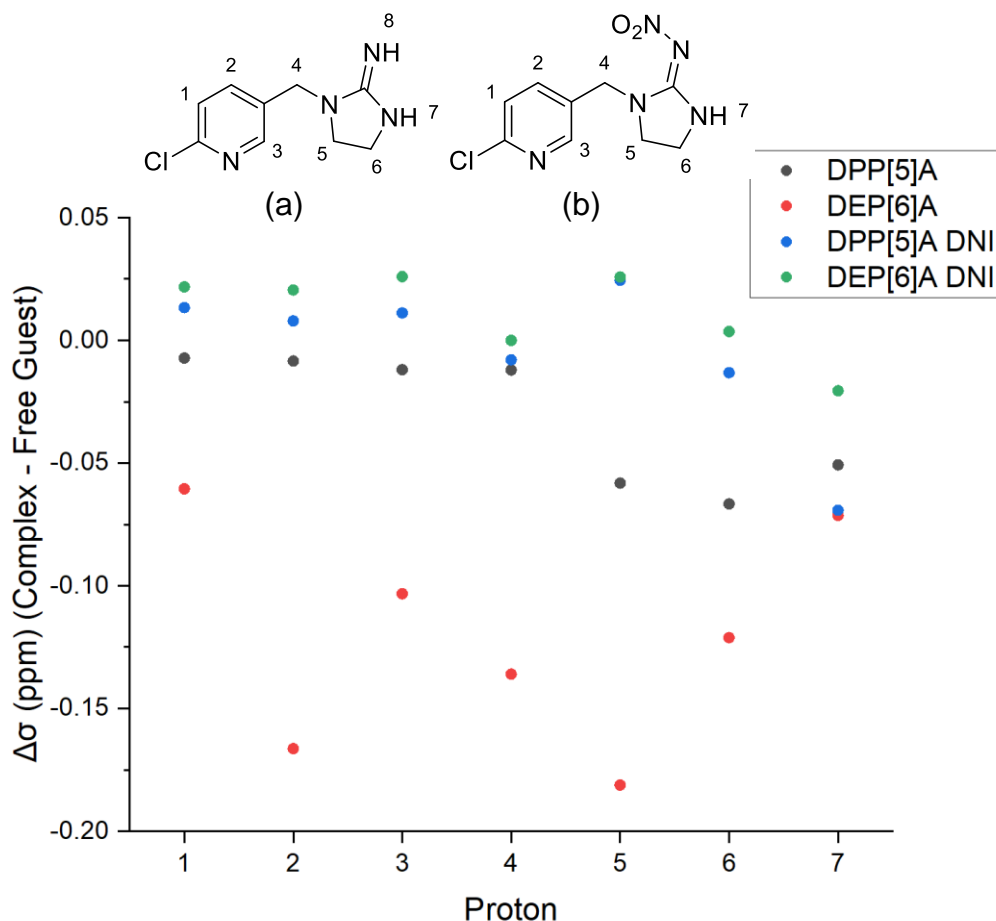


Figure 32. Graph showing the differences between imidacloprid (b) and desnitro-imidacloprid's (a) (DNI) upfield shifts when with dipropylpillar[5]arene and diethoxypillar[6]arene. (The ¹H NMR spectra of imidacloprid pillar[n]arene complexes were performed in CDCl₃, whereas from desnitroimidacloprid 10 % DMSO had to be added for solubility).

2.4.9. Desnitro-Imidacloprid NMR Titrations

Due to the low solubility of desnitro-imidacloprid in chloroform the same method for NMR titrations could not be used. To trial the maximum ratio of chloroform to DMSO before desnitro-imidacloprid precipitates, to a solution of the metabolite in DMSO chloroform was added. With this test it was estimated that for the titrations to be completed in full, a ratio of 4:1 chloroform:DMSO was required to ensure the guest does not precipitate throughout the titration. The pillar[n]arene guest was as before with a 1 mM concentration.

To ensure that solvent was not the contributing factor to peak shifting, a reference titration was added where a guestless solution of 4:1 chloroform:DMSO was added to

a solution of pillar[*n*]arene in the same volumes as for the guest. Initially, a titration from 0 to 2.5 equivalents was trialled using this method. Unfortunately, when the data was analysed, it was clear the addition of DMSO did have a drastic effect on the peak shift and the results were not usable. Even though there was downfield shifting seen in the pillar[6]arene peak when the guest was added, the distortion of the peak due to DMSO's addition rendered the data unjustifiable. Therefore, the NMR titrations of desnitro-imidacloprid were terminated.

The solution to this problem is evident in retrospect, if the starting solution of pillar[*n*]arene was also 4:1 chloroform:DMSO the effects of DMSO addition would not be present. Equally though, for said results to be comparable to the previous imidacloprid titrations, the imidacloprid titrations would also need to be in the same solvent parameters due to the known effects of solvent in pillar[*n*]arene-guest binding constants.¹⁶⁵

Host	Guest	K_a
DEP[5]A	N-Ethylnicotinium	$(3.09 \pm 0.55) \times 10^2 \text{ M}^{-1}$
DEP[6]A	N-Ethylnicotinium	$(8.21 \pm 0.25) \times 10 \text{ M}^{-1}$
DEP[5]A	Imidacloprid	$(5.51 \pm 0.53) \times 10^2 \text{ M}^{-1}$
DEP[6]A	Imidacloprid	$(1.39 \pm 0.09) \times 10^2 \text{ M}^{-1}$

Table 5. Binding constants calculated in this study.

2.5. Conclusions and Further Work

To conclude this chapter, a series of nicotinium candidates were synthesised and the binding constant of *N*-ethylnicotinium and different pillar[*n*]arenes were measured. What was observed was the preferential binding of nicotinium towards the smaller pillar[5]arene compared to pillar[6]arene. This is most likely due to the stronger non-covalent intermolecular bonds between the host and guest, caused by the closer π -electron contact within pillar[5]arenes cavity. Imidacloprid and its metabolite desnitro-imidacloprid were equally synthesised, and imidacloprid's binding constant with

pillar[*n*]arenes was assessed. Similarly to the nicotinium, the smaller pillar[5]arene provided the larger binding constant for imidacloprid, most likely for similar reasons. Importantly, it was noted that the binding constant of imidacloprid was larger than for the cationic *N*-ethylnicotinium. This is an interesting result as it indicates that an estimate on the strength of binding between pillar[*n*]arene's and a guest cannot be reduced to only electrostatic interactions. In fact, it gives a strong indication that there are secondary intermolecular connection points that aid in binding. This could also be seen in the initial upfield shift studies of the desnitro-imidacloprid, where lesser shifts are seen in the guest indicating a weaker binding. What can be estimated from these results that the nitro group in imidacloprid must be providing secondary intermolecular interactions with the rim of the pillar[5]arene; stabilising the host-guest complex.

These results ultimately countered the initial hypothesis that the metabolite would be the more favourable guest, but nonetheless provides insight into the future of selective host-neonicotinoid systems.

In future work it is essential that the titrations between the pillar[*n*]arenes and imidacloprid and its metabolite are performed in the chloroform:DMSO solvent mentioned earlier. Once that is complete a greater understanding of the selectivity of the macrocycle would be gained. Equally, to better understand the hypothesised secondary intermolecular interactions, chemically similar molecules should be trialled.

In an attempt to rationalise the apparent increase in binding between longer alkyl chain decorated pillar[5]arenes and *N*-ethylnicototinium, and expanded scope of guests should be examined with pillar[5]arene. With the data provided from the NMR upshield studies, the cationic ethylpyridinium's protons are the most shifted, and therefore the pyridinium be assumed to be the major driving force towards host-guest

encapsulation. Therefore, by altering the substituents on the meta position on the pyridinium unit, a greater understanding on how the guests interactions with the pillar[5]arene's alkyl chain can be understood. A rational approach, would be to choose a range of substituents that will either differ in electron density to the pyrrolidine, or that of which alters the size of said substituent. For the exploration of electronic effects in the host-guest binding, furan, imidazoline, pyrrole, and cyclopentane would be appropriate candidates. Equally, to examine steric contributions, the size of the substituent ring can be changed, with aziridine, azetidione, piperidine, and azepane being achievable substituent substitutes (*figure 33*).

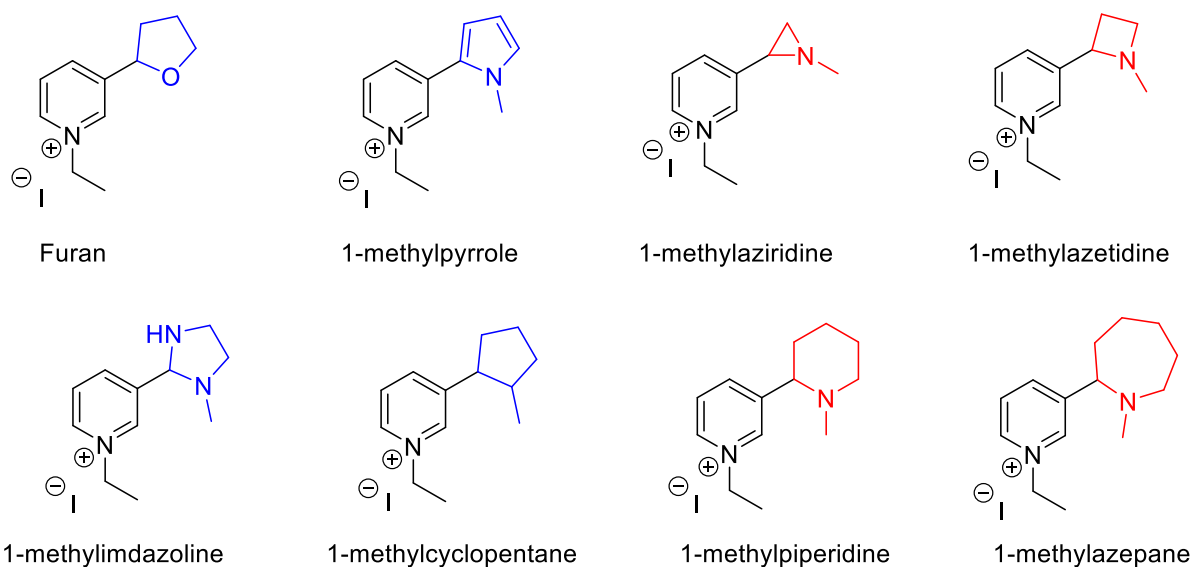


Figure 33. Extended substituent scope for further studies, with electronically altered substituents in blue and sterically altered rings in red.

The neonicotinoid research should follow a similar path; altering the imidazolidine substituents to try and better understand the key factors in effective host-guest encapsulation. The most practical approach would be to examine further metabolites of imidacloprid, as this would further the goal of sequestering neonicotinoid metabolites. Additional to the desnitro-imidacloprid examined herein, other major metabolites for example, urea-imidacloprid and olefin-imidacloprid, which

are metabolites found in groundwater, would be useful additions. These metabolites, paired with additional 2-imidazolidine substituted neonicotinoids, could provide evidence on the effect that different electron donating or withdrawing groups have on the favourability of encapsulation within pillar[*n*]arene (figure 34). The synthetic route for the imidacloprid variants, could proceed *via* reaction between the N1-((6-chloropyridin-3-yl)methyl)ethane-1,2-diamine synthesised herein, and the relevant dimethyl carbonimidodithiolate. This is a known reaction for the synthesis of 5 and 6 membered substituted heterocyclic rings and is performed in basic conditions (figure 35).¹⁸²

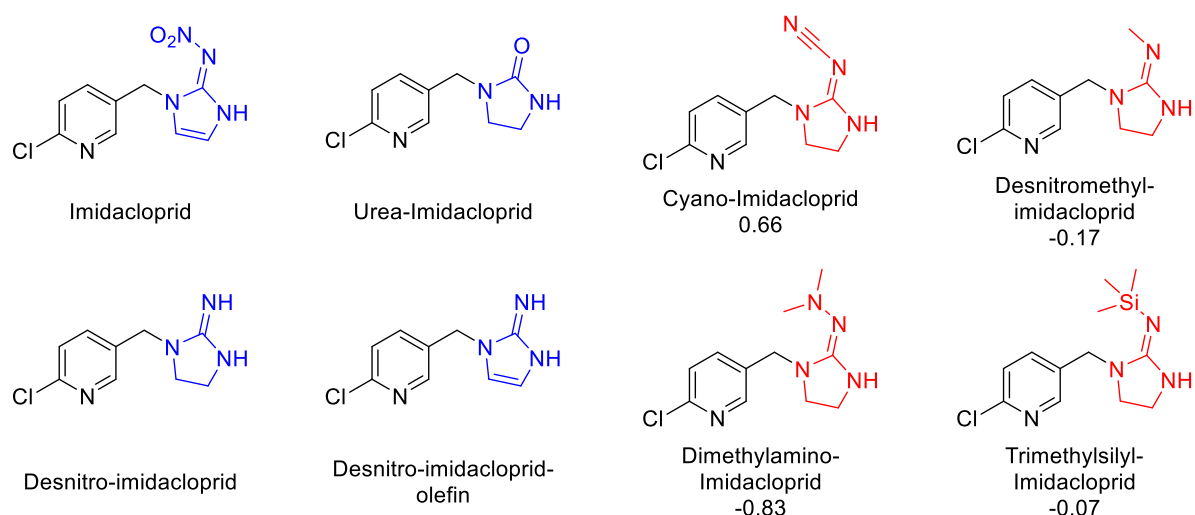


Figure 34. Extended substituent scope for further imidacloprid binding studies. Naturally formed metabolites in blue, substituted imidacloprids with a range of electron withdrawing/donating groups shown in red, with Hammett values (σ_P) below.

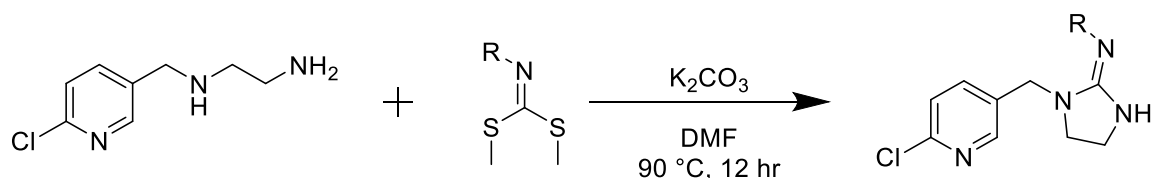
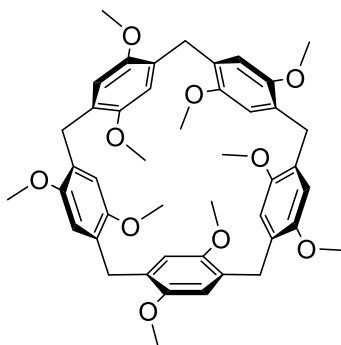


Figure 35. Proposed route for the synthesis of substituted imidacloprid derivatives.

2.6. Materials and Methods

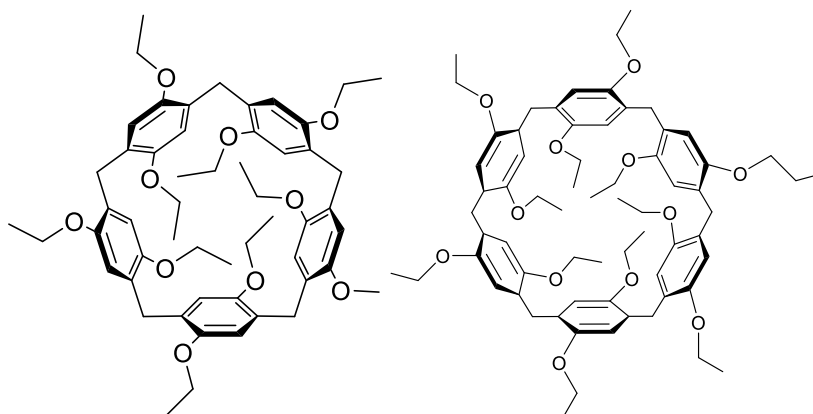
2.6.1. Synthesis

2.6.1.1. Dimethoxypillar[5]arene



1,4-Dimethoxybenzene (13.82 g, 100 mmol) and paraformaldehyde (3.00 g, 100 mmol) was stirred in 1,2-dichloroethane (1000 mL) for 15 minutes. Trifluoroacetic acid (50 mL) was added, and the solution was stirred at 90 °C for 2.5 hours. The resulting solution was added to methanol (1000 mL). The green precipitate was collected by filtration and was dissolved in chloroform (*ca* 250 mL), acetone (*ca* 250 mL) was added, and a yellow precipitate formed. The yellow precipitate was collected by filtration and dissolved in chloroform; the solvent was removed *in vacuo* after treatment with activated carbon. Giving pillar[5]arene as a white solid (12.0 g, 16.0 mmol, 80 %). Spectroscopic data for the title compound were consistent with the literature. ¹H NMR (400 MHz, Chloroform-*d*) δ (ppm): 6.82 (s, 10H), 3.79 (s, 10H), 3.69 (s, 30H); ¹³C NMR (101 MHz, Chloroform-*d*) δ (ppm): 150.41 128.26, 113.31, 55.41, 29.24; MALDI-TOF *m/z* for [M] calc'd as 750.33, found 750.14.

2.6.1.2. Diethoxypillar[5/6]arene



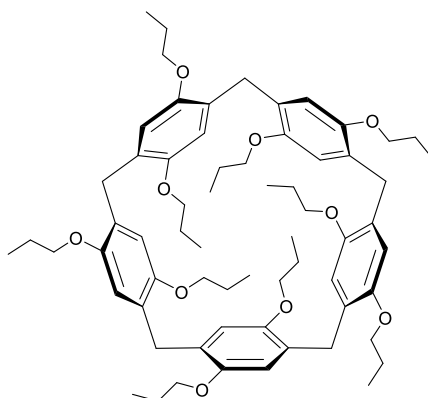
1,4-Diethoxybenzene (5.00 g, 30.1 mmol) and paraformaldehyde (2.70 g, 90.0 mmol) were stirred in degassed chloroform (500 mL) for 10 minutes. Anhydrous Iron (II) chloride (0.73 g, 5.76 mmol) was then added to the mixture, and the green solution was stirred for 3 hours at room temperature in a nitrogen environment. Water (ca 500 mL) was then added to the reaction mixture. The organic layer was washed with water (2 x 250 mL) and added to silica (ca 5 g). The solvent was removed *in vacuo* and the compound purified *via* column chromatography on silica gel with DCM/Hexane 1:1 as the solvent mixture. Giving diethoxypillar[5]arene (DEP[5]A), and diethoxypillar[6]arene (DEP[6]A) as white solids. Spectroscopic data for the title compound were consistent with the literature. DEP[5]A (2.10 g, 2.35 mmol, 39 %), DEP[6]A (1.40 g, 1.31 mmol, 24 %).

DEP[5]A ^1H NMR (400 MHz, CDCl_3) δ (ppm) 6.65 (s, 10H), 3.75 (q, $J = 7.0$ Hz, 20H), 3.69 (s, 10H), 1.19 (t, $J = 6.9$ Hz, 30H); MALDI-TOF m/z for [M] calc'd as 891.16, found 890.74.

DEP[6]A ^1H NMR (400 MHz, CDCl_3) δ (ppm) 6.62 (s, 12H), 3.75 (q, $J = 7.0$ Hz, 24H), 3.71 (s, 12H), 1.21 (t, $J = 6.9$ Hz, 36H); ^{13}C NMR (101 MHz, DMSO) δ (ppm) 150.43,

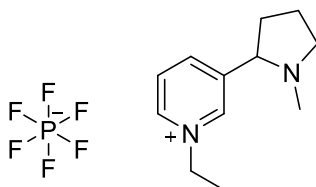
127.86, 115.25, 64.02, 30.95, 15.19; MALDI-TOF m/z for [M] calc'd as 1069.39, found 1068.91.

2.6.1.3 Dipropoxypillar[5]arene



1,4-Dipropoxybenzene (6.00 g, 31.0 mmol) and paraformaldehyde (2.78 g, 92.6 mmol) were stirred in degassed dichloromethane (ca 500 mL) for 10 minutes. Anhydrous Iron (II) chloride (0.73 g, 5.76 mmol) was then added to the mixture, and the green solution was stirred for 3 hours at room temperature in a nitrogen environment. Water (ca 500 mL) was then added to the reaction mixture. The organic layer was washed with water (2 x 250 mL) and added to silica (ca 5 g). The solvent was removed *in vacuo* and the compound purified *via* column chromatography on silica gel with DCM as the solvent mixture. Dipropoxypillar[5]arene was yielded as a white solid (2.10 g, 2.04 mmol, 32 %). Spectroscopic data for the title compound were consistent with the literature. ^1H NMR (400 MHz, CDCl_3) δ (ppm) 6.73 (s, 10H), 3.74 – 3.69 (m, 30H), 1.67 (h, $J = 7.1$ Hz, 20 H), 0.93 (t, $J = 7.4$ Hz, 30H); ^{13}C NMR (101 MHz, DMSO) δ (ppm) 149.82, 128.29, 115.01, 69.92, 29.59, 23.00, 10.77; MALDI-TOF m/z for [M] calc'd as 1031.42, found 1031.98.

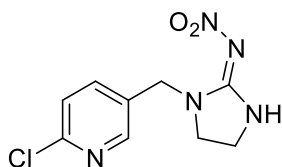
2.6.1.4 *N*-ethylnicotinium Hexafluorophosphate



(*S*)-Nicotine (5.00 g, 30.8 mmol) and iodoethane (38.8 g, 248 mmol) were stirred in acetic acid (*ca* 150 mL) overnight at 50 °C. The solvent was removed *in vacuo* and the resulting oil was redissolved in chloroform and washed with water (2 x 25 mL), sodium hydrogen carbonate (25 mL) and brine (25 mL). The organic layer was separated and dried over magnesium sulfate, and the solvent was removed *in vacuo* to give crude *N*-ethylnicotinium iodide as an orange solid. Crude *N*-ethylnicotinium iodide (5.00 g, 15.7 mmol) and ammonium hexafluorophosphate (10.0 g, 61.3 mmol) were dissolved in an acetone:water mixture (20 mL 7:1). The solution was stirred for 4 hours at room temperature, then the solvent was removed *in vacuo*. The residue was redissolved in chloroform and washed with water (3 x 25 mL). The organic layer was separated and dried over magnesium sulfate, then the solvent was removed *in vacuo* to give a yellow solid. The solid was collected and washed with water to give *N*-ethylnicotinium hexafluorophosphate as a yellow solid (3.00 g, 8.92 mmol, 28 %). Spectroscopic data for the title compound were consistent with the literature. ¹H NMR (400 MHz, CDCl₃) δ (ppm) 8.65 (s, 1H), 8.64 (d, *J* = 5.8 Hz, 1H), 8.45 (dt, *J* = 7.9, 1.5 Hz, 1H), 7.97 (dd, *J* = 8.0, 6.0 Hz, 1H), 4.64 (q, *J* = 7.4 Hz, 2H), 3.51 (t, *J* = 8.1 Hz, 1H), 3.25 (ddd, *J* = 9.6, 7.5, 2.4 Hz, 1H), 2.45 (q, *J* = 9.0 Hz, 1H), 2.42 – 2.32 (m, 1H), 2.24 (s, 3H), 2.02 – 1.79 (m, 1H), 1.67 (t, *J* = 7.3 Hz, 4H). ¹³C NMR (101 MHz, DMSO)

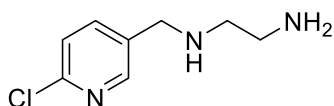
δ (ppm) 147.85, 147.75, 147.42, 146.35, 131.16, 74.47, 58.56, 57.36, 41.63, , 26.14, 19.43, 18.98, 16.67, 8.77, 7.65. ^{31}P NMR (162 MHz, DMSO- d_6) δ (ppm) -144.21 (hept, $J = 711.2$ Hz). ^{19}F NMR (377 MHz, DMSO- d_6) δ -72.71 (d, $J = 707.2$ Hz).

2.6.1.3. Imidacloprid



Sodium hydroxide (2.48 g, 62.0 mmol) and 2-(nitroimino)imidazolidine (6.60 g, 50.7 mmol) were stirred in dimethylformamide (20 mL) for 10 minutes at 50 °C. 2-chloro-5-(chloromethyl)pyridine (8.26 g, 51.0 mmol) was then added and the mixture was stirred overnight at 50 °C. Upon cooling the solvent was removed *in vacuo*, and hydrochloric acid was added until the pH of the solution reached pH 4. The precipitate formed was filtered and washed with methanol to afford imidacloprid as a pale-yellow powder (4.40 g, 17.2 mmol, 27 %). Spectroscopic data for the title compound were consistent with the literature. ^1H NMR (400 MHz, Chloroform- d) (ppm) δ 8.26 (s, 1H), 8.15 (s, 1H), 7.63 (dd, $J = 8.3, 2.3$ Hz, 1H), 7.29 (d, $J = 8.2$ Hz, 1H), 4.47 (s, 2H), 3.75 (t, $J = 9.1$ Hz, 2H), 3.46 (t, $J = 9.0$ Hz, 2H); ^{13}C NMR (101 MHz, DMSO) δ (ppm) 161.32, 151.71, 149.32, 139.11, 129.71, 124.82, 45.36, 45.16, 41.47.

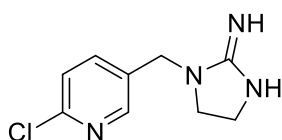
2.6.1.4. N1-((6-chloropyridin-3-yl)methyl)ethane-1,2-diamine



A solution of sodium hydroxide (1.90 g, 47.5 mmol) in water (0.78 mL) was added to a solution of ethane-1,2-diamine (3.72 g, 23.3 mmol) in acetonitrile (ca 20 mL). After stirring at room temperature for 10 minutes a solution of 2-chloro-5-

(chloromethyl)pyridine (2.00 g, 12.3 mmol) in acetonitrile (ca 20 mL) was slowly added over 10 minutes. The mixture was then stirred overnight at room temperature. Solvent was then removed *in vacuo* and the residue was dissolved in 20 mL of 2 M sodium hydroxide. Chloroform (ca 60 mL) was then used to extract the product, and the organic layer was separated and dried over magnesium sulfate. The solvent was then removed *in vacuo* to give the crude *N*¹-((6-chloropyridin-3-yl)methyl)ethane-1,2-diamine as a yellow oil (1.90 g, 10.4 mmol, 85 %). Spectroscopic data for the title compound were consistent with the literature. ¹H NMR (400 MHz, Chloroform-*d*) δ (ppm) 8.33 (d, *J* = 2.5 Hz, 1H), 7.69 (dd, *J* = 8.2, 2.5 Hz), 7.28 (dd, *J* = 8.1, 1.5 Hz, 1H), 3.80 (s, 2H), 2.82 (t, *J* = 5.7 Hz, 2H), 2.67 (t, *J* = 5.9 Hz, 2H), 2.01 (s, 1H), 1.23 (s, 1H). ¹³C NMR (101 MHz, DMSO) δ (ppm) 147.98, 147.41, 136.87, 133.12, 122.08, 50.00, 48.42, 29.74.

2.6.1.5. Desnitro-imidacloprid



Cyanogen bromide (1.00 g, 9.44 mmol) was dissolved in degassed toluene (ca 10 mL). *N*¹-((6-chloropyridin-3-yl)methyl)ethane-1,2-diamine (1.35 g, 7.27 mmol) was then slowly added. The solution was stirred at room temperature for 3 hours, and the formed precipitate was filtered and washed with diethylether to give desnitro-imidacloprid as a white solid (1.10 g, 5.23 mmol, 72 %). Spectroscopic data for the title compound were consistent with the literature. ¹H NMR (400 MHz, Chloroform-*d*) δ 8.20 (dd, *J* = 2.4, 0.8 Hz, 1H), 7.58 (dd, *J* = 8.2, 2.5 Hz, 1H), 7.16 (dd, *J* = 8.2, 0.7 Hz, 1H), 3.44 (s, 2H).

2.7. References

- 1 FAOSTAT, <https://www.fao.org/faostat/en/#data/RP/visualize>, (accessed June 27, 2022).
- 2 C. Bass, I. Denholm, M. S. Williamson and R. Nauen, *Pestic. Biochem. Physiol.*, 2015, **121**, 78–87.
- 3 H. A. Craddock, D. Huang, P. C. Turner, L. Quirós-Alcalá and D. C. Payne-Sturges, *Environ. Health.*, 2019, **18**, 7.
- 4 European Commission, *European Commission Press Release*, 2013, 1–2.
- 5 Ville de Montréal - Portail officiel - Détail du communiqué, https://web.archive.org/web/20180427151714/http://ville.montreal.qc.ca/portal/page?_pageid=5798%2C42657625&_dad=portal&_schema=PORTAL&id=26124&ret=http%3A%2F%2Fville.montreal.qc.ca%2Fpls%2Fportal%2Furl%2Fpage%2Fprt_vdm_fr%2Frep_annonces_ville%2Frep_communiques%2Fcommuniques, (accessed June 27, 2022).
- 6 Health Canada releases decisions on neonicotinoid pesticides for impact on aquatic insects, <https://www.newswire.ca/news-releases/health-canada-releases-decisions-on-neonicotinoid-pesticides-for-impact-on-aquatic-insects-831625166.html>, (accessed June 27, 2022).
- 7 Fijian Government - PARAQUAT AND IMIDACLOPRID PESTICIDE BANNED FROM 1ST JAN 2020, <https://www.fiji.gov.fj/Media-Centre/News/PARAQUAT-AND-IMIDACLOPRID-PESTICIDE-BANNED-FROM-1S>, (accessed June 27, 2022).
- 8 B. Siegmund, E. Leitner and W. Pfannhauser, *J. Agric. Food. Chem.*, 1999, **47**, 3113–3120.
- 9 A. Steppuhn, K. Gase, B. Krock, R. Halitschke and I. T. Baldwin, *PLoS Biol.*, 2004, **2**, e217.
- 10 N. E. (Norman E. McIndoo and U. States. O. of E. Stations., *Insecticidal uses of nicotine and tobacco: a condensed summary of the literature, 1690-1934*, U.S. Dept. of Agriculture. Agricultural Research Administration. Bureau of Entomology and Plant Quarantine, [Washington?], 1943.
- 11 D. Duke, E. Wohlgemuth, K. R. Adams, A. Armstrong-Ingram, S. K. Rice and D. C. Young, *Nat. Hum. Behav.*, 2022, **6**, 183–192.
- 12 E. Alderete, P. I. Erickson, C. P. Kaplan and E. J. Pérez-Stable, *Anthropol. Med.*, 2010, **17**, 27–39.
- 13 Z. Dorner, *Chest.*, 2021, **159**, 2099–2103.
- 14 N. L. Benowitz, J. Hukkanen and P. Jacob 3rd, *Handb. Exp. Pharmacol.*, 2009, **192**, 29–60.
- 15 M. Bergmann, *Science*, 1944, **99**, 537–538.
- 16 D. Pogocki, T. Ruman, M. Danilczuk, M. Danilczuk, M. Celuch and E. Wałajtys-Rode, *Eur. J. Pharmacol.*, 2007, **563**, 18–39.

- 17 B. Le Foll and S. R. Goldberg, *Handb. Exp. Pharmacol.*, 2009, 335–367.
- 18 K. A. Perkins, *Behav. Genet.*, 1995, **25**, 119–132.
- 19 N. L. Benowitz and P. 3rd Jacob, *NIDA Res. Monogr.*, 1997, **173**, 48–64.
- 20 D. B. ;Hu Kandel M. C.;Schaffran, C.;Udry, J. R.;Benowitz, N. L., *Am. J. Epidemiol.*, 2007, 165, 901–910.
- 21 A. B. Elgoyhen, D. E. Vetter, E. Katz, C. V Rothlin, S. F. Heinemann and J. Boulter, *Proc. Natl. Acad. Sci. U S A*, 2001, **98**, 3501–3506.
- 22 N. L. Benowitz, *Annu. Rev. Pharmacol. Toxicol.*, 2009, **49**, 57–71.
- 23 E. Quattrocki, A. Baird and D. Yurgelun-Todd, *Harv. Rev. Psychiatry.*, 2000, **8**, 99–110.
- 24 H. D. Mansvelder and D. S. McGehee, *J. Neurobiol.*, 2002, **53**, 606–617.
- 25 J. Hukkanen, P. Jacob and N. L. Benowitz, *Pharmacol. Rev.*, 2005, **57**, 79 LP – 115.
- 26 C. G. Nwosu and P. A. Crooks, *Xenobiotica*, 1988, **18**, 1361–1372.
- 27 P. A. Crooks and C. S. Godin, *J. Pharm. Pharmacol.*, 1988, **40**, 153–154.
- 28 K. C. Cundy, P. A. Crooks and C. Steven Godin, *Biochem. Biophys. Res. Commun.*, 1985, **128**, 312–316.
- 29 P. A. Crooks, J. T. Ayers, R. Xu, S. P. Sumithran, V. P. Grinevich, L. H. Wilkins, A. G. Deaciuc, D. D. Allen and L. P. Dvoskin, *Bioorg. Med. Chem. Lett.*, 2004, **14**, 1869–1874.
- 30 R. Nirogi, A. R. Mohammed, A. K. Shinde, S. R. Ravella, N. Bogaraju, R. Subramanian, V. R. Mekala, R. C. Palacharla, N. Muddana, J. B. Thentu, G. Bhyrapuneni, R. Abraham and V. Jasti, *J. Med. Chem.*, 2020, **63**, 2833–2853.
- 31 R. Carmelo and G. Avram, *Science*, 1980, **210**, 647–650.
- 32 J. T. Ayers, L. P. Dvoskin, A. G. Deaciuc, V. P. Grinevich, J. Zhu and P. A. Crooks, *Bioorg. Med. Chem. Lett.*, 2002, **12**, 3067–3071.
- 33 C. Matera, L. Pucci, C. Fiorentini, S. Fucile, C. Missale, G. Grazioso, F. Clementi, M. Zoli, M. De Amici, C. Gotti and C. Dallanoce, *Eur. J. Med. Chem.*, 2015, **101**, 367–383.
- 34 M. D. Joyce, M. C. Jennings, C. N. Santiago, M. H. Fletcher, W. M. Wuest and K. P. C. Minbiole, *J. Antibiot. (Tokyo)*, 2016, **69**, 344–347.
- 35 D. W. Kolpin, E. T. Furlong, M. T. Meyer, E. M. Thurman, S. D. Zaugg, L. B. Barber and H. T. Buxton, *Environ. Sci. Technol.*, 2002, **36**, 1202–1211.
- 36 D. A. Dawson, D. J. Fort, G. J. Smith, D. L. Newell and J. A. Bantle, *Teratog. Carcinog. Mutagen.*, 1988, **8**, 329–338.
- 37 C. Gómez-Canela, E. Prats, S. Lacorte, D. Raldúa, B. Piña and R. Tauler, *Ecotoxicol. Environ. Saf.*, 2018, **164**, 388–397.
- 38 F. Gagné, C. Blaise and C. André, *Ecotoxicol. Environ. Saf.*, 2006, **64**, 329–336.

- 39 I. J. Buerge, M. Kahle, H.-R. Buser, M. D. Müller and T. Poiger, *Environ. Sci. Technol.*, 2008, **42**, 6354–6360.
- 40 N. Turner, N. Woodruff, D. H. Saunders and A. Eisner, *Toxicity of Nicotine, Nicotinium Salts and Related Compounds by Injection*, 1948, vol. 521.
- 41 G. P. Carlson, *Toxicol Lett*, 1996, **85**, 173–178.
- 42 H. Weidel and M. Russo, *Monatsh. Chem.*, 1882, **3**, 850–885.
- 43 2018 Pesticide Use Maps -, https://water.usgs.gov/nawqa/pnsp/usage/maps/show_map.php?year=2018&map=PARAQUAT&hilo=H, (accessed June 28, 2022).
- 44 R. E. Murray and J. E. Gibson, *Exp. Mol. Pathol.*, 1972, **17**, 317–325.
- 45 K. S. M. Abdul, P. M. C. S. De Silva, E. M. D. V Ekanayake, W. A. K. G. Thakshila, S. D. Gunarathna, T. D. K. S. C. Gunasekara, S. S. Jayasinghe, H. B. Asanthi, E. P. S. Chandana, G. G. T. Chaminda, S. H. Siribaddana and N. Jayasundara, *Int. J. Environ. Res. Public Health*, 2021, **18**, 3278.
- 46 F. Hossain, O. Ali, U. J. A. D'Souza and D. K. S. Naing, *J. Occup. Health*, 2010, **52**, 353–360.
- 47 J. Kim, Y. Ko and W. J. Lee, *Occup. Environ. Med.*, 2013, **70**, 303–309.
- 48 K. de Jong, H. M. Boezen, H. Kromhout, R. Vermeulen, D. S. Postma and J. M. Vonk, *Am. J. Epidemiol.*, 2014, **179**, 1323–1330.
- 49 S. Narayan, Z. Liew, J. M. Bronstein and B. Ritz, *Environ. Int.*, 2017, **107**, 266–273.
- 50 T. Wiwasuku, A. Chuaephon, U. Habarakada, J. Boonmak, T. Puangmali, F. Kielar, D. J. Harding and S. Youngme, *ACS Sustain. Chem. Eng.*, 2022, **10**, 2761–2771.
- 51 B. Zhao, Q. Yang, J.-S. Wang, F.-Y. Xie, H.-Y. Yu, Y. Li, Y.-X. Ma and W.-J. Ruan, *New J. Chem.*, 2021, **45**, 4401–4407.
- 52 A. Walcarius and R. Mouchotte, *Arch. Environ. Contam. Toxicol.*, 2004, **46**, 135–140.
- 53 C. Keawkumay, W. Rongchapo, N. Sosa, S. Suthirakun, I. Z. Koleva, H. A. Aleksandrov, G. N. Vayssilov and J. Wittayakun, *Mater. Chem. Phys.*, 2019, **238**, 121824.
- 54 E. Martwong, N. Sukhawipat and J. Junthip, *Polymers (Basel)*, 2022, **14**, 2199.
- 55 S. Rasmussen, K. H. Horkan and M. Kotler, *Clin. Pharmacol. Drug Dev.*, 2018, **7**, 506–512.
- 56 E. Martwong, S. Chuetor and J. Junthip, *Polymers*, 2021, **13**, 4110.
- 57 P. Kumari, Alka, S. Kumar, K. Nisa and D. Kumar Sharma, *J. Environ. Chem. Eng.*, 2019, **7**, 103130.
- 58 F. Huang, L. Zhou, J. W. Jones, H. W. Gibson and M. Ashraf-Khorassani, *Chem. Commun.*, **2004**, 2670–2671.

- 59 T. Ogoshi, S. Kanai, S. Fujinami, T. A. Yamagishi and Y. Nakamoto, *J. Am. Chem. Soc.*, 2008, **130**, 5022–5023.
- 60 G. Yu, X. Zhou, Z. Zhang, C. Han, Z. Mao, C. Gao and F. Huang, *J. Am. Chem. Soc.*, 2012, **134**, 19489–19497.
- 61 K. Noworyta, W. Kutner, C. A. Wijesinghe, S. G. Srour and F. D'Souza, *Anal. Chem.*, 2012, **84**, 2154–2163.
- 62 D. Balestri, D. Capucci, N. Demitri, A. Bacchi and P. Pelagatti, *Materials (Basel)*, 2017, **10**, 727.
- 63 A. V Davis, D. Fiedler, M. Ziegler, A. Terpin and K. N. Raymond, *J. Am. Chem. Soc.*, 2007, **129**, 15354–15363.
- 64 S. Borsley, J. A. Cooper, P. J. Lusby and S. L. Cockroft, *Chem. Eur. J.*, 2018, **24**, 4542–4546.
- 65 M. Tlustý, P. Slavík, M. Kohout, V. Eigner and P. Lhoták, *Org. Lett.*, 2017, **19**, 2933–2936.
- 66 M. D. Joyce, M. C. Jennings, C. N. Santiago, M. H. Fletcher, W. M. Wuest and K. P. Minbiole, *J. Antibio.*, 2016, **69**, 344–347.
- 67 C. Matera, L. Pucci, C. Fiorentini, S. Fucile, C. Missale, G. Grazioso, F. Clementi, M. Zoli, M. De Amici, C. Gotti and C. Dallanocce, *Eur. J. Med. Chem.*, 2015, **101**, 367–383.
- 68 S. Gabriel, *Ber. Dtsch. Chem.*, 1887, **20**, 2224–2236.
- 69 A. Hantzsch and M. Kalb, *Ber. Dtsch. Chem.*, 1899, **32**, 3109–3131.
- 70 A. Hantzsch and O. K. Hofmann, *Ber. Dtsch. Chem.*, 1911, **44**, 1776–1783.
- 71 E. A. Lock and M. F. Wilks, eds. R. I. Krieger and W. C. B. T.-H. of P. T. (Second E. Krieger, Academic Press, San Diego, 2001, pp. 1559–1603.
- 72 J. I. Seeman and J. F. Whidby, *J. Org. Chem.*, 1976, **41**, 3824–3826.
- 73 T. Heckel, A. Winkel and R. Wilhelm, *Tetrahedron Asymmetry*, 2013, **24**, 1127–1133.
- 74 S. Gogoi and U. Barthakur, *Int. J. Chem. Stud.*, 2019, **7**, 62–67.
- 75 L. G. Costa, eds. L. G. Costa, C. L. Galli and S. D. Murphy, Springer Berlin Heidelberg, Berlin, Heidelberg, 1987, pp. 1–10.
- 76 J. Gloser, *Biol Plant*, 2002, **45**, 128–128.
- 77 Y. Abubakar, H. Tijjani, C. Egbuna, C. O. Adetunji, S. Kala, T. L. Kryeziu and K. C. Patrick-Iwuanyanwu, in *Natural Remedies for Pest, Disease and Weed Control*, Academic Press, 2019, pp. 29–42.
- 78 The Nobel Prize in Physiology or Medicine 1948, <https://www.nobelprize.org/prizes/medicine/1948/summary/>, (accessed June 29, 2022).
- 79 O. Zeidler, *Ber. Dtsch. Chem.*, 1874, **7**, 1180–1181.

- 80 G. Patterson, *Am. Hist. Rev.*, 2012, **117**, 1619–1620.
- 81 H. Luce, *Time magazine*, 1945, 28.
- 82 C. Rachel, *Silent Spring*, Houghton Mifflin, 1962.
- 83 DDT - A Brief History and Status | US EPA, <https://www.epa.gov/ingredients-used-pesticide-products/ddt-brief-history-and-status>, (accessed June 29, 2022).
- 84 R. T. Delfino, T. S. Ribeiro and J. D. Figueroa-Villar, *J. Braz. Chem. Soc.*, 2009, **20**, 407–428.
- 85 G. KOELLE, *Fundamental and Applied Toxicology*, 1981, **1**, 129–134.
- 86 Pesticides Industry Sales and Usage 2008 - 2012 Market Estimates | US EPA, <https://www.epa.gov/pesticides/pesticides-industry-sales-and-usage-2008-2012-market-estimates>, (accessed June 29, 2022).
- 87 P. Jeschke, R. Nauen, M. Schindler and A. Elbert, *J. Agric. Food. Chem.*, 2011, **59**, 2897–2908.
- 88 H. Feuer and J. P. Lawrence, *J. Org. Chem.*, 1972, **37**, 3662–3670.
- 89 S. B. Soloway, A. C. Henry, W. D. Kollmeyer, W. M. Padgett, J. E. Powell, S. A. Roman, C. H. Tieman, R. A. Corey and C. A. Horne, eds. D. L. Shankland, R. M. Hollingworth and T. Smyth, Springer US, Boston, MA, 1978, pp. 153–158.
- 90 S. Kagabu and S. Medej, *Biosci. Biotechnol. Biochem.*, 2014, **59**, 980–985.
- 91 A. Elbert, R. Nauen and W. Leicht, in *Insecticides with Novel Modes of Action*, 1998, pp. 50–73.
- 92 A. Elbert, B. Becker, J. Hartwig and C. Erdelen, *PflanzenschutzNachrichten Bayer*, 1991, **44**, 107–112.
- 93 M. Tomizawa and J. E. Casida, *Annu. Rev. Pharmacol. Toxicol.*, 2005, **45**, 247–268.
- 94 A. Nakayama, M. Sukekawa and Y. Eguchi, *Pestic. Sci.*, 1997, **51**, 157–164.
- 95 A. Akayama and I. Minamida, in *Nicotinoid Insecticides and the Nicotinic Acetylcholine Receptor*, 1999, pp. 127–148.
- 96 M. Schuld and R. Schmuck, *Ecotoxicology*, 2000, **9**, 197–205.
- 97 T. Wakita, K. Kinoshita, E. Yamada, N. Yasui, N. Kawahara, A. Naoi, M. Nakaya, K. Ebihara, H. Matsuno and K. Kodaka, *Pest. Manag. Sci.*, 2003, **59**, 1016–1022.
- 98 L. L. Carlock and T. A. Dotson, ed. R. B. T.-H. H. of P. T. (Third E. Krieger, Academic Press, New York, 2010, pp. 2293–2306.
- 99 S. O. Duke and S. B. Powles, in *Pest Manag. Sci.*, 2008, **64**, 319–325.
- 100 N. Simon-Delso, V. Amaral-Rogers, L. P. Belzunces, J. M. Bonmatin, M. Chagnon, C. Downs, L. Furlan, D. W. Gibbons, C. Giorio, V. Girolami, D. Goulson, D. P. Kreuzweiser, C. H. Krupke, M. Liess, E. Long, M. Mcfield, P. Mineau, E. A. Mitchell, C. A. Morrissey, D. A. Noome, L. Pisa, J. Settele, J. D. Stark, A. Tapparo, H. Van Dyck, J. Van Praagh, J. P. Van Der Sluijs, P. R. Whitehorn and M.

- Wiemers, *Environ. Sci. Pollut. Res.*, 2015, **22**, 5–34.
- 101 Global Metam Sodium Market Report, History and Forecast 2016-2027, <https://www.marketresearch.com/QYResearch-Group-v3531/Global-Metam-Sodium-History-Forecast-30441997/>, (accessed June 30, 2022).
- 102 Glyphosate Market | Global Industry Report, 2031, <https://www.transparencymarketresearch.com/glyphosate-market.html>, (accessed June 30, 2022).
- 103 T. Iwasa, N. Motoyama, J. T. Ambrose and R. M. Roe, *Crop Prot.*, 2004, **23**, 371–378.
- 104 E. E. D. Rand, S. Smit, M. Beukes, Z. Apostolides, C. W. W. Pirk and S. W. Nicolson, *Sci. Rep.*, 2015, **5**, 1–11.
- 105 A. Vaughan, *Review of Metham*, US EPA, 1981.
- 106 Q. H. Luo, J. Gao, Y. Guo, C. Liu, Y. Z. Ma, Z. Y. Zhou, P. L. Dai, C. S. Hou, Y. Y. Wu and Q. Y. Diao, *Sci. Rep.*, 2021, **11**, 1–8.
- 107 I. Yamamoto, K. Nagai and R. Inoki, *Jpn. J. Pharmacol.*, 1966, **16**, 295–305.
- 108 A. M. Henderson, J. A. Gervais, B. Luukinen, K. Buhl, D. Stone, A. Strid, A. Cross and J. Jenkins, 2010, **Glyphosate Technical Fact Sheet**; National Pesticide Information Center, Oregon State University Extension Services
- 109 M. Elliott, *Am. Chem. Soc.*, 1977, **42**, 1-28
- 110 M. Ihara and K. Matsuda, *Curr. Opin. Insect. Sci.*, 2018, **30**, 86–92.
- 111 H. A. Tennekes, *Toxicology*, 2011, **280**, 173–175.
- 112 R. Zwart, M. Oortgiesen and H. P. M. Vijverberg, *Environ. Toxicol. Pharmacol.*, 1992, **228**, 165–169.
- 113 M. Y. Liu and J. E. Casida, *Pestic. Biochem. Physiol.*, 1993, **46**, 40–46.
- 114 M. Y. Liu, J. Lanford and J. E. Casida, *Pestic. Biochem. Physiol.*, 1993, **46**, 200–206.
- 115 K. Matsuda, S. D. Buckingham, J. C. Freeman, M. D. Squire, H. A. Baylis and D. B. Sattelle, *Br. J. Pharmacol.*, 1998, **123**, 518–524.
- 116 M. Tomizawa and J. E. Casida, *Annu. Rev. Entomol.*, 2003, **48**, 339–364.
- 117 S. Kagabu and H. Matsuno, *J. Agric. Food. Chem.*, 1997, **45**, 276–281.
- 118 I. Yamamoto, *Adv. Pest Control Res.*, 1965, **6**, 231–260.
- 119 K. Matsuda, S. Kanaoka, M. Akamatsu and D. B. Sattelle, *Mol. Pharmacol.*, 2009, **76**, 1–10.
- 120 M. Tomizawa, Z. Wen, H.-L. Chin, H. Morimoto, H. Kayser and J. E. Casida, *J. Neurochem.*, 2001, **78**, 1359–1366.
- 121 M. Tomizawa, T. T. Talley, D. Maltby, K. A. Durkin, K. F. Medzihradzsky, A. L. Burlingame, P. Taylor and J. E. Casida, *Proc. Natl. Acad. Sci. U S A*, 2007, **104**, 9075–9080.

- 122 S. J. Lansdell and N. S. Millar, *Neuropharmacology*, 2000, **39**, 671–679.
- 123 M. Tomizawa, D. L. Lee and J. E. Casida, *J. Agric. Food. Chem.*, 2000, **48**, 6016–6024.
- 124 Z. Lu, J. K. Challis and C. S. Wong, *Environ. Sci. Technol. Lett.*, 2015, **2**, 188–192.
- 125 T. Ding, D. Jacobs and B. K. Lavine, *Microchem. J.*, 2011, **99**, 535–541.
- 126 N. Schippers and W. Schwack, *J. Agric. Food Chem.*, 2008, **56**, 8023–8029.
- 127 D. Redlich, N. Shahin, P. Ekici, A. Friess and H. Parlar, *Clean (Weinh)*, 2007, **35**, 452–458.
- 128 K. Z. Aregahegn, D. Shemesh, R. B. Gerber and B. J. Finlayson-Pitts, *Environ. Sci. Technol.*, 2017, **51**, 2660–2668.
- 129 K. L. Klarich Wong, D. T. Webb, M. R. Nagorzanski, D. W. Kolpin, M. L. Hladik, D. M. Cwiertny and G. H. Lefevre, *Environ. Sci. Technol. Lett.*, 2019, **6**, 98–105.
- 130 S. Kagabu, K. Yokoyama, K. Iwaya and M. Tanaka, *Biosci. Biotechnol. Biochem.*, 1998, **62**, 1216–1224.
- 131 R. Karmakar, S. B. Singh and G. Kulshrestha, *J. Environ. Sci. Health. B*, 2009, **44**, 435–441.
- 132 S. A. Todey, A. M. Fallon and W. A. Arnold, *Environ. Toxicol. Chem.*, 2018, **37**, 2797–2809.
- 133 R. Karmakar, S. B. Singh and G. Kulshrestha, *Bull. Environ. Contam. Toxicol.*, 2006, **76**, 400–406.
- 134 K. L. Klarich, N. C. Pflug, E. M. DeWald, M. L. Hladik, D. W. Kolpin, D. M. Cwiertny and G. H. LeFevre, *Environ. Sci. Technol. Lett.*, 2017, **4**, 168–173.
- 135 K. A. Ford and J. E. Casida, *J. Agric. Food. Chem.*, 2008, **56**, 10168–10175.
- 136 G. Pandey, S. J. Dorrian, R. J. Russell and J. G. Oakeshott, *Biochem. Biophys. Res. Commun.*, 2009, **380**, 710–714.
- 137 Y. J. Dai, S. Yuan, F. Ge, T. Chen, S. C. Xu and J. P. Ni, *Appl. Microbiol. Biotechnol.*, 2006, **71**, 927–934.
- 138 F. Ge, L. Y. Zhou, Y. Wang, Y. Ma, S. Zhai, Z. H. Liu, Y. J. Dai and S. Yuan, *Int. Biodeterior. Biodegrad.*, 2014, **93**, 10–17.
- 139 H. J. Zhang, Q. W. Zhou, G. C. Zhou, Y. M. Cao, Y. J. Dai, W. W. Ji, G. D. Shang and S. Yuan, *J. Agric. Food. Chem.*, 2012, **60**, 153–159.
- 140 L. Y. Zhou, L. J. Zhang, S. L. Sun, F. Ge, S. Y. Mao, Y. Ma, Z. H. Liu, Y. J. Dai and S. Yuan, *J. Agric. Food. Chem.*, 2014, **62**, 9957–9964.
- 141 X. Shi, R. A. Dick, K. A. Ford and J. E. Casida, *J. Agric. Food. Chem.*, 2009, **57**, 4861–4866.
- 142 J. E. Casida, *J. Agric. Food. Chem.*, 2011, **59**, 2923–2931.
- 143 K. Khidkhan, Y. Ikenaka, T. Ichise, S. M. M. Nakayama, H. Mizukawa, K.

- Nomiyama, H. Iwata, K. Arizono, K. Takahashi, K. Kato and M. Ishizuka, *Comp. Biochem. Physiol. Part - C: Toxicol. Pharmacol.*, 2021, **239**, 108898.
- 144 K. Taira, K. Fujioka and Y. Aoyama, *PLoS One*, 2013, **8**, 1–11.
- 145 K. M. Kasiotis and K. Machera, *Hell. Plant Prot. J.*, 2015, **8**, 33–45.
- 146 K. H. Harada, K. Tanaka, H. Sakamoto, M. Imanaka, T. Niisoe, T. Hitomi, H. Kobayashi, H. Okuda, S. Inoue, K. Kusakawa, M. Oshima, K. Watanabe, M. Yasojima, T. Takasuga and A. Koizumi, *PLoS One*, 2016, **11**, 1–10.
- 147 T. Ogoshi, N. Ueshima, F. Sakakibara, T. A. Yamagishi and T. Haino, *Org. Lett.*, 2014, **16**, 2896–2899.
- 148 N. K. Dalley, in *Synthetic Multidentate Macrocyclic Compounds*, Academic Press, 1978, pp. 207–243.
- 149 F. Qu, X. Zhou, J. Xu, H. Li and G. Xie, *Talanta*, 2009, **78**, 1359–1363.
- 150 M. L. Alonso, E. Sebastián, L. S. Felices, P. Vitoria and R. M. Alonso, *J. Incl. Phenom. Macrocycl. Chem.*, 2016, **86**, 103–110.
- 151 G. Utzeri, L. Verissimo, D. Murtinho, A. A. C. C. Pais, F. X. Perrin, F. Ziarelli, T. V. Iordache, A. Sarbu and A. J. M. Valente, *Molecules*, 2021, **26**, 1426.
- 152 A. C. Turan, İ. Özen, H. K. Gürakın and E. Fatarella, *J. Eng. Fiber. Fabr.*, 2017, **12**, 75–83.
- 153 G. Liu, L. Li, D. Xu, X. Huang, X. Xu, S. Zheng, Y. Zhang and H. Lin, *Carbohydr. Polym.*, 2017, **175**, 584–591.
- 154 C. Negro, H. Martínez Pérez-Cejuela, E. F. Simó-Alfonso, J. M. Herrero-Martínez, R. Bruno, D. Armentano, J. Ferrando-Soria and E. Pardo, *ACS Appl. Mater. Interfaces.*, 2021, **13**, 28424–28432.
- 155 T. Boinski and A. Szumna, *Tetrahedron*, 2012, **68**, 9419–9422.
- 156 A. Williamson, *The London, Edinburgh, and Dublin Philosophical Magazine and Journal of Science*, 1850, **37**, 350–356.
- 157 L. Liu, D. Cao, Y. Jin, H. Tao, Y. Kou and H. Meier, *Org. Biomol. Chem.*, 2011, **9**, 7007–7010.
- 158 *US Pat.*, US2007/197792, 2007.
- 159 M. Söftje, S. Acker, R. Plarre, J. C. Namyslo and D. E. Kaufmann, *RSC Adv.*, 2020, **10**, 15726–15733.
- 160 B. Latli, C. Than, H. Morimoto, P. G. Williams and J. E. Casida, *J. Labelled. Comp. Radiopharm.*, 1996, **38**, 971–978.
- 161 K. Han, Y. Zhang, J. Li, Y. Yu, X. Jia and C. Li, *Eur. J. Org. Chem.*, 2013, **2013**, 2057–2060.
- 162 C. Li, S. Chen, J. Li, K. Han, M. Xu, B. Hu, Y. Yu and X. Jia, *Chem. Commun.*, 2011, **47**, 11294–11296.
- 163 M. L. Martin and G. J. Martin, *Analisis*, 1999, **27**, 209–212.

- 164 T. K. Ronson, W. Meng and J. R. Nitschke, *J. Am. Chem. Soc.*, 2017, **139**, 9698–9707.
- 165 Y. Wang, G. Ping and C. Li, *Chem. Commun.*, 2016, **52**, 9858–9872.
- 166 T. Ogoshi, T. A. Yamagishi and Y. Nakamoto, *Chem. Rev.*, 2016, 116, 7937–8002.
- 167 Y. Ma, X. Chi, X. Yan, J. Liu, Y. Yao, W. Chen, F. Huang and J. L. Hou, *Org. Lett.*, 2012, **14**, 1532–1535.
- 168 D. Brynn Hibbert and P. Thordarson, *Chem. Commun.*, 2016, **52**, 12792–12805.
- 169 P. Thordarson, *Chem. Soc. Rev.*, 2011, **40**, 1305–1323.
- 170 BindFit v0.5 | Supramolecular, <http://app.supramolecular.org/bindfit/>, (accessed August 12, 2022).
- 171 D. M. Wang, Y. Aso, H. Ohara and T. Tanaka, *Polymers (Basel)*, 2018, **10**, 1095.
- 172 A. A. G. Moreira, P. De Lima-Neto, E. W. S. Caetano, I. L. Barroso-Neto and V. N. Freire, *New J. Chem.*, 2016, **40**, 10353–10362.
- 173 K. Chamberlain, A. A. Evans and R. H. Bromilow, *Pestic. Sci.*, 1996, **47**, 265–271.
- 174 N. L. Strutt, R. S. Forgan, J. M. Spruell, Y. Y. Botros and J. F. Stoddart, *J. Am. Chem. Soc.*, 2011, **133**, 5668–5671.
- 175 P. Metrangolo, F. Meyer, T. Pilati, G. Resnati and G. Terraneo, *Angew. Chem., Int. Ed. Engl.*, 2008, **47**, 6114–6127.
- 176 A. Forni, P. Metrangolo, T. Pilati and G. Resnati, *Cryst. Growth Des.*, 2004, **4**, 291–295.
- 177 M. Nishio, *Phys. Chem. Chem. Phys.*, 2011, 13, 13873–13900.
- 178 J. C. Dearden and W. F. Forbes, *Can. J. Chem.*, 1960, **38**, 896–910.
- 179 M. Daszkiewicz and A. Mielcarek, *Acta Crystallogr. B Struct. Sci. Cryst. Eng. Mater.*, 2016, **72**, 916–926.
- 180 O. Trott and A. J. Olson, *J. Comput. Chem.*, 2009, 455–461.
- 181 Z. Zhang, H. Liang, M. Li, L. Shao and B. Hua, *Org. Lett.*, 2020, **22**, 1552–1556.
- 182 *US Pat.*, US2018/65981, 2018.

CHAPTER 3. PILLAR[5]ARENE FOR THE SYNTHESIS OF ROTAXANE DECORATED METAL ORGANIC FRAMEWORKS

3.1. Introduction

Metal organic frameworks (MOFs) are porous materials constructed from rigid organic linkers connected *via* metal nodes. MOFs have garnered a lot of attention due to their tunability, porosity, and long-range order. Since the start of the century the number of publications on MOFs has seen a sharp increase, and equally the Cambridge Structural Database has estimated that 10% of its library is from just MOFs, with over 100,000 entries.^{1,2} The incorporation of rotaxanes within the MOF structure (so called MORFs) has been reported previously with numerous examples, however the covalent attachment of a rotaxane directly to a MOFs surface has yet to be seen.³

In this chapter, a method for the synthesis and analysis of a surface functionalised rotaxane MOF is proposed, and possible applications for such a system are discussed.

3.2. Rotaxanes

Rotaxanes are a subset of supramolecular chemistry within the wider umbrella of mechanically interlocked molecules (MIMs). Mechanically interlocked molecules are comprised of two or more molecular components being bound together, but unlike conventional organic systems, the molecules are not held together by covalent or ionic bonds. They are instead connected due to their topology, and are locked together by, for example bulky stopper groups inhibiting movement, or by ring closure. Examples of such systems are rotaxanes; a macrocycle threaded onto a dumbbell shaped rod with a bulky group on each end to help stop the macrocycle from dethreading,

catenanes; two or more mechanically interlocked macrocycles, and Borromean rings; three interlocked macrocycles (*figure 1*).⁴

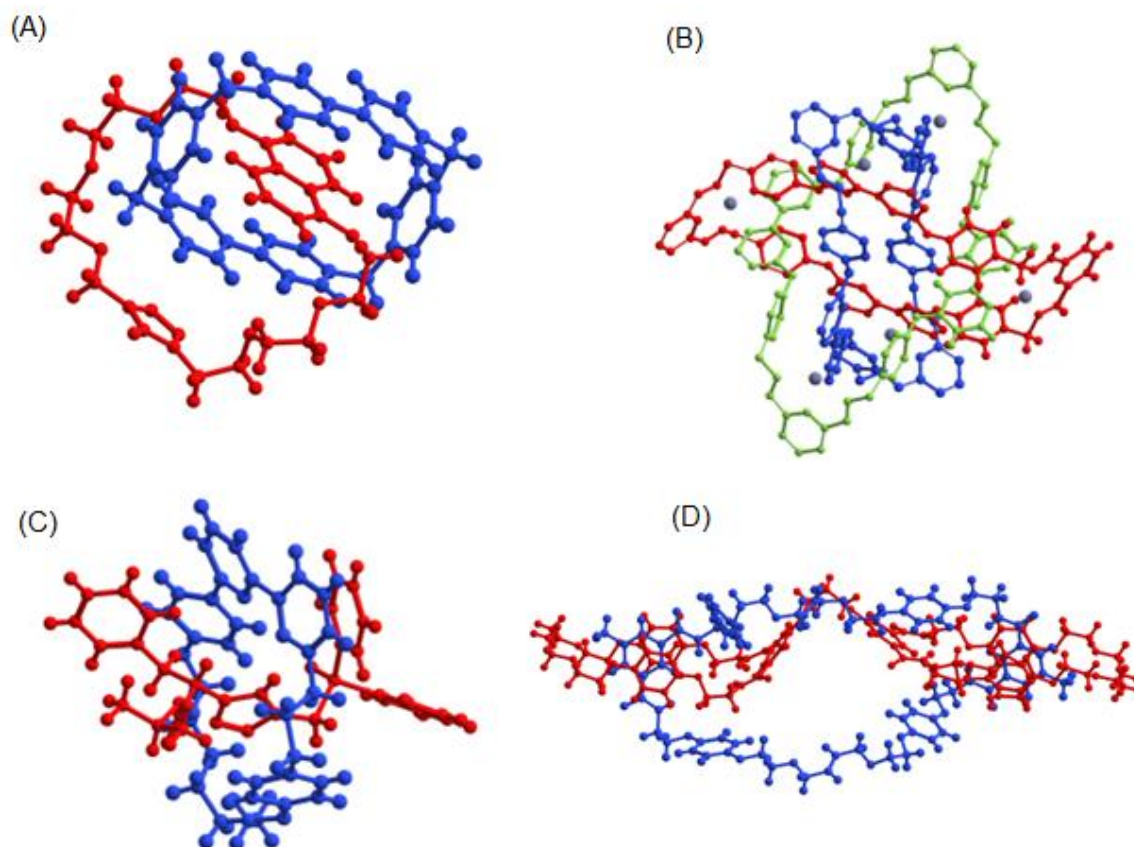


Figure 1. Examples of mechanically interlocked systems, with crystal structures of catenane (A), Borromean rings (B), rotaxane (C), and a handcuff catenane (D).⁵⁻⁸

3.2.1. Synthesis of Rotaxanes

There are three main synthetic routes for rotaxane formation: capping (also known as threading and stoppering), clipping, and slipping (*figure 2*). Firstly, capping is where the macrocycle is threaded through the rod, then a bulky stopper group is placed on the end to stop the macrocycle from dethreading. This process relies on there being a thermodynamic driving force for threading, this can be achieved via hydrophobic/hydrophilic interactions, hydrogen bonding or coulombic attractions between the rod

and macrocycle.⁹⁻¹¹ Secondly, for clipping, in this process the rod contains 'recognition sites'; where there is some intermolecular interaction to template the partial macrocycle to the rod. This induces a specific orientation of the partial macrocycle about the rod, at which point a subsequent ring closing reaction leads to formation of the rotaxane. The whole process may be controlled thermodynamically or kinetically depending on the precursors.¹² Finally, the slipping mechanism entails the mixing of the rod complete with stopper groups and the free macrocycle, energy is then supplied to the system *via* heat. This allows the macrocycle to overcome the energy barrier for threading, and due to positive noncovalent interactions between macrocycle and rod, the energy barrier for dethreading is higher than for the previous threading. Subsequent cooling will also aid prevention of dethreading. This method does require careful consideration of the sizes of both components, as slipping is only achievable if the macrocycle is capable of threading over the stopper groups.

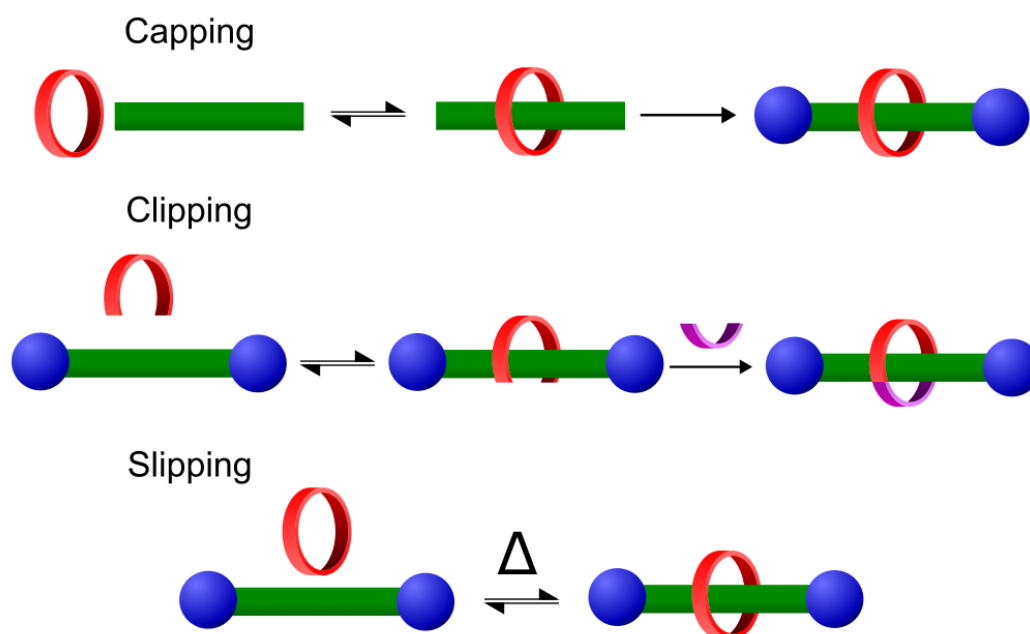


Figure 2. Generalised synthetic routes for the formation of rotaxanes

3.2.2. Dynamics of Rotaxanes

One of the most quintessential qualities of the rotaxane is the range of dynamic processes the molecule can perform. Compared to covalently bound molecules, rotaxanes contain components which are not intrinsically bound. Therefore, the macrocycle has largely free movement, both laterally and rotationally, relative to the rod it encompasses. The inherently dynamic nature of the rotaxane, and equally the mechanical bond, allows for application in the production of molecular machines.

Molecular machines encompass a wide range of different supramolecules, containing a wide range of motifs and fundamental components. However, the overarching theme of the molecular machine is that they will contain 'moveable parts that undergo reversible, positional displacements.'¹³ A wide variety of molecular machines have been reported, with examples of molecular motors, shuttles, cars, balances, hinges, tweezers and assemblers being synthesised.¹⁴⁻²¹ However, for this report only molecular shuttles are germane.

3.2.3. Molecular Shuttles

A molecular shuttle refers to an interlocked system where one component of the supramolecular structure has free movement back and forth between two or more 'stations' on the molecule it is encapsulating. This term is most commonly used when referring to rotaxanes, and the 'shuttling' of the macrocycle along the axle (*figure 3*). A rotaxane can often contain two or more distinct stations for the macrocycle to access, whereby an external stimulus can alter the equilibria to make one of the stations more favourable for the macrocycle to sit upon. That is not necessary however, as shown by *Langer et al*, wherein a symmetric axle was used with a macrocycle, and an external stimuli was applied that disabled shuttling altogether.²²

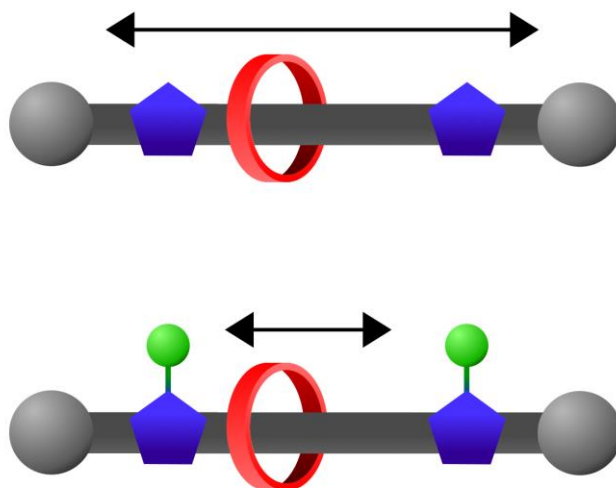


Figure 3. Diagram of a symmetric rotaxane system where the pillar[5]arene macrocycle has free movement between the two imidazole stations (top). And after addition of a coordinating metal, blocking the shuttling of the macrocycle (bottom). Adapted from from *Langer et al.*²²

There have been many examples of a two station rotaxane systems where control of the position of the macrocycle can be altered with an external stimulus. One such example from *Bissell et al* used a dicationic bis(paraquat) macrocycle, this was used alongside an axle with two different polyether linked stations (*figure 4*).²³ One of the stations was a biphenol unit, and the other station was a similarly sized benzidine. In a pH neutral environment, the macrocycle would shuttle between both stations on the NMR timescale, as was evident with ‘extreme broadening of many NMR signals’. However, when trifluoroacetic acid was added, the macrocycle could be isolated to be only situated around the biphenol unit. This phenomenon was attributed to the coulombic repulsions from the cationic cyclophane and the protonated amines in the benzidine unit. Importantly, when pyridine was added to neutralise the rotaxane, the shuttling could be reintroduced, thus indicating a reversible switchable molecular shuttle.²³

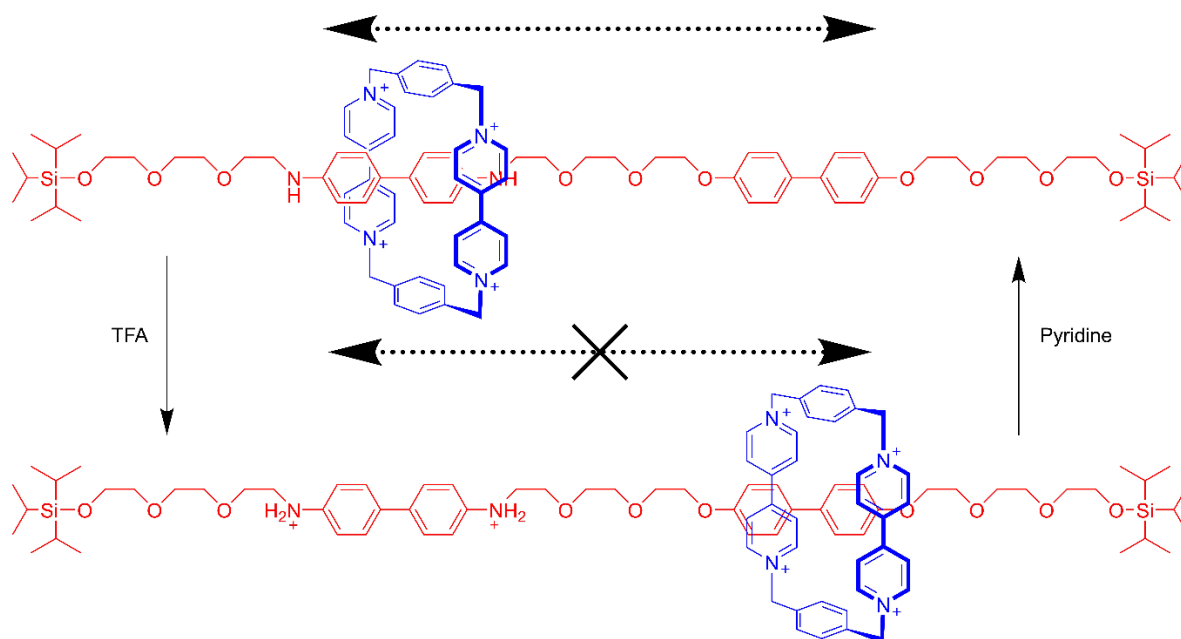


Figure 4. Example of a pH switchable molecular shuttle. Adapted with permission from *Bissell et al.*²³

3.2.4. Rotaxanes on Surfaces

Whilst there are a great many of examples of solution based rotaxanes with a myriad of molecular designs and characteristics, there have only been a select few examples of the study of a rotaxanes affixed to a 2D surface. With our collective understanding on the wide breadth of possible applications of rotaxanes in sensing, data storage and molecular logic-gates, it is pertinent to access how these properties will transfer once positioned upon a stationary platform.²⁴ The formation of such self-assembled monolayers, equally, gives an opportunity to project the inherent properties of the rotaxane upon a much larger macromolecular system.

As rotaxanes are most commonly bimolecular systems, it is evident that the synthetic routes to producing a rotaxane capable of surface modification is equally twofold in nature. Hence, either the macrocycle or rod component can contain the necessary functional group for surface binding. Equally, for the formation of rotaxane modified surfaces, it is possible for the rotaxane to be formed *post* or *pre* surface attachment.

The functional group necessary for surface modification is not fixed, but as the choice in functional group is dictated primarily by the surface, and the options for surfaces are limited, there are some reoccurring motifs observed in literature.

Sulfur-gold bonds (that of which will be explored further in chapter 4) are a popular motif, where a sulfur functionalised rotaxane is paired with a gold surface or with gold nanoparticles. An example of such a system reported by *Zhao et al*, used a rotaxane with a thiolane terminated rod and an anion templated isophthalamide macrocycle.²⁵ This rotaxane was then capable of chemisorption to a gold surface. An example of rotaxane formation upon an already adsorbed rod component was reported by *Nikitin et al*, wherein a tripodal axle with a viologen station and three thiol anchoring groups was adsorbed upon a gold surface. Subsequent additions of a cyclic ether macrocycle and a larger terminal stopper group, produced the rotaxane complete, as was evident by cyclic voltammetry.²⁶

Another route for the synthesis of rotaxane modified surfaces uses organic coupling reactions, often seen in conventional solution based synthetic chemistry. The copper-catalysed alkyne-azide cycloaddition, is a popular binding motif in surface assembly. For rotaxanes, this is especially prevalent when attachment is upon a polymer surface or bead. An inherent advantage of using polymer systems is that they can contain monomer units with either the azide or alkyne functionality, hence allowing for a wider range of rotaxanes to be introduced. *Asthana et al*, produced a rotaxane covered polymer bead (*figure 5*).²⁷ The polymer in question was functionalised with terminal azide groups, and the assembled rotaxane was functionalised with an alkyne group. A heterogeneous click reaction produced the intended rotaxane functionalised polymer bead, with an estimated 10^{14} rotaxanes per bead. Such a macromolecular structure could also be produced *in situ*, as was demonstrated by *Wilson et al*, who

used a similar azide-polymer, but performed the click reaction with the unthreaded rod and the macrocycle pre-rotaxane synthesis.²⁸

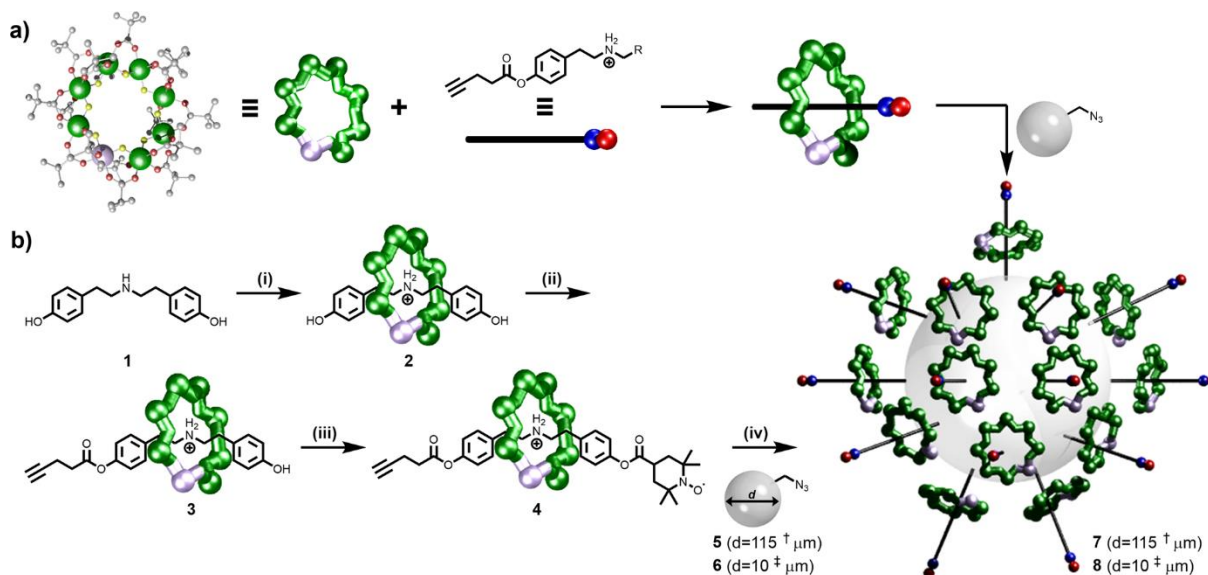


Figure 5. Synthetic route for rotaxane capped polymer beads *via* click chemistry. Extracted with permission from *Asthana et al.*²⁷

3.3. Metal Organic Frameworks

Porous materials have amassed great interest within a wide range of scientific fields. With potential applications in gas absorption, drug delivery, catalysis, and molecular separations, significant effort has been applied in creating such materials. The deliberate use of porous materials has been seen throughout history. With charcoal being used medicinally in ancient Greece, and as a water purification method in 450 BCE India.²⁹ The first documented study of the adsorption properties of porous materials was in 1780, when *Scheele* heated charcoal and measured the amount of gas expelled.³⁰

During this time another porous material; zeolite was first discovered, with naturally occurring stilbite being reported in 1756.³¹ It would not be until 1948 however, when

the first modern synthesis of a zeolite was reported by *Barrer*.³² Within 10 years, *Milton* reported the successful utilisation of synthetic zeolites as catalysts for hydrocarbon cracking.³³ From then onwards zeolites have been trialled in a number of scientific fields, with potential industrial applications being reported for energy storage, gas capture, host-guest assembly and drug delivery.^{34–36}

Whilst progressing in almost parallel timelines to zeolites, were the likes of porous polymer networks, and mesoporous silicas. It would not be until the 90s however, when MOFs would become fully established, with work by Hoskins and Robson in 1990.³⁷ With two further significant MOFs; MOF-5 and HKUST-1 being documented in 1999 (*figure 6*).^{38,39}

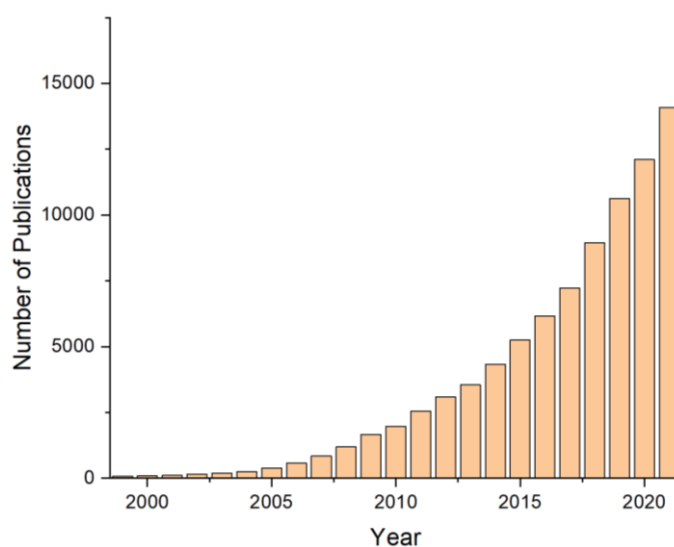


Figure 6. Number of publications per year from 1999-2021 from Web of Science containing 'metal organic framework'

3.3.1. Synthesis of MOFs

MOFs as previously mentioned contain at least two components; an organic linker and a metal node. The topology and properties of the MOF are largely defined by two factors: the geometry of the organic components and the preferred coordination

environment for the metal. By tailoring one or both of these components, one can attempt to dictate the structure, pore size and configuration of the MOF. The choice in linker and metal has been stated as being almost limitless, but there are some motifs that are often seen. The linkers most commonly used will utilise either carboxylate or pyridyl nodes, however imidazolate, phosphonate and tetrazolate nodes have also been reported.⁴⁰ As far as metals are concerned, as highlighted by *Griffin et al*: 'MOF research has touched on every part of the periodic table', with each group of metals showing unique properties and functionalities.⁴¹

The methods of synthesising MOFs have progressed significantly in the last 20 years, with methods involving, microwaves, electrochemistry and sonication being reported more regularly. However, for this work all MOFs were synthesised using 'conventional syntheses', that is using only thermal energy. That is, a reaction vessel is placed in a temperature controlled electric oven containing precise amounts of the metal salt and linker and heated at a specific temperature and time. The temperature of a reaction is a large contributor to the success of a reaction, and as such must be carefully controlled to ensure MOF growth. The other pertinent parameters in MOF synthesis are reaction time, concentration, and the use of a modulator. The first two are self-explanatory, but the application of a modulator within a reaction has only recently become better understood.

A modulator is an additional reagent that is added to a MOF synthesis, which does not necessarily appear within the MOF structure intact, but can alter and define the physical properties of the MOF. Properties including the crystallinity, particle size, porosity, morphology and surface chemistry of the MOF can all be altered *via* the use of a modulator, and as such have become important ingredients in MOF synthesis.⁴² The modulators used in MOF syntheses are many and varied, and they can perform

a myriad of roles within the MOF synthesis. However, generally, the modulator will resemble a monotopic ligand.

3.3.2. Surface Modification of MOFs

Whilst specific functionality can be presented to a MOF pre-synthesis *via* the use of specially tailored organic linkers, there also exists methods to alter a MOF's properties post-synthetically. Although there have been multiple reported routes for the post-synthetic modifications of MOFs, these methods can be largely reduced to two main directions.⁴³ Coordinative post-synthetic modification entails the introduction of a new organic group capable of metal ligation, which will either replace the original organic linker, or form additional bonds to the inorganic secondary building units within the MOF. An example of such modification would be the 'grafting' of ethylenediamine to the unsaturated metal sites in MIL-101, as shown by *Hwang et al.*⁴⁴ Alternatively, a covalent method to post-synthetic modification uses the existing organic linkers, and a reagent is used to directly modify these groups. Copper catalysed azide-alkyne click chemistry is often used for covalent modification due to its high success rate in a multitude of conditions including in heterogenous reactions, and the ease of incorporating azides or alkynes within a MOF architecture.⁴⁵

Whereas most cases of post-synthetic modification introduce functionality throughout the MOF, there have been fewer examples of modification solely on the MOFs surface. The few examples however, have provided interesting insight into potential applications for such surface-modified MOFs in biomedical, catalytic and selective uptake chemistry.⁴⁶ Akin to bulk post-synthetic modification, coordinative and covalent methods can be used for surface modification. The key difference between surface

and bulk methods is the relative size of the reagents available for addition to the MOF. For bulk post-synthetic modification of a MOF, the reagent to be added to the MOF is restricted by the size of the pores within the MOF. However, for surface modification, the size of the reagent is almost limitless, with larger macromolecules such as DNA, polypeptides and polymers being reported.⁴⁷⁻⁴⁹

Relevant to this work are covalent methods which, as mentioned previously, is where a MOF with tailored linkers containing functionalisable groups, are modified post-MOF formation. Akin to the rotaxane surface modification methods mentioned previously, this can be performed with a range of organic motifs. *Jiang et al*, used a series of azide containing linkers to synthesise a series of MOFs, and by varying the ratios of azide groups within the MOF, controlled loading of alkyne bearing molecules were able to be grafted within the MOF.⁵⁰ Equally, with copper catalysed azide-alkyne reactions *Zhang et al*, was able to further functionalise a MOF which contained two linkers, one incorporating azide functionality and the other alkyne. With this MOF, specific organic groups could be grafted into the MOF structure in precise positions within the framework, selected by either the alkyne or azide on the newly incorporated organic molecule.⁵¹ Both the previously stated examples functionalised throughout the MOF and were not isolated solely to the surface. However, the same principles can be applied when attaching larger molecules to the surface of MOFs *via* click chemistry. An example of such was reported by *Morris et al*, where azide containing MOFs were surface modified with strands of DNA (*figure 7*). In this example however, due to the DNA being functionalised with dibenzocyclooctyne the click reaction could be performed without a copper catalyst.⁵²

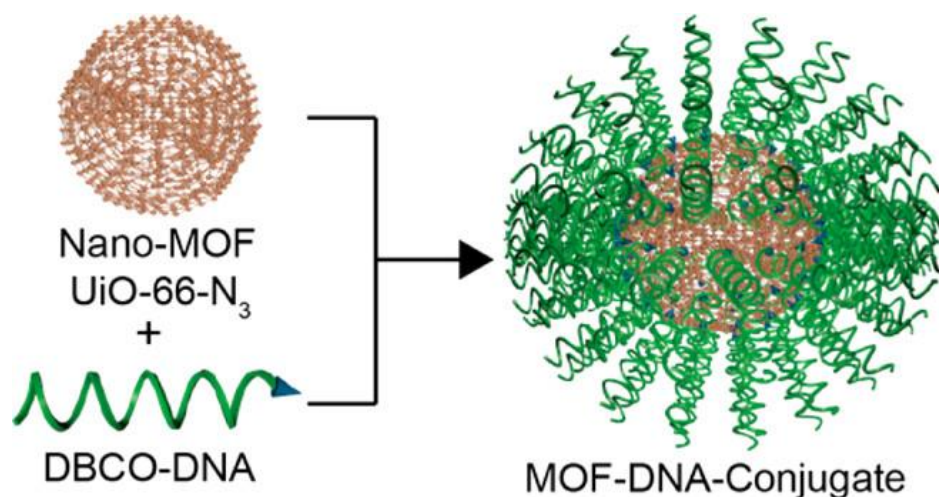


Figure 7. Schematic of the grafting of dibenzocyclooctyne terminated DNA onto an azide containing MOF. Reproduced with permission from *Morris et al.*⁵²

3.3.3. Rotaxanes and MOFs

As far as rotaxanes post-synthetically affixed to MOFs are concerned, there are no reports of such a system being reported at the time of writing. *Feng et al.*, reported a similar system using a Zr-BTB (4,4',4''-benzene-1,3,5-triyl-tris(benzoic acid)) MOF as a starting point, however the MOF was exfoliated to give single 2D sheets (*figure 8*).⁵³ In this example the axle component was grafted upon the 2D sheet *via* a terminal carboxylate group on the axle, with this group, ligand exchange on the zirconium could be undertaken from the OH⁻/H₂O to the axle. The rotaxane could then be synthesised upon the surface after radical reduction of both components, from bipyridine²⁺ to bipyridine^{•+} on the rod. Equally, the bis(paraquat) macrocycle which has been detailed in the rotaxane section was reduced from 2⁺ to 1^{•+}. These reductions led to a favourable trisradical-tricationic complexation. However, after a subsequent oxidation, the coulombic interactions between both cationic components leads to the macrocycle moving away from the bipyridine unit and down towards the surface. Importantly, after the addition of hydrochloric acid, the rotaxane could be released, returning the

zirconium surface to its un-grafted state. The surface assisted rotaxane formation reaction could then be performed again with new organic components.

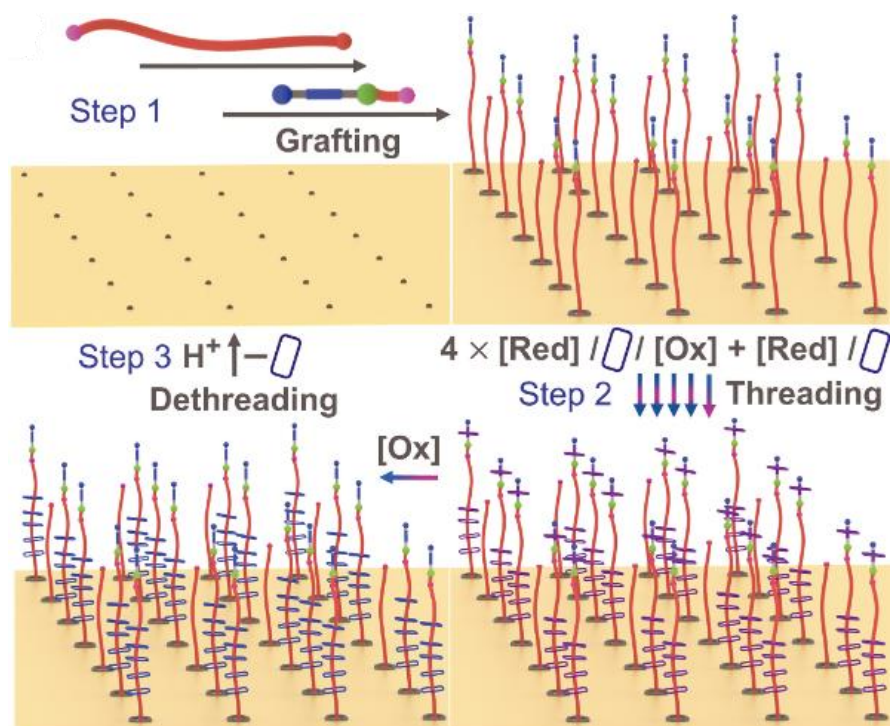


Figure 8. Graphical schematic of the mechanisorption of a rotaxane upon an exfoliated MOF 2D sheet. Step 1: grafting of a carboxylate terminated polymer upon the surface, and a subsequent click reaction to attach the bipyridine containing section (blue square). Step 2: Adsorption of cyclophane macrocycle after redox cycling. Step 3: Desorption of rotaxane after addition of acid. From L. Feng, Y. Qiu, Q. H. Guo, Z. Chen, J. S. W. Seale, K. He, H. Wu, Y. Feng, O. K. Farha, R. Dean Astumian and J. Fraser Stoddart, *Science* (80-.), 2021, **374**, 1215–1221. Reprinted with permission from AAAS.⁵³

Aside from this one example however the only combination of rotaxanes and MOFs arises in the form of metal-organic rotaxane frameworks (MORFs) where the rotaxane is part of the MOF structure. There have been several examples of rotaxane ligands being used within metal-organic frameworks, with a range of 1D, 2D, and 3D frameworks being documented. The synthesis of MORFs is not wholly representative of this work, but it does offer insights into the possibilities that can arise with the merging of rotaxanes and MOFs.^{3,54}

3.4. Results and Discussion

Within in this chapter a detailed plan of multiple routes to the surface modification of MOFs with rotaxanes will be presented. Alongside, will be a detailed discussion on the synthetic routes trialled for this research, with focus both on the organic linkers for the MOF and for surface-grafting capable rotaxanes. The rotaxane designs will arrive from a semi-modular approach to rotaxane synthesis, that is a dissection and evaluation of the individual components of the rotaxane. This alternative approach to rotaxane design should allow for a greater freedom of customisability, and guided tailoring towards specific surfaces and applications. This chapter will be organised to partition between three possible routes for the rotaxane-MOF, and ultimately conclusions will be drawn from all three methods.

3.5. Surface Modification of MOFs With Rotaxanes *Via CuAAC Click Chemistry*

As previously discussed, the copper-catalysed alkyne-azide cycloaddition is a popular method for the joining of two molecular components and can be performed in a heterogenous reaction. For this study, functionalising the MOF with azide moieties, whilst focussing on synthesizing a rotaxane with an alkyne appendage, was ultimately decided upon.

3.5.1. Synthesis of an Azide Functionalised MOF

To yield a MOF with azide functionality, the initial step was to synthesise a linker which has both azide appendages and carboxylate groups for metal ligation.

3.5.1.1. Synthesis of Dimethyl 2',5'-dimethyl-[1,1':4',1''-terphenyl]-4,4''-dicarboxylate

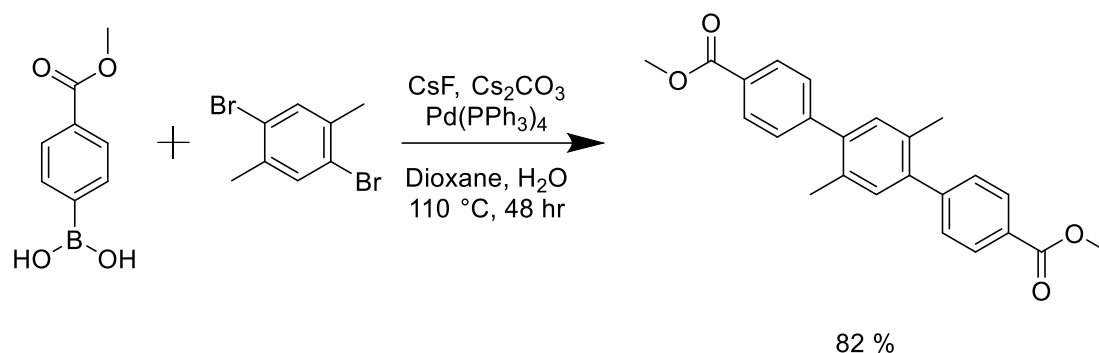


Figure 9. Reaction scheme for the synthesis of 2',5'-dimethyl-[1,1':4',1''-terphenyl]-4,4''-dicarboxylate

The synthesis of the organic linker proceeded *via* a method adapted from *Goto et al* (*figure 9*).⁵⁵ The initial Suzuki reaction to form the terphenyl, deviated from *Goto et al's* method by using 1,4-dibromo-,2,5-dimethylbenzene instead of the diiodo derivative, this was due to availability of the compound. Equally, the boronic acid was used, instead of the pinacol ester. The result of this was that for the reaction to be completed in high yield, caesium carbonate had to be added as an additional base. Equally, for this reaction to successfully proceed the palladium catalyst was changed from [1,1'-Bis(diphenylphosphino)ferrocene]dichloropalladium(II) (Pd(dppf)Cl₂) to tetrakis(triphenylphosphine)palladium(0) (Pd(PPh₃)₄). After 2 days of heating at reflux, the reaction mixture was redistributed into chloroform then filtered through celite to remove palladium metal. Crystallisation from acetone would then yield the final product as a white solid.

3.5.1.2. Synthesis of Dimethyl 2',5'-bis(bromomethyl)-[1,1':4',1''-terphenyl]-4,4''-dicarboxylate

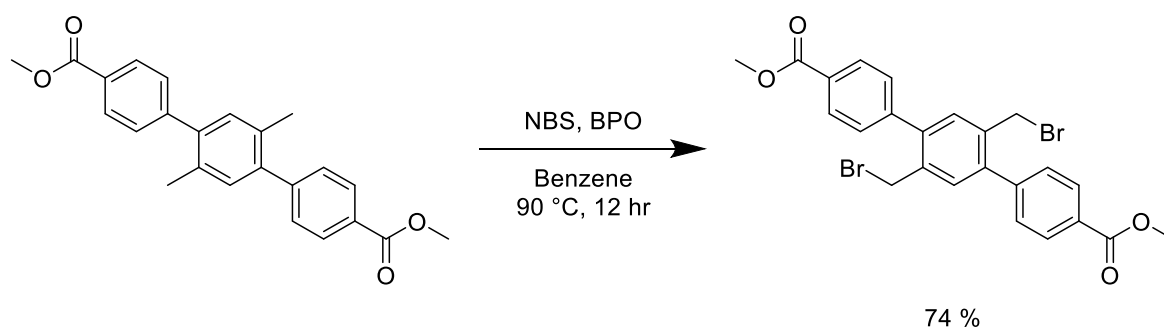


Figure 10. Reaction scheme for the synthesis of 2',5'-bis(bromomethyl)-[1,1':4',1''-terphenyl]-4,4''-dicarboxylate

Bromination of the previous methyl derivative proceeded *via* the Wohl-Ziegler bromination (*figure 10*). Within this reaction N-bromosuccinimide was used as the bromine source, and benzoyl peroxide was used as the radical initiator. After the reaction mixture had heated overnight at reflux, the benzene was removed. The final product could then be retrieved after washing with methanol to remove excess succinimide and benzoyl peroxide. It is important to note that initial proton NMR spectrum still showed benzoyl peroxide in the product, but after subsequent methanol washes, this impurity was removed.

3.5.1.3. Synthesis of Dimethyl 2',5'-bis(azidomethyl)-[1,1':4',1''-terphenyl]-4,4''-dicarboxylate

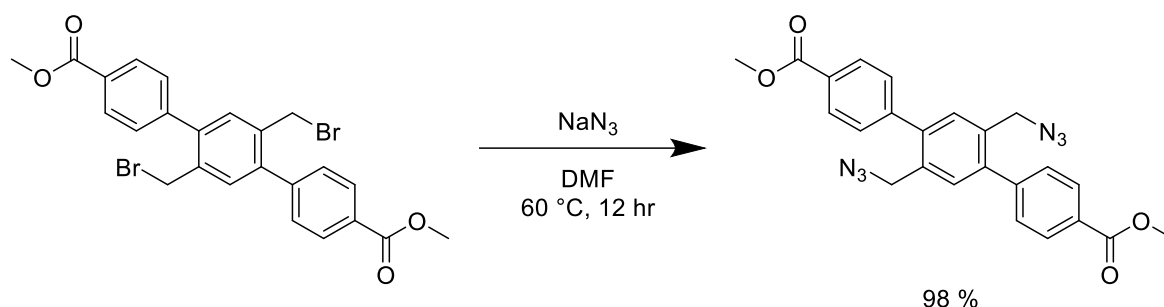


Figure 11. Reaction scheme for the synthesis of 2',5'-bis(azidomethyl)-[1,1':4',1''-terphenyl]-4,4''-dicarboxylate

The azidation of the dibromomethyl starting material used sodium azide in *N,N*-dimethylformamide solvent (*figure 11*). This reaction was performed under nitrogen and in anhydrous conditions to prevent the degradation of sodium azide in water. After the reaction was complete the reaction mixture was added to brine then the product was extracted with ethyl acetate. Removal of the ethyl acetate *in vacuo* gave the final product as a white solid.

Sodium azide can be extremely dangerous, although we experienced no issues when handling sodium azide, care must always be taken. Sodium azide reacts violently with water, and can explode in contact with acids, metals, and with shock, concussion or friction. It is also extremely toxic to both users and aquatic life, releasing hydrazoic acid in contact with acid or water. As such, all reactions must proceed cautiously with adequate PPE and with understanding of the relevant safety measures of both reagents and products.

3.5.1.4. Synthesis of 2',5'-Bis(azidomethyl)-[1,1':4',1''-terphenyl]-4,4''-dicarboxylic acid

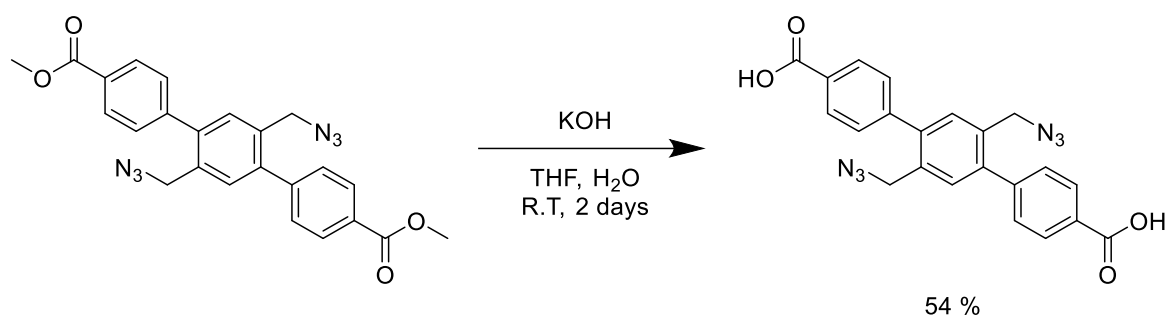


Figure 12. Reaction scheme for the synthesis of 2',5'-Bis(azidomethyl)-[1,1':4',1''-terphenyl]-4,4''-dicarboxylic acid

Saponification of the ester utilised potassium hydroxide as the base (*figure 12*). Hydrochloric acid was then used after the reaction had completed to protonate the carboxylic acids. The reaction mixture was added to ethyl acetate, and after several water washes, the organic layer was removed *in vacuo* to yield the linker complete as a light-yellow solid.

3.5.1.5. Synthesis of UIO-68 N₃ MOF

The synthesis of the MOF was performed by a Dr Sarah Griffin by a solvothermal method. The azide linker, zirconium chloride and a benzoic acid modulator, was added to DMF. This mixture was then heated in an oven at 120 °C overnight.

3.5.2. Design and Synthesis of Rotaxane for Surface Modification of an Azide Functionalised MOF

For the rotaxane component, the incorporation of an alkyne group capable of azide-alkyne cycloaddition was paramount. The other essential components were, a rod section with moieties available for pillar[5]arene intermolecular non-covalent binding, and a fluorescent component for the analysis of the modified MOF. With a rotaxane

consisting of three components, rod, stopper group and macrocycle, the potential structure of the rotaxane could take many forms. A few different rotaxane motifs were trialled, but after careful consideration the following rotaxane design was favoured.

3.5.2.1. Design of Rod Component

Firstly, the rod component would contain both an imidazole group and an amine, these groups will assist in attaching the stopper groups, but equally will act as stations for the pillar[5]arene to shuttle between. Additionally, as shown with previous switchable molecular shuttles, the incorporation of an amine moiety on the rod can be a prerequisite for potential pH-controlled switching. The length of the alkyl chain that joined the imidazole and amine was incredibly important, as large discrepancies can be seen between the binding constants between pillar[5]arene and varying alkanes with neutral groups appendaged. For example, for a bis(imidazole)alkane *Li et al* reported a 25 times decrease in the binding constant between the butyl and pentyl derivatives.⁵⁶ However, for the rotaxane to have the potential as a molecular switch a butyl chain would be too small to allow for sufficient shuttling. Therefore, to allow for both efficient binding, and a long enough chain for switchable shuttling a chain length of 6 was decided upon.

3.5.2.2. Synthesis of Rod Component

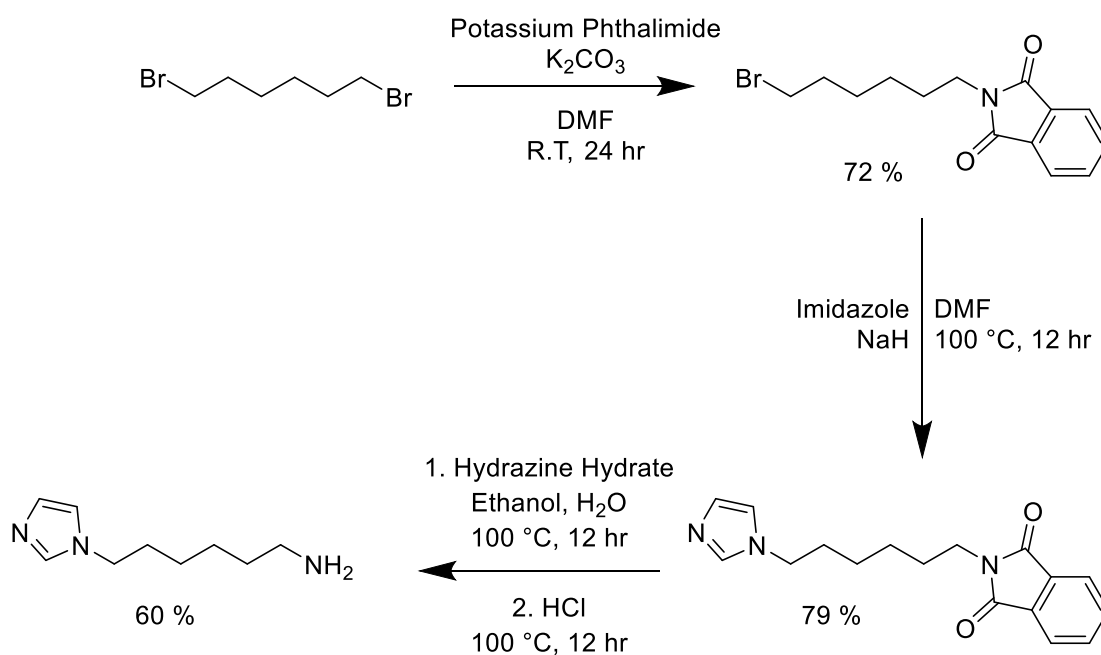


Figure 13. Reaction scheme for the synthesis of the rod component from 1,6-dibromohexane via the Gabriel Synthesis method.

The synthesis of the rod component proceeded via the Gabriel syntheses of amines from alkyl halides (figure 13). The initial step was the asymmetric addition of phthalimide to 1,6-dibromohexane. To ensure this reaction produced only the mono-substituted alkylphthalimide the alkene was used in large excess (ca 10 times). After the reaction had gone to completion, and the solvent removed, the excess alkylhalide could then be removed by recrystallisation in hexane. This gave the pure product as white crystals in good yields (ca 90 %).

The next stage would be to affix the imidazole component to the other end of the chain. As the asymmetric property of the rod was already established by the addition of the phthalimide, the addition of the imidazole could be performed easily. Two methods were possible for this transformation: sodium hydride as the base in DMF, or potassium carbonate as the base in acetone. Although success was seen with both

methods, the better yields and shorter reaction times of the method employing sodium hydride, made it a more attractive option. After the reaction had been completed, as indicated by the disappearance of the starting material in thin layer chromatography, the solvent was removed *in vacuo*. After dissolution in chloroform and subsequent aqueous washes, the product was purified *via* column chromatography to remove excess imidazole.

The final step of the reaction was the formation of the primary amine from the phthalimide group *via* the Ing-Manske procedure (*figure 14*). For this sequence within the Gabriel synthesis, acidic hydrolysis to give the amine salt is also possible. However, this reaction is known to give low yields and side products, so the aforementioned Ing-Manske procedure using hydrazine was favoured instead. The substitution advances through a known mechanism, firstly the hydrazine performs a nucleophilic acyl substitution towards the phthalimide's carbonyl group. The protonated hydrazine is then deprotonated by the parallel anionic nitrogen, and finally the unreacted NH₂ on the hydrazine attacks the other carbonyl *via* the nucleophilic acyl substitution mechanism. After protonation, this gives the primary amine and phthalhydrazide as a side product. In practice, this reaction is carried out by firstly reacting the phthalimide containing starting material and hydrazine monohydrate overnight at room temperature. To remove the phthalhydrazide, the reaction mixture is first acidified with hydrochloric acid to protonate the primary amine. The side product could then be removed by washing the aqueous layer with dichloromethane. Subsequent basification will neutralise the amine, which can be extracted with dichloromethane. After the solvent is removed *in vacuo* the final product is obtained as a yellow oil.

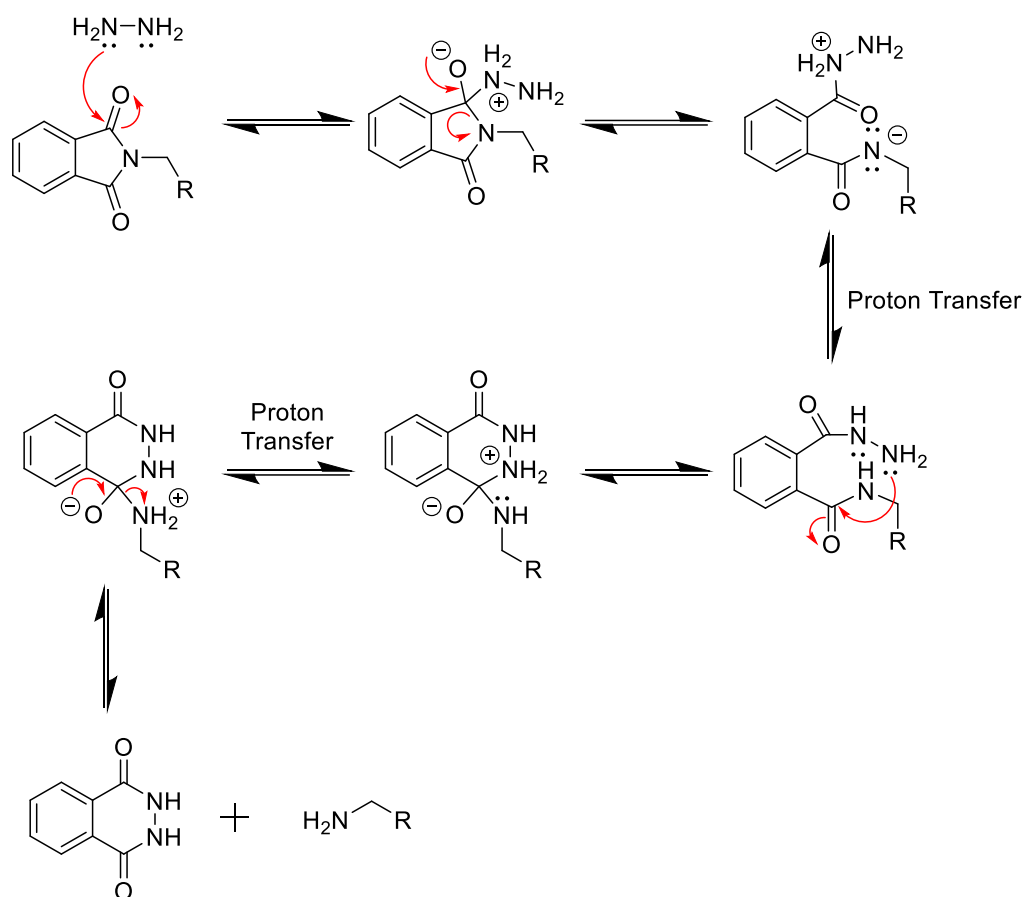


Figure 14. Mechanism of the Ing-Manske Procedure. Adapted from *Valiulin*.⁵⁷

3.5.2.3. Design of Stopper Groups

For the stopper groups there were three criteria that had to be fulfilled. Firstly, like all stopper groups, the group itself must be big enough to prevent dethreading of the macrocycle from the rod. Secondly, there must be an alkyne group on at least one of the stopper groups to allow for surface attachment to the MOF. Finally, due to the predicted difficulty in analysing the surface modified MOF, there would need to be a fluorescent group on one of the stoppers so that successful adoption of the rotaxane can be proven. To adhere to these principles two inequivalent stopper groups were devised and synthesised. Hence the synthesis of both a fluorescent stopper, and an alkyne bearing stopper.

3.5.2.4. Synthesis of Alkyne Functionalised Stopper

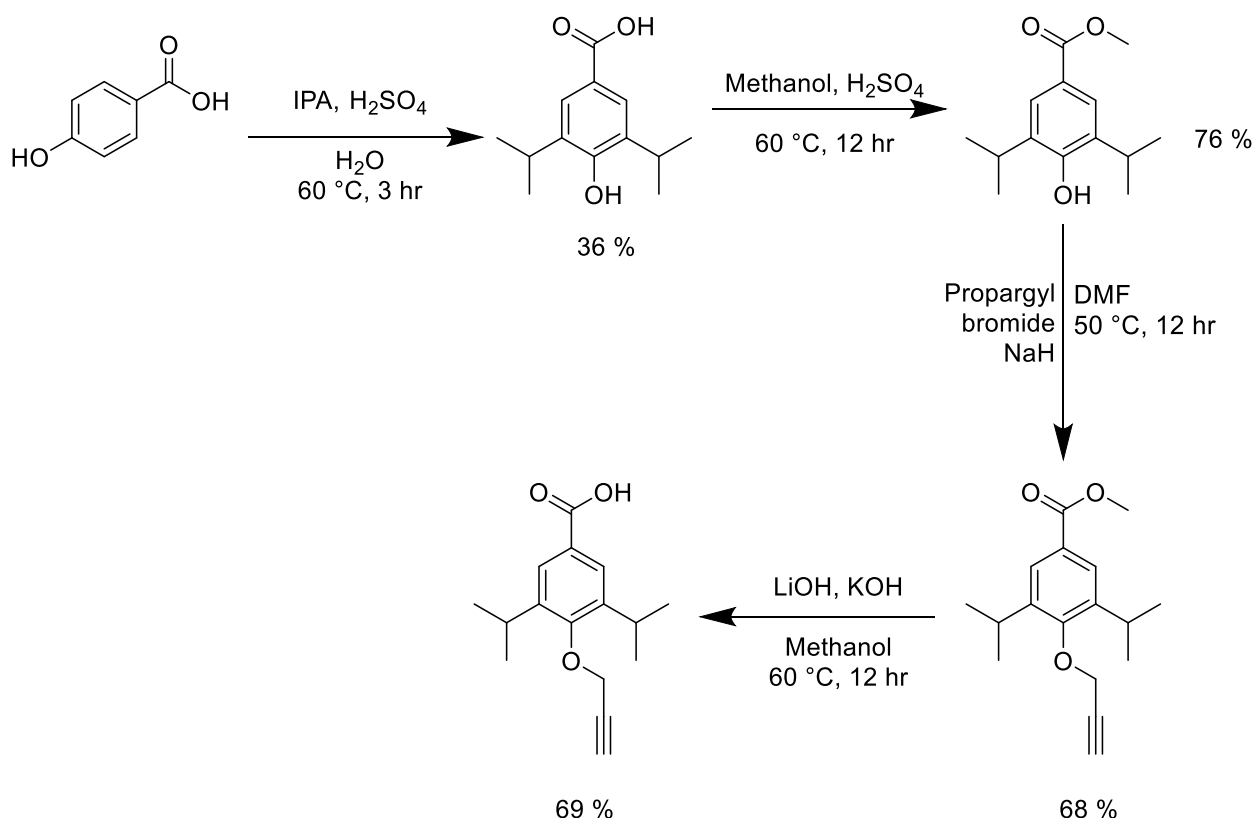


Figure 15. Reaction scheme for the synthesis of the alkyne functionalised stopper group

As previously mentioned, the alkyne functionalised stopper will need not only the aforementioned alkyne group, but also large bulky groups and a method for grafting to the rod component. For the stopper group steric bulk was ensured with the attachment of two isopropyl groups to the phenyl stopper (*figure 15*). This reaction proceeded through a Friedel-Crafts alkylation with sulfuric acid as the catalyst. After the reaction was completed the purification method was as follows. Firstly, the acidic mixture was basified with lithium hydroxide until the mixture was pH 12, this had to be done slowly and carefully because of the exothermic reaction between lithium hydroxide and sulfuric acid. The reaction mixture will go from yellow to pink when sufficient base has been added, indicating the conversion of the product from carboxylic acid to carboxylate. The alkaline solution can then be washed with toluene

to remove starting material and any side products. To retrieve the carboxylic acid, the mixture was reacidified to pH 3, the white precipitate could then be collected and washed with methanol to give the final product as a white crystalline solid.

Before attachment of the alkyne group, the carboxylic acid requires conversion to the methyl ester. This is to ensure the etherification of the alkyne group towards the phenol, and to avoid esterification with the carboxylic acid. The esterification proceeded *via* a Fischer esterification, with sulfuric acid as the catalyst. The reaction mixture was stirred overnight, and the solvent was removed *in vacuo* and washed with water to give the ester as a white crystalline solid.

To add the alkyne group, a Williamson etherification of the phenol with propargyl bromide was implemented. Due to the low boiling point of propargyl bromide (89 °C), the choice of base was steered towards a stronger base to avoid the need for higher temperatures. Therefore, instead of potassium carbonate (pKa 10.25) which was seen used previously for an etherification, the stronger sodium hydride (pKa 35) was used. After the solvent and excess propargyl bromide had been removed, the crude product could be purified *via* recrystallisation from hexane. The final product was obtained as a white crystalline solid.

Finally, to retrieve the stopper group as a carboxylic acid, the methyl ester was saponified using a mixture of potassium hydroxide and lithium hydroxide. Two bases were used, as when previously trialled with only one base there was not efficient removal of the methyl ester. The reaction mixture was acidified with hydrochloric acid to give a white precipitate which was collected and washed with methanol, giving the final alkyne bearing stopper group as a white powder.

To assess the viability of this alkyne functionalised molecule as a stopper group the crystal structure of the ester was assessed (*figure 16*). What was evident from the structure was that the maximum width of the molecule from one isopropyl group to the other was 6.4 Å, larger than the cavity of pillar[5]arene (ca 5 Å). Indicating that this stopper group was sufficiently bulky to act as a barrier to dethreading.

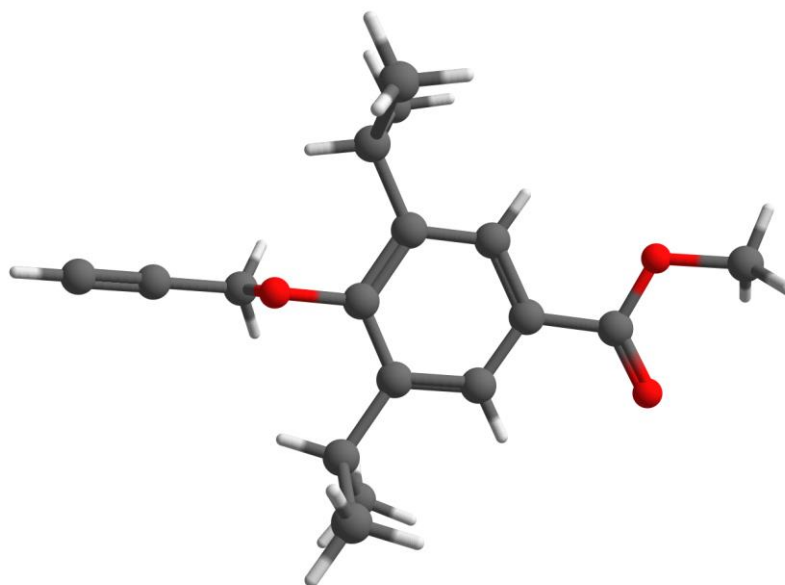


Figure 16. Crystal structure of the ester derivative of the alkyne functionalised stopper group.

3.5.2.5. Coupling of Alkyne Functionalised Stopper to Rod Component

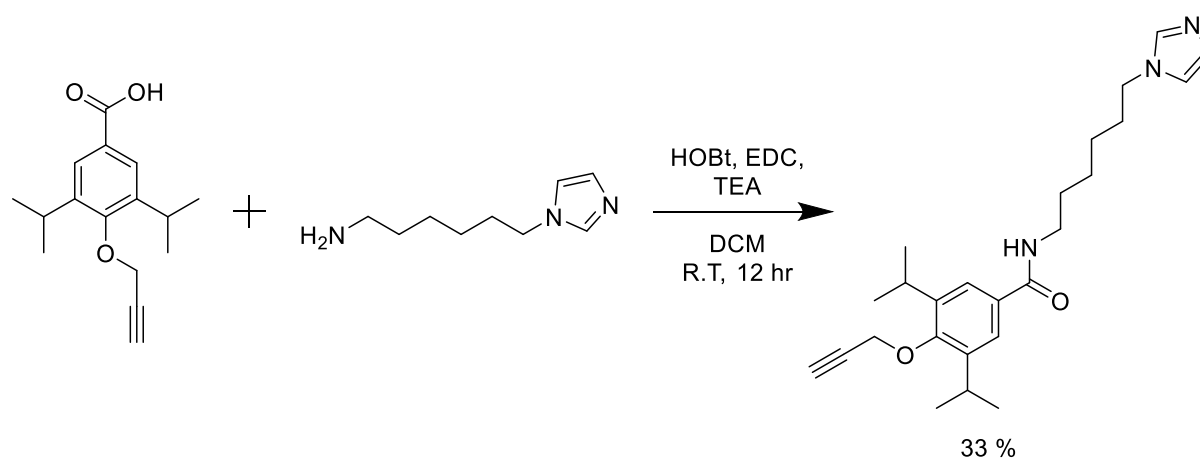


Figure 17. Reaction scheme for the amide coupling between the alkyne functionalised stopper and the rod component.

Before the rotaxane syntheses, the alkyne bearing stopper group was attached to the rod *via* an EDC amide coupling reaction (*figure 17*). Although other coupling reagents could be used (dicyclohexylcarbodiimide (DCC) or diisopropylcarbodiimide (DIC)) the advantage of 1-ethyl-3-(3-dimethylaminopropyl)carbodiimide (EDC) is that the by-product formed from this reaction is a water soluble urea, therefore the purification is easily achieved by washing with water. This is compared to the dicyclohexylurea by-product of DCC and *N,N'*-diisopropylurea of DIC, both of which are soluble only in organic solvents, hence harder to separate from an organic solvent soluble product. 1-Hydroxybenzotriazole (HOBt) was used as an auxiliary reagent within this amide formation, HOBt's role in the reaction is twofold; supressing racemization in the coupling reaction and increasing the reactivity of the ester intermediate (*figure 18*). *N,N*-Diisopropylethylamine (DIPEA) is an organic base that will deprotonate both the carboxylic acid and the HOBt, again increasing the efficiency of the reaction.

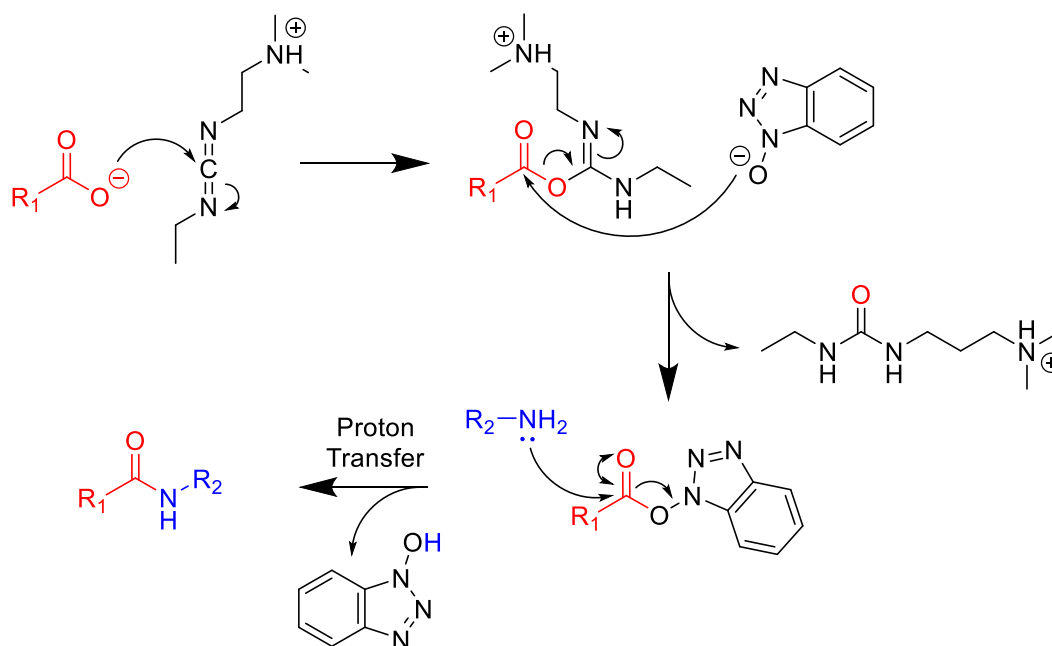


Figure 18. Mechanism of EDC amide coupling with HOBt. Adapted from *Montalbetti et al.*⁵⁸

3.5.2.6. *Design of Fluorescent Stopper*

The other crucial component for the rotaxane would be a fluorescent component. There is a myriad of fluorophores available, however for this rotaxane system, specific criterium would need to be fulfilled. Firstly, the fluorophore would have to be large enough to also function as a stopper group. Equally, the molecule will have to be able to be functionalised with an organic group that will attach to the imidazole component of the rod. The prerequisite that ultimately would guide towards the appropriate fluorophore, was the emission wavelength guidelines (450-600 nm) that were set for the instrument that was to be used to measure adsorption to the surface.

The final fluorophore that was chosen, therefore, was a 4,4-difluoro-4-bora-3a,4a-diaza-s-indacene (BODIPY), based fluorophore. This fluorophore was chosen due to its ease of functionalisation, stability in organic solvents, and tuneable fluorescent emission. More specifically, 2,6-diethyl-4,4-difluoro-1,3,5,7-tetramethyl-8-phenyl-4-bora-3a,4a-diaza-s-indecene was used as the scaffold to build the stopper group from. This specific BODIPY variant was highlighted as the most suitable candidate for its increased stability at higher temperatures and relatively high emission wavelength of ca 530 nm.⁵⁹

3.5.2.7. *Testing of Fluorophore for Confocal Microscopy*

Prior to synthesis of the rotaxane, the fluorophore was trialled for its effectiveness as a marker for surface modification. This step was performed not only to trial the fluorophore, but also to ensure the MOF and the method of surface functionalisation would be applicable. What was needed therefore, was the same BODIPY motif that would be used in the rotaxane, but with a pendant alkyne group to attach *via* the azide groups to the MOF.

3.5.2.8. Synthesis of Alkyne BODIPY

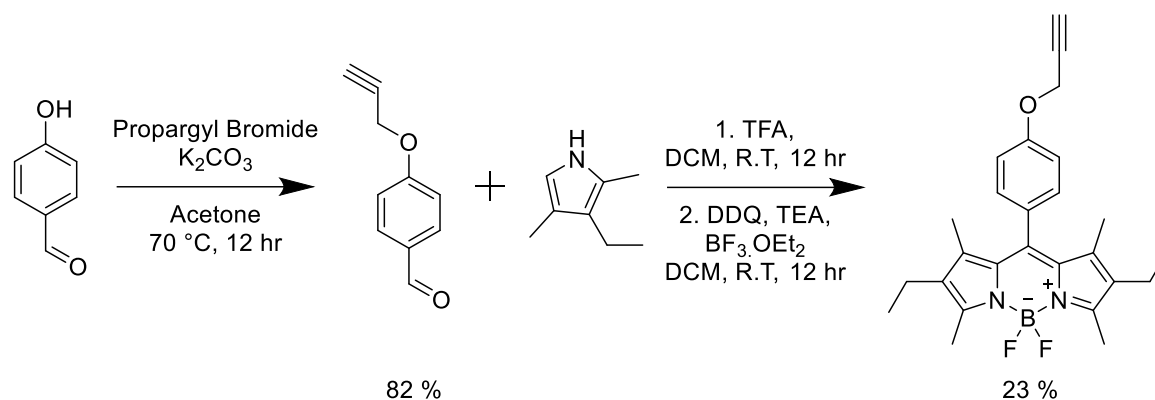


Figure 19. Reaction scheme for the synthesis of alkyne functionalised BODIPY

The synthesis of the alkyne functionalised BODIPY proceeded via the initial preparation of 4-(prop-2-yn-1-yloxy)benzaldehyde from 4-hydroxybenzaldehyde and propargyl bromide (*figure 19*). For this Williamson ether synthesis, potassium carbonate was used as the base and acetone the solvent. Similarly, to the etherification of the alkyne bearing stopper group, the product in this step was purified by hexane recrystallisation to give 4-(prop-2-yn-1-yloxy)benzaldehyde as a white solid.

To construct the BODIPY fluorophore 4-(prop-2-yn-1-yloxy)benzaldehyde, 3-ethyl-2,4-dimethyl-1H-pyrrole and a catalytic amount of trifluoroacetic acid, were stirred in dichloromethane overnight at room temperature. Dehydrogenation of the formed intermediate would then be completed with the oxidant 2,3-dichloro-5,6-dicyano-1,4-benzoquinone (DDQ). This could then be reacted with boron trifluoride diethyl etherate (BF₃·OEt₂) and a base (in this case triethylamine (TEA)) to form the BODIPY. Subsequent purification with column chromatography yielded the intended BODIPY in low yields (*ca* 20 %). This low yield could be ascribed to the preferential formation of the unsubstituted BODIPY. The unsubstituted BODIPY is said to arise from the

dichloromethane solvent acting as the *meso*-carbon source as outlined by *Auguiar et al.*⁶⁰ They found that when other solvents were used, whilst yielding only the intended substituted BODIPY, the yields were lower than that of the reaction with dichloromethane even after accounting for the unsubstituted impurity (*figure 20*).⁶⁰

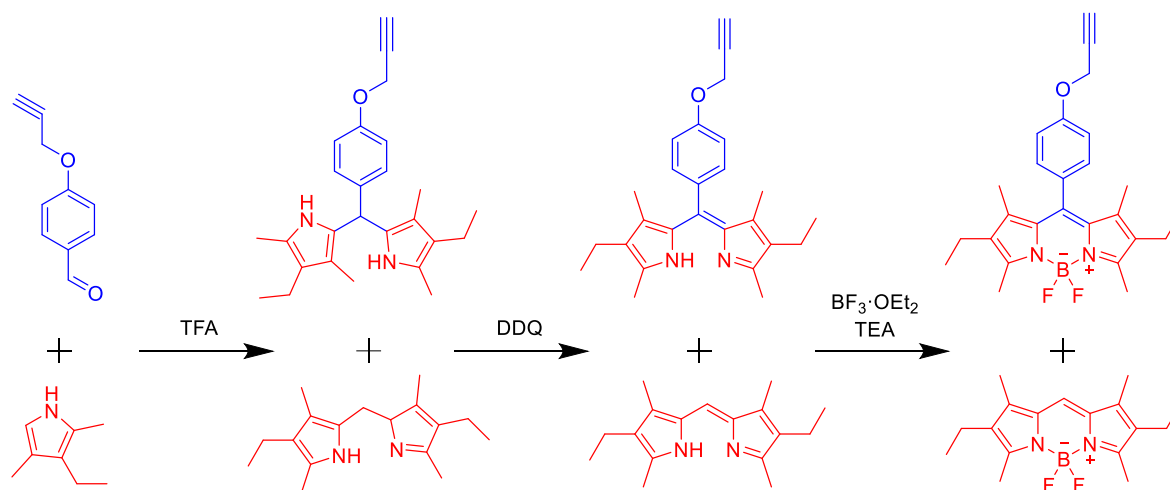


Figure 20. Reaction scheme showing the intermediates in BODIPY synthesis and highlighting the competitive formation of the alkyne BODIPY (top), and unsubstituted BODIPY (bottom).

For the surface modification of the MOF, the reaction conditions used were typical of a heterogeneous copper(I)-catalysed alkyne-azide cycloaddition. Several crystals of UIO-68 azide MOF were suspended in degassed dimethylformamide, the alkyne BODIPY was then added alongside: copper sulfate, sodium ascorbate and catalytic amounts of copper metal. After stirring overnight at room temperature, the crystals were carefully pipetted out of the solution and washed multiple times with dimethylformamide, acetone, methanol, water and dichloromethane.

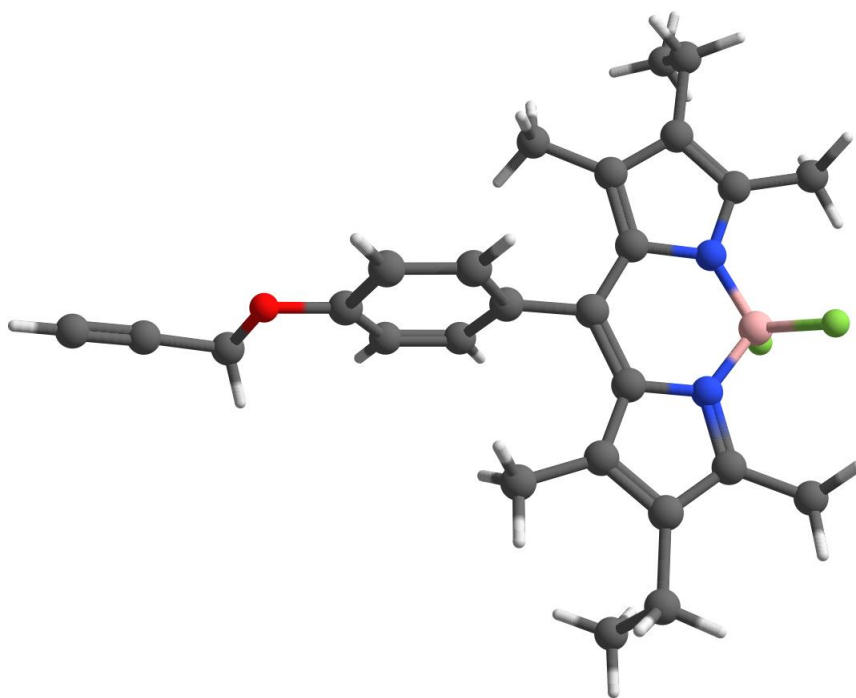


Figure 21. Crystal structure of alkyne BODIPY, with boron (pink), fluorine (green), nitrogen (blue) and oxygen (red).

To assess whether the fluorescent BODIPY was large enough to perform as a stopper group a crystal structure was examined. The structure showed us that the width of the BODIPY was 9.7 Å and its height from oxygen to boron was 8.6 Å, much larger than the cavity size of 5 Å for pillar[5]arene (*figure 21*).

3.5.2.9. Confocal Microscopy of BODIPY functionalised MOF

All confocal microscopy measurements were performed by Dr Stanimir Tashev under the supervision of Professor Dirk-Peter Herten. Reference images of the bottom edge and inner core of UIO-68 azide without the BODIPY were obtained in dimethylformamide and 10 Mm MgCl₂ in phosphate-buffered saline (PBS). These images were compared to those of the MOF after the cycloaddition with the alkyne BODIPY (*figures 22 and 23*).. Confocal z-scans were taken at a wavelength of 470 nm.

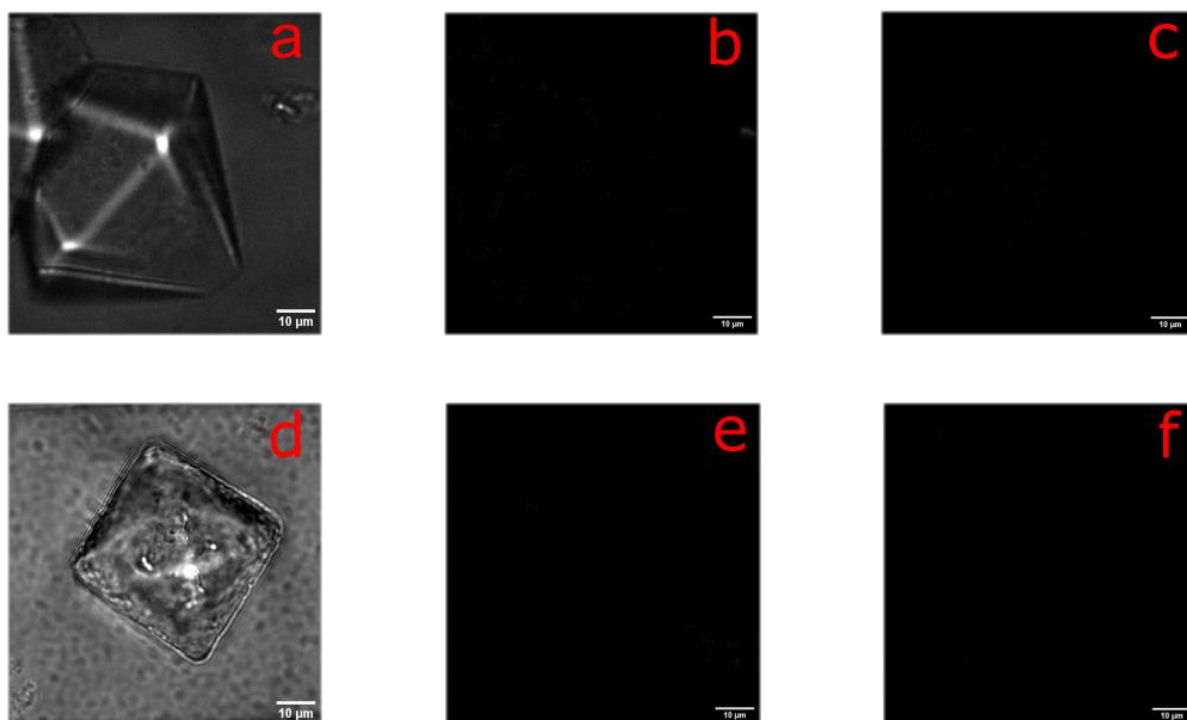


Figure 22. Confocal microscopy images of UIO-68 azide, without BODIPY performed with an excitation wavelength of 470 nm. a) brightfield in PBS, b) bottom face scan in PBS, c) internal scan in PBS, d) brightfield in DMF, e) bottom face scan in DMF, f) internal scan in DMF.

The reference images show that in both solvents the MOF crystal shows no fluorescent emission at 470 nm throughout its pores or on its surface. In contrast the BODIPY decorated MOF shows a clear indication of fluorescence focussed along the edges of the MOF crystal. Hence, indicating successful addition of the fluorophore to the surface of the MOF. Additionally, as is clear in *figure 23*, when measurements in DMF are compared to that of the same system in PBS, there is a large qualitative discrepancy in the intensity of fluorescent emission. This supports several literature reports which find that the intensity of fluorescence can be lessened in more polar solvents.^{61,62}

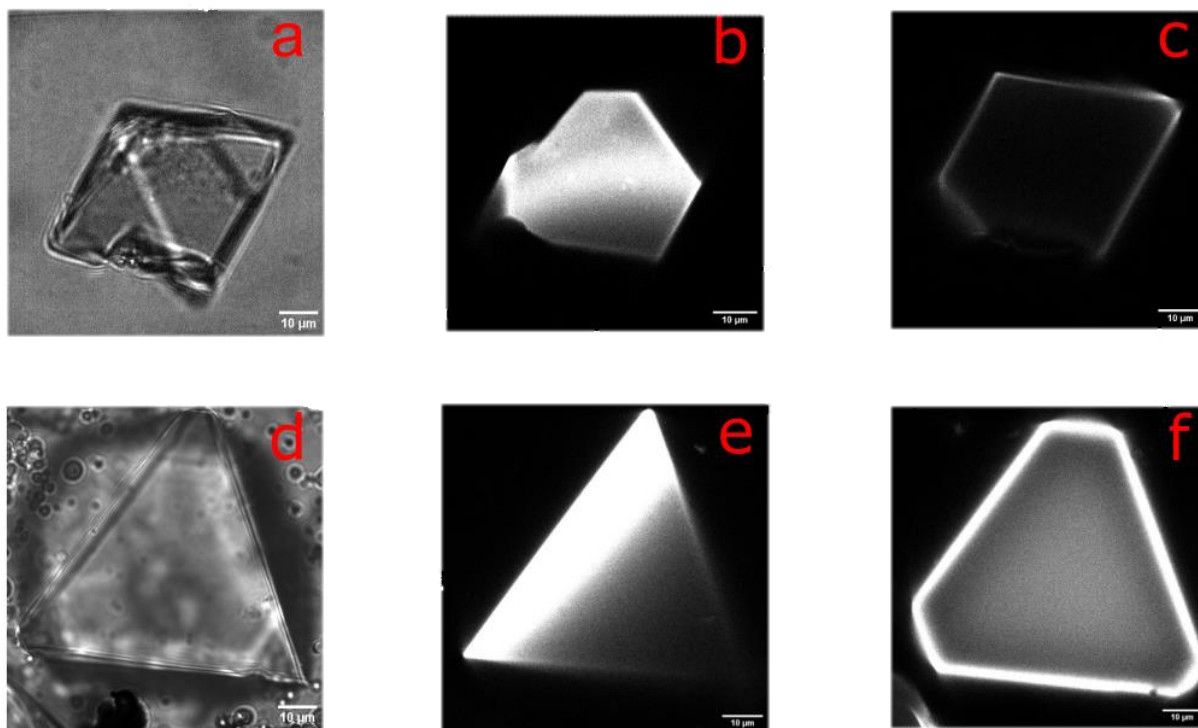


Figure 23. Confocal microscopy images of UIO-68 azide after BODIPY cycloaddition performed at an excitation wavelength of 470 nm. a) brightfield in PBS, b) bottom face scan in PBS, c) internal scan in PBS, d) brightfield in DMF, e) bottom face scan in DMF, f) internal scan in DMF.

3.5.2.10. Synthesis of Fluorescent Stopper Group

After positive confirmation that the BODIPY design was applicable for confocal microscopy, and that the performed method for cycloaddition was successful, a BODIPY stopper was synthesised. For the stopper to be able to react efficiently with the imidazole group on the rod, the stopper group requires a pendant methylhalide group. This motif is widely used within rotaxane synthesis, and has been demonstrated previously within the group to provide stoppered rotaxanes at room temperature and in good yields.^{22,63}

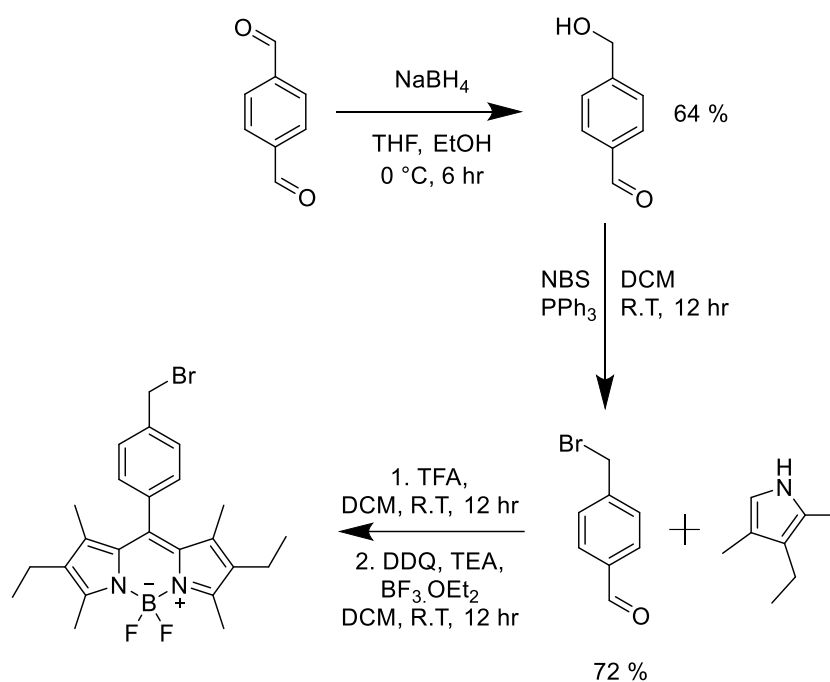


Figure 24. Reaction scheme for the synthesis of the fluorescent stopper group.

The initial step in the synthetic process produced an aryl group with both an aldehyde capable of BODIPY formation, and a methylhalide for the rotaxane syntheses (figure 24). Terephthalaldehyde was chosen as the starting product due to its low cost, good solubility in organic solvents and availability. Asymmetric reduction of the carbonyl to a methyl alcohol was then achieved using sodium borohydride (NaBH_4). The mono-reduced product was separated from the 1,4-benzenedimethanol by-product *via* column chromatography. Substitution of the alcohol to a bromide could then be achieved by reacting with a *N*-bromosuccinimide and triphenylphosphine. 4-(Bromomethyl)benzaldehyde could then be isolated by removing the organic solvent *in vacuo* and purifying with column chromatography to give the product as a white solid. For the final BODIPY synthesis an analogous method to that of the alkyne BODIPY was performed, however even after multiple attempts to remove the unsubstituted BODIPY there was still evidence of small amounts of the impurity within the final product (< 20 %). However, as the stopper group was to be used in excess,

and with the unsubstituted BODIPY not having a method of interacting with the rotaxane, the crude BODIPY stopper was used.

3.5.2.11. Design and Synthesis of Pillar[5]arene Macrocycle

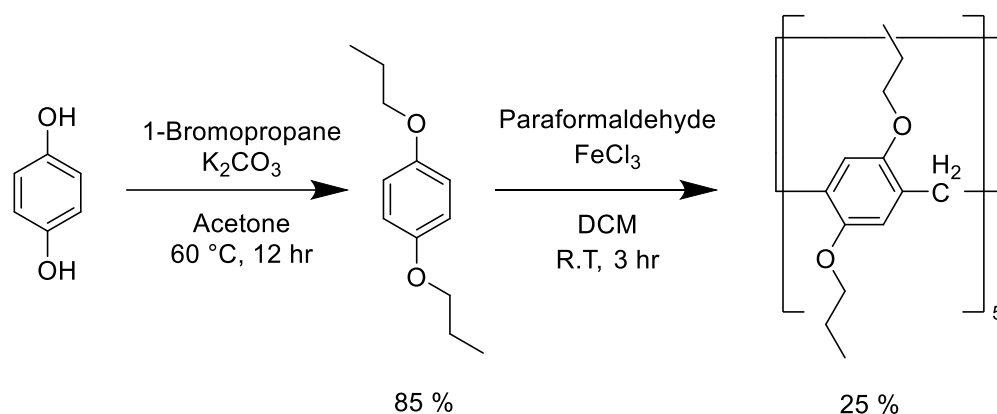


Figure 25. Reaction scheme for the synthesis of dipropoxypillar[5]arene

The choice in macrocycle was pillar[5]arene, due to its good solubility in halogenated solvents, strong host-guest complexation with cationic and electron poor groups, and its ease of synthesis. The choice in pillar[5]arene derivative was based upon literature data regarding the binding constants between differing pillar[5]arenes and imidazole-based guests. As highlighted in the review of neutral guests and pillar[5]arenes by *Wang et al*, pillar[5]arenes bearing alkane chains between 2 and 4 show the largest binding constants towards neutral guests including imidazoles.⁶⁴ The propyl chain was therefore elected as a compromise between the good binding towards imidazole, but also not too long as to prevent shuttling along the rod.

The synthesis of the pillar[5]arene subunit and the pillar[5]arene complete were as described in chapter section 2.4.1 (*figure 25*).

3.5.2.12. Attempted Rotaxane Synthesis

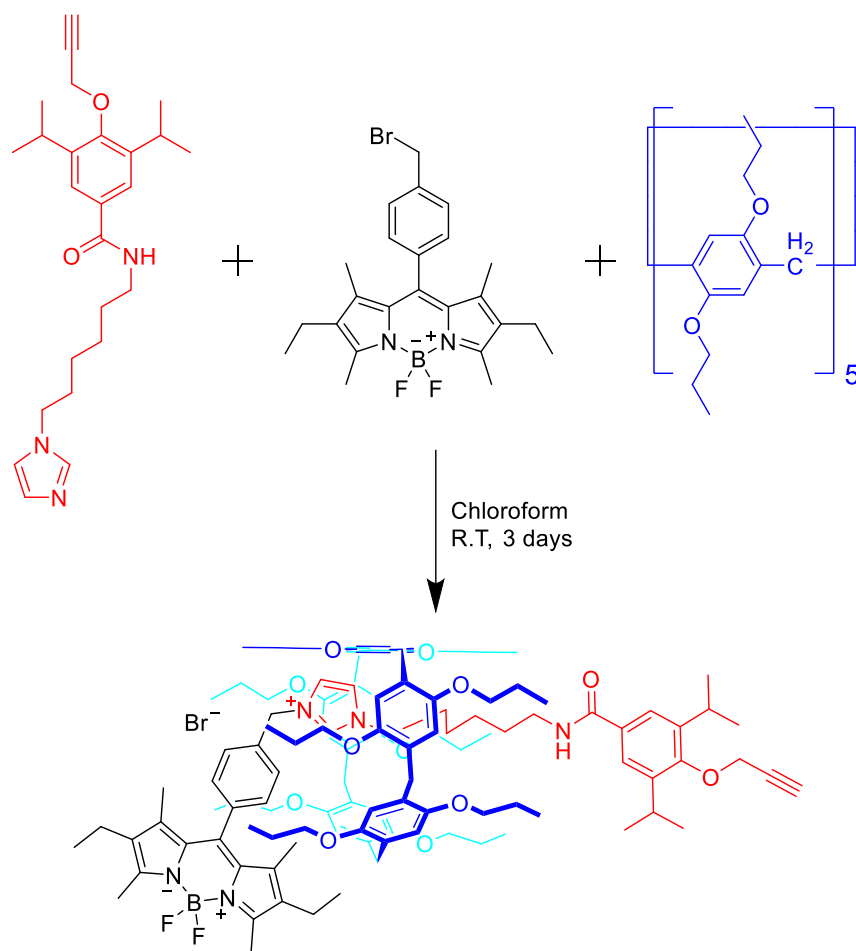


Figure 26. Reaction scheme for the synthesis of the intended rotaxane with the rod (red), fluorescent stopper (black) and pillar[5]arene macrocycle (blue).

The synthesis of the rotaxane was performed in a method adapted from *Langer et al.*²² Wherein, one equivalent of the rod component is dissolved alongside two equivalents of macrocycle in a minimum amount of chloroform (*figure 26*). This solution is stirred for 30 minutes in an ice/salt bath to ensure threading has occurred. Subsequent addition of an excess of the stopper group aims to stopper the pseudo-rotaxane before dethreading occurs. This solution was allowed to warm to room temperature and was stirred for three days.

An initial investigation using thin layer chromatography with DCM as the eluent was promising, indicating four spots: pillar[5]arene, BODIPY stopper, rod, and a secondary fluorescent spot (in order of R_f value). Each of these spots was then mixed with methanol and analysed by matrix-assisted laser desorption/ionization mass spectrometry (MALDI-TOF). The first spot indicated a mass of 1315 m/z, this mass initially seemed to not correspond to any likely products. However, when the mass of the dipropoxypillar[5]arene encapsulating the unsubstituted BODIPY was analysed, shown in *figure 20*, the mass was calculated as 1315 Da. This could be due to the low amounts of the unsubstituted BODIPY in the reaction mixture, or equally the unsubstituted BODIPY could be a product of the decomposition of the BODIPY stopper. If it was caused by decomposition there would have to be an evaluation as to whether the decomposition was caused by the relatively mild rotaxane synthesis conditions, or by the ionization from MALDI. To provide evidence to support either hypothesis, analysis using proton NMR analysis on the TLC spot was performed. Surprisingly, the proton NMR spectra indicated that indeed the spot with the highest R_f value corresponded to a pillar[5]arene/BODIPY complex, but in fact it was with both the methylbromide BODIPY stopper and unsubstituted BODIPY impurity equally. Additionally, more evidence of complexation arose from the relative upfield shifting of the peaks that corresponded to the BODIPY compounds (*figure 27*).

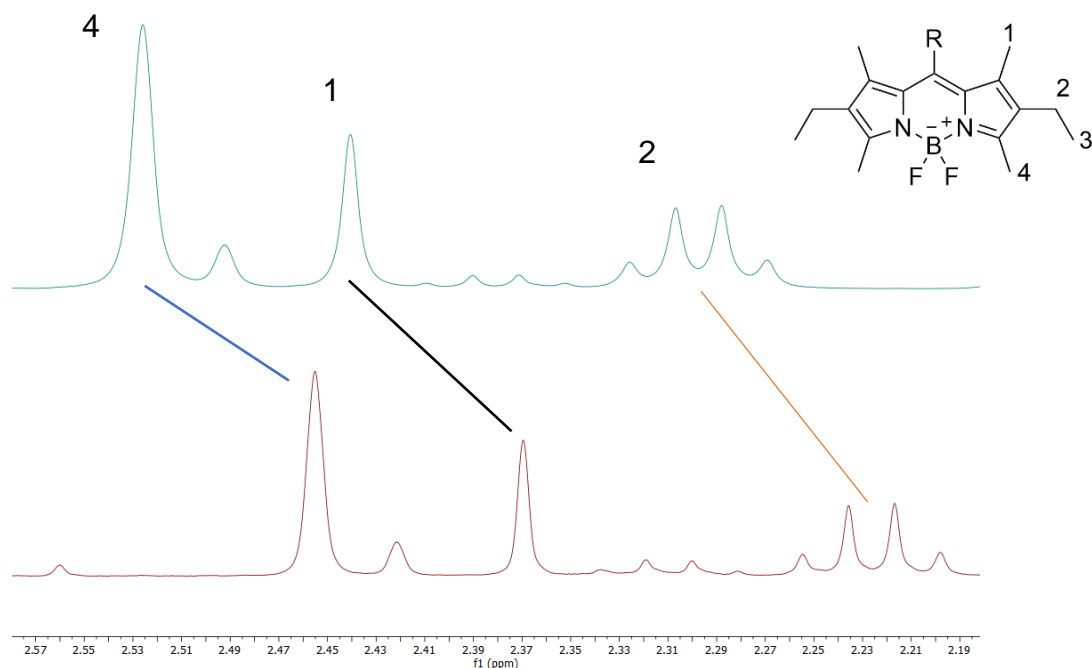


Figure 27. Highlighted region of the ^1H NMR spectra of BODIPY stopper (top) and the complex found after rotaxane synthesis (bottom). Showing upfield shifting of the BODIPY peaks.

What was unfortunate about these results was that it strongly indicated that there were competitive host-guest interactions between the rod and the stopper. This competitive binding would ultimately disrupt the pseudo-rotaxane formed between the macrocycle and the rod and would lower, or possibly extinguish the yields of the rotaxane. Ultimately, this would be the case, an initial MALDI-TOF study would indicate the rotaxane was formed showing a peak at 1833 m/z, corresponding to the rotaxane complete (without bromide counter anion). However, when an attempt to isolate the compound related to the TLC spot was attempted, no tangible amount of material was recoverable.

3.5.3. Conclusions of Surface Modification of MOFs With Rotaxanes Via CuAAC Click Chemistry

To conclude this section, it is evident that a potential system for MOF functionalisation has been developed. Confocal microscopy has been used to successfully demonstrate

that surface modification is possible using this approach, and there is good visibility of the BODIPY stopper group using this technique. However, issues arose which were mainly centred around the BODIPY group being encapsulated within the macrocycle during rotaxane synthesis, hence lowering the efficiency of rotaxane formation. There are multiple possible routes to solve this issue, the simplest would be to add bulkier groups to the (bromomethyl)phenylene moiety in the BODIPY stopper group. This could be achieved facily by starting with tetramethylterephthaldehyde instead of the terephthaldehyde previously used. Equally, a Finkelstein reaction replacing the bromomethyl group to an iodomethyl group on the BODIPY stopper, would significantly speed up the attachment of the stopper group to the imidazole group which could aid in ensuring quicker and more efficient rotaxane stoppering.

3.6. Design and Synthesis of a MOF Capable of Methylhalide Functionalisation

The second path to functionalising a MOF's surface with a rotaxane sought to employ the relative ease in alkylating pyridines. As was reported with nicotine in the previous chapter, pyridines can be readily alkylated with alkylhalides, forming cationic pyridiniums. The hypothesis was, that if a MOF that was constructed from a linker with a pendant or free pyridine group could be synthesised, then a rotaxane with a terminal alkylbromide would be able to perform the alkylation highlighted above and form a MOF with not only rotaxane adornment but also a cationic surface.

3.6.1. Design of Pyridine Containing MOF

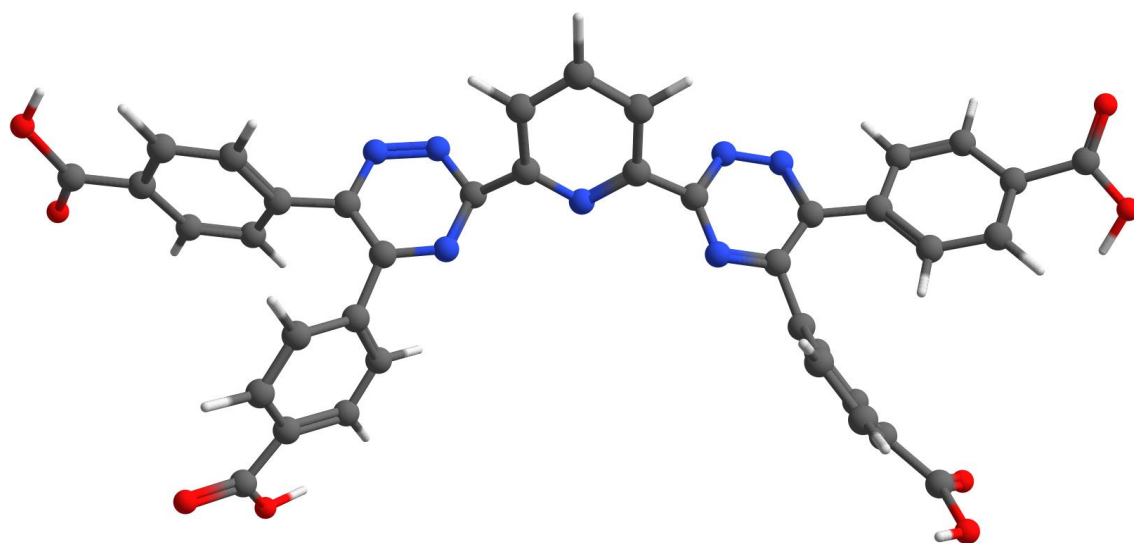


Figure 28. Energy minimized structure of MOF linker N7, calculated using density functional theory employing the 6-31+G* basis set and B3LYP functional with D3BJ dispersion correction, geometrical counterpoise correction and CPCM (chloroform) solvent model.

The greatest consideration that needed to be attended to was that pyridine's are also capable of metal ligation. Therefore, to assemble a MOF where the linker contained a pyridine that did not interact with the metal there would need to be adjacent steric hindrance. The design therefore used a central pyridine moiety with large 1,2,4-triazine groups attached in the 2 and 6 positions of the pyridine ring (*figure 28*). For metal ligation sites four benzoic acid groups attached *via* the four carbons in the triazine molecules was used. This large tetradentate ligand would have two potential post synthetic applications, firstly the above highlighted alkylation, and equally the central bis(triazyl)pyridyl system has the potential to bind metal centres.

3.6.2. Synthesis of Shielded Pyridine MOF

The synthesis of the MOF linker detailed above was conducted by ‘telescoped’ condensation of pyridine-2,6-dicarbohydrazide with the appropriate 1,2-dicarbonyl. The formation of these pyridinyl-1,2,4-triazine ligands has been previously reported, along with their successful use as tridentate ligands with ruthenium.^{65,66}

3.6.2.1. Synthesis of Dimethyl 4,4'-(2-hydroxyacetyl)dibenzoate

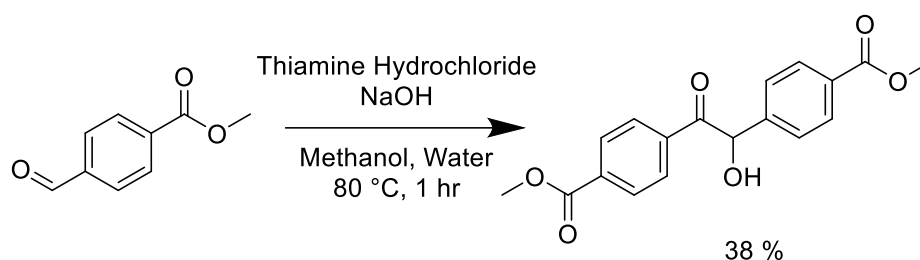


Figure 29. Reaction scheme showing the synthesis of dimethyl 4,4'-(2-hydroxyacetyl)dibenzoate.

For the 1,2-dicarbonyl component, a benzil with benzoic acid groups attached was required (*figure 29*). The initial step was a benzoin addition reaction between aldehydes, this reaction was previously reported using potassium cyanide as the catalyst.⁶⁷ However, the usage of thiamine hydrochloride was preferred, due to the relative toxicity of both reagents. The reaction proceeds firstly with the deprotonation of the thiazole forming a vinylic carbanion. The carbanion subsequently attacks the carbonyl carbon of the benzaldehyde forming an alkoxide intermediate, which will deprotonate an adjacent water molecule, forming a secondary alcohol and a hydroxide ion. Further deprotonation of the newly formed tertiary carbon, and therefore formation of a further carbanion is achievable due to the bonding of the thiamine, owing to the thiamine allowing for the stabilisation of the carbanion intermediate, through the delocalisation of the anion through resonance. The carbanion will then proceed to

attack a carbonyl carbon of another benzaldehyde as before. Finally, the second alkoxide will reform its π -bond, and break the bond to the thiamine, forming the benzoin and reforming the thiamine hydrochloride (figure 30).

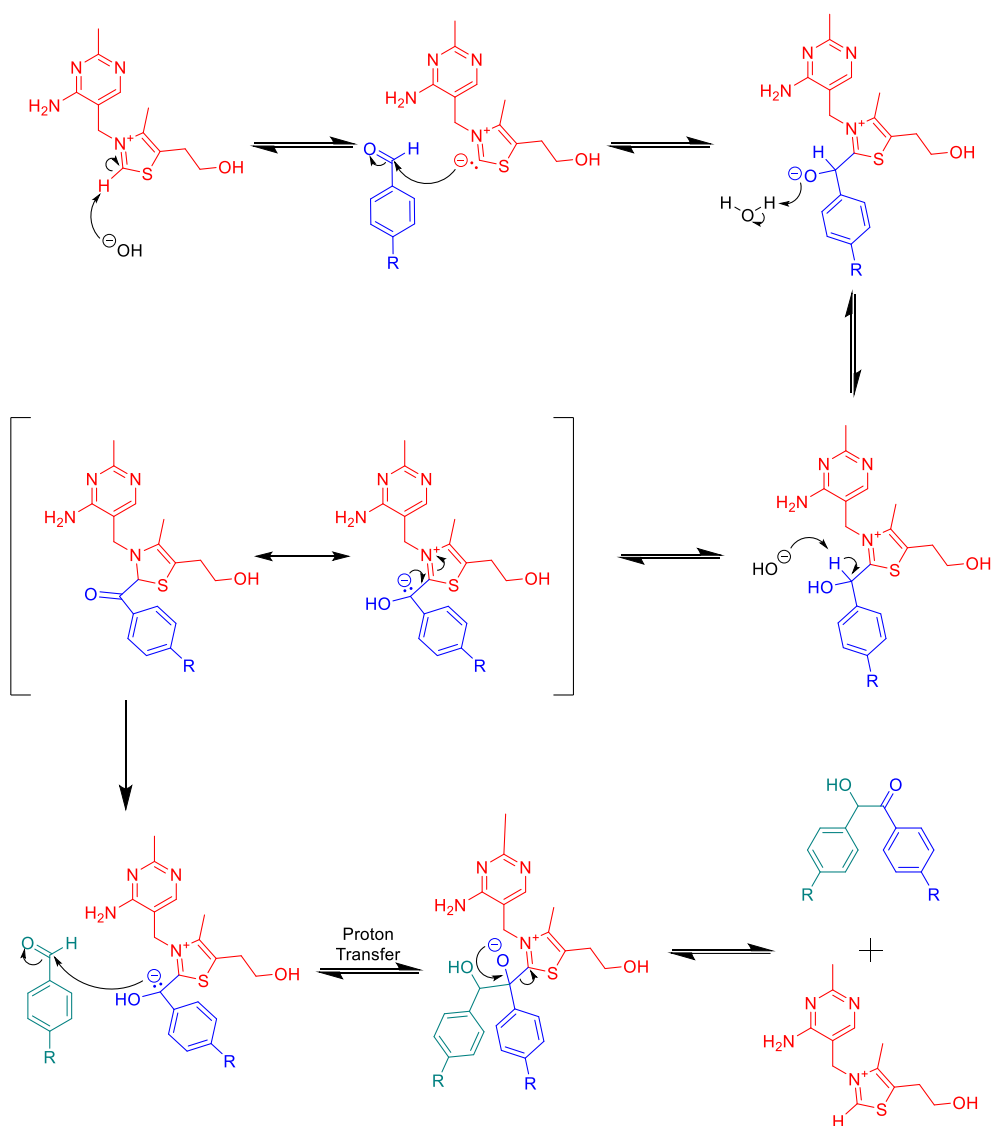


Figure 30. Mechanism for the formation of the benzoin from *para*-substituted benzaldehyde and thiamine hydrochloride. Adapted from Soderberg.⁶⁸

Experimentally the reaction involved the simple mixing of the three reagents with refluxing for an hour. Once cooled, the pale-yellow solid was collected and washed with water and corresponded to the intended benzoin. Equally, any unreacted thiamine

hydrochloride and sodium hydroxide was washed away with water. Making this reaction a simple one-pot synthesis.

3.6.3. Synthesis of Dimethyl 4,4'-oxalyldibenzoate

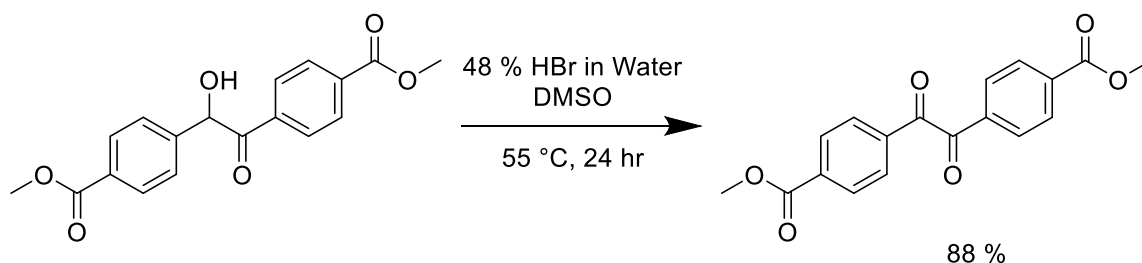


Figure 31. Reaction scheme for the synthesis of dimethyl 4,4'-oxalyldibenzoate.

For the conversion of benzoin to benzil a Kornblum oxidation was chosen, *via* an acid catalysed alcohol-halide substitution reaction (*figure 31*). This is not however the only viable route for the oxidation of benzoin; chlorine, iodine, nitric acid, copper sulfate and pyridine, lithium nitrate and acetic anhydride, and ammonium nitrate and copper diacetate are also previously reported reagents for this reaction.^{69–74} However, due to most of these experimental conditions involving caustic gases or explosive metal salts, the aforementioned Kornblum oxidation method was preferred.

The initial step is the protonation of the alcohol with hydrobromic acid, due to the alcohol being a secondary alcohol the reaction will proceed *via* an S_N1 nucleophilic substitution, compared to the S_N2 of primary alcohols (*figure 32*). Hence, the next stage is the elimination of water forming the carbocation intermediate. Then the carbocation will be attacked by the bromide nucleophile to form the methyl bromide derivative. The next stage is the Kornblum oxidation, this is an S_N2 displacement, with an attack from the lone pair of DMSO's oxygen, and the bromide now acting as a leaving group. Subsequently, deprotonation of the sulfonium salt leads to the forming of the carbonyl and elimination of dimethylsulfide.

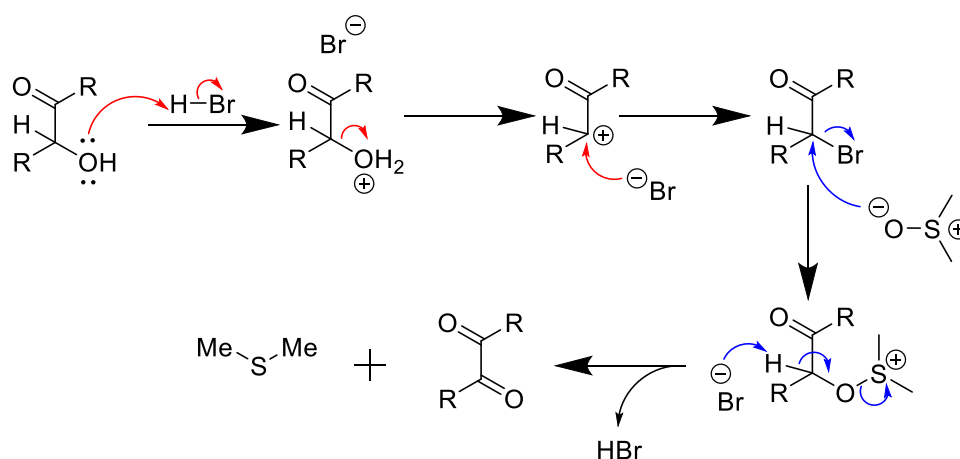


Figure 32. Reaction mechanism for the conversion of benzoin to benzil with a Kornblum oxidation reaction (blue), via a halide substitution (red).

Practically this high yielding reaction was performed facily by heating all reagents overnight. Subsequent addition of water will precipitate the benzil as a pale-yellow solid.

3.6.4. Synthesis of 4,4'-oxalyldibenzoic acid

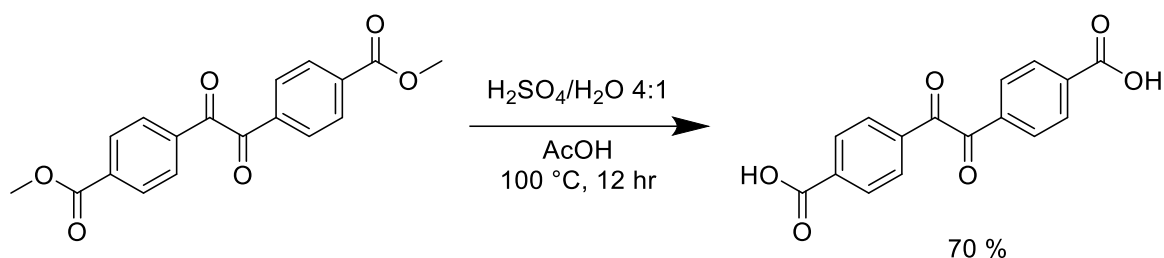


Figure 33. Reaction scheme for the synthesis of 4,4'-oxalyldibenzoic acid

For the hydrolysis of esters, the usual procedure would be a saponification using an alkaline base, e.g. sodium hydroxide or potassium hydroxide. However, due to benzils undergoing a 1,2-rearrangement to form an α -hydroxy-carboxylic acid in the presence of base, acid hydrolysis was preferred (figure 33).⁷⁵ The reaction itself requires both an acid and water, this is due to the initial protonation of the carbonyl oxygen being followed by an attack from a water molecule towards the now electrophilic carbon. A

proton transfer between the water molecule and the ester leads to the elimination of the alcohol. Additional water can then be added which will deprotonate the carbonyl forming the carboxylic acid. This reaction yielded a yellow solid after washing with water and drying at 60 °C in vacuum

3.6.5. Synthesis of Pyridine-2,6-bis(carboximidhydrazide)

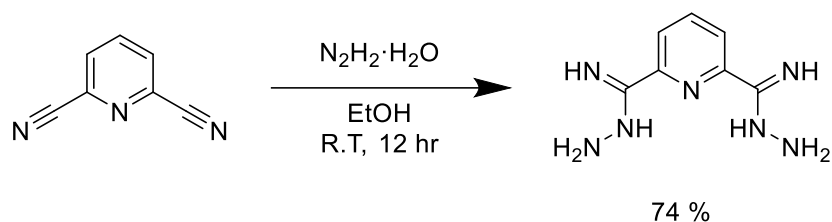


Figure 34. Reaction scheme for the synthesis of pyridine-2,6-bis(carboximidhydrazide)

For the triazine formation with the benzil to be successful, an appropriate pyridyl would have to be synthesised. The reactive bis(carboximidhydrazide)pyridine was obtained by reacting pyridine-2,6-dicarbonitrile with hydrazine monohydrate (*figure 34*). This was performed *via* a method adapted from *Sagot et al.*⁷⁶ After a day of stirring the pyridine and hydrazide in ethanol at room temperature, the precipitate could be collected and washed with ethanol to give pyridine-2,6-bis(carboximidhydrazide) as a white solid.

3.6.6. Synthesis of MOF-N7 linker

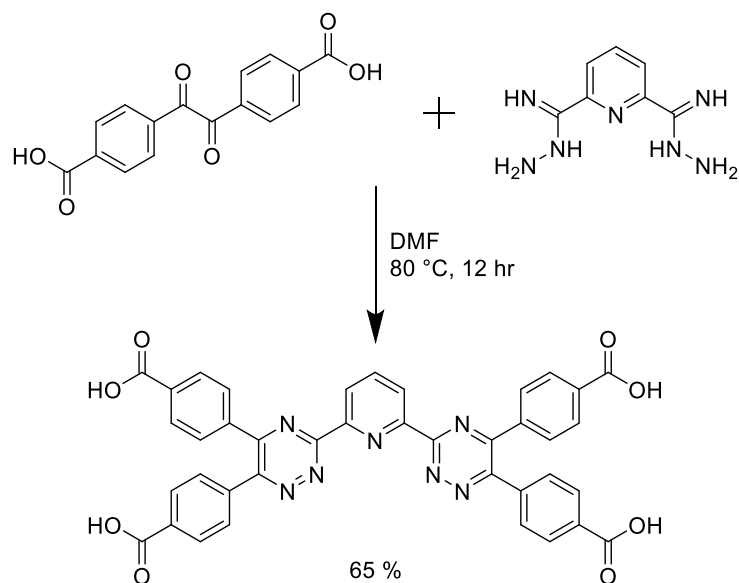


Figure 35. Reaction scheme for the synthesis of MOF linker N7

The synthesis of MOF linker N7, proceeded *via* a method adapted from *Tai et al.*⁶⁶ The reaction involved dissolving both reagents in a minimum volume of DMF followed by heating at 80 °C overnight (*figure 35*). After cooling a pale-green precipitate was formed that corresponded to MOF-N7 linker. The DMF could also be removed *in vacuo* and the resulting brown solid recrystallised in methanol to yield a further crop of MOF-N7 linker. The reaction was high yielding (*ca* 65 %) and was found to be replicable within the group. The MOF-N7 linker was further studied by single crystal X-ray diffraction, with the crystals being prepared by slow evaporation of the linker in *N,N*-dimethylformamide (*figure 36*). The crystal structure obtained of the linker, solved by Dr Griffin, indicates that two of the four carboxylic acid groups have been deprotonated by the decomposition product of *N,N*-dimethylformamide, dimethylamine. Hence, within the gathered structure, as well as the linker, and two molecules of *N,N*-dimethylformamide, there are two dimethylammonium cations.

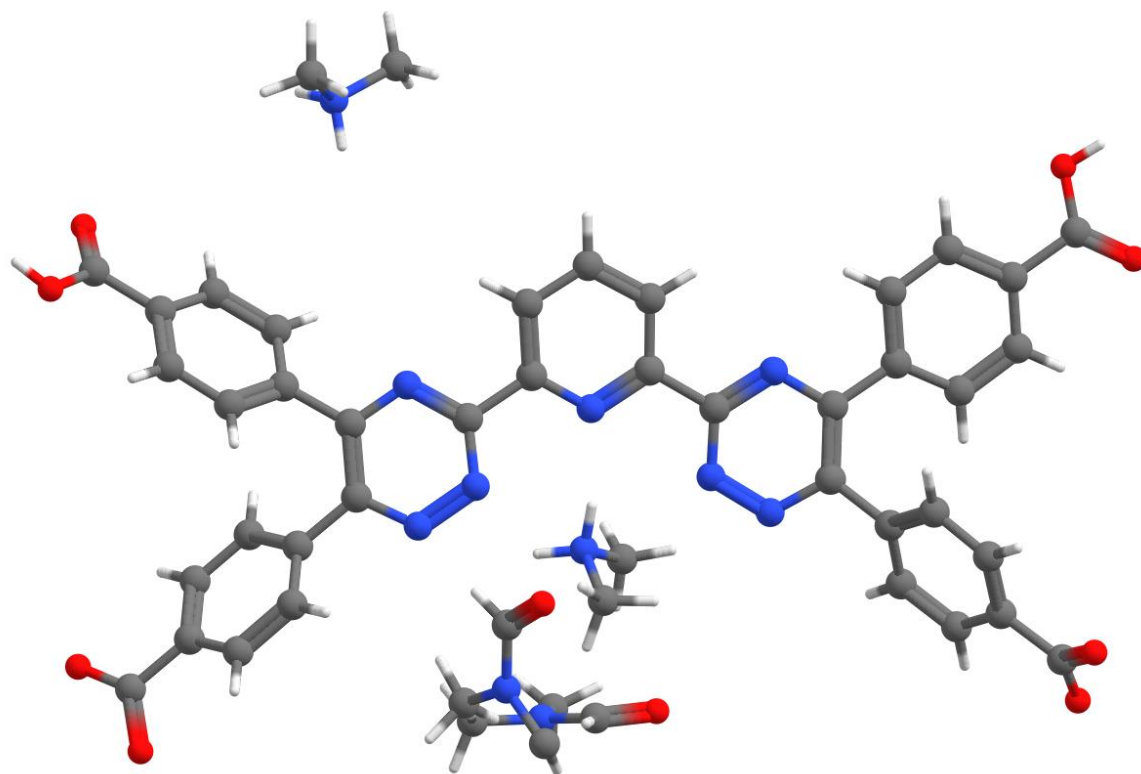


Figure 36. Crystal structure of the MOF-N7 linker. With carbon shown in black, oxygen in red, nitrogen in blue, and hydrogen in white.

Additional linkers were trialed with this method and similar methods. Including a reaction between the benzil, ammonium acetate, zinc chloride, urea and terephthalaldehyde, in a manner adapted from *López et al.*⁷⁷ The intended molecule (MOF-N4) would be equally tetradentate with a central bis(imidazolyl)benzene which would be used in a similar manner to the pyridine in the above example (*figure 37*). However, solubility of this linker in a wide range of solvents was sparing, so MOF- N7 linker was the only linker studied further.

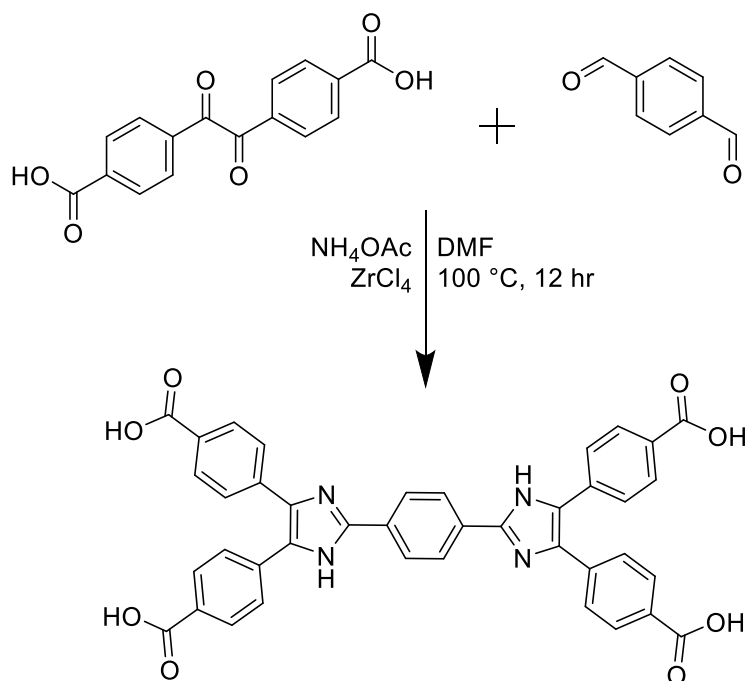


Figure 37. Reaction scheme showing the attempted synthesis of MOF-N4 linker.

3.6.7. Synthesis of Shielded Pyridine MOF

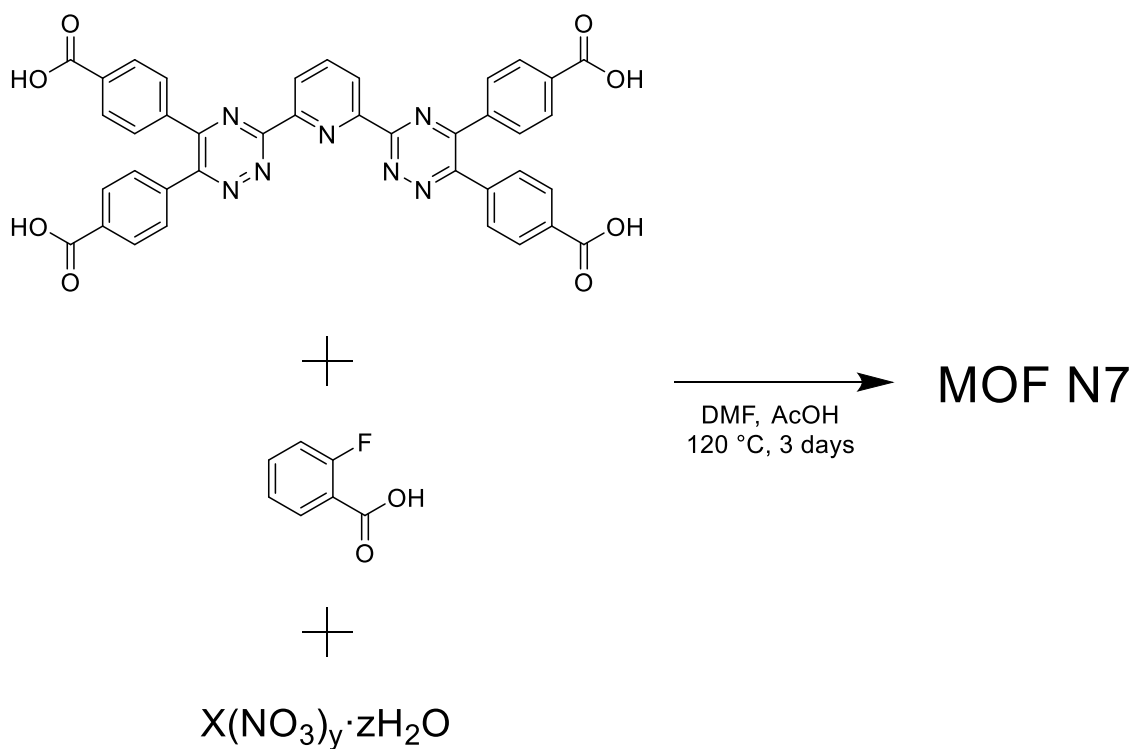


Figure 38. Reaction scheme for the synthesis of MOF N7, Lanthanide metal = X, number of nitrate ligands = y, stoichiometry of hydration = z.

A method was devised, with consideration to previous MOF syntheses using tetracarboxylate ligands and lanthanide metals, to prepare a MOF using MOF-N7 (*figure 38*).⁷⁸ The choice of a lanthanide metal node was established due to their hard nature which will enhance carboxylate coordination in preference to the pyridyl sites. Stability of lanthanide based MOFs towards desolvation and temperature, and their interesting conformations caused by their variable coordination numbers were also viewed as potentially beneficial.⁴¹ 2-Fluorobenzoic acid was implemented as the modulator system as this organic acid is widely used for its structure directing properties.⁷⁹ Multiple reaction conditions were trialled, including varying the acid, solvent, reaction time and temperature. However, the first conditions used were the most successful so were implemented in further reactions. The optimised conditions were that 9 μmol of MOF-N7 linker, 34 μmol of lanthanide nitrate salt and 1.4 mmol of σ -fluorobenzoic acid, was dissolved in 3 mL of *N,N*-dimethylformamide and 0.75 mL of acetic acid. The vessel was closed and heated in an oven at 120 °C for three days. After cooling, yellow hexagonal crystals were present for the reaction containing yttrium nitrate, no other lanthanides were successful initially. However, using crystals from the successful yttrium synthesis as seeds, holmium and dysprosium syntheses produced crystalline samples. This is performed by simply adding 3 or 4 of the yttrium MOF crystals in the reaction vial

Although the crystals were of adequate size, and of a good qualitative quality, the crystal data obtained was poor (*figure 39*). The linker being difficult to model, most likely due to the molecule's high degree of rotational freedom, leading ultimately to a highly disordered structure. That withstanding, the crystal structure does still give some indication as to the packing arrangement of MOF-N7

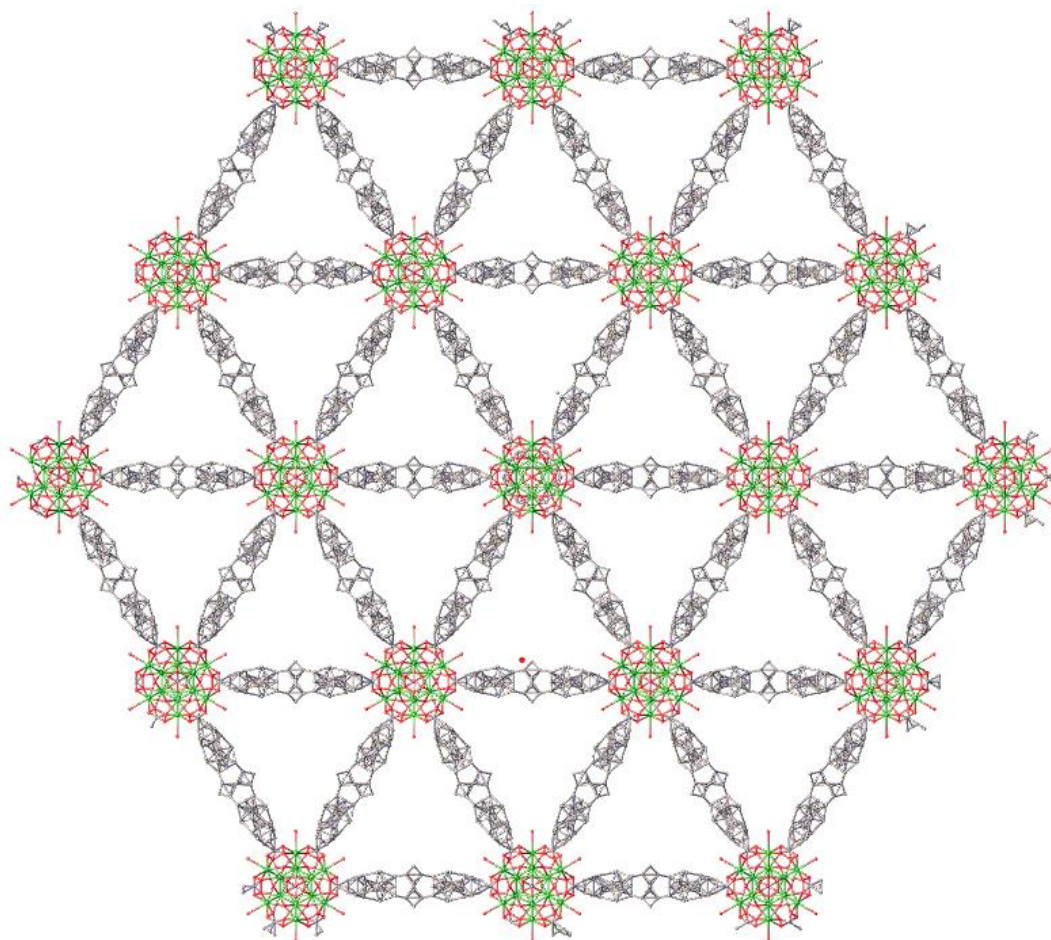


Figure 39. Crystal structure of MOF-N7 with dysprosium as the metal node. Carbon shown in black, oxygen in red, and dysprosium in green. With neither the hydrogen's or nitrogen's being possible to model due to disorder.

3.6.8. Conclusion of the Synthesis of a MOF Capable of Methylhalide Functionalisation

This chapter section detailed the synthesis of a novel tetracarboxylate MOF linker, with a bis(triazyl)pyridyl core. A MOF was successfully synthesised using an adaptation of a method using a similar linker.

The next stages of this research could take multiple routes. Firstly, as originally stated, the next step would be the synthesis of an alkylhalide terminated rotaxane as highlighted above. This rotaxane could then be attached to the surface with a method akin to the alkylation of nicotine's reported in chapter 2. Equally, with a longer

alkylhalide group on the rotaxane it is feasible that the rotaxane could be synthesised *in situ* upon the MOF surface.

Another possible route for MOF-N7 could be to examine a method of MOF formation after the ligand has been bound to a square planar metal *via* the central nitrogen rich heterocyclic core. The synthesis of a ruthenium complex for example, has already been reported with a ligand of equivalent core functionality.⁶⁵ Therefore, by expanding such a complex into a MOF, there is an opportunity to produce a bimetallic MOF system which could mimic or improve the transfer hydrogenation properties of the aforementioned complex reported by *Wang et al.* Equally, it is theorised that the difficulty in obtaining crystallographic data from this MOF can be attributed to the various modes of rotational freedom of the ligand. The introduction of a metal node within the core of the ligand could aid in reducing such movements and help gain clarity of the MOF structure.

3.7. Design and Synthesis of a MOF for Thiol-ene Surface Modification

Our third route to surface modification of MOFs was to use a thiol-ene click reaction to adhere the potential rotaxane to the MOF surface. The thiol-ene reaction, also known as alkene hydrothiolation, is an example of click chemistry that describes the organic reaction between an alkene and a thiol to form a thioether. For the intended purpose the free-radical addition mechanism for the thiol-ene formation would be exploited. However, a base or nucleophile can also be used, and the reaction will proceed *via* a Michael addition pathway. As the intended pathway would use a radical initiator, the product formed will follow the anti-Markovnikov rule for regiochemistry; a new group will form on the least substituted carbon. One of the largest issues with

radical initiated thiol-ene reactions is that due to no terminating point for the radical, a series of cascade reactions can form, including cyclisation's and polymerisation's. Therefore, it is difficult to accurately predict and model the intended products of the reaction.

For this proposed system, a MOF linker functionalised with an alkene containing moiety was intended, therefore requiring the rotaxane to contain the thiol group.

3.7.1. Design and Synthesis of bis(alkene) Linker

The MOF will follow the same MOF synthetic route as the azide MOF previously shown, therefore belonging to the UiO-68 family of MOFs. The linker therefore also needed to be a linear dicarboxylate ligand, consisting of three para-bound phenyl rings. As in the azide, the central phenyl unit would contain the difunctionalised 'arms', but for this linker they are alkene functionalised (*figure 40*).

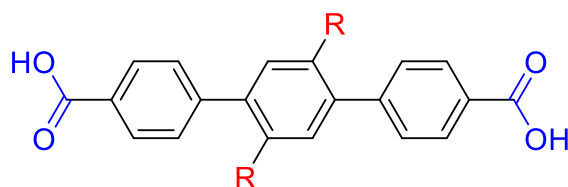


Figure 40. Molecular structure of the generic UiO-68 linker, where the blue carboxylic acids form the MOF structure through interactions with the metal nodes, and the red 'R' groups represent potential sites for functional groups, and by extension post-synthetic modification.

3.7.1.1. Synthesis of 1,4-Dibromo-2,5-bis(bromomethyl)benzene

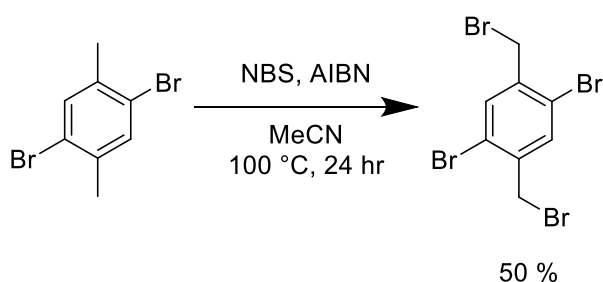


Figure 41. Reaction scheme for the synthesis of 1,4-dibromo-2,5-bis(bromomethyl)benzene.

The synthetic method for the synthesis of 1,4-dibromo-2,5-bis(bromomethyl)benzene was adapted from *García et al.*⁸⁰ As in chapter section 3.5.1.2, the di-bromination of the starting material proceeded using *N*-bromosuccinimide (NBS), and a radical initiator, but this time using azobisisobutyronitrile (AIBN) (*figure 41*). All reagents were dissolved in acetonitrile (MeCN) and stirred at reflux overnight. The solution was then cooled, and the solvent was removed *in vacuo*. Purification was performed by washing the resulting solid in hot methanol, to give the final product as a white solid.

3.7.1.2. Synthesis of 1,4-Dibromo-2,5-divinylbenzene

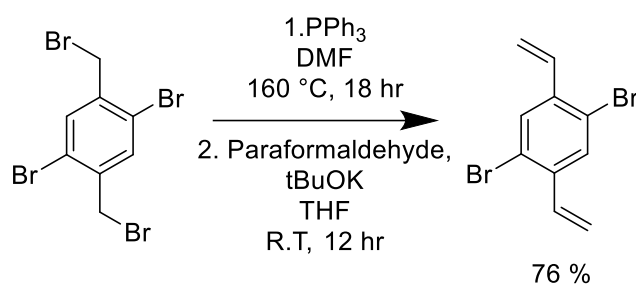


Figure 42. Reaction scheme for the synthesis of 1,4-dibromo-2,5-divinylbenzene

The synthesis of 1,4-dibromo-2,5-divinylbenzene followed a procedure adapted from *Bonifacio et al.*⁸¹ The reaction proceeds *via* a double Wittig olefination with paraformaldehyde (*figure 42*). The initial step was to synthesise the bis(triphenylphosphonium) derivative of the previously synthesised product. This was performed easily by refluxing the starting material and triphenylphosphine (PPh₃) in DMF overnight. After complete removal of the solvent *in vacuo* 1,4-dibromo-2,5-*p*-xylenebis(triphenylphosphonium) dibromide could be retrieved as a white solid. The next step introduced paraformaldehyde and potassium-*tert*-butoxide in tetrahydrofuran. The reaction was then stirred overnight at room temperature and the solvent was removed *in vacuo* to obtain the crude product. Further purification was

performed using column chromatography with hexane as the eluent. The styrene product was obtained as a white powder.

As previously stated, this reaction proceeds *via* a double Wittig olefination (*figure 43*). The initial reaction of the bis(methylbromo)benzene derivative and triphenylphosphonium, accessing the di(triphenylphosphonium)benzene required for the formation of the phosphonium ylide. This proceeds *via* an S_N2 pathway, with the bromide acting as a leaving group. The introduction of potassium-*tert*-butoxide as a base deprotonates methylcarbon, leading to the double phosphonium ylide, potassium bromide (KBr) and *tert*-butyl alcohol (tBA). The carboanion that has been subsequently formed performs a nucleophilic attack on the carbonyl of paraformaldehyde. This in turn forms a dipolar, charge-separated species commonly referred to as a betaine. The anionic alkoxide will then form the oxaphosphetane intermediate by attacking the cationic phosphine. A reverse [2+2] cycloaddition will then yield the di-alkene product and phosphonium oxide as a by-product.

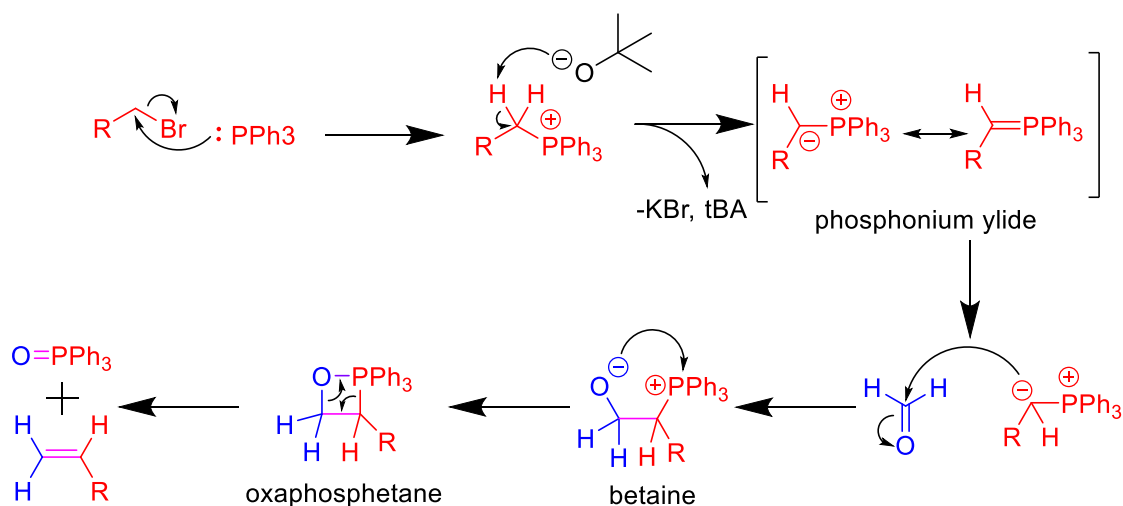


Figure 43. Reaction mechanism for the conversion from methylbromide to alkene *via* a Wittig olefination.

3.7.1.3. Synthesis of bis(alkene) Linker

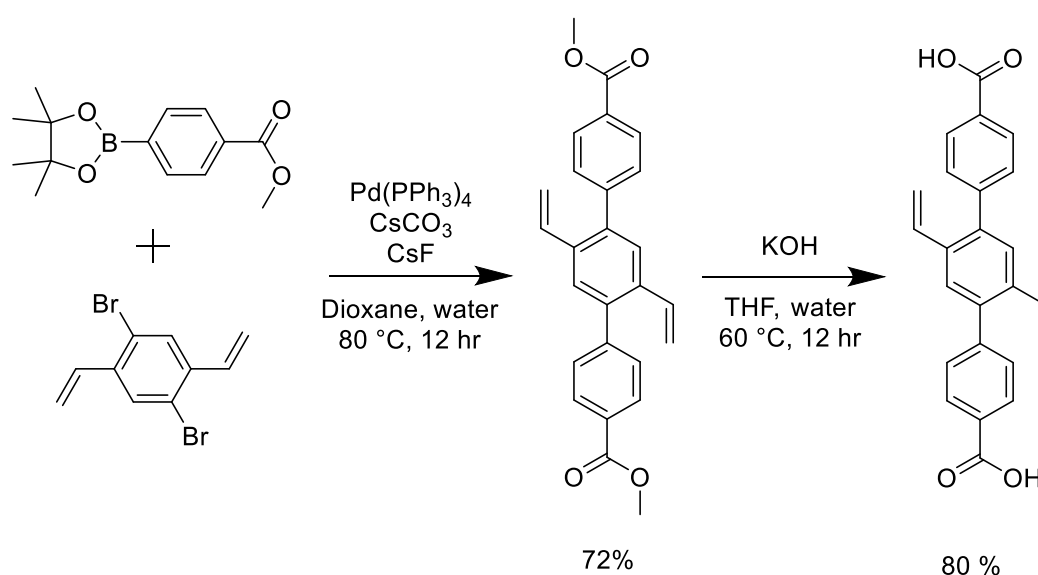


Figure 44. Reaction scheme for the synthesis of bis(alkene) linker

The previously synthesised divinyl compound was functionalised with benzoic acids group using a Suzuki reaction with the corresponding pinacolborane (*figure 44*). The reaction conditions are the same as for chapter section 3.5.1.1 the only significant difference is that the temperature was lowered from 110°C to 80°C , solely for practical considerations. For the purification of this product, column chromatography was used with dichloromethane:hexane 1:1 as the eluent mixture.

The final stage was the saponification of the two ester groups to form the ligating carboxylates. This step was performed in a similar manner as in chapter section 3.5.1.4, wherein potassium hydroxide (KOH) was used as the base in a tetrahydrofuran (THF), water solvent mixture. Acidification of the mixture with hydrochloric acid, gave a white precipitate which was isolated as the alkene linker.

3.7.2. Synthesis of UiO-68 bis(alkene) MOF

The synthesis of the UiO-68 bis alkene MOF proceeded in a method not dissimilar to that outlined in 3.5.1.5. The linker and zirconium tetrachloride are dissolved in

dimethylformamide in a 1:1 ratio, benzoic acid (20 equivalents) were added as a modulator. The reaction mixture was sealed and heated for a day at 120 °C. Colourless crystals were obtained and analysed using X-ray Diffraction (*figure 45*). The alkene bonds of the linker could not be modelled due to disorder, most likely due to the rotational freedom of the central phenyl unit in the linker. The crystal structure does however, show the extended cubic closed-packed structure characteristic for UiO-68 MOFs. Combining the crystal structure, with the spectroscopic data obtained of the linker, one can gain confidence in successful synthesis of the intended UiO MOF synthesis.

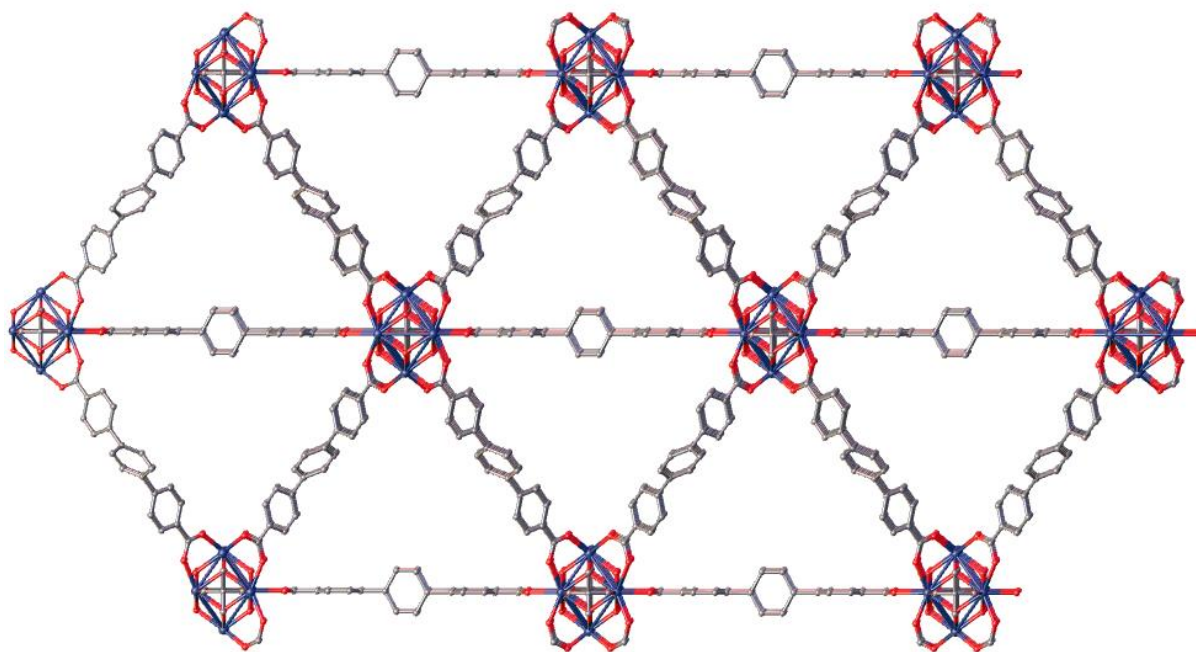


Figure 45. Crystal structure of UiO-68 bis(alkene) MOF. With carbon in black, oxygen in red, and zirconium in blue.

3.7.3. Conclusions of the Synthesis of a MOF for Thiol-ene Surface Modification

Reported herein is a novel UiO-68 based MOF with pendent alkene groups on the linker, with the intention of providing a platform for post-synthetic modification *via*

hydrothiolation. It is important to note that initial tests were performed using the thiol functionalised copillar[4+1]arene detailed in chapter 4, however methods of analysis were limited due to the lack of visible fluorescence in pillar[5]arenes. Other methods of analysis, for example single crystal X-ray diffraction and powder X-ray diffraction were trialled but were unsuccessful.

Therefore, to obtain a measure of the success of the thiol-ene reaction for post-synthetic modification of a MOFs surface, a similar fluorophore containing rotaxane as the one in section 3.5.2 must first be synthesised. The incorporation of a thiol into the rotaxane could follow any route from *figure 38*, either using the phenol or carboxylic acid functional group of the isopropyl stopper.

3.8. Conclusions and Further Work

Within this chapter multiple possible routes to functionalising the surface of MOFs are discussed. Although each method has its merits and issues, it has been made clear that there are several feasible routes to a rotaxane decorated MOF system. An alkyne functionalised molecule which has the ability to selectively attach to a MOFs surface if steric bulk is added was demonstrated. Equally, by using confocal microscopy a qualitative method for the evaluation of the coverage of the MOFs surface has been put forward.

Two novel MOFs have been synthesised, one using the popular UiO-68 motif, and one that required an exploratory approach with a unique nitrogen rich linker, based on a known organic motif. Potential rotaxane designs to compliment these MOFs have been put forward with justification for their construction.

Discussed herein is a semi-modular approach to custom rotaxane synthesis, in future work it is pertinent that further development of these rotaxane templates is undertaken.

Using a 'dual-stopper' approach has brought forth alternative avenues for asymmetric rotaxane synthesis, but for this work to be applicable for a wide range of MOF designs, it is essential that there is an expansion on the available stopper groups.

To address the issues of the pillar[5]arene preferentially encapsulating the BODIPY stopper, steric bulk could be added to the BODIPY to dissuade binding. This could be performed facily, by starting with an aldehyde with bulky groups in the 2, 3, 5, and 6 positions on the benzene ring. Methyl groups have been shown previously to successfully stopper pillar[5]arene, so should suffice for this purpose. Equally, starting from 2,3,5,6-tetramethylbenzene the BODIPY should be achievable using known literature procedures (*figure 46*).^{82–86}

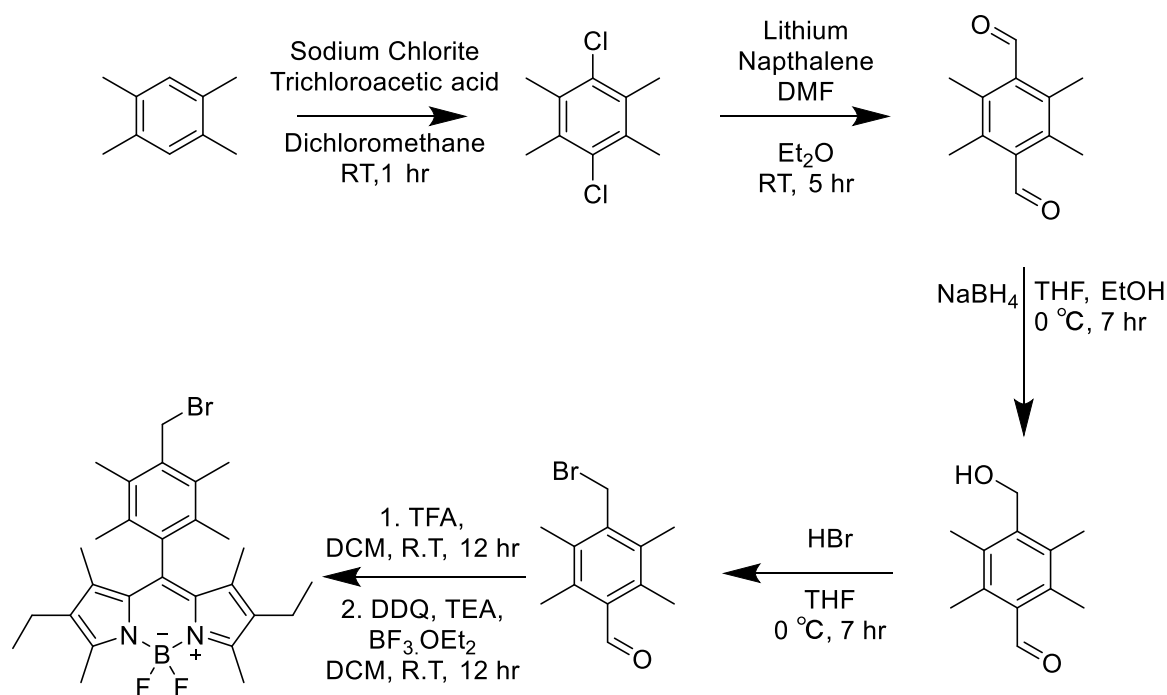


Figure 46. Reaction scheme showing potential synthetic route for a sterically hindered BODIPY stopper.

Ongoing work performed by Dr Griffin has indicated MOF-N7 linker can be successfully used in the formation of lanthanide MOFs using the procedure here reported. Equally, preliminary results have indicated the formation of 3D columnar

structures when first row transition metals are used. Furthermore, post-synthetic modification has been successfully performed with both dichlorotricarbonylruthenium(II), and bromopentacarbonylmanganese(I). With the metal carbonyl coordinating to the (bis)triazine-pyridine core of the linker. These early results further highlight the potential that MOF-N7 has as a platform for post-synthetic modification, with both covalently bonded organic groups, and previously mentioned metal coordination. The expansion of this work could include altering the shape of the MOF-N7 linker, this would alter the resulting MOFs architecture, and allow for the potential of new properties emerging. An 'H' shaped linker could be synthesised following a similar procedure as that described for the MOF-N7 linker, but the starting reagent would be methyl 3-formylbenzoate, instead of the *para*-formylbenzoate used for the MOF-N7 linker (*figure 47*).

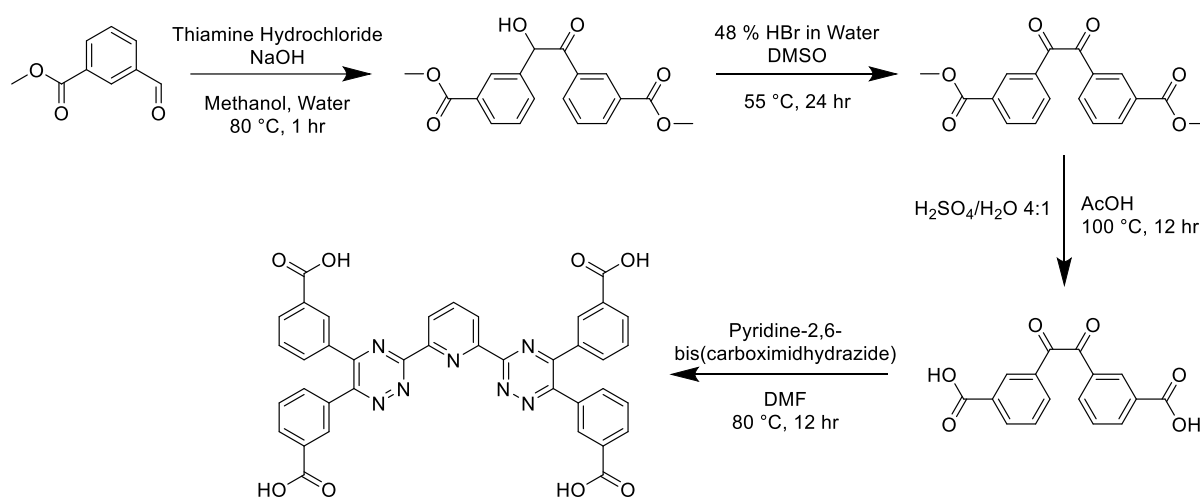
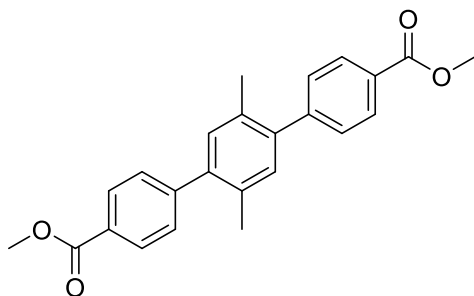


Figure 47. Reaction scheme showing potential synthetic route for a 'H'-MOF-N7 linker.

3.9 Materials and Methods

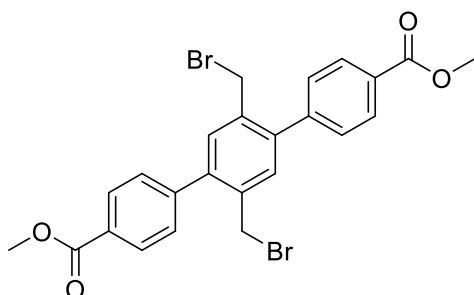
3.9.1 Synthesis of UiO6-8-N₃ MOF

3.9.1.1. 2',5'-dimethyl-[1,1':4',1''-terphenyl]-4,4''-dicarboxylate



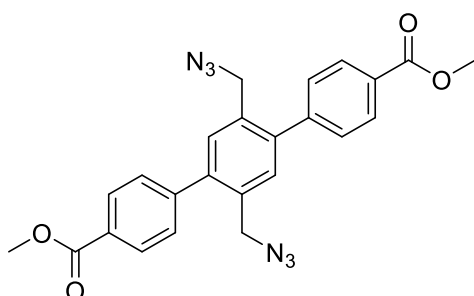
Caesium carbonate (11.1 g, 34.1 mmol) and caesium fluoride (0.80 g, 5.26 mmol) were stirred in degassed dioxane (100 mL) and water (3 mL) and stirred under nitrogen for 10 minutes. 2,5-Dibromo-*p*-xylene (3.0 g, 11.3 mmol), 4-methoxycarbonylphenylboronic acid (6.2 g, 37.4 mmol), and tetrakis(triphenylphosphine)palladium(0) (1.31 g, 1.13 mmol) were then added and the mixture was stirred over 2 days at 110 °C in a nitrogen environment. Upon cooling the mixture was extracted into dichloromethane (ca 250 mL) and washed with water (ca 300 mL x 3). The organic layer was separated and dried over magnesium sulfate, the solvent was then removed *in vacuo* to give the crude product. The crude product was further purified with column chromatography using silica gel and dichloromethane as the eluent, to give 2',5'-dimethyl-[1,1':4',1''-terphenyl]-4,4''-dicarboxylate as a white solid. (3.50 g, 10.1 mmol, 82 %). Spectroscopic data for the title compound were consistent with the literature. ¹H NMR (300 MHz, Chloroform-*d*) δ (ppm) 8.04 (dt, *J* = 8.4, 1.8 Hz, 4H), 7.37 (dt, *J* = 8.4, 1.7 Hz, 4H), 7.09 (s, 2H), 3.89 (s, 6H), 2.20 (s, 6H).

3.9.1.2. Dimethyl 2',5'-bis(bromomethyl)-[1,1':4',1''-terphenyl]-4,4''-dicarboxylate



2',5'-Dimethyl-[1,1':4',1''-terphenyl]-4,4''-dicarboxylate (1.70 g, 4.91 mmol) and *N*-bromosuccinimide (2.00 g, 11.3 mmol) were dissolved in benzene (ca 20 mL) and stirred at room temperature for 10 minutes. Benzoyl peroxide (0.50 g, 2.06 mmol) was then added, and the mixture was heated to 90 °C and stirred overnight. After cooling, the solvent was removed *in vacuo* and the residue was collected and washed with methanol to give methyl 2',5'-bis(bromomethyl)-[1,1':4',1''-terphenyl]-4,4''-dicarboxylate as a white solid (2.00 g, 3.76 mmol, 74 %). Spectroscopic data for the title compound were consistent with the literature. ¹H NMR (400 MHz, Chloroform-*d*) δ 8.09 (dt, *J* = 8.4, 1.8 Hz 4H), 7.53 – 7.48 (dt, *J* = 8.4, 1.8 Hz 4H), 7.37 (s, 2H), 4.35 (s, 4H), 3.90 (s, 6H).

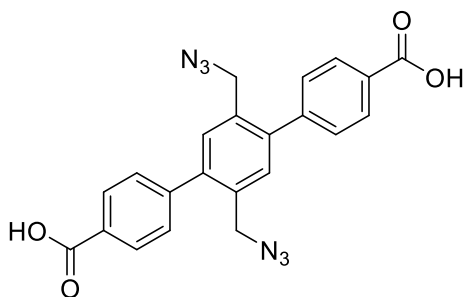
3.9.1.3. Dimethyl 2',5'-bis(azidomethyl)-[1,1':4',1''-terphenyl]-4,4''-dicarboxylate



Dimethyl 2',5'-bis(bromomethyl)-[1,1':4',1''-terphenyl]-4,4''-dicarboxylate (0.70 g, 1.31 mmol) was dissolved in anhydrous degassed dimethylformamide (ca 20 mL). Sodium

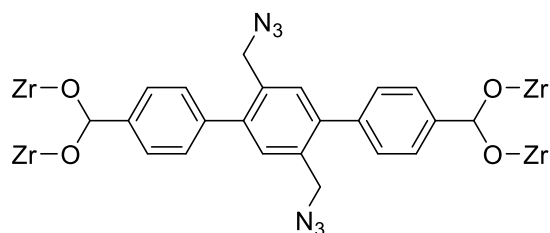
azide (0.50 g, 7.70 mmol) was then added, and the reaction mixture was allowed to heat to 60 °C and stirred overnight in a nitrogen environment. Upon cooling, water (ca 250 mL) was added to the solution and the solid was collected and washed with acetone and diethyl ether to give Dimethyl 2',5'-bis(azidomethyl)-[1,1':4',1''-terphenyl]-4,4''-dicarboxylate as a white solid (0.60 g, 1.32 mmol, 98 %). Spectroscopic data for the title compound were consistent with the literature. ¹H NMR (400 MHz, Chloroform-*d*) δ 8.09 (d, *J* = 8.0 Hz, 4H), 7.43 (d, *J* = 8.3 Hz, 4H), 7.36 (s, 2H), 4.27 (s, 4H), 3.90 (s, 6H); ¹³C NMR (101 MHz, CDCl₃) δ 171.09, 166.68, 143.84, 140.99, 133.09, 131.46, 129.77, 129.64, 129.32, 129.21, 52.23, 52.06, 36.47, 20.99.

3.9.1.4. 2',5'-Bis(azidomethyl)-[1,1':4',1''-terphenyl]-4,4''-dicarboxylic acid



Dimethyl 2',5'-bis(azidomethyl)-[1,1':4',1''-terphenyl]-4,4''-dicarboxylate (0.60 g, 1.32 mmol) and potassium hydroxide (3.00 g, 53.6 mmol) were stirred in tetrahydrofuran (20 mL) and water (10 mL) over 2 days. Hydrochloric acid was then added and the white solid was collected and washed with methanol to give 2',5'-Bis(azidomethyl)-[1,1':4',1''-terphenyl]-4,4''-dicarboxylic acid as a white solid (0.30 g, 0.70 mmol, 54 %). Spectroscopic data for the title compound were consistent with the literature. ¹H NMR (400 MHz, DMSO-*d*₆) δ 13.1 (s, 2H, br) 8.08 (d, *J* = 7.9 Hz, 4H), 7.58 (d, *J* = 8.2 Hz, 4H), 7.56 (s, 2H), 4.50 (s, 4H); ¹³C NMR (101 MHz, DMSO) δ (ppm) 166.49, 143.89, 140.74, 133.71, 132.27, 130.00, 129.85, 129.67, 51.71.

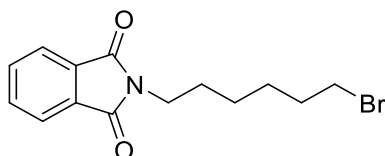
3.9.1.5. UIO-68 N₃ MOF



2',5'-Bis(azidomethyl)-[1,1':4',1''-terphenyl]-4,4''-dicarboxylic acid (26.0 mg, 60 μ mol), zirconium tetrachloride (24.0 mg, 103 μ mol) and benzoic acid (240 mg, 1960 μ mol) were dissolved in dimethylformamide (3 mL) in a screw topped vial. The reaction mixture was then heated in a temperature controlled electric oven at 120 °C for a day. Single crystals were then collected and solved by Dr Sarah Griffin.

3.9.2. Synthesis of Alkene Rotaxane

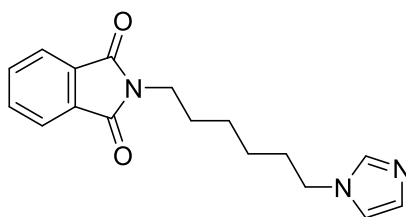
3.9.2.1. 2-(6-bromohexyl)isoindole-1,3-dione



Potassium phthalimide (10.0 g, 53.9 mmol) and 1,6-dibromohexane (40.0 g, 164 mmol) were dissolved in dimethylformamide (125 mL) and the solution was stirred overnight at room temperature in a nitrogen environment. The suspension was then filtered, and the filtrate was reduced *in vacuo* and extracted with chloroform (*ca* 250 mL). The solution was washed with water (*ca* 2 x 100 mL), ammonium chloride solution (*ca* 100 mL) and brine (*ca* 100 mL) and the organic layer was dried over magnesium sulfate. The solvent was removed *in vacuo* to give a yellow oil which was recrystallised in hexane to give 2-(6-bromohexyl)isoindole-1,3-dione as a white solid (12.1 g, 39.1 mmol, 72% yield). Spectroscopic data for the title compound were consistent with the

literature. ^1H NMR (400 MHz, Chloroform-*d*) δ 7.84 (dt, $J = 5.6, 2.8$ Hz, 2H), 7.71 (dt, $J = 5.9, 3.0$ Hz, 2H), 3.67 (td, $J = 7.3, 5.5$ Hz, 2H), 3.39 (t, $J = 6.8$ Hz, 2H), 1.84 (p, $J = 6.9$ Hz, 2H), 1.68 (p, $J = 7.1$ Hz, 2H), 1.43 (h, $J = 7.5, 6.6$ Hz, 2H), 1.38 – 1.27 (m, 6H); ^{13}C NMR (101 MHz, CDCl_3) δ 168.44, 133.82, 132.17, 123.14, 38.00, 33.96, 32.73, 29.04, 28.55, 26.78.

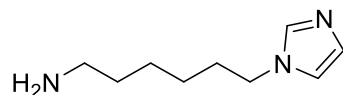
3.9.2.2. 2-(6-(1H-imidazol-1-yl)hexyl)isoindoline-1,3-dione



Imidazole (1.80 g, 26.5 mmol) and sodium hydride (0.70 g, 29.2 mmol) were dissolved in degassed dimethylformamide (20 mL) and stirred for 1 hour at room temperature. 2-(6-Bromohexyl)isoindole-1,3-dione (5.50 g, 17.7 mmol) was then added and the reaction mixture was stirred overnight at room temperature. The solvent was removed *in vacuo* and the residue redistributed in chloroform (ca 100 mL) and washed with water (ca 2 x 250 mL). The organic layer was separated and dried over magnesium sulfate, the solvent was subsequently removed *in vacuo*. The crude residue was purified *via* column chromatography using silica gel with dichloromethane as the eluent. 2-(6-(1H-imidazol-1-yl)hexyl)isoindoline-1,3-dione was collected as a white solid (4.00 g, 13.5 mmol, 79 %). Spectroscopic data for the title compound were consistent with the literature. ^1H NMR (400 MHz, Chloroform-*d*) δ (ppm) 7.77 (dd, $J = 5.4, 3.0$ Hz, 2H), 7.65 (dd, $J = 5.4, 3.0$ Hz, 2H), 7.38 (s, 1H), 6.97 (s, $J = 1.6$ Hz, 1H), 6.83 (t, $J = 1.3$ Hz, 1H), 3.85 (t, $J = 7.1$ Hz, 2H), 3.60 (t, $J = 7.2$ Hz, 2H), 1.71 (p, $J = 7.1$ Hz, 2H), 1.60 (p, $J = 7.2$ Hz, 2H), 1.39 – 1.22 (m, 4H); ^{13}C NMR (101 MHz,

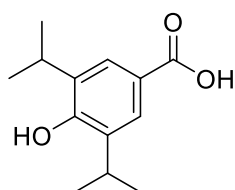
Chloroform-*d*) δ 168.45, 133.95, 132.09, 129.43, 123.21, 118.72, 46.91, 37.70, 30.93, 28.36, 26.27, 26.10.

3.9.2.3. 6-(1H-imidazol-1-yl)hexan-1-amine



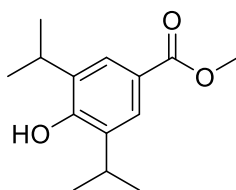
2-(6-(1H-imidazol-1-yl)hexyl)isoindoline-1,3-dione (1.00 g, 3.36 mmol) was dissolved in ethanol (23 mL) and water (7 mL). Hydrazine monohydrate (0.40 mL, 7.99 mmol) was then added, and the reaction mixture was stirred overnight at 110 °C. Hydrochloric acid (ca 0.1 mL) was then added and the reaction mixture was stirred overnight at 110 °C. Upon cooling the solvent was removed *in vacuo* and the residue was added to water and basified to pH 12 with sodium hydroxide. The solution was extracted with chloroform (ca 100 mL) and the organic layer was separated and dried over magnesium sulfate. The solvent was removed *in vacuo* to give 6-(1H-imidazol-1-yl)hexan-1-amine as a yellow oil (0.30 g, 1.79 mmol, 60 %). Spectroscopic data for the title compound were consistent with the literature. ¹H NMR (400 MHz, Chloroform-*d*) δ (ppm) 7.45 (d, *J* = 1.2 Hz, 1H), 7.03 (t, *J* = 1.1 Hz, 1H), 6.90 (t, *J* = 1.3 Hz, 1H), 4.90 (s, 1H, br), 3.93 (t, *J* = 7.1 Hz, 2H), 2.66 (t, *J* = 6.8 Hz, 2H), 1.82 – 1.75 (m, 2H), 1.47 – 1.27 (m, 6H); ¹³C NMR (101 MHz, Chloroform-*d*) δ 136.43, 128.22, 118.31, 46.26, 40.80, 31.82, 30.40, 28.56, 25.76.

3.9.2.4. 4-Hydroxy-3,5-diisopropylbenzoic acid



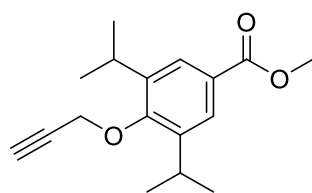
4-Hydroxybenzoic acid (20.0 g, 151 mmol) was dissolved in isopropyl alcohol (40 mL), sulfuric acid (72 mL) and water (5 mL). The mixture was then stirred for 4 hours at 60 °C. Upon cooling the mixture was basified to 12 pH with potassium hydroxide and washed with toluene. The aqueous layer was then separated and acidified to pH 3 with hydrochloric acid. A white precipitate was then collected and washed with methanol and hexane to give 4-Hydroxy-3,5-diisopropylbenzoic acid as a white solid (12.0 g, 54.1 mmol, 36 %). Spectroscopic data for the title compound were consistent with the literature. ¹H NMR (400 MHz, Chloroform-*d*) δ (ppm) 7.79 (s, 2H), 5.25 (s, 1H, br), 3.09 (hept, *J* = 6.9 Hz, 2H), 1.24 (d, *J* = 6.9 Hz, 12H); ¹³C NMR (101 MHz, Chloroform-*d*) δ (ppm) 171.81, 155.03, 133.64, 126.44, 121.35, 27.18, 22.55.

3.9.2.5. Methyl 4-hydroxy-3,5-diisopropylbenzoate



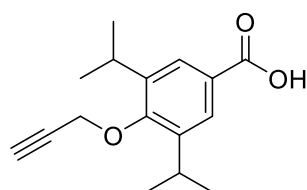
4-Hydroxy-3,5-diisopropylbenzoic acid (3.00 g, 13.5 mmol) was dissolved in methanol (ca 300 mL) and sulfuric acid (2 mL) was slowly added. The mixture was stirred overnight at 60 °C, and upon cooling the solvent was removed *in vacuo*. The resulting residue was collected and washed with water to give Methyl 4-hydroxy-3,5-diisopropylbenzoate as a white solid (2.50 g, 10.6 mmol, 76 %). Spectroscopic data for the title compound were consistent with the literature. ¹H NMR (400 MHz, Chloroform-*d*) δ (ppm) 7.78 (s, 2H), 3.89 (s, 3H), 3.15 (hept, *J* = 6.9 Hz, 2H), 1.29 (d, *J* = 6.9 Hz, 12H); ¹³C NMR (101 MHz, Chloroform-*d*) δ (ppm) 167.49, 154.27, 133.52, 125.67, 122.34, 51.82, 27.17, 22.60.

3.9.2.6. Methyl 3,5-diisopropyl-4-(prop-2-yn-1-yloxy)benzoate



Methyl 4-hydroxy-3,5-diisopropylbenzoate (1.90 g, 8.04 mmol) and sodium hydride (1.00 g, 41.6 mmol) were dissolved in degassed dimethylformamide (ca 50 mL) and stirred for 1 hour. Propargyl bromide (2.00 g, 16.8 mmol) was then added and the mixture was stirred overnight at 50 °C. Upon cooling the solvent was removed, and the residue was recrystallised in hexane to give methyl 3,5-diisopropyl-4-(prop-2-yn-1-yloxy)benzoate as a pale-yellow solid (1.50 g, 5.52 mmol, 68 %). Novel compound. ¹H NMR (400 MHz, Chloroform-*d*) δ (ppm) 7.74 (s, 2H), 4.43 (d *J* = 2.5 Hz, 2H), 3.83 (s, 3H), 3.32 (hept, *J* = 7.1 Hz, 2H), 2.49 (t, *J* = 2.5 Hz, 1H), 1.19 (d, *J* = 6.9 Hz, 12H); ¹³C NMR (101 MHz, Chloroform-*d*) δ (ppm) 167.10, 156.58, 142.43, 126.95, 126.00, 75.59, 61.96, 52.03, 26.85, 23.91.

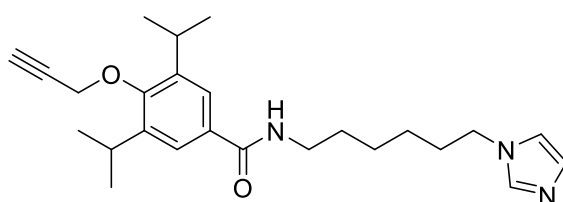
3.9.2.7. 3,5-Diisopropyl-4-(prop-2-yn-1-yloxy)benzoic acid



Methyl 3,5-diisopropyl-4-(prop-2-yn-1-yloxy)benzoate (1.50 g, 5.47 mmol), potassium hydroxide (1.00 g, 17.8 mmol) and lithium hydroxide (1.00 g, 41.6 mmol) were dissolved in methanol (100 mL). The reaction mixture was then stirred overnight at 80 °C. Upon cooling the solvent was removed *in vacuo* and the resulting residue was acidified to pH 1 with hydrochloric acid. The precipitate was collected and washed with water and methanol to give crude 3,5-Diisopropyl-4-(prop-2-yn-1-yloxy)benzoic acid

as a pale-yellow solid (1.00 g, 3.84 mmol, 69 %) and was used immediately in the next reaction without further purification. Novel compound. ^1H NMR (400 MHz, Chloroform-*d*) δ (ppm) 7.81 (2, 2H), 4.46 (d, $J = 2.4$ Hz), 3.33 (hept, $J = 6.9$ Hz, 2H), 2.50 (t, $J = 2.4$ Hz, 1H), 1.20 (d, $J = 6.9$ Hz, 12H); ^{13}C NMR (101 MHz, Chloroform-*d*) δ (ppm) 142.69, 126.70, 125.86, 78.53, 75.50, 61.99, 26.89, 23.88.

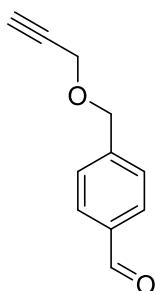
3.9.2.8. *N*-(6-(1*H*-imidazol-1-yl)hexyl)-3,5-diisopropyl-4-(prop-2-yn-1-yloxy)benzamide



6-(1*H*-imidazol-1-yl)hexan-1-amine (0.50 g, 2.99 mmol) and 3,5-Diisopropyl-4-(prop-2-yn-1-yloxy)benzoic acid (0.77 g, 29.6 mmol) were dissolved in degassed dichloromethane (25 mL) and stirred for 10 minutes. *N,N*-Diisopropylethylamine (0.07 g, 0.54 mmol), 1-ethyl-3-(3-dimethylaminopropyl)carbodiimide hydrochloride (0.85 g, 5.47 mmol) and 1-hydroxybenzotriazole (0.60 g, 4.44 mmol) were then added and the mixture was stirred overnight at room temperature in a nitrogen environment. The reaction mixture was then washed with water (*ca* 200 mL x 2) and the organic layer was separated and dried over magnesium sulfate. The solvent was removed *in vacuo* and the residue was purified using column chromatography with ethyl acetate as the eluent. The third fraction was collected as a yellow oil and corresponded to *N*-(6-(1*H*-imidazol-1-yl)hexyl)-3,5-diisopropyl-4-(prop-2-yn-1-yloxy)benzamide (0.45 g, 1.03 mmol, 33 %). Novel compound. ^1H NMR (400 MHz, Chloroform-*d*) δ (ppm) 7.49 (s, 2H), 7.47 (s, 1H), 6.90 (s, 1H), 6.23 (t, $J = 5.3$ Hz, 1H), 4.49 (d, $J = 2.4$ Hz, 2H), 3.93 (t, $J = 7.1$ Hz, 2H), 3.47-3.27 (m, 4H), 2.56 (t, $J = 2.4$ Hz, 1H), 1.79 (p, $J = 7.2$ Hz, 2H),

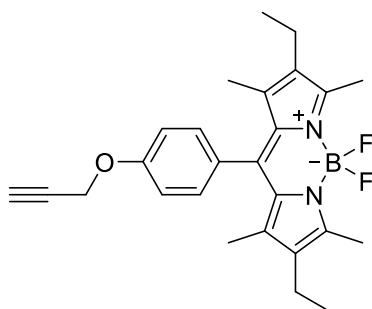
1.48-1.28 (m , 4H), 1.25 (d, $J = 6.9$ Hz, 12H); ^{13}C NMR (101 MHz, Chloroform- d) δ (ppm) 67.76, 155.27, 142.54, 137.03, 131.66, 129.31, 123.02, 118.81, 78.61, 77.36, 77.05, 76.73, 75.56, 61.97, 46.99, 39.86, 30/96, 29.70, 26.89, 26.44, 26.28, 23.92.

3.9.2.9. 4-(Prop-2-yn-1-yloxy)benzaldehyde



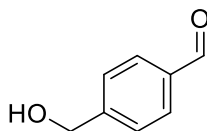
4-Hydroxybenzaldehyde (3.00 g, 24.5 mmol), potassium carbonate (13.6 g, 98.6 mmol) and propargyl bromide (9.30 g, 78.2 mmol) were mixed in acetone (250 mL) and stirred overnight at 70 °C. Upon cooling the solvent was removed *in vacuo* and the resulting residue recrystallised in hexane to give 4-(Prop-2-yn-1-yloxy)benzaldehyde as a yellow oil (3.30 g, 20.6 mmol, 82 %). Spectroscopic data for the title compound were consistent with the literature. ^1H NMR (400 MHz, Chloroform- d) δ (ppm) 9.84 (s, 1H), 7.79 (dt, $J = 8.9, 2.0$ Hz, 2H), 7.02 (td, $J = 8.8, 1.9$ Hz, 2H), 4.72 (d, $J = 2.4$ Hz, 2H), 2.50 (t, $J = 2.4$ Hz, 1H); ^{13}C NMR (101 MHz, Chloroform- d) δ (ppm) 190.78, 162.38, 131.91, 130.63, 115.20, 77.55, 76.36, 55.96.

3.9.2.10 Alkyne BODIPY



3-Ethyl-2,4-dimethyl-1H-pyrrole (2.00 g, 16.3 mmol) and 4-(Prop-2-yn-1-yloxy)benzaldehyde (1.29 g, 8.05 mmol) were dissolved in degassed dichloromethane (150 mL) and stirred for 10 minutes at room temperature. Trifluoroacetic acid (0.6 g, 5 mmol) was subsequently added and the mixture was stirred overnight at room temperature overnight in a nitrogen environment. A solution of 2,3-dichloro-5,6-dicyano-1,4-benzoquinone (1.80 g, 7.92 mmol) in dichloromethane (15 mL) was slowly added to the reaction mixture and was stirred for a further 10 minutes. Triethylamine (8 mL) and boron trifluoride etherate (11 mL) were then added, and the reaction mixture was stirred overnight at room temperature in a nitrogen environment. The reaction mixture was then quenched with water and the organic layer was separated and was washed with water (ca 100 mL x 3). The organic layer was separated and dried over magnesium sulfate, then the solvent was removed *in vacuo*. The black residue was then purified with column chromatography using silica gel and dichloromethane:hexane (1:1) as the eluent. Alkyne BODIPY was achieved as a red solid. (0.82 g, 1.90 mmol, 23 %). Spectroscopic data for the title compound were consistent with the literature. ^1H NMR (400 MHz, Chloroform-*d*) δ (ppm) 7.13 (d, $J = 8.6$ Hz, 2H), 7.01 (d, $J = 8.7$ Hz, 2H), 4.70 (d, $J = 2.4$ Hz, 2H), 2.49 (t, $J = 2.4$ Hz, 1H), 2.46 (s, 6H), 2.23 (q, $J = 7.5$ Hz, 4H), 1.25 (s, 6H), 0.91 (t, $J = 7.5$ Hz, 6H), ^{19}F NMR (377 MHz, Chloroform-*d*) δ (ppm) -142.47 (dd, $J = 68.0, 33.9$ Hz, 2F).

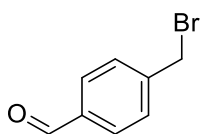
3.9.2.10 4-(hydroxymethyl)benzaldehyde



Terephthalaldehyde (10.0 g, 74.6 mmol) was dissolved in ethanol (40 mL) and tetrahydrofuran (60 mL) and stirred for 10 minutes and cooled to 0 °C. Sodium

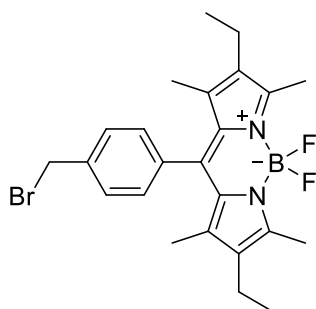
borohydride (0.70 g, 18.5 mmol) was quickly added and stirred for a further 6 hours at 0 °C. The solvent was then removed and the residue was purified by column chromatography using silica gel with hexane:dichloromethane (1:1) as the eluent 4-(hydroxymethyl)benzaldehyde was retrieved as a white solid (1.60 g, 11.9 mmol, 64 %). Spectroscopic data for the title compound were consistent with the literature.

3.9.2.11. 4-(Bromomethyl)benzaldehyde



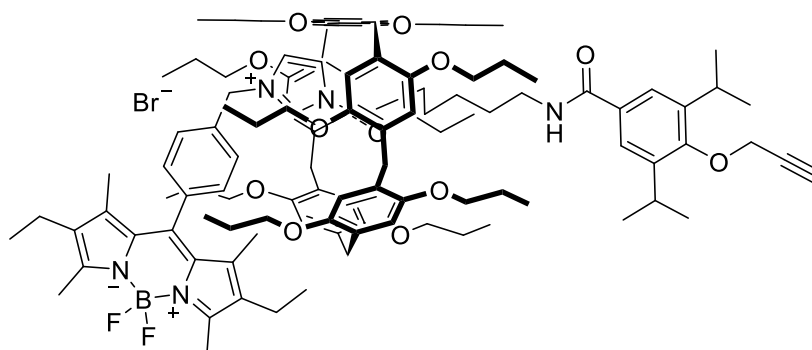
4-(hydroxymethyl)benzaldehyde (5.80 g, 42.6 mmol), triphenylphosphine (27.8 g, 106 mmol) and *N*-bromosuccinimide (14.8 g, 83.1 mmol) was dissolved in dichloromethane (400 mL) and stirred overnight at room temperature. Water (*ca* 400 mL) was added to the reaction mixture, and the organic layer was separated and washed with water (*ca* 2 x 200 mL) and brine (*ca* 150 mL). The organic layer was separated, dried over magnesium solvent, and the solvent was removed *in vacuo*. The residue was purified with column chromatography using silica gel and dichloromethane:hexane (1:1) as the eluent. 4-(Bromomethyl)benzaldehyde was retrieved as a white solid (6.10 g, 30.7 mmol, 72 %). Spectroscopic data for the title compound were consistent with the literature.

3.9.2.12. Bromomethyl BODIPY



4-(Bromomethyl)benzaldehyde (2.60 g, 13.1 mmol) and 3-Ethyl-2,4-dimethyl-1H-pyrrole (3.00 g, 24.4 mmol) were stirred in degassed dichloromethane (300 mL) for 10 minutes in a nitrogen environment. Trifluoroacetic acid (0.18 g, 1.57 mmol) was then added and the mixture was stirred overnight at room temperature in a nitrogen environment. A solution of 2,3-dichloro-5,6-dicyano-1,4-benzoquinone (2.20 g, 10.1 mmol) in dichloromethane (20 mL) was slowly added to the reaction mixture and was stirred for a further 10 minutes. *N,N*-Diisopropylethylamine (20 mL) and boron trifluoride etherate (20 mL) were then added, and the reaction mixture was stirred overnight at room temperature in a nitrogen environment. Water (500 mL) was then added to quench the reaction, and the organic layer was separated and washed with water (*ca* 2 x 250 mL). The organic layer was separated, dried over magnesium sulfate and the solvent was removed *in vacuo*. The resulting residue was purified with column chromatography using silica gel and dichloromethane:hexane (1:1), however separation from the unsubstituted BODIPY could not be achieved and a small amount of impurity (*calculated 20 %*) was present. Spectroscopic data for the title compound were consistent with the literature. ¹H NMR (400 MHz, Chloroform-*d*) δ (ppm) 7.27 (d, *J* = 8.0 Hz, 3H, *contains impurity*), 7.14 (d, *J* = 7.7 Hz, 2H), 4.56 (s, 1H), 2.53 (s, 6H), 2.44 (s, 3H, *impurity*), 2.30 (q, *J* = 7.6 Hz, 4H), 2.17 (d, *J* = 3.0 Hz, 1H, *impurity*), 1.30 (s, 6H), 1.06 (t, *J* = 7.6 Hz 1H, *impurity*), 0.98 (t, *J* = 7.5 Hz, 6H), 0.91 – 0.78 (m, 2H, *impurity*); ¹³C NMR (101 MHz, Chloroform-*d*) δ (ppm) 153.46, 140.61, 138.57, 132.75, 132.62, 130.95, 129.68, 128.09, 58.48, 29.71, 21.44, 17.29, 17.08, 14.63, 14.59, 12.49, 11.73, 9.40; ¹⁹F NMR (377 MHz, Chloroform-*d*) δ (ppm) -146.35 (dd, *J* = 67.5, 33.7 Hz, 2F).

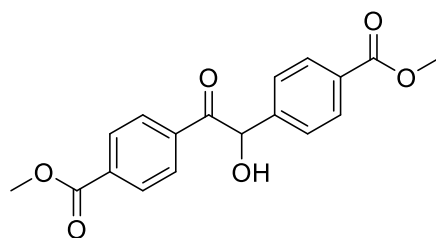
3.9.2.13. Attempted Rotaxane Synthesis



N-(6-(1H-imidazol-1-yl)hexyl)-3,5-diisopropyl-4-(prop-2-yn-1-yloxy)benzamide (36 mg, 87.1 μmol) and dipropoxypillar[5]arene (100 mg, 96.9 μmol) were stirred in 1 mL of chloroform for 30 minutes in an ice/salt cooling bath (*ca* -10 $^{\circ}\text{C}$). The bromomethyl BODIPY (60.0 mg, 140 μmol) was then added and the mixture was stirred for three days at room temperature. Thin layer chromatography was performed on the reaction mixture (eluent dichloromethane) and three fluorescent spots were examined by MALDI-TOF. Spot one referred to the unsubstituted BODIPY – dipropoxypillar[5]arene complex 1314.04 m/z . Spot was ambiguous but could related to the BODIPY stoppered rod after amide bond breaking 555.53 m/z . Spot three related to the rotaxane complete 1833.39 m/z . Column chromatography was performed on the reaction mixture using dichloromethane:methanol (100:5) as the eluent. Unfortunately, the rotaxane was not retrieved in a high enough yield to perform spectroscopic analysis.

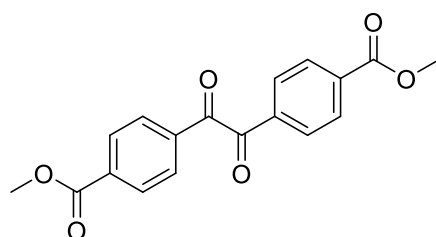
3.9.3. Synthesis of MOF-N7

3.9.3.1. Dimethyl 4,4'-(1-hydroxy-2-oxoethane-1,2-diyl)dibenzoate



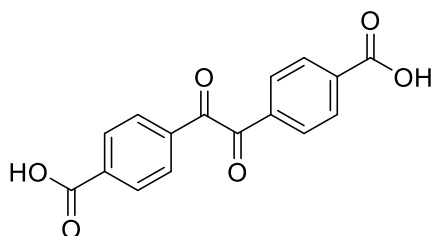
Thiamine hydrochloride (1.80 g, 5.34 mmol) was dissolved in water (7 mL) and methanol (13 mL). A sodium hydroxide solution (2 M, 5 mL) was then added, and the mixture was stirred for 5 minutes. Upon cooling, the reaction mixture was filtered, and the solid product was washed with water, methanol and diethylether to give dimethyl 4,4'-(1-hydroxy-2-oxoethane-1,2-diyl)dibenzoate as a pale-yellow solid (5.70 g, 17.4 mmol, 38 %). Spectroscopic data for the title compound were consistent with the literature. ^1H NMR (400 MHz, DMSO) δ (ppm) 7.98 (dt, $J = 8.5, 2.2$ Hz, 2H), 7.87 (dt, $J = 8.4, 1.6$ Hz, 2H), 7.78 (dt, $J = 8.2, 1.6$ Hz, 2H), 7.44 (dt, $J = 8.4, 1.6$ Hz, 2H), 6.37 (d, $J = 5.7$ Hz, 1H), 6.04 (t, $J = 1.6$ Hz, 1H), 3.71 (s, 3H), 3.67 (s, 3H); ^{13}C NMR (101 MHz, DMSO) δ (ppm) 199.02, 166.39, 165.91, 145.02, 138.78, 130.67, 130.39, 130.27, 130.09, 130.05, 129.80, 129.78, 129.75, 129.66, 129.48, 129.26, 129.14, 127.93, 76.17, 53.15, 53.03, 52.90, 52.55, 40.23.

3.9.3.2. Dimethyl 4,4'-oxalyldibenzoate



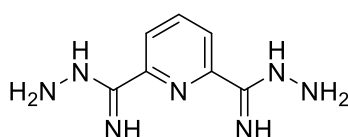
Dimethyl 4,4'-(1-hydroxy-2-oxoethane-1,2-diyl)dibenzoate (5.70 g, 17.4 mmol) was dissolved in dimethylsulfoxide (50 mL), hydrobromic acid (40 % in water, 9 mL) was then slowly added and the mixture was stirred at 55 °C overnight. Upon cooling the reaction mixture was filtered and the solid was washed with water and dried in a vacuum oven at 70 °C overnight. Dimethyl 4,4'-oxalyldibenzoate was then collected as a pale-yellow solid (5.00 g, 15.3 mmol, 88 %). Spectroscopic data for the title compound were consistent with the literature. ¹H NMR (400 MHz, DMSO) δ (ppm) 8.11 (dt, *J* = 8.7, 1.5 Hz, 4H), 7.98 (dt, *J* = 8.6, 1.9 Hz, 4H), 3.90 (s, 6H).

3.9.3.3. 4,4'-Oxalyldibenzoic acid



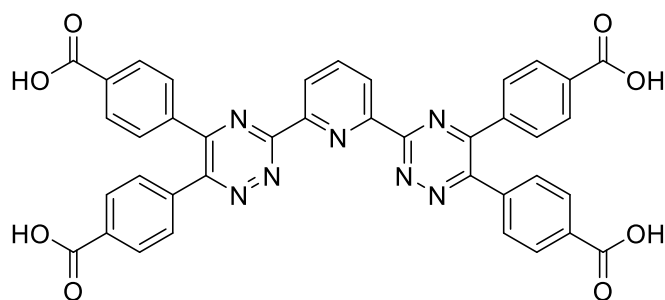
Dimethyl 4,4'-oxalyldibenzoate (3.20 g, 10.2 mmol) was dissolved in sulfuric acid (50 mL) and water (10 mL). Acetic acid was then added, and the reaction mixture was heated at 100 °C and stirred overnight. Upon cooling, the reaction mixture was filtered and the solid was washed with water, methanol, and diethyl ether to give 4,4'-oxalyldibenzoic acid as a yellow solid (2.10 g, 7.04 mmol, 70 %). Spectroscopic data for the title compound were consistent with the literature. ¹H NMR (400 MHz, DMSO) δ (ppm) 13.46 (s, 2H, br), 8.15 (d, *J* = 8.1 Hz, 4H), 8.09 (d, *J* = 8.1 Hz, 4H); ¹³C NMR (101 MHz, DMSO) δ (ppm) 193.82, 166.78, 136.90, 135.48, 130.56, 130.53.

3.9.3.4. Pyridine-2,6-bis(carboximidhydrazide)



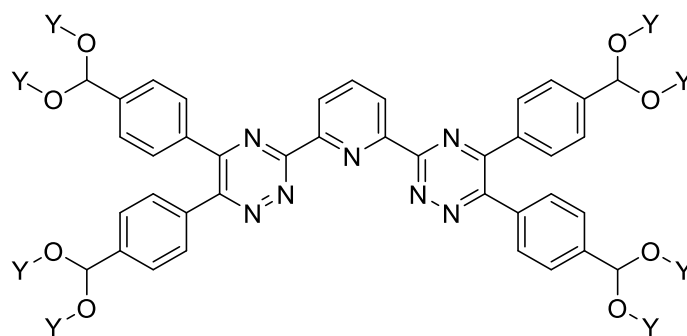
Pyridine-2,6-dicarbonitrile (2.00 g, 15.4 mmol) was dissolved in ethanol (8 mL) and stirred for 10 minutes. Hydrazine monohydrate (9.60 g, 19.2 mmol) was then slowly added and the mixture was stirred overnight at room temperature. The reaction mixture was then filtered, and the solid was washed with ethanol to give pyridine-2,6-bis(carboximidhydrazide) as a white solid (2.30 g, 11.9 mmol, 74 %). Spectroscopic data for the title compound were consistent with the literature.. ^1H NMR (400 MHz, DMSO) δ (ppm) 7.66 (d, $J = 7.8$ Hz, 2H), 7.50 (td, 7.9, 0.8 Hz, 1H), 5.89 (s, 4H, br), (*other amine hydrogens enveloped within water peak*); ^{13}C NMR (101 MHz, DMSO) δ (ppm) 150.79, 144.09, 136.45, 118.43.

3.9.3.5. MOF-N7 linker



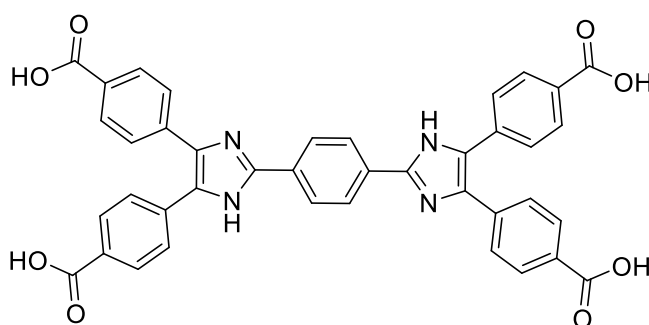
Pyridine-2,6-bis(carboximidhydrazide) (0.50 g, 2.59 mmol) and 4,4'-Oxalyldibenzoic acid (1.60 g, 5.36 mmol) were stirred in dimethylformamide (25 mL) overnight at 80 °C. Upon cooling, the solid was filtered and washed with methanol to give MOF-N7 linker. A further crop was obtained by removing the filtrate solvent *in vacuo* then recrystallising in methanol to give further MOF-N7 as a yellow solid (total 1.20 g, 1.71 mmol, 65 %). Novel compound. ^1H NMR (400 MHz, DMSO) δ (ppm) 13.27 (s, 4H, br), 8.81 (d, $J = 7.8$ Hz, 2H), 8.42 (t, $J = 7.9$ Hz, 1H), 8.10 - 7.90 (m, 8H), 7.82 - 7.63 (m, 8H). ^{13}C NMR (101 MHz, DMSO) δ (ppm) 193.85, 167.31, 167.17, 166.79, 156.07, 136.97, 135.46, 132.24, 130.66, 130.56, 130.53, 130.34, 129.94, 129.80.

3.9.3.6. MOF-N7 Synthesis



MOF-N7 linker (6.40 mg, 9 μmol), yttrium (III) nitrate hexahydrate (13.0 mg, 34 μmol), and σ -fluorobenzoic acid (0.60 g, 1.4 mmol) was dissolved in dimethylformamide (0.3 mL) and sonicated till solvation. Acetic acid (0.75 mL) was then added and the reaction vessel was sealed and placed in an electric heating oven at 120 $^{\circ}\text{C}$ for 3 days. Upon cooling yellow hexagonal crystals were separated and washed with dimethylformamide. Single crystal X-ray diffraction was performed and the data was solved by Dr Sarah Griffin.

3.9.3.7. MOF-N4 Linker Synthesis

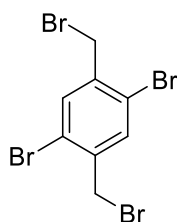


4,4'-Oxalyldibenzoic acid (0.58 g, 1.94 mmol) and terephthalaldehyde (0.13 g, 0.97 mmol) were dissolved in dimethylformamide (10 mL) and stirred for 10 minutes. Ammonium acetate (0.39 g, 50.6 mmol) and zirconium (IV) tetrachloride (0.05 g, 0.21 mmol) were then added and the mixture was stirred overnight at 100 $^{\circ}\text{C}$. Upon cooling,

the reaction mixture was filtered, giving MOF-N4 linker as a pale-yellow solid (0.30 g, 0.42 mmol, 43 %).

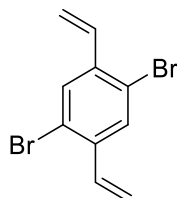
3.9.4. Synthesis of UIO-68 Alkene

3.9.4.1. 1,4-Dibromo-2,5-bis(bromomethyl)benzene



1,4-dibromo-2,5-dimethylbenzene (10.0 g, 37.8 mmol), *N*-bromosuccinimide (14.2 g, 79.7 mmol) and azobisisobutyronitrile (0.30 g, 1.82 mmol) was dissolved in acetonitrile (ca 75 mL) and stirred overnight at 100 °C. Upon cooling, the solvent was removed *in vacuo* and the residue was washed with hot methanol to give 1,4-dibromo-2,5-bis(bromomethyl)benzene as a white solid. (8.00 g, 19.0 mmol, 50 %). Spectroscopic data for the title compound were consistent with the literature. ¹H NMR (400 MHz, Chloroform-*d*) δ (ppm) 7.68 (s, 2H), 4.52 (s, 4H); ¹³C NMR (101 MHz, Chloroform-*d*) δ (ppm) 138.3, 134.7, 122.8, 31.2.

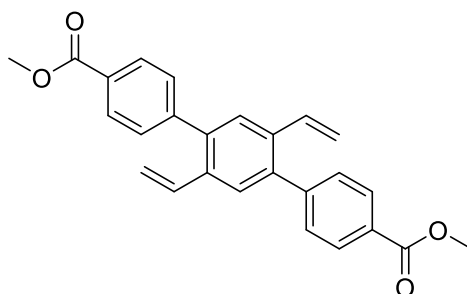
3.9.4.2. 1,4-Dibromo-2,5-divinylbenzene



1,4-dibromo-2,5-bis(bromomethyl)benzene (4.40 g, 10.4 mmol) and triphenylphosphine (6.20 g, 23.6 mmol) were dissolved in dimethylformamide (50 mL) and stirred at 160 °C overnight. Upon cooling the solvent was removed *in vacuo* and the residue redissolved in tetrahydrofuran (ca 100 mL). Paraformaldehyde (7.10 g,

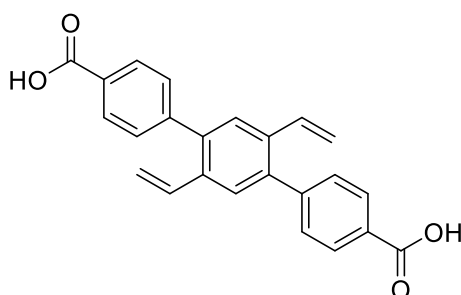
236 mmol) and potassium *tert*-butoxide (3.50 g, 31.2 mmol) were then added and stirred overnight at room temperature. The solvent was then removed and the residue was purified with column chromatography using silica gel and hexane as the eluent. 1,4-Dibromo-2,5-divinylbenzene could then be retrieved as a white powder (2.20 g, 7.63 mmol, 76 %). Spectroscopic data for the title compound were consistent with the literature. ¹H NMR (400 MHz, Chloroform-*d*) δ (ppm) 7.65 (s, 2H), 6.88 (dd, $J = 17.4$, 11.0 Hz, 2H), 5.64 (dd, $J = 17.4$, 0.8 Hz, 2H), 5.33 (dd, $J = 10.9$, 0.8 Hz, 2H).

3.9.4.3. Dimethyl 2',5'-divinyl-[1,1':4',1''-terphenyl]-4,4''-dicarboxylate



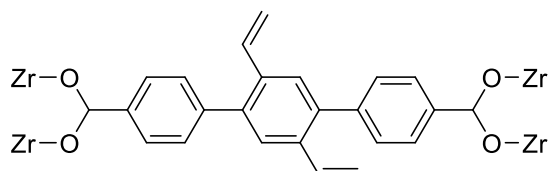
1,4-Dibromo-2,5-divinylbenzene (0.40 g, 1.38 mmol), methyl 4-(4,4,5,5-tetramethyl-1,3,2-dioxaborolan-2-yl)benzoate (1.40 g, 5.34 mmol), caesium carbonate (1.90 g, 5.85 mmol) and caesium fluoride (0.20 g, 1.32 mmol) were stirred in degassed dioxane (50 mL) and water (3 mL). Tetrakis(triphenylphosphine)palladium (0) (0.20 g, 0.17 mmol) was then added and the reaction was stirred at 80 °C overnight. Upon cooling the reaction mixture was filtered through celite and the solvent was removed *in vacuo*. The residue was then purified with column chromatography using silica gel and dichloromethane:hexane (1:1) as the eluent. Dimethyl 2',5'-divinyl-[1,1':4',1''-terphenyl]-4,4''-dicarboxylate was retrieved as a white solid (0.40 g, 1.00 mmol, 72 %). Novel compound. ¹H NMR (400 MHz, Chloroform-*d*) δ (ppm) 8.12 - 7.99 (m, 4H), 7.46 - 7.37 (m, 4H), 6.59 (dd, $J = 17.4$, 11.0 Hz, 2H), 5.66 (dd, $J = 17.5$, 1.2 Hz, 2H), 5.16 (dd, $J = 11.0$, 1.1 Hz, 2H), 3.89 (s, 6H).

3.9.4.4. 2',5'-divinyl-[1,1':4',1''-terphenyl]-4,4''-dicarboxylic acid (bis(alkene) linker)



Dimethyl 2',5'-divinyl-[1,1':4',1''-terphenyl]-4,4''-dicarboxylate (0.40 g, 1.00 mmol) was dissolved in tetrahydrofuran (15 mL) and water (3 mL) and stirred for 10 minutes. Potassium hydroxide (1.00 g, 17.8 mmol) was then added, and the reaction mixture was stirred overnight at 60 °C. Upon cooling, the solvent was removed *in vacuo*, and hydrochloric acid (2 M, 25 mL) was added. The mixture was filtered and the solid was washed with water, methanol and diethylether to give bis(alkene) linker as a white solid (0.30 g, 0.84 mmol, 80 %). Novel compound. ¹H NMR (300 MHz, DMSO) δ (ppm) 13.08 (s, 2H), 8.05 (d, $J = 7.9$ Hz, 4H), 7.64 (s, 2H), 7.53 (d, $J = 8.0$ Hz, 4H), 6.61 (dd, $J = 17.4, 11.0$ Hz, 2H), 5.88 (d, $J = 17.4$ Hz, 2H), 5.29 (d, $J = 11.2$ Hz, 2H).

3.9.4.5. UiO-68 bis(alkene) MOF



Bis(alkene) linker (37.0 mg, 97.3 μ mol), zirconium tetrachloride (24.0 mg, 103 μ mol) and benzoic acid (240 mg, 2.97 mmol) were added to dimethylformamide (3 mL) and sonicated until dissolved. The reaction mixture was then sealed and placed in a

temperature controlled electric oven at 120 °C overnight. Crystals could then be retrieved. Single crystal X-ray diffraction was then performed, and the data was solved by Dr Sarah Griffin.

3.10. References

- 1 P. Z. Moghadam, A. Li, S. B. Wiggin, A. Tao, A. G. P. Maloney, P. A. Wood, S. C. Ward and D. Fairen-Jimenez, *Chem. Mater.*, 2017, **29**, 2618–2625
- 2 Case: How many MOFs are there in the CSD? - The Cambridge Crystallographic Data Centre (CCDC), <https://www.ccdc.cam.ac.uk/support-and-resources/support/case/?caseid=9833bd2c-27f9-4ff7-8186-71a9b415f012>, (accessed September 22, 2022).
- 3 S. J. Loeb, *Chem. Commun.*, 2005, **12**, 1511-1418.
- 4 D. Sluysmans and J. F. Stoddart, *Trends Chem.*, 2019, **1**, 185-197.
- 5 P. R. Ashton, C. L. Brown, E. J. T. Chrystal, T. T. Goodnow, A. E. Kaifer, K. P. Parry, D. Philp, A. M. Z. Slawin, N. Spencer, J. F. Stoddart and D. J. Williams, *J. Chem. Soc.*, 1991, **9**, 634–639.
- 6 K. S. Chichak, S. J. Cantrill, A. R. Pease, S. H. Chiu, G. W. V. Cave, J. L. Atwood and J. F. Stoddart, *Science*, 2004, **304**, 1308–1312.
- 7 A. W. Heard and S. M. Goldup, *Chem.*, 2020, **6**, 994–1006.
- 8 N. H. Evans, C. J. Serpell and P. D. Beer, *Angew. Chem., Int. Ed. Engl.*, 2011, **50**, 2507–2510.
- 9 S. Shinoda, T. Maeda, H. Miyake and H. Tsukube, *Supramol. Chem.*, 2011, **23**, 244–248.
- 10 R. Jimenez, C. Martin and P. Lopez-Cornejo, *J. Phys. Chem. B*, 2008, **112**, 11610–11615.
- 11 Y. Domoto, S. Sase and K. Goto, *Chem. Eur. J.*, 2014, **20**, 15998–16005.
- 12 P. T. Glink, A. I. Oliva, J. Fraser Stoddart, A. J. P. White and D. J. Williams, *Angew. Chem., Int. Ed. Engl.*, 2001, **40**, 1870–1875.
- 13 V. Richards, *Nat. Chem.*, 2016, **8**, 1090.
- 14 M. Schliwa and G. Woehlke, *Nature*, 2003, **422**, 759–765.
- 15 D. Trauner, *Beilstein J. Org. Chem.*, 2012, **8**, 870–871.
- 16 Y. Shirai, A. J. Osgood, Y. Zhao, K. F. Kelly and J. M. Tour, *Nano. Lett.*, 2005, **5**, 2330–2334.
- 17 P. R. Ashton, R. Ballardini, V. Balzani, I. Baxter, A. Credi, M. C. T. Fyfe, M. T. Gandolfi, M. Gómez-López, M.-V. Martínez-Díaz, A. Piersanti, N. Spencer, J. F. Stoddart, M. Venturi, A. J. P. White and D. J. Williams, *J. Am. Chem. Soc.*, 1998, **120**, 11932–11942.
- 18 S. Paliwal, S. Geib and C. S. Wilcox, *J. Am. Chem. Soc.*, 1994, **116**, 4497–4498.
- 19 Y. Ai, M. H.-Y. Chan, A. K.-W. Chan, M. Ng, Y. Li and V. W.-W. Yam, *Proc. Natl. Acad. Sci.*, 2019, **116**, 13856–13861.
- 20 I. Hadrovic, P. Rebmann, F. G. Klärner, G. Bitan and T. Schrader, *Front. Chem.*, 2019, **7**.

- 21 W. Meng, R. A. Muscat, M. L. McKee, P. J. Milnes, A. H. El-Sagheer, J. Bath, B. G. Davis, T. Brown, R. K. O'Reilly and A. J. Turberfield, *Nat. Chem.*, 2016, **8**, 542–548.
- 22 P. Langer, L. Yang, C. R. Pfeiffer, W. Lewis and N. R. Champness, *Dalton Transactions*, 2019, **48**, 58–64.
- 23 R. A. Bissell, E. Córdova, A. E. Kaifer and J. F. Stoddart, *Nature*, 1994, **369**, 133–137.
- 24 M. Xue, Y. Yang, X. Chi, X. Yan and F. Huang, *Chem. Rev.*, 2015, **115**, 7398–7501.
- 25 L. Zhao, J. J. Davis, K. M. Mullen, M. J. Chmielewski, R. M. J. Jacobs, A. Brown and P. D. Beer, *Langmuir*, 2009, **25**, 2935–2940.
- 26 K. Nikitin, E. Lestini, M. Lazzari, S. Altobello and D. Fitzmaurice, *Langmuir*, 2007, **23**, 12147–12153.
- 27 D. Asthana, D. Thomas, S. J. Lockyer, A. Brookfield, G. A. Timco, I. J. Vitorica-Yrezabal, G. F. S. Whitehead, E. J. L. McInnes, D. Collison, D. A. Leigh and R. E. P. Winpenny, *Commun. Chem.*, 2022, **5**, 73.
- 28 H. Wilson, S. Byrne, N. Bampos and K. M. Mullen, *Org. Biomol. Chem.*, 2013, **11**, 2105–2115.
- 29 F. Çeçen and Ö. Aktaş, in *Activated Carbon for Water and Wastewater Treatment*, 2011.
- 30 C. W. Scheele, *Carl Wilhelm Scheele's d. Königl. Schwed. Acad. d. Wissenschaft. Mitgliebes, Chemische Abhandlung von der Luft und dem Feuer*, 1777.
- 31 E. F. Sousa-Aguiar, P. A. Arroyo, M. A. S. D. de Barros and J. L. de Miranda, in *Zeolites and Metal-Organic Frameworks*, 2019, pp. 307–342.
- 32 R. M. Barrer, *J. Chem. Soc.*, 1948, **1**, 127–132.
- 33 R. M. Milton, in *Molecular sieve science and technology: a historical perspective in Zeolite Synthesis*, 1989, pp. 1–10.
- 34 Y. Li, L. Li and J. Yu, *Chem*, 2017, **3**, 928-949.
- 35 T. Bein, in *Studies in Surface Science and Catalysis*, 2007, vol. 168.
- 36 M. Servatan, P. Zarrintaj, G. Mahmodi, S. J. Kim, M. R. Ganjali, M. R. Saeb and M. Mozafari, *Drug Discov. Today*, 2020, **25**, 642-656.
- 37 B. F. Hoskin and R. Robson, *J. Am. Chem. Soc.*, **4**, 1546-1554.
- 38 H. Li, M. Eddaoudi, M. O'Keeffe and O. M. Yaghi, *Nature*, 1999, **402**, 276–279.
- 39 S. S. Y. Chui, S. M. F. Lo, J. P. H. Charmant, A. G. Orpen and I. D. Williams, *Science*, 1999, **283**, 1148–1150.
- 40 N. Stock and S. Biswas, *Chem. Rev.*, 2012, **112**, 933–969.
- 41 S. L. Griffin and N. R. Champness, *Coord. Chem. Rev.*, 2020, **414**, 213295.

- 42 R. S. Forgan, *Chem. Sci.*, 2020, **11**, 4546–4562.
- 43 M. Kalaj and S. M. Cohen, *ACS. Cent. Sci.*, 2020, **6**, 1046–1057.
- 44 Y. K. Hwang, D. Y. Hong, J. S. Chang, S. H. Jhung, Y. K. Seo, J. Kim, A. Vimont, M. Daturi, C. Serre and G. Férey, *Angew. Chem., Int. Ed. Engl.*, 2008, **47**, 4144–4148.
- 45 X. Zhang, T. Xia, K. Jiang, Y. Cui, Y. Yang and G. Qian, *J. Solid State Chem.*, 2017, **253**, 277–281.
- 46 R. S. Forgan, *Dalton Transactions*, 2019, **48**, 9037–9042.
- 47 S. Wang, Y. Chen, S. Wang, P. Li, C. A. Mirkin and O. K. Farha, *J. Am. Chem. Soc.*, 2019, **141**, 2215–2219.
- 48 R. Röder, T. Preiß, P. Hirschle, B. Steinborn, A. Zimpel, M. Höhn, J. O. Rädler, T. Bein, E. Wagner, S. Wuttke and U. Lächelt, *J. Am. Chem. Soc.*, 2017, **139**, 2359–2368.
- 49 I. Abánades Lázaro, S. Haddad, S. Sacca, C. Orellana-Tavra, D. Fairen-Jimenez and R. S. Forgan, *Chem*, 2017, **2**, 561–578.
- 50 H. L. Jiang, D. Feng, T. F. Liu, J. R. Li and H. C. Zhou, *J. Am. Chem. Soc.*, 2012, **134**, 14690–14693.
- 51 Y. Zhang, B. Gui, R. Chen, G. Hu, Y. Meng, D. Yuan, M. Zeller and C. Wang, *Inorg. Chem.*, 2018, **57**, 2288–2295.
- 52 W. Morris, W. E. Briley, E. Auyeung, M. D. Cabezas and C. A. Mirkin, *J. Am. Chem. Soc.*, 2014, **136**, 7261–7264.
- 53 L. Feng, Y. Qiu, Q. H. Guo, Z. Chen, J. S. W. Seale, K. He, H. Wu, Y. Feng, O. K. Farha, R. Dean Astumian and J. Fraser Stoddart, *Science*, 2021, **374**, 1215–1221.
- 54 S. J. Loeb, *Chem. Soc. Rev.*, 2007, **36**, 226–235.
- 55 Y. Goto, H. Sato, S. Shinkai and K. Sada, *J. Am. Chem. Soc.*, 2008, **130**, 14354–14355.
- 56 C. Li, S. Chen, J. Li, K. Han, M. Xu, B. Hu, Y. Yu and X. Jia, *Chem. Commun.*, 2011, **47**, 11294–11296.
- 57 R. Valiulin, in *Organic Chemistry: 100 Must-Know Mechanisms*, De Gruyter, 2020, pp. 94–95.
- 58 C. A. G. N. Montalbetti and V. Falque, *Tetrahedron*, 2005, **61**, 10827–10852.
- 59 Y. Gabe, Y. Urano, K. Kikuchi, H. Kojima and T. Nagano, *J. Am. Chem. Soc.*, 2004, **126**, 3357–3367.
- 60 A. Aguiar, J. Farinhas, W. da Silva, M. Susano, M. R. Silva, L. Alcácer, S. Kumar, C. M. A. Brett, J. Morgado and A. J. F. N. Sobral, *Dyes and Pigm.*, 2020, **172**, 107842.
- 61 Y. S. Marfin, D. A. Merkushev, S. D. Usoltsev, M. V. Shipalova and E. V. Rummyantsev, *J. Fluoresc.*, 2015, **25**, 1517–1526.

- 62 X. Yang, X. F. Zhang, X. Lu, C. Yu and L. Jiao, *J. Photochem. Photobiol. A Chem.*, 2015, **297**, 39–44.
- 63 L. Yang, P. Langer, E. S. Davies, M. Baldoni, K. Wickham, N. A. Besley, E. Besley and N. R. Champness, *Chem. Sci.*, 2019, **10**, 3723–3732.
- 64 Y. Wang, G. Ping and C. Li, *Chem. Commun.*, 2016, **52**, 9858–9872.
- 65 L. Wang and T. Liu, *Tetrahedron Lett.*, 2019, **60**, 150993.
- 66 S. Tai, S. V Marchi and J. D. Carrick, *J. Heterocycl. Chem.*, 2016, **53**, 1138–1146.
- 67 M. H. Petersen, S. A. Gevorgyan and F. C. Krebs, *Macromolecules*, 2008, **41**, 8986–8994.
- 68 Timothy Soderberg, in *Organic Chemistry with a Biological Emphasis Volume II*, 2019.
- 69 M. Weiss and M. Appel, *J. Am. Chem. Soc.*, 1948, **70**, 3666–3667.
- 70 A. Laurent, *Annalen der Pharmacie*, 1836, **17**, 88–94.
- 71 B. B. Corson and R. W. McAllister, *J. Am. Chem. Soc.*, 1929, **51**, 2822–2825.
- 72 N. Zinin, *Justus Liebigs Ann. Chem.*, 1840, **34**, 186–192.
- 73 H. T. Clarke, E. E. Dreger, *Org. Syn.*, 1926, **6**, 6.
- 74 G. Bacharach and J. E. Brolles Jr., *Recl. Trav. Chim. Pays-Bas*, 1931, **50**, 732–735.
- 75 J. Liebig, *Ann. Phar.*, 1838, **25**, 1–31.
- 76 E. Sagot, A. Le Roux, C. Soulivet, E. Pasquinet, D. Poullain, E. Girard and P. Palmas, *Tetrahedron*, 2007, **63**, 11189–11194.
- 77 N. L. Higuera, D. Peña-Solórzano and C. Ochoa-Puentes, *Synlett*, 2019, **30**, 225–229.
- 78 P. Wu, L. Xia, M. Huangfu, F. Fu, M. Wang, B. Wen, Z. Yang and J. Wang, *Inorg. Chem.*, 2020, **59**, 264–273.
- 79 D. X. Xue, Y. Belmabkhout, O. Shekhah, H. Jiang, K. Adil, A. J. Cairns and M. Eddaoudi, *J. Am. Chem. Soc.*, 2015, **137**, 5034–5040.
- 80 J. Bello-García, D. Padín, J. A. Varela and C. Saá, *Org. Lett.*, 2021, **23**, 5539–5544.
- 81 M. C. Bonifacio, C. R. Robertson, J.-Y. Jung and B. T. King, *J. Org. Chem.*, 2005, **70**, 8522–8526.
- 82 X. Yang, B. Cheng, Y. Xiao, M. Xue, T. Liu, H. Cao and J. Chen, *Eur. J. Med. Chem.*, 2021, **213**, 113058.
- 83 S. J. Park, S. K. Yeon, Y. Kim, H. J. Kim, S. Kim, J. Kim, J. W. Choi, B. Kim, E. H. Lee, R. Kim, S. H. Seo, J. Lee, J. W. Kim, H.-Y. Lee, H. Hwang, Y.-S. Bahn, E. Cheong, J.-H. Park and K. D. Park, *J. Med. Chem.*, 2022, **65**, 3539–3562.

- 84 S. J. Park, S. K. Yeon, Y. Kim, H. J. Kim, S. Kim, J. Kim, J. W. Choi, B. Kim, E. H. Lee, R. Kim, S. H. Seo, J. Lee, J. W. Kim, H.-Y. Lee, H. Hwang, Y.-S. Bahn, E. Cheong, J.-H. Park and K. D. Park, *J. Med. Chem.*, 2022, **65**, 3539–3562.
- 85 C. G. Screttas, B. R. Steele, M. Micha-Screttas and G. A. Heropoulos, *Org. Lett.*, 2012, **14**, 5680–5683.
- 86 H. A. Muathen, *Monatsh. Chem.*, 1999, **130**, 1493–1497.

CHAPTER 4. THIOLATED PILLAR[5]ARENES ON GOLD SURFACES

4.1. Introduction

The adsorption of macrocycles upon a 2D surface is an intriguing prospect for the future of porous materials. Although specific stated applications are often varied, the aims can be broadly reduced into the extension of the intrinsic molecular porosity of macrocycles on to a macromolecular scale. As discussed in *chapter 3*, porous materials are well established, with applications in gas storage, molecular separation, catalysis, and ion exchange being reported.¹⁻⁴ However, where some porous materials falter is in permanent porosity, that is the ability of a material to sustain well defined cavities after chemical or physical changes, such as solvent loss, temperature variation, and pressure increases and decreases. The implementation of macrocycles upon surfaces aims to alleviate this issue, by building from the starting point of a rigid and chemically stable molecular ring system. Adsorbed macrocycles can also be used to enhance or support the structure they are placed upon. For example, controlling aggregation of gold nanoparticles, or to aid in stabilising a guest towards a reactive surface.^{5,6}

4.2. Self-Assembled Monolayers

The emergence of self-assembled monolayers within scientific fields did not arise in a vacuum. From *Franklin's* observations of oil's 'stilling of waves' when placed upon water's surface, to the implementation of solid substrates for heterogenous catalysis by *Haber* and *Sabatier*, the chemistry of surfaces has always been widely noted, even if not fully understood.^{7,8} As our understanding of surfaces increased through works

from the likes of *Langmuir*, *Pockels*, and *Blodgett*, so did the number of works on novel surface functionalisation methods.^{9–11} Subsequently, from the mid-20th century onwards appeared reports detailing the surface modification of metals with hydrocarbons, glass with silanes, and gold with sulfides.^{12–14} Self-assembled monolayers, therefore provided a unique opportunity to modify the properties of a metal, glass or metal oxide surface, without disrupting the bulk properties of the material.

Self-assembled monolayers can be defined as molecular assemblies formed *via* adsorption of organic molecules onto a solid substrate.¹⁵ There is a large variation of both adsorbents and substrates, and from this arises a range of interaction strengths between the constituent parts. This scales from the relatively weak, aromatic molecules on a metal surface; where the main interaction is the phenyl π -system interacting with the d-electrons in the metal.¹⁶ Conversely, an example of a strong surface-adsorbent interaction, uses covalent bonds between the adsorbent and the surface, an example of which uses a perfluorodecyltrichlorosilane adsorbent on a hydroxyl based substrate, forming a strong Si-O covalent bond.¹⁷

Aside from the substrate, which as previously stated can take multiple forms, the adsorbent is the other key component in the self-assembled monolayer (*figure 1*). The adsorbent can be further divided into three parts: the terminal group, the spacer, and the functional group.

The terminal group (often called the headgroup) is the binding group on the adsorbent, it can be one of multiple functional groups, including but not limited to: -OH, -NH₂ -SH, or -COOH, and binds *via* spontaneous exothermic chemisorption with the surface. The

specificity of a terminal group towards an individual surface varies, but there are key motifs which will be discussed later.

The spacer is most commonly an alkyl chain and acts as the backbone of the adsorbent and connects the terminal group to the functional group. It contributes to the stacking, rigidity, and distribution of the adsorbent.

Finally, the functional group (often called tailgroup) at the top of the adsorbent can take numerous forms, and in theory can be any moderately sized organic molecule. The functional group is almost solely dependent on the intended application, and as self-assembled monolayers have been used in a large variety of applications, such as for protective layers for metals, modifying electrodes, nano fabrication etc, a large number of functional groups have been reported.^{18–20}

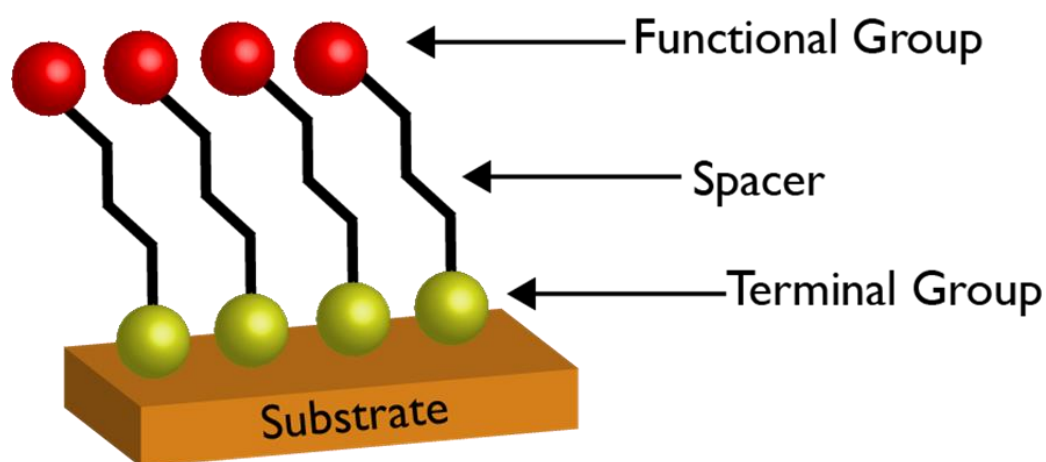


Figure 1. Diagram showing the components of a self-assembled monolayer

4.2.1. Common Self-Assembled Monolayer Motifs

Although there exists a plethora of substrates with an equally voluminous number of adsorbents, there are a few combinations which have prevailed in the research of self-assembled monolayers. Firstly, partially due to their abundance and versatility in

necessary surface composition, and equally due to their biological importance, carboxylic acids have been some of the first and most widely studied terminal groups for self-assembled monolayers. Carboxylic acid terminated adsorbents will form monolayers upon a large number of metals, with the driving force being the formation of a carboxylate salt with the cationic metallic surface. *Timmons and Zisman*, for example, reported successful monolayer formation between stearic acid and 19 polished metal surfaces, including noble metals like platinum, gold and silver, p-block metals, and a wide range of transition metals.²¹ This also extends to metal oxide surfaces, with *Tao* introducing similar *n*-alkanoic acids to copper, silver, and aluminium oxide surfaces.²²

Equal in surface diversity, organosilicon derivatives are adsorbents that can be applied to a wide range of oxygen containing surfaces. The formation of strong silicon-oxygen bonds is the driving force that accelerates the assembly of such monolayers and provides a strong and stable foundation for macromolecular systems to be built upon. However, the strength of the silicon-oxygen bond and reactivity of the organosilicon reagents hinders the reproducibility of such surfaces. As an example, *Brandriss and Margel* reported large variations in the quality and coverage of their self-assembled monolayers depending on the storage method and pre-treatment heating temperature that was applied to their substrate.²³ This was due to water playing a pivotal role in both the formation of the self-assembled monolayer, but equally in formation of siloxane polymers which can form multi-layers onto the surface.

Conversely, an opposing method can be used which exchanges the organosilicon adsorbent and oxide surface. By using a silicon surface and a hydroxyl terminated adsorbent, the same strong silicon-oxide covalent bond can be formed, but with the advantages of the ease in handling and preparing organic alcohols compared to

organosilicons. An attractive option due to the dependence of silicon in areas such as computing, hydroxyl-silicon self-assembled monolayers have been extensively studied to advance our electronic transport systems.²⁴

Finally, and most relevant to this work, is the use of organosulfurs as adsorbents to be used on metal surfaces. Although organosulfur based self-assembled monolayers have been seen with a myriad of substrates such as, nickel, palladium, silver, and platinum. It is their interactions with gold surfaces which are the best understood.²⁵

4.2.2. Self-Assembled Monolayers of Thiolates on Gold

Although the terminal group for the adsorbent in sulfur-gold self-assembled monolayer formation is most commonly an alkanethiol, other sulfur containing terminal groups have been demonstrated. Those of which include, dialkyl disulfides, dialkyl sulfides, thiophenols, thiophenes, dithiocarbamates, xanthates, thionocarbamates, thioureas, and the related alkaneselenols (*figure 2*).^{14,26–34}

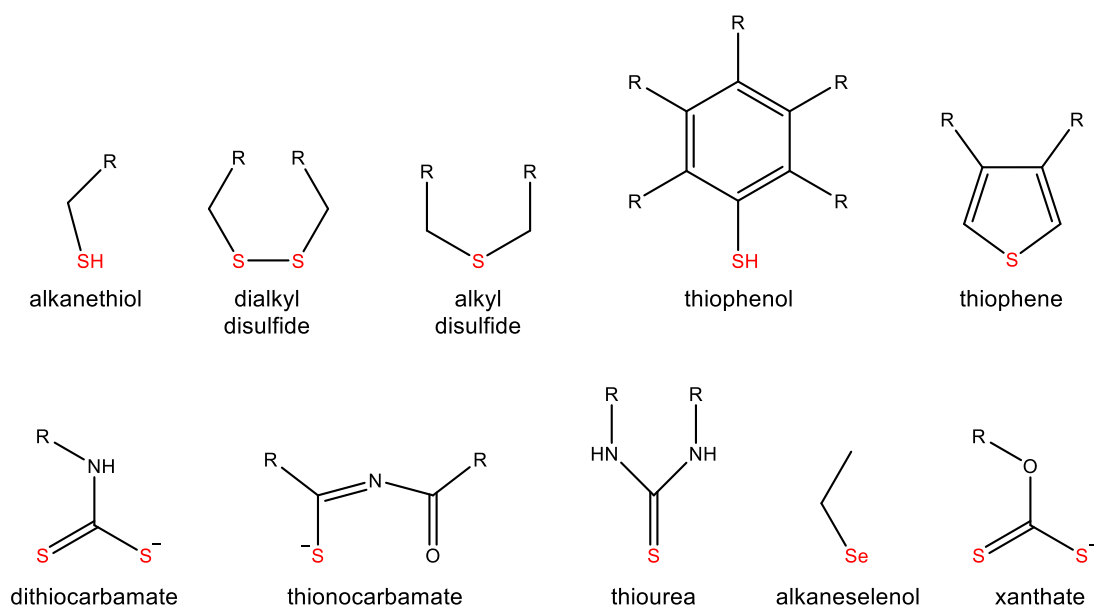


Figure 2. Possible terminal groups for the formation of chalcogen-gold self-assembled monolayers.

Equally, the substrate most commonly used and studied is a Au(111) surface, however there have been some studies on thiolate self-assembled monolayers on Au(100) (figure 3).^{35,36} Nevertheless, as this research will only use alkanethiols and Au(111) substrates, the complexities of differing terminal groups and substrate composition will not be further examined.

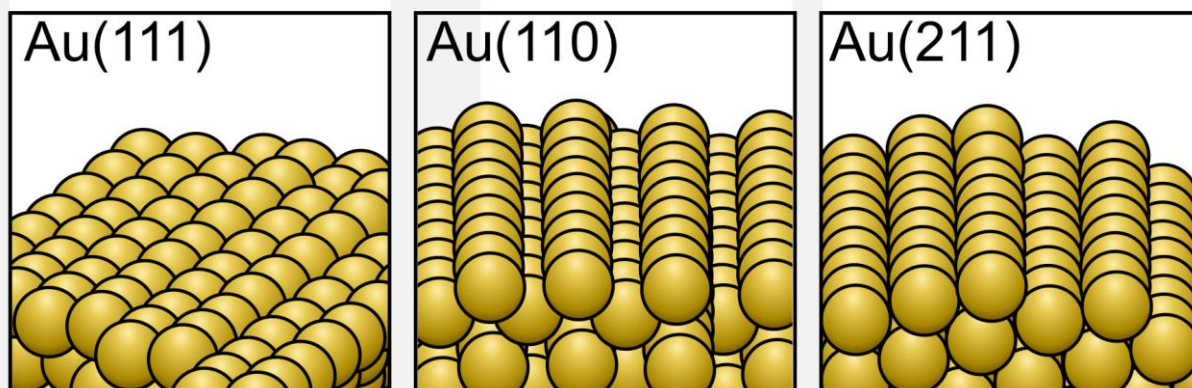


Figure 3. Structures of Au(111), Au(110) and Au(211) surfaces.

With the versatility of the thiolate-gold self-assembled monolayer, paired with their relative ease of preparation, and strong S-Au bond leading to good stability, this has propelled this pairing as the most widely studied SAM.

4.2.3. Mechanism of Thiolate-Gold SAM Formation

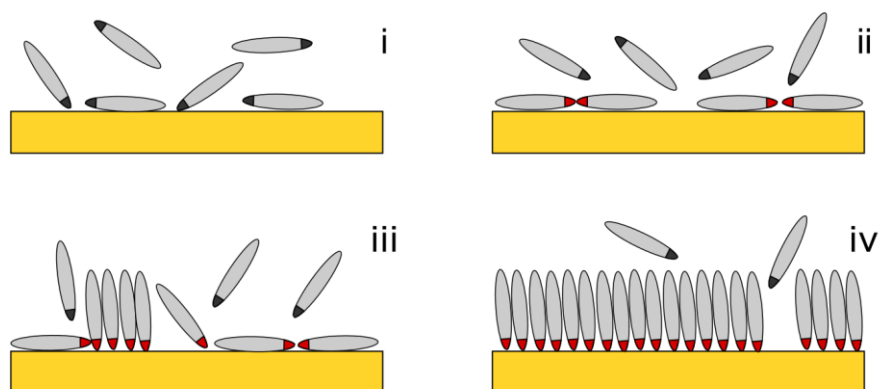


Figure 4. Schematic of the stages of self-assembly in regard to the formation of alkanethiol on Au(111) SAMs. i) physisorption, ii) lying down phase formation, iii) nucleation of standing phase, iv) completion of standing phase. Adapted from *Vericat et al.*³⁷

There are some discrepancies when examining the nature of the mechanism of thiolate gold SAM formation. However, the most widely accepted hypothesis is that the mechanism of self-assembly can be broadly split into: physisorption, chemisorption, followed by ordering and rearrangement (*figure 4*). The initial physisorption state resembles a highly disordered gas-like system, where the alkanethiols are arranged sporadically. Although the exact nature of this state is difficult to assert, due to the 'mobile' nature of the physisorbed molecules, evidence about the behaviour of this state has been brought forth. *Torelles et al*, proposed the physisorption stage is almost entirely directed by Van der Waals interactions between both the molecules and the gold substrate, and between neighbouring molecules. Equally, they suggested that the physisorbed and chemisorbed species are not independent, and that there will be a coexisting of both states as the adsorbent rearranges to more energetically favourable positions upon the surface.³⁸

The mechanism of chemisorption is also not completely understood, with disagreements regarding the intermediary binding stage. Some studies suggest that the binding of alkanethiols onto a gold surface can occur *via* a non-dissociative adsorption, in select cases such as for short chain alkanethiols, and for the attachment to gold clusters.^{39,40} For the majority of cases, scission of the sulfur-hydrogen bond, and formation of dihydrogen is assumed as necessary for the formation of the SAM. What is not clear however, is the order in which the adsorption of sulfur and elimination of hydrogen occurs. *Ulman* argues the case for an initial oxidative addition of S-H to the gold surface, with a subsequent reductive elimination of hydrogen, this occurring *via* an anionic thiolate intermediate.⁴¹ *Häkkinen*, in contrast, argues that due to the interaction between S-H and gold only resembling weak lone-pair driven 'coordinative-type' bonds, the initial step would be the breaking of the sulfur-hydrogen bond, forming a thiyl radical.⁴²

In either circumstance what has been demonstrated is that this chemisorption step is relatively fast, taking only a few minutes in most cases. The kinetics of this initial step follows a diffusion-controlled Langmuir adsorption model, and as such is dependent mainly on the concentration of the adsorbent.⁴³ There can also be contributory factors arising from the molecular structure of the adsorbent, as to how quick or slowly chemisorption occurs. These effects are governed primarily by the electron density of the binding sulfur. There is also a secondary kinetic stage, which is the rearrangement of the adsorbents upon the surface to their least disordered states. Often described as a quasi-crystallisation, this manoeuvring of the thiol adsorbents into discrete unit cells, is a slow step, with some examples of this process lasting several hours.²⁵ The rate of this step varies, and has numerous contributory factors, with the intermolecular

interactions between neighbouring adsorbents, as well as the surface mobility of the adsorbents proving key factors.⁴¹

4.2.4. Structure and Bonding of Thiolate-Gold SAM

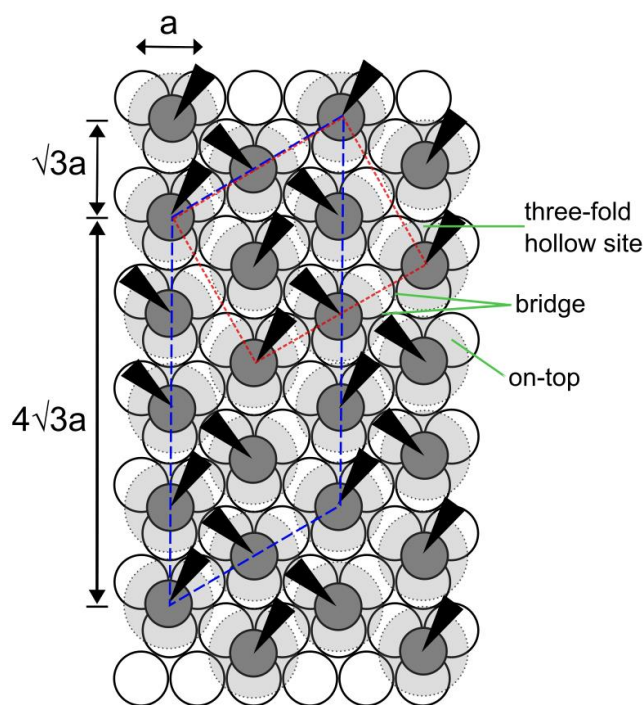


Figure 5. Structural model of the monolayer formed by thiol adsorbents on a Au(111) surface. Denoting a $(\sqrt{3}\times\sqrt{3})R30^\circ$ structure where the sulfur atoms (grey) are sitting within the 3-fold hollows of the gold lattice (white circles with $a = 2.88 \text{ \AA}$). The estimated surface areas occupied by the alkyl chains are denoted by the dashed circles, with the wedges indicating the projection of the CC plane of the alkyl chain onto the gold surface. A $c(4\times 2)$ superlattice formed from the alternating of the alkane chains is shown with the box constructed of large blue dashes. Equally, a $2\sqrt{3}\times\sqrt{3}$ unit cell is shown with short red dashes. Figure adapted from *Love et al.*¹⁵

The defining of the surface structure of the thiolate-gold SAM was mainly analysed using *n*-alkanethiols, and as such may not directly compare with larger adsorbents. However, what was observed using alkanethiol adsorbents was that they would form a $(\sqrt{3}\times\sqrt{3})R30^\circ$ overlayer, with a secondary $c(4\times 2)$ superlattice being formed *via* the preferred orientation of the alkyl chains (*figure 5*).^{35,44–46} *Strong and Whiteside*, were among the first to study the structure of alkanethiol on Au(111), and in addition to the

previous ordering remarks calculated the intermolecular spacing of the alkanethiol groups as 4.97 Å, with an area per molecule of 21.4 Å².³⁵ The preferential binding of alkanethiols towards the three-fold hollow sites of Au(111) has been shown experimentally and theoretically. With this site being calculated as the most stable binding site with the lowest surface energy, when compared to the bridge and on-top positions.

As previously described, the preferred orientation of the alkyl chains upon the surface are determined partially by the intermolecular interactions between the spacers and functional groups of neighbouring adsorbents. However, generalisations can be made with regards to the Au-S-C angle in the gold hollow sites. The average tilt angles of 27°- 35° (relative to the surface) found for most alkanethiols can be described as a compromise between two opposing forces. Firstly, when examining the nature of the Au-S bond, *Ulman* prescribed the bond as having both distinct σ and π -character.⁴⁷ With the σ -bonding arising mainly from the sulfur p-orbitals and the gold 6s-orbitals, with significant contribution from the p and d orbitals of gold. The π -bonding is said to be constructed from the p-orbitals of both gold and sulfur. It is the significant π -bonding contributions of the bond that constricts the Au-S-C to an 'sp like' linear structure.⁴⁸

However, as the bond angles found deviates from linear, it is clear that there are other contributions that determine the orientation. It is in fact, the Van der Waals intermolecular forces between the spacers that cause this discrepancy. This effect can be quantified by comparing adsorbents with different spacers, for alkanethiols as previously stated the average cant angle is ca 28°, however this changes when the alkyl spacer is replaced with phenyl groups. *Kang et al*, found that by using *para*-substituted biphenyl thiols, this tilt angle can be reduced to as low as 12° for a phenol derivative.⁴⁹ This variation in angle arises from the change of the optimisation of Van

der Waals forces in alkane thiols, to a maximisation of π - π interactions for phenyl derivatives.

4.2.5. Macrocycles as Adsorbents for Thiolate-Gold SAMs

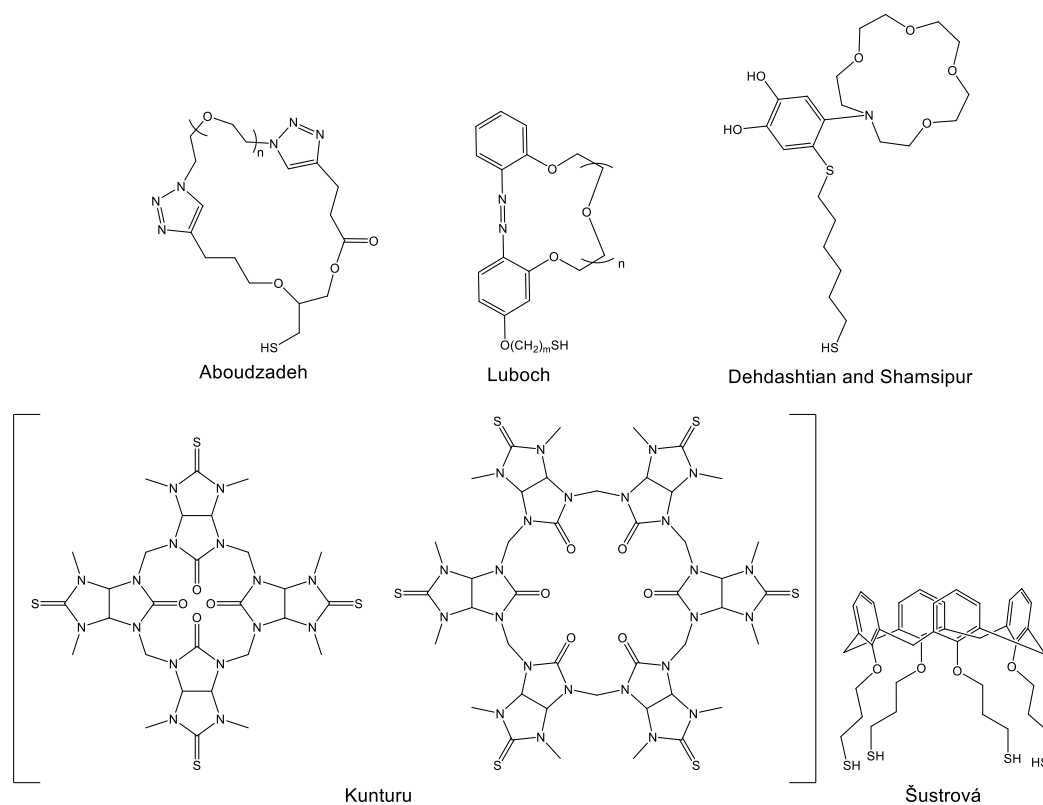


Figure 6. Structures of macrocycles mentioned in this chapter section.

Although not plentiful, there have been some reports of the successful incorporation of macrocycles into a thiolate-gold SAM (figure 6). An example of which by *Aboudzadeh et al*, used a macrocyclic poly(ethylene oxide) functionalised with a thiol group.⁵⁰ They demonstrated not only successful attachment to a gold surface, but also emphasised the increased hydrophilicity of their SAM when compared with bare gold. Similarly, *Luboch et al* reported an azobenzocrown derivative with a pendant alkanethiol chain, this macrocycle could then be bound to gold nanoparticles with a good surface coverage.⁵¹ These macrocycle covered nanoparticles were shown to display efficient encapsulation and sensing of potassium cations. With emphasis on

electrochemical sensing of cadmium, *Dehdashtian and Shamsipur* employed a thiol substituted mono aza-crown ether for gold electrode adsorption.⁵² Dissimilar to the work of *Luboch et al*, the macrocycle in this report was not initially thiolated. Contrary to this, 1,6-hexanedithiol was initially bound to the polished gold surface, then the macrocycle with a pendant catechol group was added. A subsequent Michael Addition, would then affix the catechol to the disulfide chain, finishing the macrocycle bound thiolate-gold SAM. Aside from this interesting route to functionalisation, this research also documented the materials sensitive sensing of Cd^{2+} , with a detection limit of 4.5 μM .

Some studies opted to avoid a single alkanethiol functionalisation route like those reported previously, and instead functionalised an entire rim of their macrocycle. *Šustrová et al*, functionalised the phenol rings of calix[4]arene with pendant thiol chains.⁵³ They reported that the formation of the SAM occurred on the relatively quick time scale of 300 s, and the process of adsorption was a concentration dependent Langmuir isotherm. Equally, they noted significant differences in surface coverage and reproducibility when different solvents were used in the adsorption process. *Kunturu et al*, also synthesised a rim thiolated macrocycle, this time utilising the bambusuril macrocyclic framework.⁵⁴ The chemisorption of the thiocarbonyl sulfur atoms to the gold surface could be confirmed with X-ray photoelectron spectroscopy (XPS). Equally, through scanning tunnelling microscopy (STM) they were able to qualify the structure of their SAMs, with the 4 membered bambusuril adopting a rectangular lattice, and the 6 membered macrocycle adopting a triangle/hexagonal lattice.

4.3. Thiolated Pillar[5]arenes on Gold Surfaces

As of the time of writing, only one research paper has outlined the effective adsorption of thiolated pillar[5]arene to a gold surface. *Kothur et al* in 2016 reported the successful

synthesis and deposition of a thiolated pillar[5]arene onto a gold electrode (*figure 7*).⁵⁵ Their work was later supplemented by the addition of the thiolated pillar[5]arene onto gold nanoparticles.⁵⁶

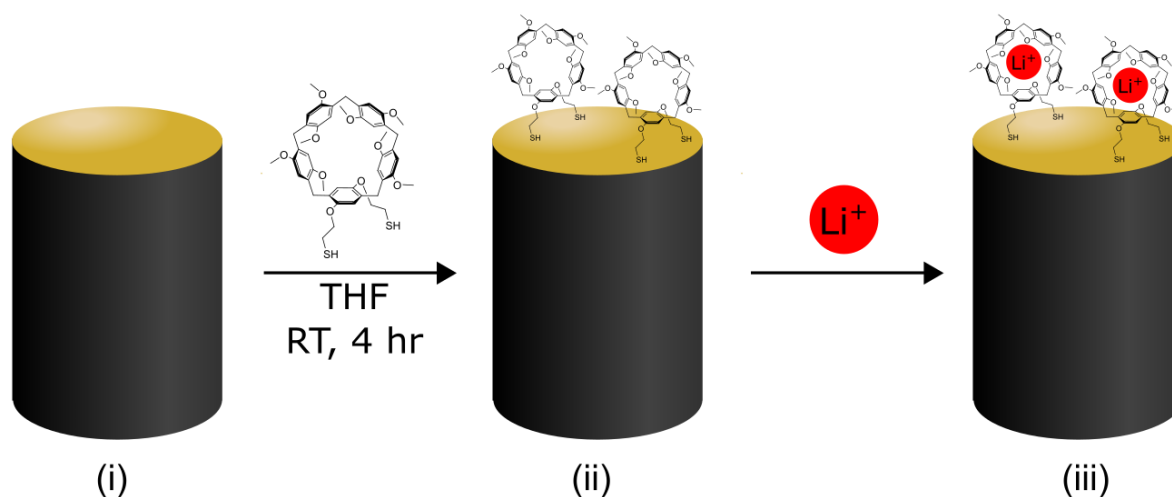


Figure 7. Diagram of work performed by Kothur et al. i) Bare gold electrode. ii) Gold electrode after soaking in a concentrated solution of thiolated pillar[5]arene in tetrahydrofuran. iii) Addition of a series of alkali salts (lithium pictured) to measure the selectivity of pillar[5]arene towards alkali cations using cyclic voltammetry.⁵⁵

4.3.1. Pillar[5]arene on Surfaces

Aside from the thiolate-gold SAM that are herein being examined, there have been multiple reports of the surface modification of other metal and non-metal surfaces with functionalised pillar[5]arenes. For gold nanoparticles there have been multiple successful attempts at capping the metal surface with functionalised pillar[5]arenes. Whether with carboxylate, ammonium, or imidazolium functionalised pillar[5]arenes, the capped nanoparticles were synthesised with a ‘bottom-up’ approach.^{57–59} That is, the functionalised pillar[5]arenes are added to a solution of H₂AuCl₄ and a reducing agent, and the surface modified nanoparticles are formed *in situ*. This compares to other methods which start with premade nanoparticles stabilised by, for example, citrate, then the intended adsorbent is added to begin the functionalisation process.⁶⁰

These pillar[5]arene decorated nanoparticles showed a range of interesting properties. Firstly, the stability of the nanoparticles towards pH changes and salt addition was enhanced, and aggregation could be limited.⁶¹ Additionally, due to the vacant pores of the bound pillar[5]arene still allowing for the encapsulation of guests, macromolecular meta structures could be constructed by introducing 'linking' guests. This is best demonstrated by the work of Yao *et al*, who reported that by adding an amphiphilic guest molecule, unique nanostructures could be constructed (*figure 8*).⁵⁸ Therein reported, was three structures observed by SEM and TEM: a micelle, an 'onion-like disk, and a vesicle.

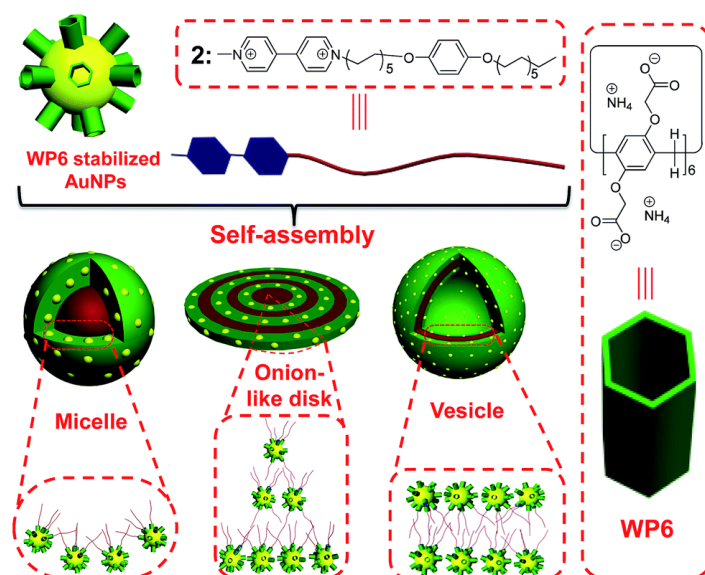


Figure 8. Structures of water-soluble pillar[6]arene (WP6), amphiphilic guest (2), and the products of self-assembly of WP6 stabilised gold nanoparticles with guest 2 in water. Extracted with permission from Yao *et al*.⁵⁸

Akin to nanoparticles, silica surfaces have also been reported with pillar[5]arene adsorption. Ogoshi *et al* for example, showed that after initially functionalising a silica surface with a cationic ammonium pillar[5]arene, consecutive additions of anionic carboxylate pillar[5]arene and the cationic pillar[5]arene can lead to the formation of an alternating layered structure.⁶² Equally, by using a silica surface, Li *et al* were able

to selectively encapsulate chiral proteins *via* the chiral induction of adsorbed amine functionalised pillar[5]arenes.

4.3.2. Thiolated Pillar[5]arenes

Before examining the sparse reports of thiolated pillar[5]arene on surfaces it is important to examine the current reports of how thiolated pillar[5]arenes are synthesised. At the time when the work herein was conducted only one viable route for thiolation had been reported by *Kothur et al.*^{55,63} However, as research into thiolated pillar[5]arenes has recently progressed, other methods have been trialled and reported.

The methods of producing thiol containing pillar[5]arenes can be split into two categories, dependent on whether the product is an alkanethiol or a thiol attached directly to the phenylene units. For the latter, the process requires the demethylated pillar[5]arene detailed in chapter 1. From then a dimethylcarbamothioate is produced with the addition of a base and *N,N*-dimethylthiocarbamoyl chloride. A high temperature Newman-Kwart rearrangement yields the *S*-aryl thiocarbamate, where a subsequent reduction with lithium aluminium hydride will give the thiolphenyl pillar[5]arene (*figure 9*).⁶⁴

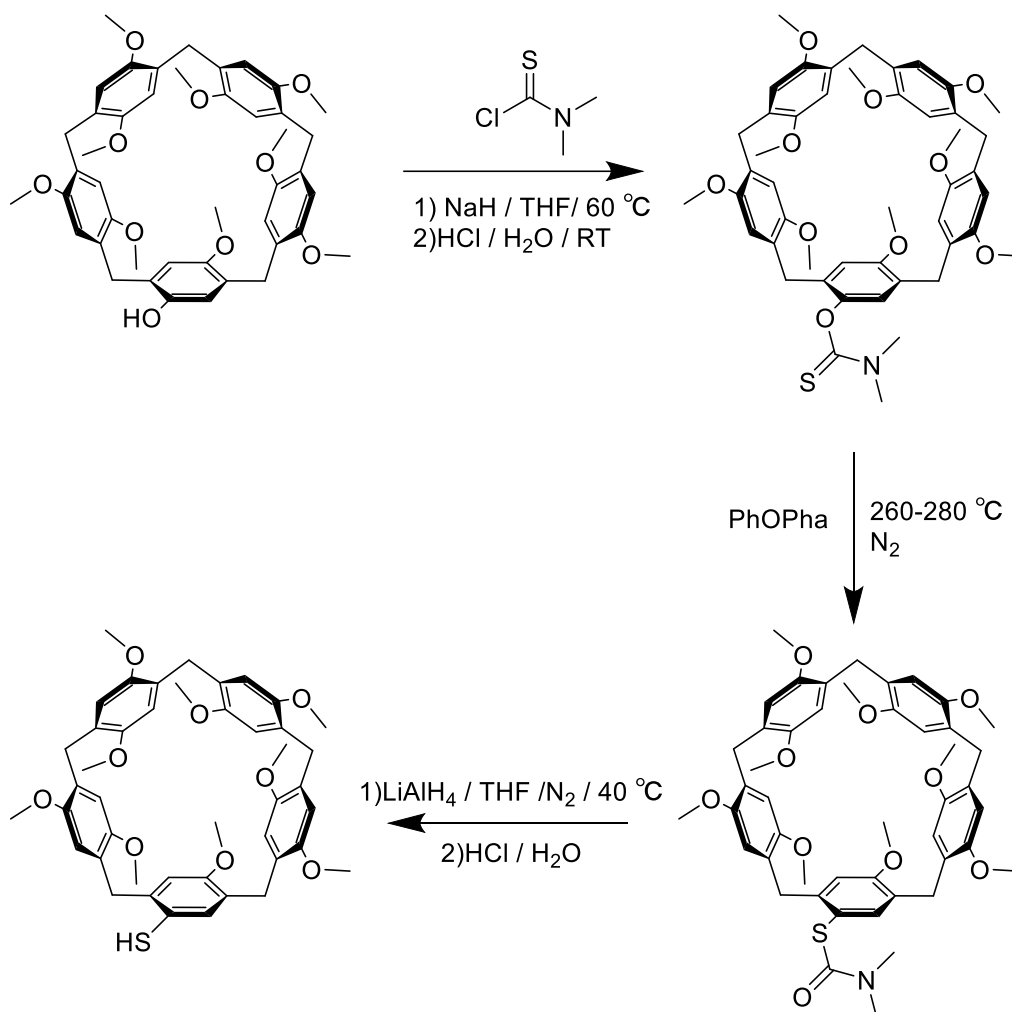


Figure 9. Synthetic route for substituted containing pillar[5]arene.⁶⁴

Alternatively, an alkanethiol group can be added to the pillar[5]arene with one of three viable routes shown so far. This can be with a silyl protected thiol and tetrabutyl ammonium fluoride, or with thiourea and base, those of which will be discussed in the results section. An additional method by *Shurpik et al*, was recently documented in May 2022 and proceeded *via* the addition of a thioacetate intermediate.⁶⁵ This intermediary step could be performed easily with an alkylbromo functionalised pillar[5]arene and potassium thioacetate. A subsequent deprotection step with hydrazine, will yield the thiolated pillar[5]arene with good yields (*ca* 70 %).

4.3.3. Pillar[5]arenes on Gold Surfaces

Kothur et al, conducted an extensive study on pillar[*n*]arene based gold electrodes and nanoparticles, the aim of this research was to investigate these pillar[*n*]arene-gold systems as potential selective molecular sensors.⁵⁵ For the modified electrodes, the gold electrodes were submerged in a solution of alkylthiol functionalised pillar[*n*]arene for approximately 4 hours. The attachment to the gold surface was confirmed *via* cyclic voltammetry, SEM and EDX. The imaging from SEM, combined with the EDX showing a near theoretical ratio of carbon to sulfur led the researchers to assert a coating of the pillar[5]arene on the gold surface. The surface modified gold electrodes were then tested against a range of both biogenic amines, and alkali metals to establish their possible sensing applications.⁶³ A high degree of selectivity towards certain alkali metals cations, and biogenic amines was asserted. This partnered with the orientation of the adsorbed pillar[*n*]arene; perpendicular to the substrate, indicated the thiol pillar[*n*]arene-gold SAM as a potential 2D sensor.

4.3.4. Scanning Tunnelling Microscopy

Scanning tunnelling microscopy (STM) is an imaging method, that yields high-resolution images of surface topography on the atomic scale. Developed in 1981 by *Binnig* and *Rohrer*, STM was one of the earliest examples of scanning probe microscopy, which would later include other commonly used imaging techniques, namely, atomic force microscopy, and scanning probe electrochemistry.

Scanning tunnelling microscopy can be fundamentally associated with the quantum mechanical notion of electron tunnelling. That is the movement of electrons through a barrier that under classical description should not be passable. For STM this is employed by passing a probe, consisting of an atomically sharp metal wire (often

tungsten or platinum), over a conductive surface. When the metal tip and the surface are sufficiently close, an overlap of the electron 'cloud' between the two is formed. A bias voltage can then be applied resulting in tunnelling across the gap between the probe and surface. This application of voltage produces a tunnelling current due to the drive for electrons to travel through the potential barrier. As the probe scans across the 2D surface, the tunnel current will map the surface's electron density. Equally, due to the tunnelling current being exponentially dependent on the distance between probe and tip, this method is highly sensitive to minor topographic differences within the surface.

For the operation of STM, there are two distinct modes that can be used: constant height mode and constant current mode. For constant height mode, the probe is scanned along the surface at a defined z value. The changes in tunnelling current can then be plotted as a function of the (x,y) position of the probe. This provides a visual representation of the electronic density of states of the surface. Although a quick method of gaining high-resolution images, this method can only be applied for extremely flat surfaces, as height discrepancies in a surface can cause the tip to crash when scanned at a constant height.

Alternatively, constant current mode, this instead limits the tunnelling current by use of a feedback loop. This requires the implementation of the piezoelectric effect. The probe used in STM is attached to a drive consisting of three piezoelectric transducers which are specific to either the x , y , or z axis. The x and y transducers control the movement of the probe across the surface by expanding or contracting in response to an applied voltage. The z piezoelectric transducer brings the tip closer or further away from the surface in response to a voltage as before. For the feedback loop to occur, and for constant current mode to work, the tunnelling current obtained from the probe

to surface interaction is amplified to a voltage. This voltage is then compared to a reference value, where the difference in voltages is applied to the z piezoelectric transducer. Thus, causing the tip to move up or down, dependent on whether the voltage formed from the tunnelling current is more or less than the reference voltage. It is the applied voltage to move the piezoelectric transducer in the z plane, that is recorded. As before, this change can be plotted against the (x,y) position of the probe to construct a 2D image (figure 10).

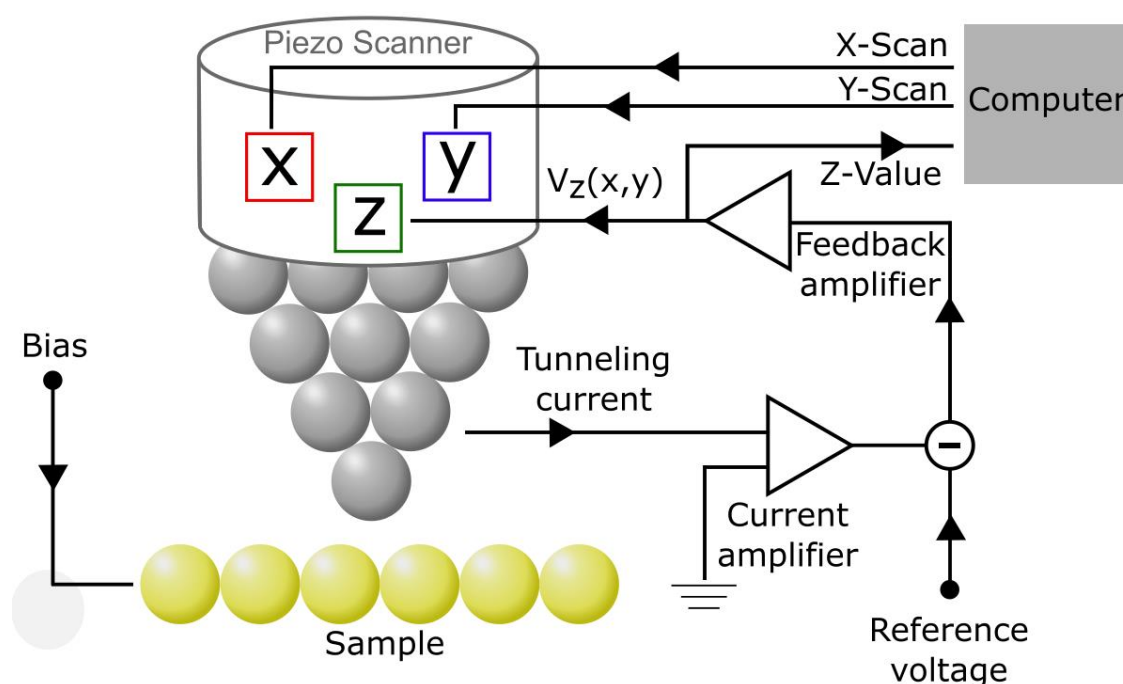


Figure 10. Schematic diagram of the principles behind STM using the constant current mode, with $V_z(x,y)$ representing the signal fed to the z piezoelectric transducer to relay information regarding the displacement from the ideal current. Adapted from *Binnig and Rohrer*.⁶⁶

4.4. Results and Discussion

Within this chapter a detailed overview of the synthetic route to both difunctionalised and per-functionalised pillar[5]arenes is discussed using two methods. Following that will be an investigation into the applicability of thiolated pillar[5]arenes in the coating of a Au(111) surface using a vapour deposition method. Scanning tunnelling

microscopy is used to investigate the surface properties of the pillar[5]arene gold surface, with a discussion on the shortcomings and possibilities for future work.

4.4.1. Synthesis of Thiolated Pillar[5]arenes

As previously mentioned, two methods were deployed for the synthesis of the di- and per-thiolated pillar[5]arenes. However, both methods required an alkylbromo functionalised pillar[5]arene to proceed. For this halogenated pillar[5]arene, an alkylbromo subunit was first synthesised, and then macrocyclization was performed either with or without dimethoxybenzene for the per- and di- functionalised pillar[5]arene respectively.

4.4.1.1 Synthesis of 1,4-Bis(2-bromoethoxy)benzene

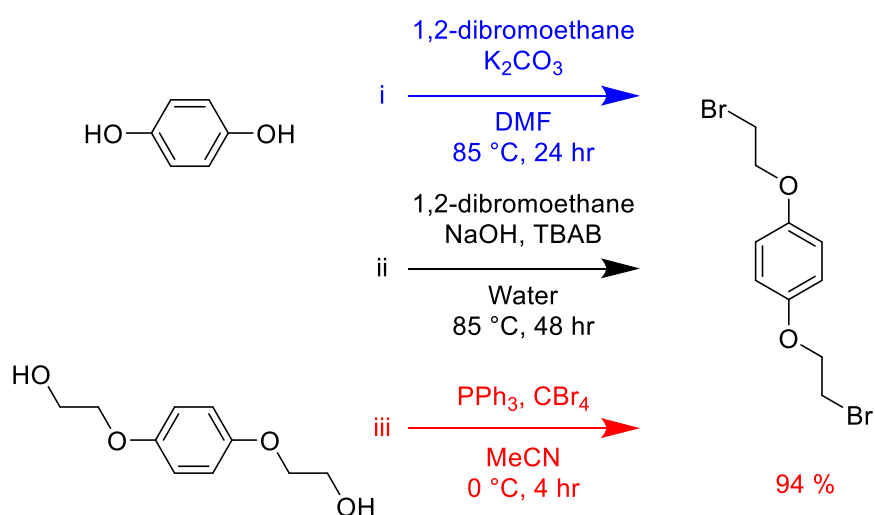


Figure 11. Experimental routes trialled for the synthesis of 1,4-bis(2-bromoethoxy)benzene

To synthesise the necessary subunits for the pillar[5]arenes, a few synthetic routes were trialled so that an effective and economic subunit synthesis can be documented for further research (*figure 11*). The first route (*figure 11i*), follows a similar procedure to other Williamson etherification's documented in chapters 2 and 3 of this thesis. Whereas the equivalent reaction conditions with the dibromobutyl or hexyl chain were

high yielding when trialled (ca 90 %), for ethylenedibromide the yields were below 20 %, which concurs with literature examples.⁶⁷ There could be a number of reasons as to why this yield was relatively low, firstly the boiling point of dibromoethane is the lowest of the haloalkanes, when discounting methyl derivatives. The high temperatures that this etherification requires, paired with the low vapour pressure (11.7 mmHg) and relatively low boiling point (ca 131 °C), could lead to the evaporation of the reagent before successful etherification. Equally, the shorter alkyl chain length could contribute to the lessening of the effectiveness of the bromine as a leaving group by the relative destabilisation of the intermediate.

Whichever the reasons may be, alternate methods were trialled so that a larger crop of the subunit could be obtained. Next, a method adapted from *Liu et al*, where the hydroquinone and 1,2-dibromoethane remain, but the base is substituted for sodium hydroxide, water is used as the solvent and tetrabutylammonium bromide is used as a phase transfer catalyst.⁶⁸ Still not satisfied with the yields (ca 50 %), and the lack of scalability (ca 5 g), another method was used, proceeding *via* the bromination of 1,4-bis(2-hydroxyethoxy)benzene. This reaction is an example of the Appel reaction, which uses a tetrahalide carbon and an organic phosphine to convert alcohols to alkylhalides (*figure 12*). For the reaction performed herein, carbon tetrabromide and triphenylphosphine were used, and the reaction itself was the shortest temporally and did not require the application of a heat source. Equally, the yields were vastly superior to the previously trialled methods (ca 95 %), and the reaction could be scaled to above 10 g.

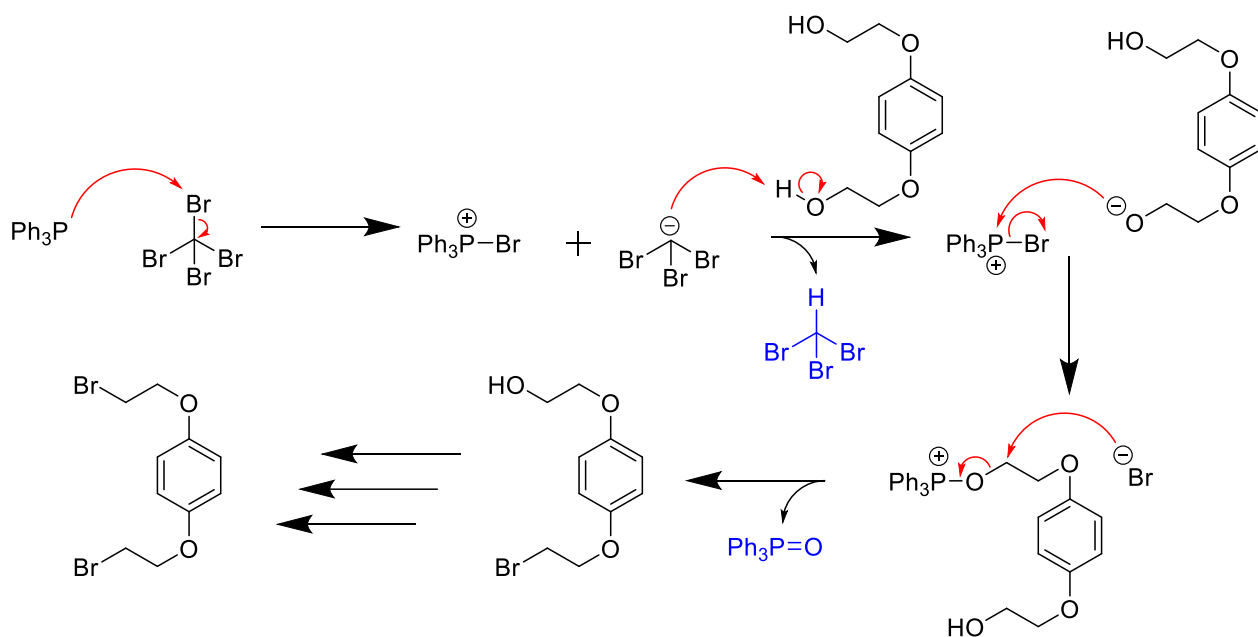


Figure 12. Reaction mechanism for the Appel Reaction, converting alcohols to alkyl bromides.⁶⁹

4.4.1.2 Synthesis of bis(bromoethoxy)-dimethoxycopillar[4+1]arene

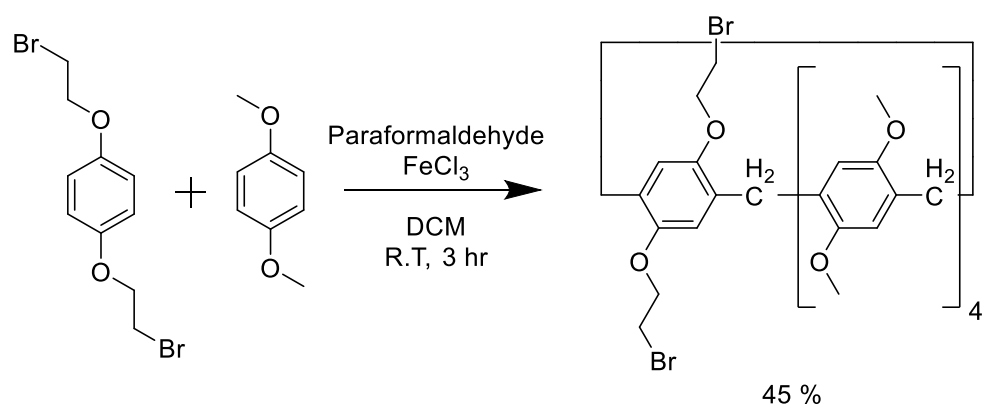


Figure 13. Reaction scheme for the synthesis of diethylbromo-dimethoxycopillar[4+1]arene

Synthesis of the copillar[4+1]arene used a method adapted from *Shao et al.*⁷⁰ The di-substituted pillar[5]arene could be synthesised by using 1:4 stoichiometric amounts of substituted hydroxybenzene and 1,4-dimethoxybenzene respectively (*figure 13*). Although, in practice the amount of 1,4-dimethoxybenzene is in large excess to avoid the formation of multiply substituted pillar[5]arenes. As in other pillar[5]arene synthesis

paraformaldehyde is used alongside iron chloride as the Lewis acid. The separation of the substituted and unsubstituted pillar[5]arene could be performed readily using column chromatography. For this particular functionalisation a less polar eluent (hexane:dichloromethane 1:1) was used, this was due to the limited polarity difference between the two products compared to that of a hexyl or octyl functionalised pillar[5]arene.

4.4.1.3 Synthesis of Bis(bromoethoxy)pillar[5+6]arene

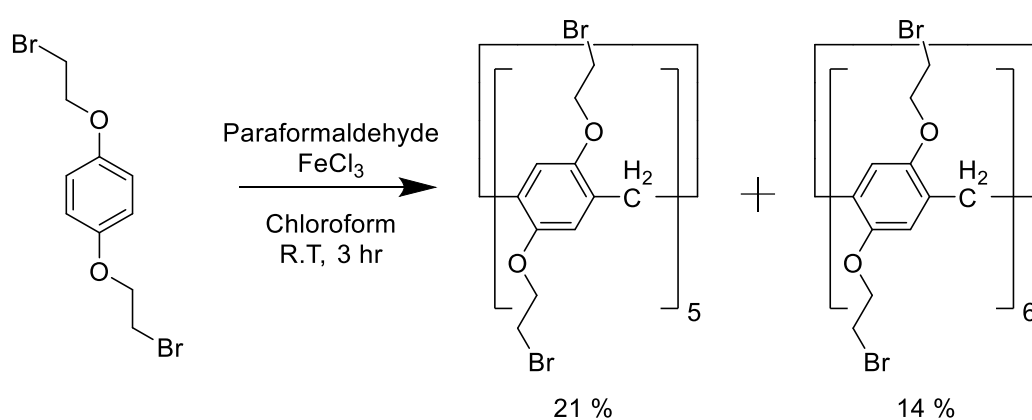


Figure 14. Reaction scheme for the synthesis of bis(bromoethoxy)pillar[5]arene and bis(bromoethoxy)pillar[6]arene.

For the synthesis of the ‘fully functionalised’ pillar[*n*]arene, the solvent was switched to chloroform to try and enable the synthesis of the 6 membered macrocycle (*figure 14*). The reason for this was to enable the future possibility of a comparison of the different sized pillar[*n*]arenes on surfaces. The other reagents were kept constant with regards to the previous procedure, aside from the solvent and the omission of dimethoxybenzene. The separation of the 5 and 6 membered macrocycle was performed using column chromatography. When this separation is compared to the diethoxypillar[*n*]arene isomer separation in chapter 2, it is significantly easier as the bromide arms help widen the gap in polarity between the pentamer and hexamer.

4.4.1.4 Structure of Bis(bromoethoxy)pillar[6]arene

In order to appreciate the conformational arrangement of bis(bromoethoxy)pillar[6]arene crystals were grown by slow evaporation in chloroform solvent, and analysed by single crystal X-ray diffraction (*figure 13*).

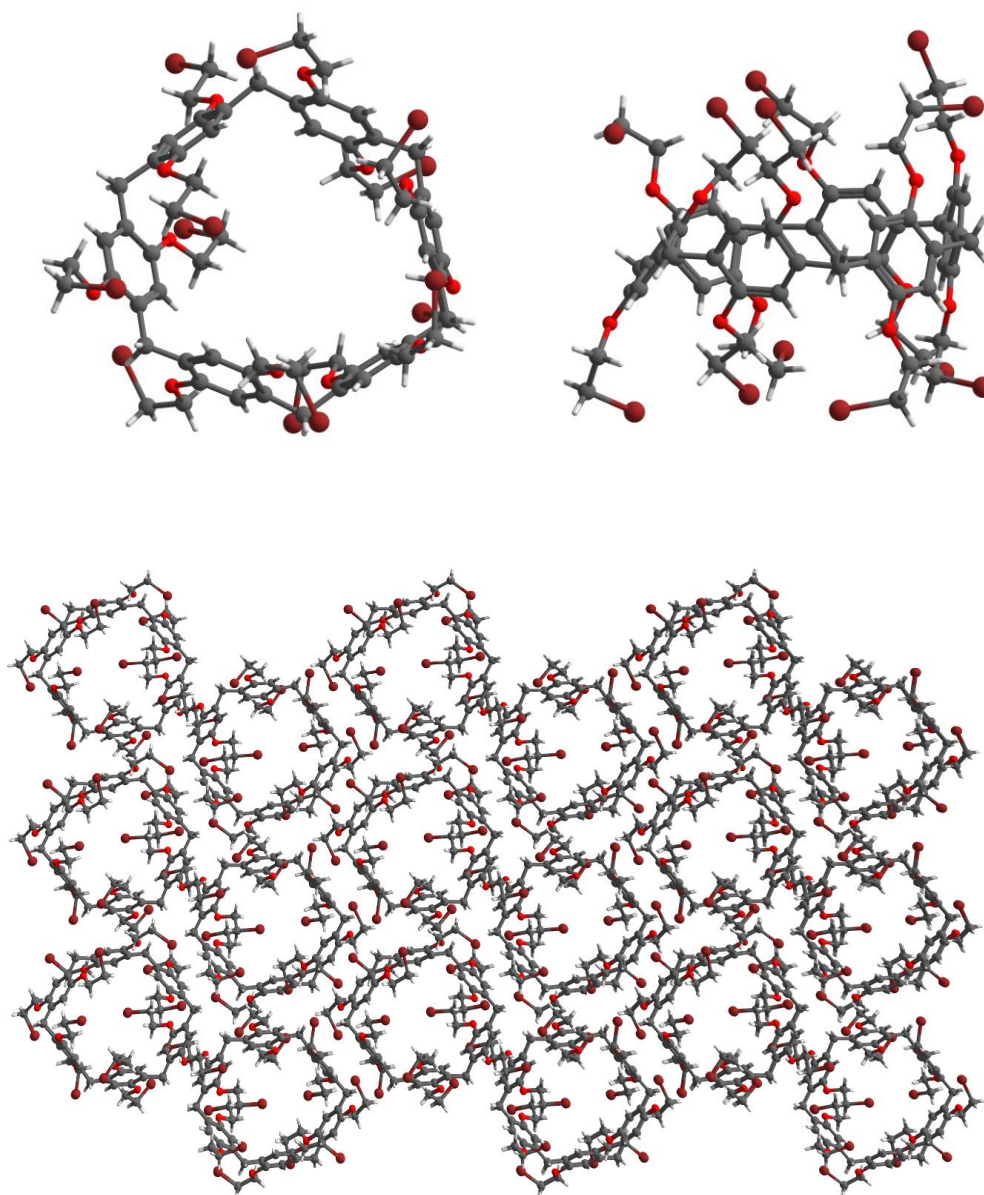


Figure 15. Crystal structure of bis(bromoethoxy)pillar[6]arene, showing top, side and packing views.

When examining the crystal structure of bis(bromoethoxy)pillar[6]arene there are a few interesting characteristics that arise (*figure 15*). Firstly, from the slow evaporation of the macrocycle in chloroform a packing formation of 1D channels arranged in a honeycomb pattern is seen. Literature reports reiterate this packing structure, with other crystallisation solvents; dichlorobenzene and methylfuran also resulting in the 1D channel/ honeycomb packing arrangement of the hexamer.^{71,72} Equally, crystal structures of the bis(bromoethoxy) pentamer show the same packing arrangement.⁷³

The other observation which was made from the crystal structure was the bending of the bromoalkyl arms away from the pillar[*n*]arenes cavity. This deviation can be seen clearly visually when examining the structure. However, to quantify the extent of deviation one can examine the bond distances between adjacent methoxy groups. If one first takes for example the crystal structure of diethoxypillar[6]arene (displayed in chapter 2). The average alkoxy-alkoxy oxygen bond distance is 5.13 Å with a standard deviation of 0.037. When this is compared with the bis(ethoxybromo)pillar[6]arene, the halogenated macrocycle shows vast differences. The average bond distance is 5.44 Å, and the standard deviation has increased to 0.52. Equally, the largest inter-oxygen distance is 6.77 Å, with the lowest distance being the adjacent subunit with 4.911 Å. The same brominated pillar[6]arene with different guest solvents show the same deviations from planarity, with a standard deviation of 0.22 for both the pillar[6]arene encapsulated with chlorobenzene and methylfuran. Although it is not possible to ascertain the explanation for this deviancy solely from the crystal data, it does provide a few possibilities to this subunit twisting. It is clear when examining the crystal structure and the other functionalised and unfunctionalized pillar[6]arenes, that the addition of bromines is a key contributor to the twisting. After examining the bond distances between the bromine atoms on adjacent pillar[6]arenes in the crystal

structure, it was clear that due to the bond distances being above 6 Å, halogen bonding was highly unlikely to be the cause of the twisting. Equally, when examining neighbouring pillar[6]arenes the bromoethoxy chains appear to twist away from each other.

Nevertheless, whatever the reasons may be, it is clear that this pillar[6]arene does not maintain planarity in all circumstances, with the aryl centres of the subunits not all facing parallel to the cavity. As such, the macrocycle may not form the intended 'open-cavity' structure when adsorbed on a surface. Although the target thiol derivative may behave quite differently, no crystal structure could be measured for that macrocycle, no further experiments were performed with the 6 membered pillar[6]arene in this study.

4.4.1.5 Synthesis of bis(ethoxythiol)-dimethoxycopillar[4+1]arene and bis(ethoxythiol)pillar[5]arene

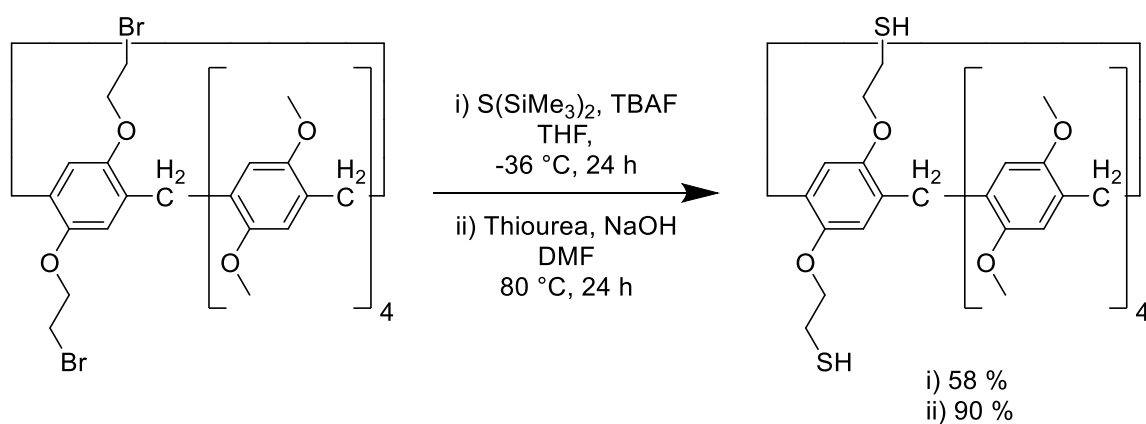


Figure 16. Reaction scheme for the thiolation of bis(bromoethoxy)-dimethoxycopillar[4+1]arene using two methods.

For the thiolation of bis(bromoethoxy)-dimethoxycopillar[4+1]arene two methods were trialled (*figure 16*). The initial thiolation reaction proceeded *via* conditions adapted from *Fox et al.*⁷⁴ In this reaction a silyl protected thiol; bis(trimethylsilyl)sulfide ($S(SiMe_3)_2$)

was deprotected by tetra-n-butylammonium fluoride (TBAF), this rapidly forms trimethylsilylthioate which can then react with the alkyl bromides on the pillar[5]arene. After stirring overnight at *ca* -30 °C, the crude product is obtained with the addition of water then filtration. Purification can then proceed *via* recrystallisation with methanol. Indication of thiols was shown in infrared spectroscopy, where peaks at around 2500 Hz indicating S-H bonds, can be observed.

Although this method gave a sufficient yield and was appropriate for the copillar[4+1]arene, there was an issue with this reaction when attempting scaling up. When this reaction was performed to *ca* 5 g scale, or when the deca-functionalised bis(ethoxythiol)pillar[5]arene was attempted, the reaction would not proceed to completion. Increasing the proportion of the bis(trimethylsilyl)sulfide and tetrabutylammonium fluoride, did alleviate these issues, but brought upon new practical issues. Firstly, the cost of the reagents is considerable, and when accounting for the large excess required to complete the fully functionalised thiolated pillar[5]arene, it proves an inefficient method. Equally, bis(trimethylsilyl)sulfide is an incredibly malodorous reagent, and so requires special experimental design considerations to avoid contamination of the working environment. Lastly, the final step of the reaction is protonation with water, as well as producing the product, excess bis(trimethylsilyl)sulfide will react to form the siloxane, but also hydrogen sulfide which is pungent and highly toxic gas.

To circumvent these issues, a number of new methods were trialled, to try and increase the scalability of the reaction, whilst also increasing the reproducibility, and negating some of the practical concerns of the previous method. Two methods that used bench stable, sulfur containing, starting materials, thiourea and potassium thioacetate, were trialled. At this point these methods were not reported in the

literature, and although thiolations with these reagents had been reported, their reactions with alkylhalide pillar[5]arenes had not.

Both methods followed an identical method, where the alkylbromide pillar[5]arene is heated with a significant excess of the thiolation reagent in DMF overnight. An aqueous solution of sodium hydroxide was added, and the reaction mixture was stirred overnight at an elevated temperature. Once the reaction was cooled, dilute hydrochloric acid was added. With thiourea, once the acid was added a white precipitate formed which corresponded to the thiolated pillar[5]arene. The potassium thioacetate method however did not produce a precipitate, and after removal of the solvent it was evident by proton NMR that the acetate group was still attached, thus thiolation had not been achieved. In retrospect, when examining the recently released research where potassium thioacetate was used successfully, it is clear that the sodium hydroxide alone was not capable of deprotecting the thiol group.⁶⁵

The advantages of the thiourea method were immediately evident, thiourea is a widely available, cheap reagent, which is relatively low in toxicity. Additionally, an excess of thiourea was easier to justify due to the previously mentioned reasons, but also due to the side products of this reaction being water soluble urea, which provided an easier purification.

4.4.2. Thermal Decomposition and Adsorption Analysis

For the deposition of the thiolated pillar[5]arene on a gold surface, a sublimation approach was attempted. For this to be possible, the macrocycle would need to be able to sublime without decomposition. The decomposition analysis was performed by using a cold finger apparatus. For bis(ethoxythiol)-dimethoxycopillar[4+1]arene the experiment was conducted at 0.70 mbar, and 100 °C was found to be the sublimation

temperature, with 130 °C being the observable decomposition temperature. Decomposition could be observed visually, wherein the white solid would darken to a light brown powder. Confirmation of decomposition was also provided by analysis with MALDI-TOF, with the mass values associated with the starting material no longer present.

To ensure the thiolated pillar[5]arenes could withstand the high voltage needed for STM, the macrocycles were deposited onto a gold electrode with a solution-based method. Due to the experiment entailing a potential range of -5 V to +5 V being scanned multiple times on the electrode, and the voltammogram showing little to no differences. One could infer that the adsorbent was capable of withstanding large voltage changes.

4.4.3. Scanning Tunnelling Microscopy of Bis(ethoxythiol)-dimethoxycopillar[4+1]arene on a Au(111) surface

To prepare the Au(111) surface, a series of sputtering and annealing cycles were carried out, and a few area scans of the cleaned surface were then gathered to ensure no build-up of residues. The thiolated pillar[5]arene was then adsorbed onto the gold surface *via* sublimation (*ca* 120 °C) under ultra-high vacuum. The initial deposition time used was 30 minutes, but after initial scans indicated minimal surface coverage, a longer deposition time of 60 minutes was performed.

The images obtained from STM, unfortunately did not provide conclusive evidence, but did have some interesting properties that could be extracted (*figures 17-19*). The images, as can be seen in the figures below, show a highly disordered surface deposition. However, there are a few areas of higher-order; firstly, as would be anticipated, the highest density of molecular deposition were along the step edges and

the herringbone reconstruction elbows.^{75,76} Secondly, and most importantly, lines of deposits roughly 4 nm apart appear, irrespective of the gold surface's contours. The circular adsorbents have an average diameter of *ca* 20 Å, an average depth of *ca* 2 Å and were arranged sporadically throughout the surface. These results could indicate a pillar[*n*]arene parallel to the gold surface, due to its similar size. Although due to the large clusters of organic matter, possibly formed from pillar[*n*]arene decomposition, it is difficult to draw definitive conclusions from the images.

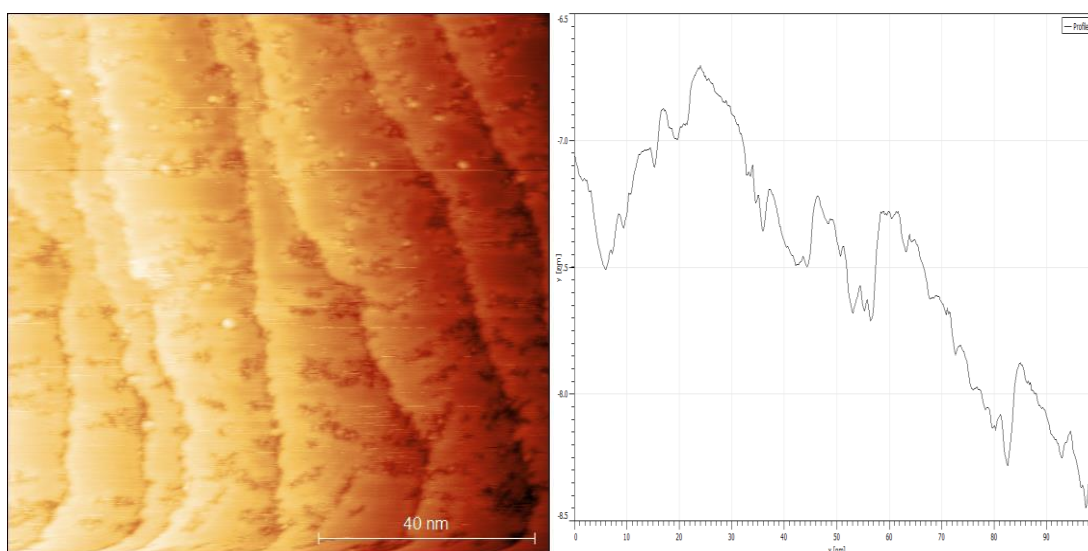


Figure 17. left: STM image showing high areas of deposition, along step edges. Right: plot of depth along the centre axis.

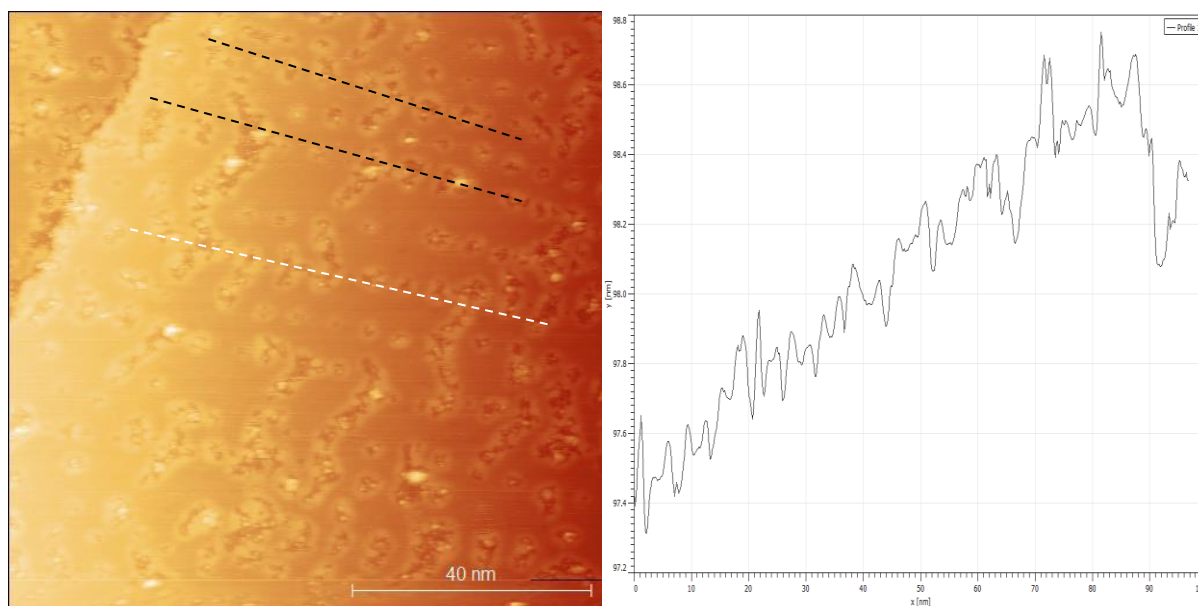


Figure 18. Left: STM image showing ordered lines of adsorbed molecules. Right: plot of depth along white line, indicating molecules depth of approximately 0.2 nm.

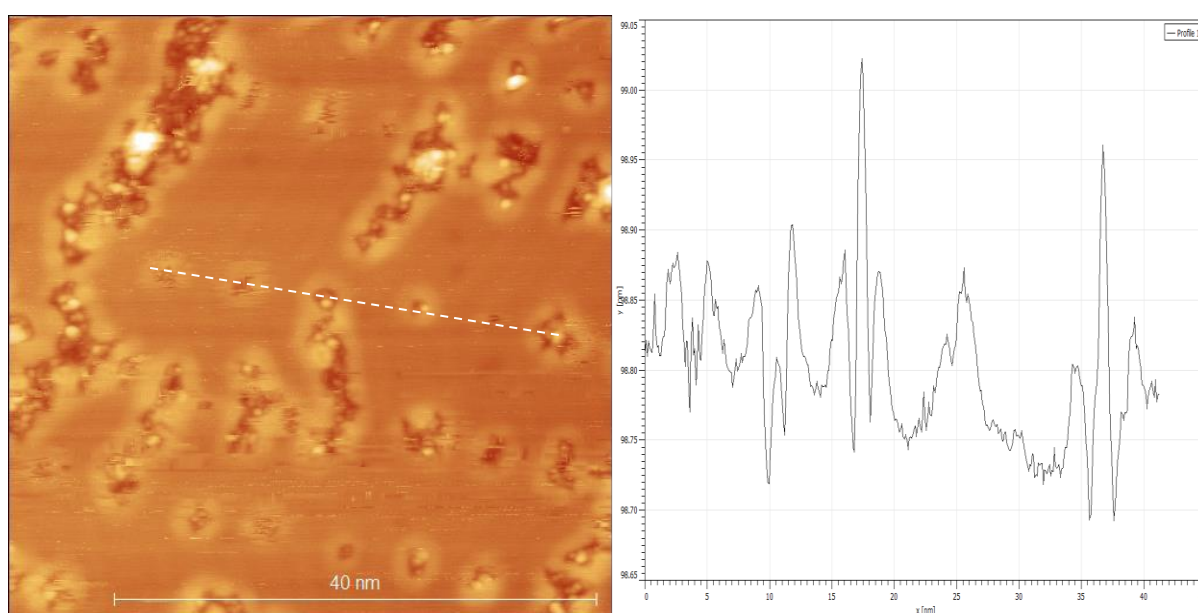


Figure 19. Higher resolution scan of figure 4, displaying ordered lines, among clusters. Right, depth plot along white line.

4.5. Conclusions and Further Work

This work has reported and compared methods of thiolating alkylbromide containing pillar[5]arenes. The discussion identified practical considerations to reagent use and commented on the nature of scalability in reactions. An attempt to adsorb the thiolated

pillar[5]arene onto a Au(111) surface was attempted and scanning tunnelling microscopy was used to visualise the surface. Although the images obtained did not conclusively qualify the pillar[5]arene gold surface, it did indicate a degree of deposition.

For this work to continue new deposition methods should be trialled, including solvent deposition. This is due to the possibility that the high temperatures needed for sublimation may be causing partial decomposition of the pillar[5]arene, forming the aggregates of residue seen in the STM. Once a suitable deposition method has been found a comparison to the decathiolated bis(thioethoxy)pillar[5]arene should be made. Alternatively, different functional groups and/or substrates could be used in substitute to the thiol-gold system, this could circumvent decomposition of the macrocycle through disulfide formation. This could include carboxylates or phosphates on a metal oxide substrate, or with a silica wafer as a substrate, organosilicons or an alcohol functionalised macrocycle could be used (*figure 20*).

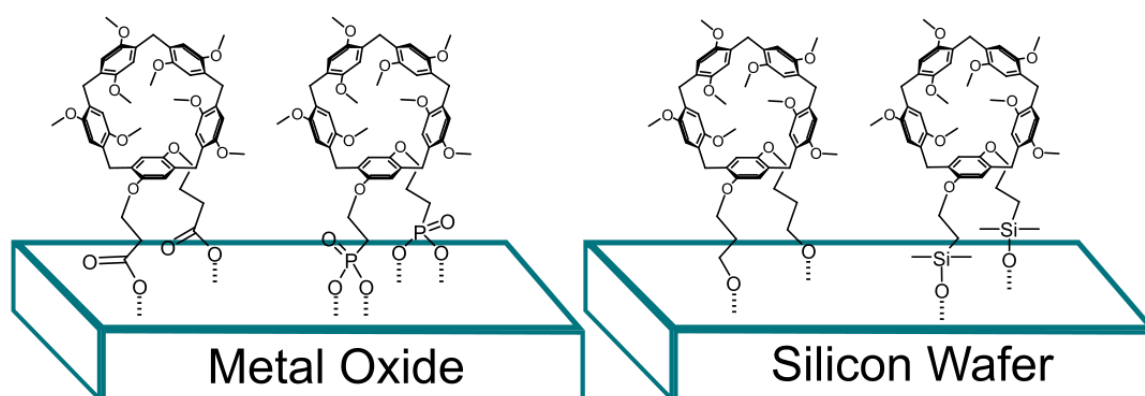
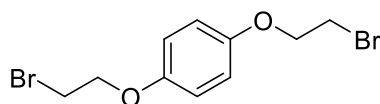


Figure 20. Alternative functional group and substrate compositions for pillar[5]arene SAMs.

4.6. Materials and Methods

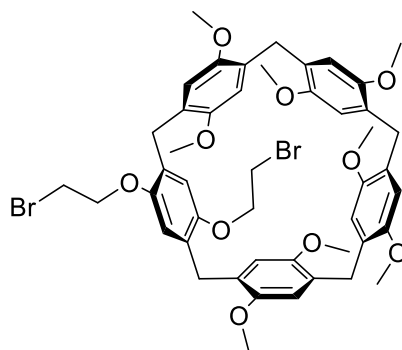
4.6.1. Synthesis of Thiolated Pillar[5]arenes

4.6.1.1. 1,4-Bis(2-bromoethoxy)benzene



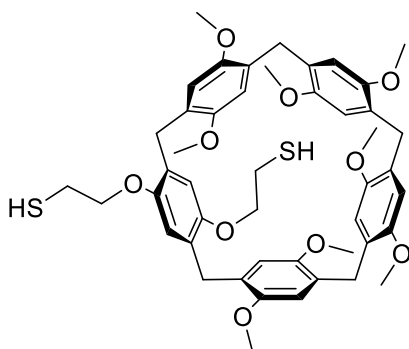
1,4-Bis(2-hydroxyethoxy)benzene (10.00 g, 50.4 mmol), triphenylphosphine (31.5 g, 120 mmol) and tetrabromomethane (40 g, 120 mmol) were dissolved in acetonitrile (250 mL) and were stirred for 4 hours at 0 °C. The solvent was removed *in vacuo*, and the residue was redissolved in dichloromethane (*ca* 250 mL), the organic layer was washed with water (*ca* 3 x150 mL) and brine (*ca* 150 mL). The organic layer was then dried over magnesium sulfate and the solvent was removed *in vacuo*. The resulting solid was then recrystallised in methanol to give 1,4-bis(2-bromoethoxy)benzene as white crystals (15.00 g, 46.2 mmol, 94 %). Spectroscopic data for the title compound were consistent with the literature. ¹H NMR (400 MHz, Chloroform-d) δ 6.87 (s, 4H), 4.26 (t, J = 6.3 Hz, 4H), 3.62 (t, J = 6.3 Hz, 4H); ¹³C NMR (101 MHz, Chloroform-d) δ 152.8, 116.0, 68.7, 29.3.

4.6.1.2. Bis(bromoethoxy)-dimethoxybenzenecopillar[4+1]arene



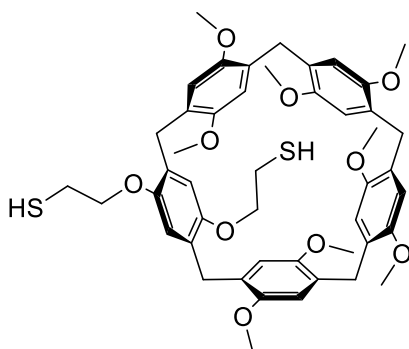
1,4-bis(2-bromoethoxy)benzene (1.75 g, 5.40 mmol), paraformaldehyde (6.25 g, 8.00 mmol) and 1,4-dimethoxybenzene (10.16 g, 73.6 mmol) were dissolved in anhydrous dichloromethane (ca 500 mL), and was stirred for 30 minutes at room temperature in a nitrogen environment. Iron (II) Chloride (1.75 g, 13.8 mmol) was then added, and the green solution was stirred for a further three hours. The suspension was then washed with water (ca 5 x 250 mL) and silica gel (ca 50 g) was added to the organic layer and the solvent was removed *in vacuo*. The crude product was purified by column chromatography on silica gel with hexane: dichloromethane (1:1) as the eluent to give bis(bromoethoxy)-dimethoxyco-pillar[4+1]arene as a white solid. (0.60 g, 0.64 mmol, 45 % yield). Spectroscopic data for the title compound were consistent with the literature. ¹H NMR (400 MHz, Chloroform-*d*) δ 6.89 – 6.80 (m, 10H), 4.14 (t, *J* = 6.2 Hz, 4H), 3.82 (t, *J* = 3.8 Hz, 10H), 3.78 – 3.69 (m, 24H), 3.54 (t, *J* = 6.2 Hz, 4H); ¹³C NMR (101 MHz, Chloroform-*d*) δ 150.75, 150.71, 129.09, 128.55, 128.22, 128.12, 127.79, 115.79, 114.36, 113.99, 113.90, 77.35, 77.04, 76.72, 68.71, 56.07, 55.82, 55.80, 55.76, 29.91, 29.79, 29.55; MALDI-TOF *m/z* for [M+H] calc'd as 937.73, found 937.12.

4.6.1.3. Bis(ethoxythiol)-dimethoxybenzenecopillar[4+1]arene – method 1



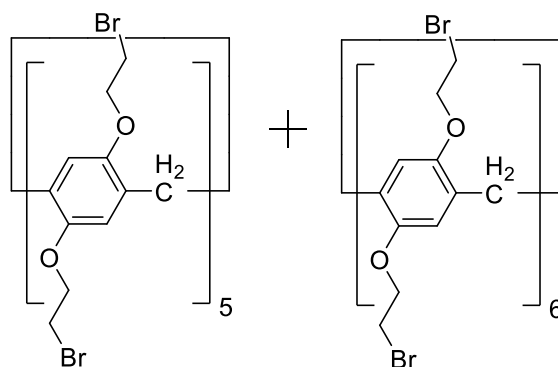
Bis(bromoethoxy)-dimethoxycopillar[4+1]arene (0.60 g, 0.64 mmol) was dissolved in anhydrous tetrahydrofuran (ca 50 mL) and was stirred at room temperature in a nitrogen environment for 30 minutes. Tetrabutylammonium fluoride (0.90 g, 3.45 mmol) and bis(trimethylsilyl) sulfide (0.22 g, 1.23 mmol) were then added and the green solution was stirred overnight at -36 °C. The solution was reduced *in vacuo* and redissolved in dichloromethane (ca 50 mL), the organic layer was then washed with water (ca 3 x 150 mL), brine (ca 100mL), hexane (ca 50 mL) and methanol (50 mL). The dichloromethane layer was separated, and the solvent was removed *in vacuo* to give Bis(ethoxythiol)-dimethoxybenzenecopillar[4+1]arene as a pale-yellow solid. (0.30 g, 0.35 mmol, 58 %). Spectroscopic data for the title compound were consistent with the literature. ¹H NMR (400 MHz, Chloroform-*d*) δ 6.87 – 6.67 (m, 10H), 4.05 (t, 4H), 3.90 – 3.75 (m, 10H), 3.72 – 3.61 (m, 24H), 3.16 – 2.86 (t, 4H), 1.24 (s, 1H, *SH*), 0.89 (s, 1H, *SH*); ¹³C NMR (101 MHz, Chloroform-*d*) δ 150.84, 150.79, 150.72, 149.90, 128.76, 128.32, 128.24, 128.03, 115.51, 114.22, 113.97, 77.35, 77.23, 77.03, 76.71, 69.42, 68.04, 55.98, 55.89, 55.80, 32.30, 29.71; MALDI-TOF *m/z* for [M⁺] calc'd as 842.32, found 841.13.

4.6.1.4. Bis(ethoxythiol)-dimethoxybenzenecopillar[4+1]arene – method 2



Bis(bromoethoxy)-dimethoxycopillar[4+1]arene (0.50 g, 0.52 mmol) and thiourea (5.00 g, 65.8 mmol) were dissolved in dimethylformamide (50 mL) and stirred overnight at 80 °C in a nitrogen environment. Sodium hydroxide (2.50 g, 62.6 mmol) in water (10 mL) was slowly added, and the mixture was stirred for a further 4 hours at 80 °C. Upon cooling, dilute hydrochloric acid was added until pH 4 was reached. The precipitate was collected *via* filtration and washed with methanol (ca 50 mL) and diethylether (50 mL) to yield 3 Bis(ethoxythiol)-dimethoxybenzenecopillar[4+1]arene as a pale-yellow solid (0.45 g, 0.48 mmol, 90 %). Spectroscopic data for the title compound were consistent with the literature. ¹H NMR (400 MHz, Chloroform-*d*) δ 6.87 – 6.67 (m, 10H), 4.05 (t, 4H), 3.90 – 3.75 (m, 10H), 3.72 – 3.61 (m, 24H), 3.16 – 2.86 (t, 4H), 1.24 (s, 1H, *SH*), 0.89 (s, 1H, *SH*); ¹³C NMR (101 MHz, Chloroform-*d*) δ 150.84, 150.79, 150.72, 149.90, 128.76, 128.32, 128.24, 128.03, 115.51, 114.22, 113.97, 77.35, 77.23, 77.03, 76.71, 69.42, 68.04, 55.98, 55.89, 55.80, 32.30, 29.71; MALDI-TOF *m/z* for [M⁺] calc'd as 842.32, found 841.13.

4.6.1.5. Bis(bromoethoxy)pillar[5]arene

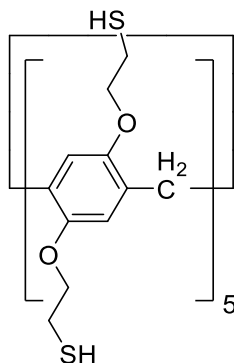


1,4-bis(4-bromoethoxy)benzene (5.00 g, 15.4 mmol) and paraformaldehyde (1.00 g, 33.3 mmol) was dissolved in anhydrous chloroform (ca 300 ml) was stirred for 30 minutes in a nitrogen environment. Iron (III) chloride (1.00 g, 7.88 mmol) was added, and the green solution was stirred for 3 hours. The suspension was washed with water

(250 ml x 3) and the solvent was removed *in vacuo*. The solid was then purified by column chromatography on silica gel with CH₂Cl₂ as the eluent. Bis(bromoethoxy)pillar[5]arene was obtained as a white solid (1.10 g, 0.64 mmol, 21% yield). Bis(bromoethoxy)pillar[6]arene was also obtained as a white solid (0.8 g, 0.40 mmol, 15 %). Spectroscopic data for the title compound were consistent with the literature.

Bis(bromoethoxy)pillar[5]arene ¹H NMR (400 MHz, Chloroform-*d*) 6.94 (s, 10H), 4.25 (t, *J* = 5.6, 20H,), 3.38 (s, 10H), 3.66 (t, *J* = 5.8, 20H,); ¹³C NMR (101 MHz, Chloroform-*d*) δ 149.67, 129.07, 116.09, 68.98, 30.60, 29.25; MALDI-TOF *m/z* for [M⁺] calc'd as 1680.12 found 1679.93. Bis(bromoethoxy)pillar[6]arene MALDI-TOF *m/z* for [M⁺] calc'd as 2016.14, found 2014.03.

4.6.1.6. Bis(ethoxythiol)pillar[5]arene



Bis(bromoethoxy)pillar[5]arene (0.20 g, 0.12 mmol) and thiourea (3.00 g, 39.5 mmol) was dissolved in dimethylformamide (75 mL) and stirred overnight at 80 °C in a nitrogen environment. Potassium hydroxide (5.00 g, 89.3 mmol) in water (10 mL) was slowly added, and the mixture was stirred for a further 4 hours at 80 °C. Upon cooling, dilute hydrochloric acid was added until pH 4 was reached. The precipitate was collected *via* filtration and washed with methanol (ca 50 mL) and diethylether (50 mL) to yield Bis(ethoxythiol)pillar[5]arene as a pale-yellow solid (0.12 g, 0.48 mmol, 90 %).

Novel Compound. ¹H NMR (400 MHz, Chloroform-d) δ 6.71 (s, 10H), 3.91 (t, J = 6.2 Hz, 20H), 3.73 (s, 10H), 2.74 (dt, J = 8.1, 6.2 Hz, 20H), 1.58 (t, J = 8.1 Hz, 10H); MALDI-TOF m/z for [M⁺] calc'd as 1210.2, found [M+K] 1247.31.

4.7. References

- 1 Y. Li and R. T. Yang, *Langmuir*, 2007, **23**, 12937–12944.
- 2 S. Aguado, G. Bergeret, C. Daniel and D. Farrusseng, *J. Am. Chem. Soc.*, 2012, **134**, 14635–14637.
- 3 T. Zhu, Y. Han, S. Liu, B. Yuan, Y. Liu and H. Ma, *Front. Chem.*, 2021, **9**.
- 4 A. Campanile, B. Liguori, C. Ferone, D. Caputo and P. Aprea, *Sci. Rep.*, 2022, **12**, 3686.
- 5 Ya. V Shalaeva, Ju. E. Morozova, A. T. Gubaidullin, A. F. Saifina, V. V Syakaev, A. M. Ermakova, I. R. Nizameev, M. K. Kadirov, A. S. Ovsyannikov and A. I. Konovalov, *J. Incl. Phenom. Macrocycl. Chem.*, 2018, **92**, 211–221.
- 6 E. Vesselli, *Nanoscale Adv.*, 2021, **3**, 1319–1330.
- 7 B. Franklin, W. Brownrigg and Farish, *Philos. Trans. R. Soc. Lond.*, 1774, **64**, 445–460.
- 8 I. Fechete, *C. R. Chim.*, 2016, **19**, 1374–1381.
- 9 I. Langmuir, *J. Am. Chem. Soc.*, 1917, **39**, 1848–1906.
- 10 A. Pockels, *Nature*, 1892, **46**, 418–419.
- 11 K. B. Blodgett, *J. Am. Chem. Soc.*, 1935, **57**, 1007–1022.
- 12 W. C. Bigelow, D. L. Pickett and W. A. Zisman, *J. Colloid. Sci.*, 1946, **1**, 513–538.
- 13 H. Kuhn, *Thin Solid Films*, 1983, **99**, 1–16.
- 14 R. G. Nuzzo and D. L. Allara, *J. Am. Chem. Soc.*, 1983, **105**, 4481–4483.
- 15 J. C. Love, L. A. Estroff, J. K. Kriebel, R. G. Nuzzo and G. M. Whitesides, *Chem. Rev.*, 2005, **105**, 1103–1169.
- 16 G. Witte and C. Wöll, *J. Mater. Res.*, 2004, **19**, 1889–1916.
- 17 U. Srinivasan, M. R. Houston, R. T. Howe and R. Maboudian, *J. Microelectromechanical Syst.*, 1998, **7**, 252–259.
- 18 I. Kaur, X. Zhao, M. R. Bryce, P. A. Schauer, P. J. Low and R. Katakya, *ChemPhysChem*, 2013, **14**, 431–440.
- 19 G. Y. Liu, S. Xu and Y. Qian, *Acc. Chem. Res.*, 2000, **33**, 457–466.
- 20 S. H. Cho, Y. U. Lee, J. S. Lee, K. M. Jo, B. S. Kim, H. S. Kong, J. Y. Kwon and M. K. Han, *IEEE/OSA Journal of Display Technology*, 2012, **8**, 35–40.
- 21 C. O. Timmons and W. A. Zisman, *J. Phys. Chem.*, 1965, **69**, 984–990.
- 22 Y. T. Tao, *J. Am. Chem. Soc.*, 1993, **115**, 4350–4358.
- 23 S. Brandriss and S. Margel, *Langmuir*, 1993, **9**, 1232–1240.
- 24 D. K. Aswal, S. Lenfant, D. Guerin, J. V Yakhmi and D. Vuillaume, *Anal. Chim.*

- Acta.*, 2006, **568**, 84–108.
- 25 C. Vericat, M. E. Vela, G. Corthey, E. Pensa, E. Cortés, M. H. Fonticelli, F. Ibañez, G. E. Benitez, P. Carro and R. C. Salvarezza, *RSC Adv.*, 2014, **4**, 27730–27754.
 - 26 E. B. Troughton, C. D. Bain, G. M. Whitesides, R. G. Nuzzo, D. L. Allara and M. D. Porter, *Langmuir*, 1988, **4**, 365–385.
 - 27 E. Sabatani, J. Cohen-Boulakia, M. Bruening and I. Rubinstein, *Langmuir*, 1993, **9**, 2974–2981.
 - 28 T. T. T. Li, H. Y. Liu and M. J. Weaver, *J. Am. Chem. Soc.*, 1984, **106**, 1233–1239.
 - 29 Th. Arndt, H. Schupp and W. Schrepp, *Thin Solid Films*, 1989, **178**, 319–326.
 - 30 J. A. Mielczarski and R. H. Yoon, *Langmuir*, 1991, **7**, 101–108.
 - 31 H. Zhu, D. M. Coleman, C. J. Dehen, I. M. Geisler, D. Zemlyanov, J. Chmielewski, G. J. Simpson and A. Wei, *Langmuir*, 2008, **24**, 8660–8666.
 - 32 W. Limbut, P. Kanatharana, B. Mattiasson, P. Asawatreratanakul and P. Thavarungkul, *Biosens. Bioelectron.*, 2006, **22**, 233–240.
 - 33 V. Chaudhari, H. M. N. Kotresh, S. Srinivasan and V. A. Esaulov, *J. Phys. Chem. C*, 2011, **115**, 16518–16523.
 - 34 A. Ihs, K. Uvdal and B. Liedberg, *Langmuir*, 1993, **9**, 733–739.
 - 35 L. Strong and G. M. Whitesides, *Langmuir*, 1988, **4**, 546–558.
 - 36 L. H. Dubois, B. R. Zegarski and R. G. Nuzzo, *J. Chem. Phys.*, 1993, **98**, 678–688.
 - 37 C. Vericat, M. E. Vela, G. Benitez, P. Carro and R. C. Salvarezza, *Chem. Soc. Rev.*, 2010, **39**, 1805–1834.
 - 38 X. Torrelles, C. Vericat, M. E. Vela, M. H. Fonticelli, M. A. Daza Millone, R. Felici, T.-L. Lee, J. Zegenhagen, G. Muñoz, J. A. Martín-Gago and R. C. Salvarezza, *J. Phys. Chem. B*, 2006, **110**, 5586–5594.
 - 39 I. I. Rzeźnicka, J. Lee, P. Maksymovych and J. T. Yates, *J. Phys. Chem. B*, 2005, **109**, 15992–15996.
 - 40 M. Hasan, D. Bethell and M. Brust, *J. Am. Chem. Soc.*, 2002, **124**, 1132–1133.
 - 41 A. Ulman, *Chem. Rev.*, 1996, **96**, 1533–1554.
 - 42 H. Häkkinen, *Nat. Chem.*, 2012, **4**, 443–455.
 - 43 C. D. Bain, E. B. Troughton, Y. T. Tao, J. Evall, G. M. Whitesides and R. G. Nuzzo, *J. Am. Chem. Soc.*, 1989, **111**, 321–335.
 - 44 C. A. Widrig, C. A. Alves and M. D. Porter, *J. Am. Chem. Soc.*, 1991, **113**, 2805–2810.
 - 45 B. Lüssem, L. Müller-Meskamp, S. Karthäuser and R. Waser, *Langmuir*, 2005, **21**, 5256–5258.

- 46 G. E. Poirier, *Chem. Rev.*, 1997, **97**, 1117–1128.
- 47 A. Ulman, in *An Introduction to Ultrathin Organic Films: From Langmuir-Blodgett to Self-Assembly*, 2013.
- 48 H. Sellers, A. Ulman, Y. Shnidman and J. E. Eilers, *J. Am. Chem. Soc.*, 1993, **115**, 9389–9401.
- 49 J. F. Kang, A. Ulman, S. Liao, R. Jordan, G. Yang and G. Liu, *Langmuir*, 2001, **17**, 95–106.
- 50 M. A. Aboudzadeh, M. Dolz, X. Monnier, E. de San Román, D. Cangialosi, M. Grzelczak and F. Barroso-Bujans, *Polym. Chem.*, 2019, **10**, 6495–6504.
- 51 E. Luboch, M. Szarmach, A. Buczkowska, E. Wagner-Wysiecka, M. Kania and W. Danikiewicz, *J. Incl. Phenom. Macrocycl. Chem.*, 2015, **83**, 321–334.
- 52 S. Dehdashtian and M. Shamsipur, *Colloids Surf. B.*, 2018, **171**, 494–500.
- 53 B. Šustrová, K. Štulík, V. Mareček and P. Janda, *Electroanalysis*, 2010, **22**, 2051–2057.
- 54 P. P. Kunturu, Ö. Kap, K. Sotthewes, P. Cazade, H. J. W. Zandvliet, D. Thompson, O. Reany and J. Huskens, *Mol. Syst. Des. Eng.*, 2020, **5**, 511–520.
- 55 R. R. Kothur, F. Fucassi, G. Dichello, L. Doudet, W. Abdalaziz, B. A. Patel, G. W. V. Cave, I. A. Gass, D. K. Sarker, S. V. Mikhalovsky and P. J. Cragg, *Supramol. Chem.*, 2016, **28**, 436–443.
- 56 R. Reddy Kothur, PhD Thesis, University of Brighton, 2016.
- 57 H. Li, D.-X. Chen, Y.-L. Sun, Y. B. Zheng, L.-L. Tan, P. S. Weiss and Y.-W. Yang, *J. Am. Chem. Soc.*, 2013, **135**, 1570–1576.
- 58 Y. Yao, Y. Wang and F. Huang, *Chem. Sci.*, 2014, **5**, 4312–4316.
- 59 Y. Yao, M. Xue, X. Chi, Y. Ma, J. He, Z. Abliz and F. Huang, *Chem. Commun.*, 2012, **48**, 6505–6507.
- 60 P. S. Ghosh, C.-K. Kim, G. Han, N. S. Forbes and V. M. Rotello, *ACS Nano.*, 2008, **2**, 2213–2218.
- 61 C. Park, E. S. Jeong, K. J. Lee, H. R. Moon and K. T. Kim, *Chem. Asian. J.*, 2014, **9**, 2761–2764.
- 62 T. Ogoshi, S. Takashima and T. Yamagishi, *J. Am. Chem. Soc.*, 2015, **137**, 10962–10964.
- 63 R. Reddy Kothur, B. Anil Patel and P. J. Cragg, *Chem. Commun.*, 2017, **53**, 9078–9080.
- 64 J. Luo, Y. Guo, P. Li, A. C.-H. Sue and C. Cheng, *Chem. Commun.*, 2022, **58**, 8646–8649.
- 65 D. N. Shurpik, Y. I. Aleksandrova, O. A. Mostovaya, V. A. Nazmutdinova, R. E. Tazieva, F. F. Murzakhanov, M. R. Gafurov, P. V Zelenikhin, E. V Subakaeva, E. A. Sokolova, A. V Gerasimov, V. V Gorodov, D. R. Islamov, P. J. Cragg and I. I. Stoikov, *Nanomaterials*, 2022, **12**, 1604.

- 66 G. Binnig and H. Rohrer, *Surf. Sci.*, 1983, **126**, 236–244.
- 67 J.-C. Gui, Z.-Q. Yan, Y. Peng, J.-G. Yi, D.-Y. Zhou, D. Su, Z.-H. Zhong, G.-W. Gao, W.-H. Wu and C. Yang, *Chin. Chem. Lett.*, 2016, **27**, 1017–1021.
- 68 Q. X. Liu, Z. Q. Yao, X. J. Zhao, A. H. Chen, X. Q. Yang, S. W. Liu and X. G. Wang, *Organometallics*, 2011, **30**, 3732–3739.
- 69 Appel Reaction, <https://www.organic-chemistry.org/namedreactions/appel-reaction.shtm>, (accessed October 28, 2022).
- 70 L. Shao, J. Zhou, B. Hua and G. Yu, *Chem. Commun.*, 2015, **51**, 7215–7218.
- 71 E. Li, Y. Zhou, R. Zhao, K. Jie and F. Huang, *Angew. Chem., Int. Ed. Engl.* 2019, **58**, 3981–3985.
- 72 Y. Wu, J. Zhou, E. Li, M. Wang, K. Jie, H. Zhu and F. Huang, *J Am Chem Soc*, 2020, **142**, 19722–19730.
- 73 Y. Wu, J. Zhou, E. Li, M. Wang, K. Jie, H. Zhu and F. Huang, *J Am Chem Soc*, 2020, **142**, 19722–19730.
- 74 J. Hu and M. A. Fox, *J. Org. Chem.*, 1999, **64**, 4959–4961.
- 75 A. Saywell, J. Schwarz, S. Hecht and L. Grill, *Angew. Chem., Int. Ed. Engl.*, 2012, **51**, 5096–5100.
- 76 M. Yu, N. Kalashnyk, W. Xu, R. Barattin, Y. Benjalal, E. Lægsgaard, I. Stensgaard, M. Hliwa, X. Bouju, A. Gourdon, C. Joachim, F. Besenbacher and T. R. Linderoth, *ACS Nano*, 2010, **4**, 4097–4109.

CHAPTER 5. CONCLUSIONS

Supramolecular chemistry stands as a burgeoning field within the sciences, and as research progresses, the applications of supramolecular systems will become more apparent. Within this field, the macrocycle forms an essential cornerstone and will undoubtedly remain so. Since its inception in 2008, pillar[5]arene has become a focal point within the discussion of macrocycles. Part of its success can be attributed to its chemical and structural properties. Equally though, the accessibility of the macrocycle brought forth by its ease of synthesis and functionalisation, has propelled pillar[5]arene into a wide variety of disciplines. Exploring the host-guest properties of macrocycles has always been an evident avenue for exploration. That is especially pronounced for the pillar[5]arene, where exploration on the capabilities and limits of the pillar[5]arene's ability to encapsulate is evident.

Within chapter 2 the exploration of pillar[5]arene's host-guest properties has been investigated. Starting from an intended guest target and application, a proposal was brought forth to a significant environmental issue, the use of neonicotinoids was discussed, and with it, a method for alleviating some of the hazards was proposed. A number of important points were established that will guide a more targeted approach to future work. Firstly, the accuracy of using proton shift studies to directly correlate the extent of encapsulation was considered. Throughout the research it was displayed that, although in this case there was correlation between the extent of shifting in peaks and the binding constants found from NMR titrations, a definitive causal link could not be isolated. This was made evident when comparing the pillar[5]arene and pillar[6]arene, where the larger macrocycle would not cause the extent of upfield shifting of the pentamer. This large discrepancy was, however, not as distinct within

the binding constants. All of which points to other intermolecular effects, for example proximity to aryl groups, being more pertinent to deciding the extent of guest proton shifting. Regardless, with all the guests, the pillar[5]arene had larger binding constants and by extension was better at binding the target guests. This points to the 'goodness of fit' being just as, if not more important in determining the attributes of a host-guest system, compared to just the number or strength of non-covalent intermolecular bonds. When observed in isolation, the upfield shift studies indicated that imidacloprid showed greater binding behaviour than its desnitro metabolite. However, these results could not be confirmed by NMR titration measurements due to solubility issues. However, for a direct comparison, a method to compare the two guests evenly was discussed.

Chapter 3 discussed the formation of rotaxanes and their attachment to the surface of a metal organic framework *via* covalent post synthetic modification. The approach that was taken reduced both the rotaxane and MOF into their constituent parts, in the pursuit of a 'semi-modular' approach to creating adaptable and tailored rotaxane decorated MOFs. With this approach, the synthesis of a number of possible MOF linkers, with a specific functionality towards a particular method for covalent post synthetic modification was discussed and reported. One such example used the CuAAC reaction as a scaffold to build the components from. Although the azide containing MOF was already known, a novel rotaxane was required to complete the structure. The design process separated the stoppers, macrocycle and rod components, and assigned each with a specific duty: MOF attachment, fluorescence and intermolecular binding. Through this, a rotaxane was designed where individual components could be interchanged towards determined functionalised MOFs. To evaluate the suitability of the rotaxane for both the attachment to the MOF and the

favoured method for analysis, confocal microscopy, a test was devised. Using an alkyne functionalised BODIPY a CuAAC reaction with the azide MOF could be performed before the rotaxane was made. What was observed through confocal microscopy was a measurable surface coverage of the fluorophore across the metal organic framework.

A novel alkene functionalised MOF linker was also reported, with a synthetic protocol for the MOF equally being reported. An example of how a thiol functionalised rotaxane could be made. Accompanying this, a proposal into how this rotaxane could be used in conjunction with the alkene MOF can be used to create a thiol-ene functionalised MOF surface was also suggested. Lastly, a unique tetra-carboxylate MOF linker with a bis(triazoyl)-pyridyl core was reported, in conjunction with a method for synthesising a lanthanide MOF using the linker. With the possibility of a wide range of post synthetic modification options, including alkylation and metalation, this MOF should lead to a series of interesting structures.

Lastly, the synthesis of two thiolated pillar[5]arenes was discussed in detail in chapter 4, with special attention paid to the synthetic procedures. A foundation was also built into the exploration of how pillar[5]arenes could be adsorbed onto a surface. Although unsuccessful, the images gained from scanning tunnelling microscopy indicate how this could be possible in the future.

For pillar[5]arenes, and by extension supramolecular chemistry, to become suitable for application, targeted explorations must be conducted. The work presented herein broadens the potential for the macrocycles use in a number of fields. Through either functionalisation, or by incorporating within a mechanically interlocked molecule, the pillar[5]arene was shown to be a versatile molecule. The host-guest chemistry

between pillar[5+6]arene was determined, and improvements to increase the binding and selectivity was suggested. Multiple methods of covalent post-synthetic modification of MOFs using rotaxanes was brought forth. Perhaps more importantly, a molecular system which allows for a wide range of functionalisation options was presented. With this and the other findings presented, a greater understanding of how pillar[*n*]arenes could be implemented was made, and more importantly, a foundation for future research was built.

CHAPTER 6. MATERIALS AND METHODS

6.1. Reagents and Purification

All solvents and chemicals were used as purchased from Merck, VWR international, Fluorochem, Alfa Aesar, or Tokyo Chemical Industry. Column Chromatography was performed using silica gel 60. Air and moisture reactions were performed using a standard glass Schlenk Line, with dinitrogen to establish an inert atmosphere. Glassware used was flame dried under vacuum and backfilled with dinitrogen.

6.2. General Equipment

6.2.1. Nuclear Magnetic Resonance Spectroscopy (NMR)

NMR spectra were recorded on either a Bruker AVIII 300 MHz or a Bruker AVANCE NEO 400 MHz spectrometer and referenced to residual solvent peaks, unless otherwise stated. Deuterated solvents were used as specified.

6.2.2. Mass Spectrometry

MALDI-TOF mass spectra were recorded with a Bruker **ultrafleXtreme** III mass spectrometer using trans-2-[3-(4-tert-butylphenyl)-2-methyl-2-propenylidene] malononitrile (DCTB) as the matrix. GCMS mass spectra was recorded using a JEOL GCv4G high-performance gas chromatograph time-of-flight mass spectrometer.

6.2.3. Infrared Spectroscopy (IR)

Infrared spectra of solids were obtained via a Agilent Fourier Transform Spectrometer, FTIR-8400S, fitted with a Diamond ATR unit.

6.2.4. Single crystal X-ray diffractometry (SCXRD)

Data were collected using a Rigaku Synergy-S dual source with a PhotonJet-S X-ray source and a HyPix-6000 detector. Data were collected at 100 K or 200 K through the use of an Oxford Cryosystems cryostream device. Crystal structures were solved by Dr Sarah Griffin.

6.2.5. Procedure for Titrations by Nuclear Magnetic Resonance Spectroscopy

For the titrations the concentration of the host pillar[*n*]arenes were constant (1 mM in CDCl₃) and aliquots of guest (50 mM) were added so that equivalents of 0.2, 0.4, 0.6, 0.8 1, 1.2, 1.4, 1.6, 2, 2.5, 4, 5 and 7, could be achieved. The lowering concentration of host due to dilution when adding the guest, were taken into consideration when calculating the binding constants. Each titration was repeated in triplicate to authenticate results, and polydimethylsiloxane was used as the NMR standard to reference peak shifts against. To calculate the association constants (K_a) and stoichiometry the Bindfit application was used.^{315–317}

6.2.6 Scanning Tunnelling Microscopy

The scanning tunnelling microscope used was a custom in-house made ultra-high vacuum instrument. The surface used was an ultra-flat Au(111) surface deposited upon a mica chip. The tip used was a tungsten hairpin filament, sharpened by carefully plunging into the gold surface.

To prepare the Au(111) surface, a series of sputtering and annealing cycles were carried out, and a few area scans of the cleaned surface were then gathered to ensure no build-up of residues. The thiolated pillar[5]arene was then adsorbed onto the gold surface *via* sublimation (*ca* 120 °C) under ultra-high vacuum. The initial deposition

time used was 30 minutes, but after initial scans indicated minimal surface coverage, a longer deposition time of 60 minutes was performed.

6.3. Computational Chemistry

Computational chemistry data was retrieved using the Orca 4.2.1 software package, or the AutoDock Vina package. Computational measurements were calculated with density functional theory employing 6-311++G(d,p) as the basis set and the M06-2X exchange correlation potential. Or for the energy minimized structures; the 6-31+G* basis set and B3LYP functional with D3BJ dispersion correction, geometrical counterpoise correction and CPCM (chloroform) solvent model. All calculations were performed using an Intel Core i5 7500K CPU, NVIDIA GeForce GTX 1060 6GB GPU, ASUSTek STRIX Z270e motherboard, and 2 x Corsair CMK16GX4M2B3000C15 DDR4 RAM.